

Biological Characterization of the Lectins  
DC-SIGN and FimH:  
Putative Targets for novel Anti-Infectives

Inauguraldissertation

Zur Erlangung der Würde eines Doktors der Philosophie  
vorgelegt der Philosophisch-Naturwissenschaftlichen Fakultät  
der Universität Basel.

von

Meike Scharenberg  
aus Hannover, Deutschland

Basel, 2013

Genehmigt von der Philosophisch-Naturwissenschaftlichen Fakultät auf Antrag von  
Prof. Dr. Beat Ernst und Prof. Dr. Rudolf Glockshuber.

Supervisor:

Prof. Dr. Beat Ernst

Institute of Molecular Pharmacy

Pharmacenter, University of Basel, Basel, Switzerland

External co-referee:

Prof. Dr. Rudolf Glockshuber

Institute of Molecular Biology and Biophysics

ETH Zürich, Zürich, Switzerland

Basel, den 13.12.2011

Prof. Dr. Martin Spiess

(Dekan)

## **Acknowledgements**

First, I would like to express what is on my mind when writing these acknowledgements. The time at the IMP was one of the best times I have experienced so far. Besides the great science that I was allowed to take part in, I met so many wonderful people who made my years there such a memorable time. I would like to thank all of you who supported me over the last years.

First and foremost, I would like to thank Prof. Dr. Beat Ernst for his excellent supervision, his great scientific support and daily guidance during all this time. I am exceedingly grateful for his encouragement, his unbelievable enthusiasm, and our humorous discussions. Beat, with your spirit you make the IMP a fantastic work place with an enjoyable and lively atmosphere.

I would like to thank Prof. Dr. Rudolf Glockshuber for accepting to be the co-referee of my thesis.

I thank Dr. Said Rabbani for his support and introduction into the lab and for our fruitful discussions during my time at the IMP. Thank you for providing me with the valuable FimH protein.

My warmest thanks go to Roland Preston for being not only my lab colleague, but also for being one of my best friends. Roland, having you as my “lab husband” was a wonderful stroke of luck. The same is true for Daniela Abgottspon. Thank you for your unconfined friendship. You both made my day, every day.

My deep and special thanks are also going to all present and former colleagues at the institute, who created the wonderful atmosphere at the IMP and provided me with proteins, new compounds, good ideas and memorable fun. Huge thanks go to Flo, Roland, Daniela, Simon, Matthias, Mo, Céline, Katrin, Luca, Kathi, Jacqueline, Mirko, Jonas, Katja, Martin, Sameh, and Adam. Special thanks also go to the members of the FimH and DC-SIGN team for all the helpful contributions and the fantastic teamwork.

I am deeply grateful to my master students Mirco, Evelin, Sabine, and Sirin for their great support of my work and all the memorable fun we had together. I also would like to thank Deniz for all his valuable advice during our hot chocolate breaks. You are a great friend.

I thank Prof. Scapozza and Dr. Lucile Péronot (University of Geneva), for introducing me to the world of crystals and helping me in generating DC-SIGN crystals and Prof. Angelo Vedani for being a big support in molecular modeling.

I thank my friends from Hannover, especially my best friend Yvonne, for accompanying me for so many years now. You helped me forgetting work and relaxing whenever I needed it. Thank you that I can always trust in you.

Finally, I am greatly indebted to my husband Matthias. Nothing I could write here would be enough to express my gratitude to you. Thank you for all your love, your endless care, your support, for cheering me up and always calming me down when I needed it. Knowing that we manage everything together gave me the strength I needed over the last years. Without you I would be a teacher now ;-). In the same sense I thank my family for their never-ending support in everything I did, their love and guidance throughout my whole life.

## Table of contents

### Part I: The Lectin FimH

<b>FimH Abstract</b> .....	<b>1</b>
<b>FimH Chapter 1: Introduction</b> .....	<b>3</b>
<b>FimH Chapter 2: Results and discussion</b> .....	<b>21</b>
<b>Publication 1: A Flow Cytometry-Based Assay for Screening FimH Antagonists</b> .....	<b>21</b>
<b>Publication 2: FimH Antagonists for the Oral Treatment of Urinary Tract Infections: From Design and Synthesis to in Vitro and in Vivo Evaluation</b> .....	<b>31</b>
<b>Publication 3: Target Selectivity of FimH Antagonists</b> .....	<b>47</b>
<b>Publication 4: Kinetic Properties of Carbohydrate-Lectin Interactions: FimH Antagonists</b> .....	<b>55</b>
<b>Publication 5: FimH Antagonists: Structure-Activity and Structure-Property Relationships for Biphenyl <math>\alpha</math>-D-Mannopyranosides</b> .....	<b>65</b>
<b>Supplementary Table</b> .....	<b>85</b>

### Part II: The Lectin DC-SIGN

<b>DC-SIGN Abstract</b> .....	<b>91</b>
<b>DC-SIGN Chapter 1: Introduction</b> .....	<b>93</b>
<b>DC-SIGN Chapter 2: Results and discussion</b> .....	<b>109</b>
<b>Manuscript 1: Optimization of Recombinant Protein Expression in the Mammalian Cell System by the Choice of the Signal Peptide</b> .....	<b>109</b>
<b>Manuscript 2: Variable Binding Modes of Lewisia-type DC-SIGN Antagonists</b> .....	<b>129</b>
<b>Supplementary Table</b> .....	<b>151</b>

## **Part I: The lectin FimH**

---

**FimH Abstract**

---

## **Abstract FimH**

Urinary tract infection (UTI) is one of the most common infections, with millions of people affected every year. Besides women, who bear a risk of 40 - 50% to experience at least one symptomatic UTI episode during a life-time, patients with diabetes, spinal cord injuries, and suppressed immune system are particularly at risk. Without treatment UTI may lead to bladder infection (cystitis) and, in a later infection state, to kidney infection (pyelonephritis). The initial and most fundamental step in the pathogenesis of UTIs is the type 1 pili-dependent adhesion of uropathogenic *Escherichia coli* (UPEC) to  $\alpha$ -mannoside-containing glycoprotein receptors on the surface of uroepithelial cells, such as uroplakin Ia (UPIa). The bacterial adhesion is mediated by the lectin FimH, localized at the tip of type 1 pili, which recognizes mono- and oligomannosides. The adhesion triggers the bacterial cell invasion, resulting in the development of an infection. FimH antagonists such as  $\alpha$ -D-mannopyranosides have been shown to interfere with the attachment of UPEC to their host cells, thus providing a novel therapeutic opportunity for the treatment and prevention of UTIs as an alternative to antibiotic treatment.

A potent FimH antagonist has to fulfill several requirements to also achieve a high *in vivo* efficacy. Besides a high affinity for FimH ( $K_D$ ), slow off-rates and irreversibility of the antagonist-FimH interaction are beneficial for the *in vivo* efficacy, as prolonged occupancy of the target by the drug results in an extended duration of the pharmacological effect. Furthermore, target selectivity of FimH antagonists is a pivotal concern, since the reported FimH antagonists are  $\alpha$ -D-mannopyranosides and therefore are potential ligands for mannose receptors of the human host system. Non-selective interactions of FimH antagonists with the various mannose receptors would have a profound impact on physiological processes and could cause severe side effects.

This thesis addresses some major issues in the development and biological evaluation of FimH antagonists:

- Development of a cell-based competition assay for the determination of  $IC_{50}$  values of FimH antagonists using flow cytometry.
- Determination of kinetic properties and  $K_D$  values of FimH antagonists by surface plasmon resonance.
- Investigation of the selectivity of FimH antagonists towards human mannose binding receptors.

## **Part I: The lectin FimH**

---

### **FimH Chapter 1: Introduction**

---



## **FimH Introduction**

### **Microbial lectins**

Glycoconjugates on mammalian cell surfaces are often exploited as receptors for cell adhesion by pathogenic microorganisms, leading to tissue invasion and colonization. This first and crucial step of an infection can either be mediated by bacterial adhesins or by viral hemagglutinins, which specifically bind to surface receptors on epithelial cells [1, 2]. Most adhesins are lectins that recognize complex carbohydrate structures located on membrane receptors such as glycoproteins, glycolipids, or proteoglycans [2]. Hemagglutinin from the influenza A virus was the first microbial lectin to be discovered in the 1950s [3, 4]. The name hemagglutinin derives from its ability to aggregate red blood cells, which it shares with many other microbial lectins.

Bacterial lectins commonly form oligomers that assemble in filamentous, fiber-like, organelles, called fimbriae or pili, such as type 1 fimbriae [5, 6], P fimbriae [7, 8] and F17 fimbriae [9, 10], which are important for *Escherichia coli* infections. The terminal subunit of each fimbriae functions as carbohydrate recognition domain (CRD), which recognizes distinct carbohydrate structures (subunit FimH on type 1 fimbriae [11], PapG on P-fimbriae [12], and F17G on F17 fimbriae [13]). The ligand specificity of these fimbrial lectins determines the tissue tropism of the microorganism. P-fimbriae favorably bind to galabiose (Gal $\alpha$ 1-4Gal $\beta$ )-structures, expressed in the upper part of the kidney [14], whereas type 1 fimbriae prefer high-mannose containing glycoconjugates that are highly abundant on urothelial bladder cells [15, 16]. The receptor interaction triggers signal transduction pathways in the host cells, which are often crucial for the host invasion and infection. Type 1 fimbriae bind to uroplakin protein complexes on the bladder urothelium, and thereby trigger the cytoskeletal reorganization that is critical for the internalization of the microorganism, as well as the activation of apoptosis cascades within the urothelial cells [17, 18].

### **Type 1 fimbriae and urinary tract infections**

Type 1 fimbriae are abundantly expressed on invasive uropathogenic *E.coli* (UPECs), which are the etiological agent in more than 80% of the reported cases of urinary tract infections [19-21]. The lectin FimH being located on the tip of each pilus, allows the bacteria to adhere to oligomannosides of the glycoprotein uroplakin Ia (UPIa) on uroepithelial cells [15, 16]. This initial adhesion is the most crucial step during the entire infection process. It prevents the

rapid clearance of *E. coli* from the urinary tract by the bulk flow of urine and, at the same time, enables the invasion of the host cells [22, 23]. This finally leads to a urinary tract infection (UTI), one of the most common infections, with millions of people affected every year. Particularly affected beside women, who bear a 40 - 50% risk to experience at least one symptomatic UTI episode during a life-time [20], are patients with diabetes, spinal cord injuries, and suppressed immune system [24, 25]. An untreated UTI can lead to a bladder infection (cystitis) and in a later infection stage to kidney infection (pyelonephritis) [21], both serious infections. The adherence of UPEC to the urothelium activates the innate immune defense, triggering the exfoliation of infected bladder cells, the influx of neutrophils, and other inflammatory responses [18]. Nevertheless, UPEC can evade innate host defense mechanisms and invade deeper into the tissue. There they can adopt a quiescent state by forming intracellular bacterial communities (IBCs), in which the bacteria are well protected from exogenous influences and therefore are thought to be the cause for the high incidence of recurrence of UTIs [18] (Figure 1). Antibiotic treatment does not always eradicate UPEC, resulting in the emergence of microbial resistance [26]. Therefore, over 50% of all patients experience a relapse of the infection within 6 months [19, 21].

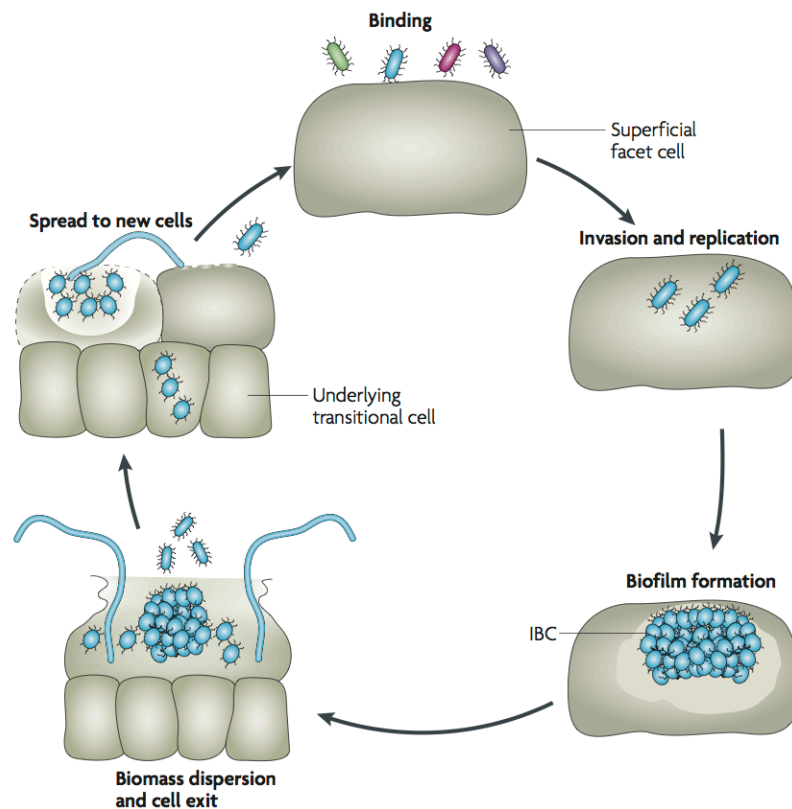


**Figure 1.** Infection cycle of uropathogenic *Escherichia coli* (UPEC), taken from [27]. UPECs bind to urothelial bladder cells via type 1 pili. They invade the host cells, replicate, and form biofilm-like intracellular bacterial communities (IBCs). Protected from immune responses and antibiotic treatment UPECs can persist for months in this quiescent state. Bacteria can re-emerge from IBCs and can form long fibers of not divided cells, which facilitate the easy infection of neighboring cells. Furthermore, UPECs can penetrate deeper into the bladder tissue and infect the underlying cells.

### Assembly and expression of type 1 fimbriae

Type 1 fimbriae are 1-3  $\mu\text{m}$  long, filamentous organelles [5, 6]. These helical rods with a diameter of 7 nm consist of thousands of FimA subunits, forming the pili rod, followed by the subunits FimF, FimG, and FimH, forming the tip of the fimbrium. The adhesin FimH, which is located at the distal end of the linear fimbrium, contains the mannose-specific carbohydrate recognition domain (FimH-CRD) [11, 28, 29].

Type 1 pili assembly takes place in the periplasmic space mediated by the chaperone/usher pathway [30] (Figure 2). This pathway is a conserved bacterial secretion system that is also used for the assembling of other fimbriae, e.g. for P fimbriae [31]. For the pilus biogenesis, the periplasmic chaperone FimC and the outer membrane assembly platform, the subunit FimD (termed the usher), are required [32]. FimD catalyzes the polymerization of the

subunits and provides the channel for the translocation of the assembled pili across the outer membrane. FimC guarantees the proper intracellular folding of the monomeric pili subunits and their delivery to the FimD platform. The subunits share similar structures, possessing an imperfect immunoglobulin (Ig)-like fold with one C-terminal  $\beta$ -strand missing. The periplasmic chaperone FimC interacts with each subunit by providing the missing  $\beta$ -strand to complete their Ig-like fold. Delivered to the FimD usher, an N-terminal extension strand (15-20 bp) of the incoming subunit replaces the FimC donor strand of the previously incorporated subunit [33]. This donor-strand complementation mechanism accounts for the strong and kinetically stable intermolecular interactions between the subunits and therefore for the remarkable stability of type 1 pili [34, 35].

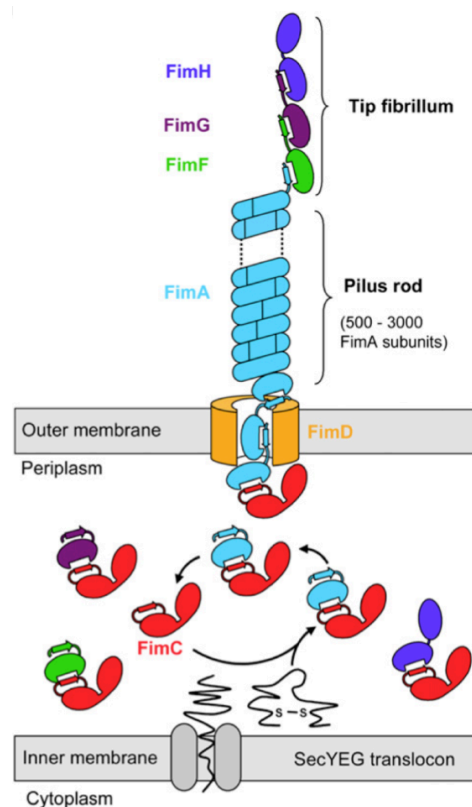


**Figure 2.** Schematic representation of the chaperone/usher pathway, taken from [35]. The fibrillum rod is composed of thousands of FimA subunits forming the pilus rod and the fibrillum tip consists of the subunits FimF, FimG, and the adhesin FimH. The chaperone FimC binds intracellular to each subunit, catalyzing folding of the subunits and delivery to the assembly platform FimD (usher) in the outer membrane. There, the donor  $\beta$ -strand of the previously incorporated subunit of the growing pilus replaces the donor strand of FimC.

The expression of type 1 pili is phase variable and switches between fimbriated and non-fimbriated states in individual cells. The genes for type 1 fimbriae are organized on a *fim* gene cluster as depicted in Figure 3.

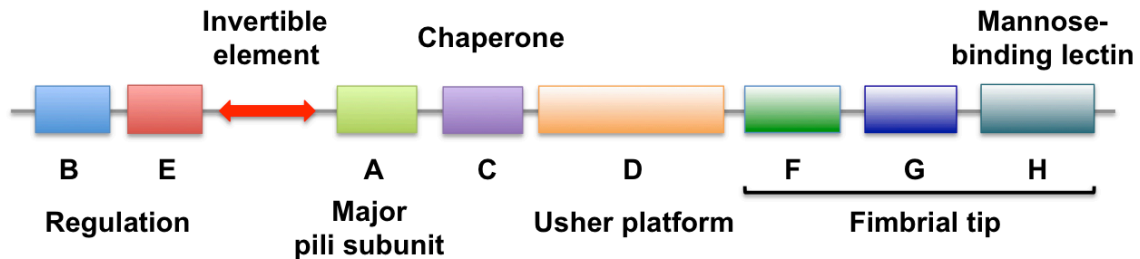


**Figure 3.** Organization of the *fim* gene cluster. The cluster encode for the pili subunits FimA, FimF, FimF, and FimH, for the chaperone FimC, the assembly platform FimD (the usher) and for the recombinases FimB and FimE. The invertible element in the promoter region is located upstream of the *fimA* gene.

The phase variation is under the control of an invertible promoter region (314 bp), which is located upstream of the *fimA* gene and promotes the transcription of the *fimA*, *fimC*, *fimF*, *fimG*, and *fimH* genes. Depending on the orientation of this promoter element, the pili expression of individual bacteria can either be in the on-phase, resulting in protein transcription or in the off-phase, where the transcription of the *fim* gene cluster is silenced [36, 37]. The inversion is regulated by the two recombinases FimB and FimE, which are encoded upstream of the invertible element within the *fim* gene cluster. It was shown that FimB promotes the switch in both directions (on-to-off and off-to-on), whereas FimE predominantly promotes the on-to-off switch [38, 39]. Several factors such as growth conditions [37, 40] (pH, osmolarity, temperature, shaking/static incubation) and the infection state [41, 42] influence the activity of the recombinases, though the underlying mechanism is not fully understood. However, it was shown that there is a cross talk between different adhesin gene clusters. For example, the activated P fimbriae gene switches the *fim* gene to phase-off orientation, thus preventing simultaneous type 1 pili expression. Expression of P fimbriae allows UPECs to ascent and infect the upper part of the urinary tract, the kidneys, resulting in a pyelonephritis. These results implicate a mutually exclusive expression of the two types of pili, depending on the infection status. This regulatory mechanism seems to be crucial for the survival and pathogenicity of the bacteria under changing environmental conditions [41].

**FimH topology and catch bond behavior**

To date, six crystal structures of FimH are accessible [29, 43-47] (Figure 4). FimH is a 30 kDa protein and consists in contrast to all other pili subunits of two immunoglobulin-like domains, the N-terminal lectin domain and the C-terminal pilin domain. The pilin domain connects FimH with the following FimG protein and is homologous to the other pili subunits. The lectin domain contains two  $\beta$ -sheets, one large and continuous, the other smaller and split. The mannose-binding site is located at the distal end of the  $\beta$ -sandwich, opposite to the region where the lectin domain is connected with the pilin domain.

The ligand binding site is a deep pocket that is negatively charged (Figure 5). FimH selects the  $\alpha$ -configuration around the free reducing anomeric oxygen of D-mannose. Hydrophilic side chains of the amino acids lining the binding pocket establish a perfect network of hydrogen bonds with the hydroxyl groups of an  $\alpha$ -D-mannopyranoside. The hydroxyl groups of D-mannose interact with residues Phe1, Asn46, Asp47, Asp54, Gln133, Asn135, Asp140, and Phe142 via hydrogen bonds and hydrophobic interactions. In addition, the entrance of the binding pocket is formed by three hydrophobic amino acids (Tyr48, Ile52 and Tyr137), which form the so called “tyrosine gate” [28, 46].

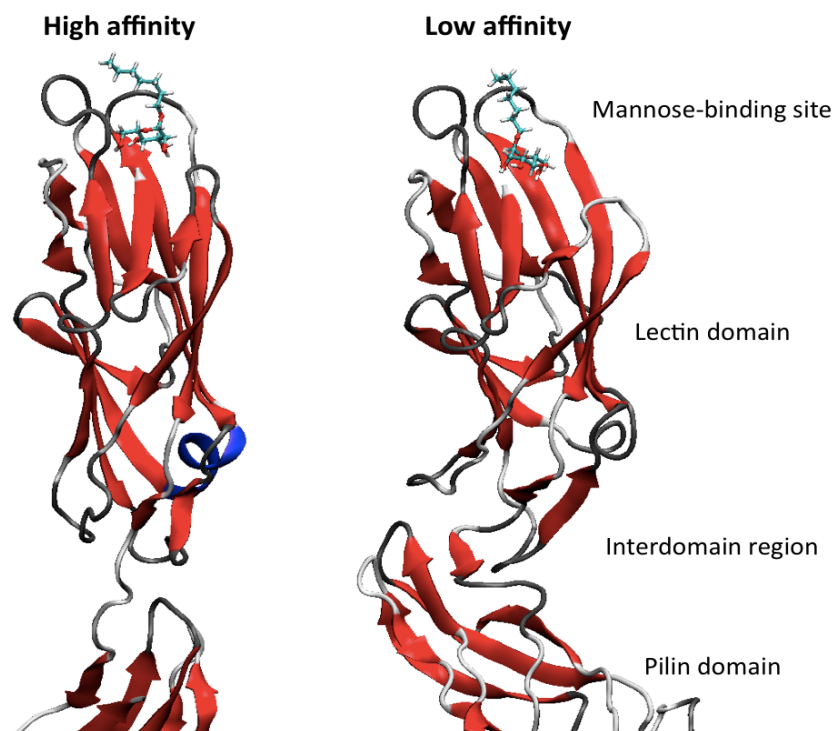


**Figure 4.** FimH lectin domain structure in the high-affinity (left side, PDB entry 1KLF) and low-affinity (right side, PDB entry 3jwn) conformation. In the high-affinity state the lectin domain is elongated with a narrow mannose-binding site. In the low-affinity state the lectin domain interacts with the pilin domain at the interdomain region with the insertion-, swing-, and linker-loop. These interdomain interactions lead to a twist in the  $\beta$ -sandwich fold of the lectin domain, which results in an opening of the distal mannose-binding site [47] (modeled by Adam Zalewski, IMP, University of Basel).

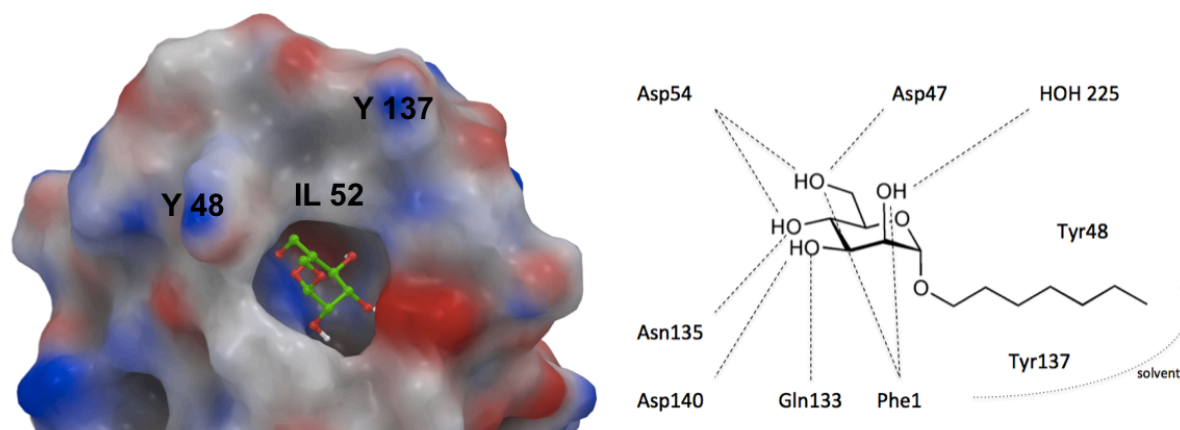


**Figure 5.** FimH mannose-binding site in complex with methyl- $\alpha$ -D-mannopyranoside (left, PDB entry 1KLF) and the interacting protein residues with n-heptyl- $\alpha$ -D-mannopyranoside (left). The hydroxyl groups of D-mannose interact with residues Phe1, Asn46 (not depicted), Asp47, Asp54, Gln133,

Asn135, Asp140, and Phe142 (not depicted) via hydrogen bonds and hydrophobic interactions. Tyr48, Ile52 and Tyr137 form the tyrosine gate at the entrance of the binding site (modeled by Adam Zalewski, IMP, University of Basel).

FimH mediates shear-dependent binding to mannosylated surfaces, facilitated via force-enhanced allosteric catch bonds [48, 49]. The physiological function of catch bonds seems to be to facilitate sustained adhesion under flow conditions, as they are found in the urinary tract. FimH can adopt two conformational states, a low and a high affinity state. Recently, the crystal structure of the low affinity FimH conformation was resolved [47] (Figure 4). In the low-affinity state the pilin and the lectin domain of FimH interact with each other via several loops of the lectin domain, which are called insertion-, swing-, and linker- loop. These interdomain interactions trigger a twist in the  $\beta$ -sandwich fold of the lectin domain, resulting in an opening of the distal mannose-binding site. In the active high-affinity state, the lectin and pilin domain are separated and thus do not interact, which leads to an untwist of the pilin domain and a tightening of the mannose binding pocket [47]. Since the low-affinity conformation is stabilized by intramolecular interactions, this mechanism is also called allosteric autoinhibition. Applying a tensile force across the bond can induce the switch from the low-affinity state to the high-affinity state. This force-induced switch and enhanced affinity to a ligand are characteristic for catch bonds. For catch bonds, the lifetime of a bond becomes longer when a tensile force is applied, in contrast to slip bonds, where the lifetime is reduced under enhanced shear force (Figure 6). The catch bond behavior of FimH was demonstrated in flow chamber assays [50] and atomic force microscopy experiments (AFM) [51]. In AFM experiments, using purified fimbrial tips, most bonds broke up at low force (<60 pN of rupture force), whereas all bonds survived when higher forces (140–180 pN of rupture force) were applied [51].



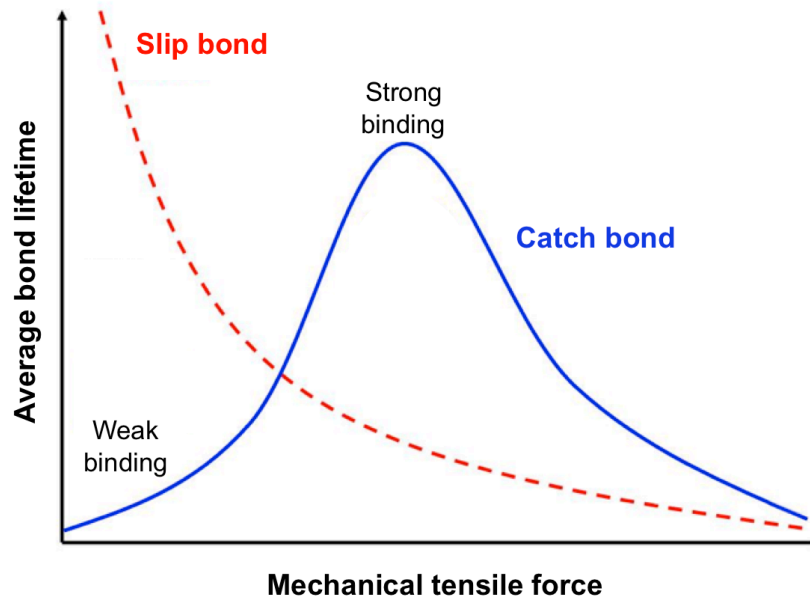


**Figure 6.** Bond-lifetime profile of catch- and slip-bond. For catch bonds, the lifetime of a bond becomes longer when a tensile force is applied across this bond. In normal slip bonds the lifetime is reduced under enhanced shear force.

Further studies showed that external factors, which keep the domains apart, force FimH into the high affinity conformation. This can be the complexation with the chaperone FimC, which wedges the two domains apart, or binding of an antibody to the interdomain region [50, 51]. Consequently, the isolated lectin domain exhibits the high-affinity state. Additionally, it was shown that the binding to a ligand and the tightening of the binding pocket around the ligand, transiently induced a switch from the twisted low-affinity to the untwisted high-affinity conformation [47].

### FimH variants

Various FimH mutant strains are found in nature. Although the mutations reside outside of the highly conserved mannose-binding site, they often lead to an enhanced mannose binding affinity [52, 53]. It is presumed that these mutations disrupt the interdomain interaction, thus shifting the equilibrium from the low-affinity to a high-affinity state [50]. In a wide study, Tchesnokova *et al.* showed that FimH possesses a ligand induced binding site (LIBS) in the interdomain region, which is constitutively exposed in FimH mutant variants with a disrupted interdomain interaction [54]. An exposed LIBS epitope, measured by the binding of a specific antibody to the LIBS epitope, correlates with a high-affinity for mannose. These results proved the allosteric link between the high affinity state of the mannose-binding site and the

open conformation of the interdomain region. Aprikian *et al.* investigated several FimH point mutations by comparing the binding strength of the LIBS antibody [50]. The study showed that most of the naturally occurring point mutations, such as the S62A and the A27V, weaken the interaction between the lectin and the pilin domain, resulting in higher mannose affinities. These mutant FimH variants evolved under positive selection, benefiting from augmented mannose binding affinity even under the static conditions, as they are found in the upper urinary tract [55]. Nevertheless, it is presumed that the allosteric catch-bond behavior still has its physiological advantages, such as better transmission potency and resistance to soluble inhibitors like the Tamm-Horsfall protein, found in the urine [56-58].

### **FimH antagonists and assay methods**

Due to increasing antibiotic resistance, efforts are made to identify novel, inexpensive, and orally available therapeutics, which inhibit bacterial adhesion with a low potential for generating resistance. FimH antagonists, such as  $\alpha$ -D-mannopyranosides, were shown to interfere with the attachment of UPEC to their host cells, thus providing a novel therapeutic opportunity for the treatment and prevention of UTIs as an alternative to antibiotic treatment [59-61].

For the evaluation of FimH antagonists, several *in vitro* assays have been reported. Most of them measure the effect of antagonists on the hemagglutination of erythrocytes [62-64] or the aggregation of yeast cells in the presence of UPECs [65-67]. In addition, FimH antagonists were evaluated with an ELISA-based assay [67, 68] and with bacterial adhesion assays using GFP tagged bacteria [69], radiolabeled mannose [44] or radiolabeled bacteria [70]. The inhibition of the binding of purified type 1 fimbriae to human granulocytes was investigated utilizing the flow cytometry technology [71]. In surface plasmon resonance (SPR) experiments, the binding of FimH to an anti-FimH blocking antibody, covalently linked to the sensor chip, enabled the determination of the affinity of antagonists [44]. Depending on the applied assay format, the reported inhibitory potencies can be different, for example  $IC_{50}$  values of D-mannose and methyl  $\alpha$ -D-mannopyranoside can vary between millimolar [62, 66] and micromolar values [44, 71]. These discrepancies can have various origins. As already discussed, FimH can adopt two different conformational states. FimH mediates weak binding at low shear stress, but shifts to strong binding at high shear [72]. The isolated CRD, which is often used in target-based assays, always adopts the high-affinity state and therefore mediates strong binding to mannose even under static conditions [50]. In cell-based assays FimH is in

its native conformation, which is usually the low affinity conformation when no shear force is applied. Furthermore, the choice of the *E.coli* strain can have a strong effect on the outcome of an assay, since strains with various FimH mutations and different binding properties exist [52].

Mannose, methyl- $\alpha$ -D-mannopyranoside and mannan were the first ligands discovered in the 70s, which inhibited yeast aggregation [73]. In the following years several reports on mannose oligosaccharides and multivalent mannose dendrimers with nanomolar affinities have been published [62, 65]. Additionally, mannosides with an aromatic aglycon, such as *p*-nitrophenyl  $\alpha$ -D-mannopyranoside (*p*-NPMAN, **2**) and derivatives thereof exhibited increased inhibitory potencies [66]. Nowadays, these findings can be rationalized based on crystal structures, such as the structure of the FimH/FimC complex, which was resolved in 1999 [29]. It was shown that aromatic aglycons interact with the so called “tyrosine gate” via  $\pi$ - $\pi$  stacking interactions with Tyr48 and Tyr137 at the entrance of the mannose-binding site. This binding mode is termed the “in-mode binding”. Since then, three main FimH antagonist families have been described, alkyl  $\alpha$ -D-mannosides [44],  $\alpha$ -D-mannosides with aromatic aglycon [46], and  $\alpha$ -D-mannosides with extended aromatic aglycons [46]. Bouckaert and co-workers showed that the affinity of alkyl  $\alpha$ -D-mannosides increases with the length of the aglycon alkyl chain [44]. Among these inhibitors *n*-heptyl  $\alpha$ -D-mannopyranoside (**1**) exhibited the best affinity, showing a  $K_D$  of 5 nM in SPR assays. In the group of  $\alpha$ -D-mannosides with an aromatic aglycon, it was shown that introduction of substituents in the ortho position of the aromatic ring (**3**) is superior to *meta* or *para* position [66, 68]. The third group, mannosides with extended aromatic aglycons, comprises the biphenyl substituted compounds with various ring substitutions [46, 74], and *p*-NPMAN compounds substituted with a squaric acid moiety [68]. Extending *p*-NPMAN with a phenyl group increased the inhibitory potency of the antagonists by a factor of 16 (**4**) [46]. Furthermore, the *m*-nitro substituted biphenyl compounds (**5**) exceeded the inhibitory potency of *p*-NPMAN by a factor of 62. They displayed nanomolar affinities in target-based assays and micromolar affinities in cellular yeast disaggregation assays [46, 75].

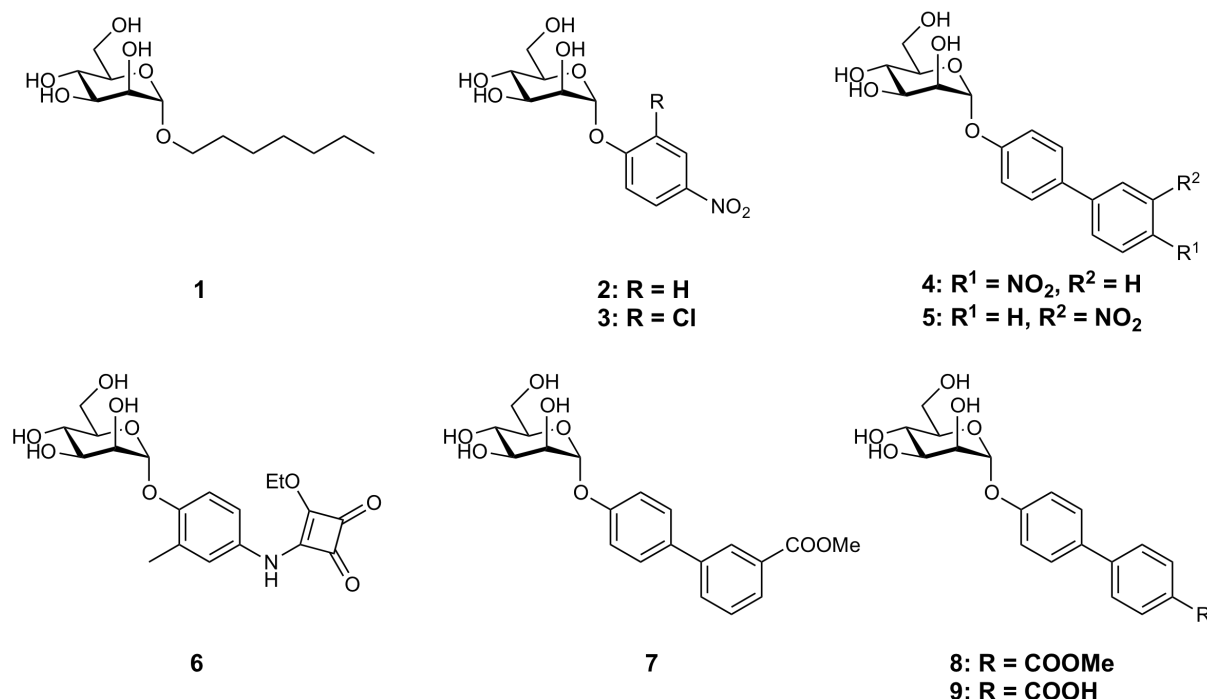


**Figure 7.** Known alkyl **1** [44] and aryl **2-9** [46, 74]  $\alpha$ -D-mannopyranoside FimH antagonists.

Recently, an unexpected binding mode of a biphenyl-substituted compound (**7**) was observed in a published crystal structure [46] (Figure 8). The X-ray structure revealed that the biphenyl aglycon was not located within the tyrosine gate, but exclusively formed  $\pi$ - $\pi$  interactions with the Tyr 48 and additional electrostatic interactions with the Arg 98/Glu 50 salt-bridge at the outer side of the CRD. This new binding mode is termed the “out-binding mode”.

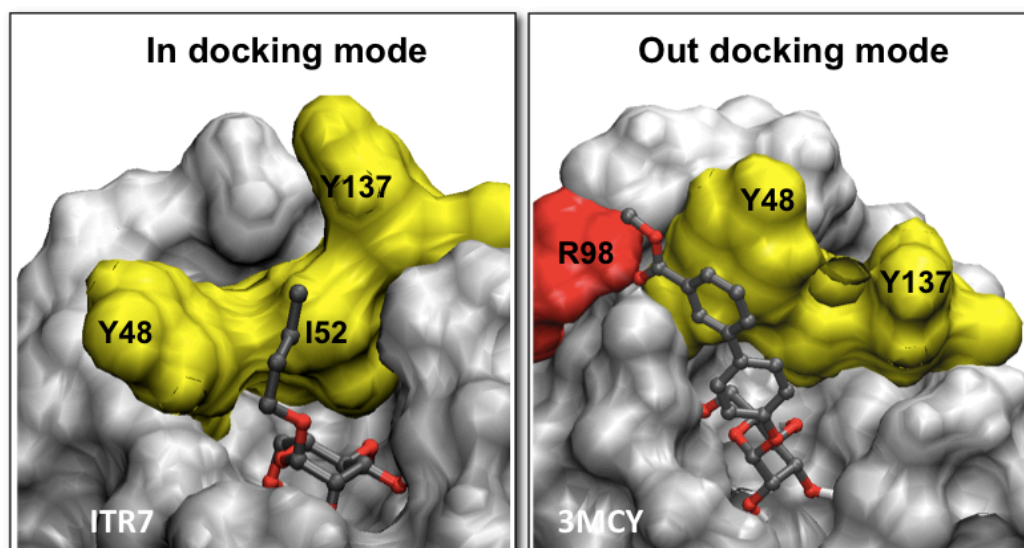


**Figure 8.** FimH mannose-binding site in complex with *n*-butyl  $\alpha$ -D-mannopyranoside in the in-binding mode (left, PDB entry ITR7), and in complex with the biphenyl derivative (**7**) in the out-binding mode (right, PDB entry 3MCY) [46] (modeled by Adam Zalewski, IMP, University of Basel).

Up to now, the squaric acid derivative (**6**) is the best monomeric antagonist with a 223-fold higher binding affinity than *p*NPMan (**2**), as determined in an ELISA based assay [68].

Furthermore, *in vivo* mouse infection studies were performed, where the antagonists were directly instilled into the bladder concomitantly with uropathogenic *E. coli*. Methyl  $\alpha$ -D-mannopyranoside [45, 75, 76] and *n*-heptyl  $\alpha$ -D-mannopyranoside [45] exhibited a considerable potential to reduce bacterial infections.

For the development of an orally available drug, good pharmacokinetic properties of FimH antagonists are a prerequisite. In regard to enhance the oral availability, an ester prodrug approach was explored in a UTI mouse model [74]. The ester (**8**) was expected to facilitate high intestinal absorption, since it increases the lipophilicity of the compounds. Ester hydrolysis, resulting in compound (**9**) by carboxyl esterases, expressed in enterocytes of the small intestine and liver, would restore the hydrophilicity and thus renal elimination of the compounds. In this approach, an orally available, low molecular weight FimH antagonist was identified with the potential to reduce the colony forming units (CFU) in the bladder by 4 orders of magnitude. These results confirmed the great potential for the effective treatment of urinary tract infections with orally available anti-infectives.

---

**Literature**

1. Patti JM, Hook M, *Curr. Opin. Cell Biol.* **1994**, 6(5):752-758.
2. Mouricout M, *Adv Exp Med Biol.* **1997**, 412:109-123.
3. Wilson IA, Skehel JJ, Wiley DC, *Nature* **1981**, 289(5796):366-373.
4. Weis W, Brown JH, Cusack S, Paulson JC, Skehel JJ, Wiley DC, *Nature* **1988**, 333(6172):426-431.
5. Russell PW, Orndorff PE, *J bacteriol* **1992**, 174(18):5923-5935.
6. Jones CH, Pinkner JS, Roth R, Heuser J, Nicholes AV, Abraham SN, Hultgren SJ, *Proc. Natl. Acad. Sci. U.S.A.* **1995**, 92(6):2081-2085.
7. Hull RA, Gill RE, Hsu P, Minshew BH, Falkow S, *Infect. Immun.* **1981**, 33(3):933-938.
8. Kuehn MJ, Heuser J, Normark S, Hultgren SJ, *Nature* **1992**, 356(6366):252-255.
9. Bertin Y, Martin C, Oswald E, Girardeau JP, *J. Clin. Microbiol.* **1996**, 34(12):2921-2928.
10. Elmazouari K, Oswald E, Hernalsteens JP, Lintermans P, Degreve H, *Infect. Immun.* **1994**, 62(6):2633-2638.
11. Hanson MS, Brinton CC, *Nature* **1988**, 332(6161):265-268.
12. Lindberg F, Lund B, Johansson L, Normark S, *Nature* **1987**, 328(6125):84-87.
13. Buts L, Wellens A, Van Molle I, Wyns L, Loris R, Lahmann M, Oscarson S, De Greve H, Bouckaert J, *Acta Crystallogr D Biol Crystallogr.* **2005**, 61:1149-1159.
14. Leffler H, Svanborgeden C, *Infect. Immun.* **1981**, 34(3):920-929.
15. Zhou G, Mo WJ, Sebbel P, Min GW, Neubert TA, Glockshuber R, Wu XR, Sun TT, Kong XP, *J Cell Sci.* **2001**, 114(22):4095-4103.
16. Xie B, Zhou G, Chan SY, Shapiro E, Kong XP, Wu XR, Sun TT, Costello CE, *J Biol Chem.* **2006**, 281(21):14644-14653.
17. Bliska JB, Galan JE, Falkow S, *Cell* **1993**, 73(5):903-920.
18. Mulvey MA, Lopez-Boado YS, Wilson CL, Roth R, Parks WC, Heuser J, Hultgren SJ, *Science* **1998**, 282(5393):1494-1497.
19. Foxman B, *Am J Public Health.* **1990**, 80(3):331-333.
20. Foxman B, Barlow R, D'Arcy H, Gillespie B, Sobel JD, *Ann Epidemiol* **2000**, 10(8):509-515.
21. Ronald A, *Am J Med.* **2002**, 113:14S-19S.
22. Wiles TJ, Kulesus RR, Mulvey MA, *Exp. Mol. Pathol.* **2008**, 85(1):11-19.

23. Mulvey MA, *Cell. Microbiol.* **2002**, 4(5):257-271.
24. Patterson JE, Andriole VT, *Infect. Dis. Clin. North Am.* **1997**, 11(3):735-&.
25. Mahan KT, Wang J, *J Am Podiatr Med Assoc* **1993**, 83(11):607-614.
26. Foxman B, Brown P, *Infect. Dis. Clin. North Am.* **2003**, 17(2):227-+.
27. Cegelski L, Marshall GR, Eldridge GR, Hultgren SJ, *Nat. Rev. Microbiol.* **2008**, 6(1):17-27.
28. Hung CS, Bouckaert J, Hung D, Pinkner J, Widberg C, DeFusco A, Auguste CG, Strouse R, Langermann S, Waksman G *et al*, *Mol Microbiol* **2002**, 44(4):903-915.
29. Choudhury D, Thompson A, Stojanoff V, Langermann S, Pinkner J, Hultgren SJ, Knight SD, *Science* 1999, 285(5430):1061-1066.
30. Hung DL, Hultgren SJ, *J. Struct. Biol.* **1998**, 124(2-3):201-220.
31. Dodson KW, Jacobdubuisson F, Striker RT, Hultgren SJ, *Proc. Natl. Acad. Sci. U.S.A.* **1993**, 90(8):3670-3674.
32. Sauer FG, Remaut H, Hultgren SJ, Waksman G, *Biochim. Biophys. Acta* **2004**, 1694(1-3):259-267.
33. Sauer FG, Futterer K, Pinkner JS, Dodson KW, Hultgren SJ, Waksman G, *Science* **1999**, 285(5430):1058-1061.
34. Nishiyama M, Glockshuber R, *J Mol Biol.* **2010**, 396(1):1-8.
35. Puorger C, Eidam O, Capitani G, Erilov D, Grutter MG, Glockshuber R, *Structure* **2008**, 16(4):631-642.
36. Sohanpal BK, Kulasekara HD, Bonnen A, Blomfield IC, *Mol. Microbiol.* **2001**, 42(2):483-494.
37. Gally DL, Rucker TJ, Blomfield IC, *J Bacteriol.* **1994**, 176(18):5665-5672.
38. Klemm P, *J Cell Biochem.* **1986**, 138-138.
39. Klemm P, *Embo J.* **1986**, 5(6):1389-1393.
40. Tsai K-W, Lai H-T, Tsai T-C, Wu Y-C, Yang Y-T, Chen K-Y, Chen C-M, Li Y-SJ, Chen C-N, *J Biomed Sci.* **2009**, 16.
41. Xia Y, Gally D, Forsman-Semb K, Uhlin BE, *Embo J* **2000**, 19(7):1450-1457.
42. Lindberg S, Xia Y, Sonden B, Goeransson M, Hacker J, Uhlin BE, *Infect. Immun.* **2008**, 76(2):771-780.
43. Hung C, Bouckaert J, Hung DL, Pinkner J, Widberg C, DeFusco A, Auguste G, Strouse R, Langermann S, Hultgren SJ, *Abstr. Gen. Meet. Am. Soc. Microbiol.* 2002, **102**:41.

44. Bouckaert J, Berglund J, Schembri M, De Genst E, Cools L, Wuhrer M, Hung CS, Pinkner J, Slattegard R, Zavialov A *et al.*, *Mol. Microbiol.* **2005**, 55(2):441-455.
45. Wellens A, Garofalo C, Nguyen H, Van Gerven N, Slattegard R, Hernalsteens J-P, Wyns L, Oscarson S, De Greve H, Hultgren S *et al.*, *Plos One* **2008**, 3(4).
46. Han Z, Pinkner JS, Ford B, Obermann R, Nolan W, Wildman SA, Hobbs D, Ellenberger T, Cusumano CK, Hultgren SJ *et al.*, *J Med Chem.* **2010**, 53(12):4779-4792.
47. Le Trong I, Aprikian P, Kidd BA, Forero-Shelton M, Tchesnokova V, Rajagopal P, Rodriguez V, Interlandi G, Klevit R, Vogel V *et al.*, *Cell* **2010**, 141(4):645-655.
48. Aprikian P, Trinchina E, Thomas WE, Tchesnokova V, Nilsson LM, Vogel V, Sokurenko EV, *Abstr. Gen. Meet. Am. Soc. Microbiol.* **2004**, 104:52.
49. Tchesnokova V, Aprikian P, Yakovenko O, Larock C, Kidd B, Vogel V, Thomas W, Sokurenko E, *J Biol Chem.* **2008**, 283(12):7823-7833.
50. Aprikian P, Tchesnokova V, Kidd B, Yakovenko O, Yarov-Yarovoy V, Trinchina E, Vogel V, Thomas W, Sokurenko E, *J Biol Chem.* **2007**, 282(32):23437-23446.
51. Yakovenko O, Tchesnokova V, Aprikian P, Forero M, Vogel V, Sokurenko E, Thomas W, *Biophys J* **2007**:348A-349A.
52. Sokurenko EV, Chesnokova V, Dykhuizen DE, Ofek I, Wu XR, Krogfelt KA, Struve C, Schembri MA, Hasty DL, *Proc. Natl. Acad. Sci. U.S.A.* **1998**, 95(15):8922-8926.
53. Sokurenko EV, Feldgarden M, Trintchina E, Weissman SJ, Avagyan S, Chattopadhyay S, Johnson JR, Dykhuizen DE, *Mol. Biol. Evol.* **2004**, 21(7):1373-1383.
54. Tchesnokova VL, Aprikian P, Yakovenko O, Thomas W, Sokurenko E, Vogel V, *Abstr. Gen. Meet. Am. Soc. Microbiol.* **2006**, 106:43.
55. Chen SL, Hung CS, Pinkner JS, Walker JN, Cusumano CK, Li Z, Bouckaert J, Gordon JI, Hultgren SJ, *Proc. Natl. Acad. Sci. U.S.A.* **2009**, 106(52):22439-22444.
56. Thomas WE, Trintchina E, Forero M, Vogel V, Sokurenko EV, *Cell* **2002**, 109(7):913-923.
57. Thomas WE, Trintchina E, Forero M, Vogel V, Sokurenko EV, *Abstr. Gen. Meet. Am. Soc. Microbiol.* **2002**, 102:41.
58. Pak J, Pu YB, Zhang ZT, Hasty DL, Wu XR, *J Biol Chem.* **2001**, 276(13):9924-9930.
59. Ofek I, Hasy DL, Sharon N, *FEMS Immunol. Med. Microbiol.* **2003**, 38(3):181-191.
60. Sharon N, *Biochim. Biophys. Acta* **2006**, 1760(4):527-537.
61. Ernst B, Magnani JL, *Nat Rev Drug Discov* **2009**, 8(8):661-677.



62. Lindhorst TK, Kieburg C, Krallmann-Wenzel U, *Glycoconj. J.* **1998**, *15*(6):605-613.
63. Nagahori N, Lee RT, Nishimura S, Page D, Roy R, Lee YC, *Chembiochem* **2002**, *3*(9):836-844.
64. Abgottspon D, Roelli G, Steinhuber A, Ernst B, Trampuz A, *J. Microbiol Methods.* **2010** *82*(3):249-55.
65. Firon N, Ofek I, Sharon N, *Carbohydr. Res.* **1983**, *120*(AUG):235-249.
66. Firon N, Ashkenazi S, Mirelman D, Ofek I, Sharon N, *Infect. Immun.* **1987**, *55*(2):472-476.
67. Sokurenko EV, Courtney HS, Ohman DE, Klemm P, Hasty DL, *J Bacteriol.* **1994**, *176*(3):748-755.
68. Sperling O, Fuchs A, Lindhorst TK, *Carbohydr. Res.* **2006**, *4*(21):3913-3922.
69. Hartmann M, Horst AK, Klemm P, Lindhorst TK, *Chem. Commun.* **2010**, *46*(2):330-332.
70. Schaeffer AJ, Amundsen SK, Schmidt LN, *Infect. Immun.* **1979**, *24*(3):753-759.
71. Horst AK, Kotter S, Lindhorst TK, Ludwig A, Brandt E, Wagener C, *Med. Microbiol. Immunol.* **2001**, *190*(3):145-149.
72. Yakovenko O, Sharma S, Forero M, Tchesnokova V, Arikian P, Kidd B, Mach A, Vogel V, Sokurenko E, Thomas WE, *J Biol Chem.* **2008**, *283*(17):11596-11605.
73. Neeser JR, Koellreutter B, Wuersch P, *Infect. Immun.* **1986**, *52*(2):428-436.
74. Klein T, Abgottspon D, Wittwer M, Rabbani S, Herold J, Jiang X, Kleeb S, Luethi C, Scharenberg M, Bezencon J *et al*, *J Med Chem.* **2010**, *53*(24):8627-8641.
75. Eden CS, Freter R, Hagberg L, Hull R, Hull S, Leffler H, Schoolnik G, *Nature* **1982**, *298*(5874):560-562.
76. Aronson M, Medalia O, Schori L, Mirelman D, Sharon N, Ofek I, *J Infect Dis.* **1979**, *139*(3):329-332.

## **Part I: The lectin FimH**

---

**FimH Chapter 2: Results and discussion**

**Publication 1**

---

# A Flow Cytometry-Based Assay for Screening FimH Antagonists

Meike Scharenberg, Daniela Abgottspon, Evelin Cicek, Xiaohua Jiang, Oliver Schwardt, Said Rabbani, and Beat Ernst

Institute of Molecular Pharmacy, Pharmacenter, University of Basel, Basel, Switzerland.

## ABSTRACT

Urinary tract infections (UTIs), including cystitis and pyelonephritis, affect a large proportion of the population and account for significant medical costs. In more than 80% of UTIs, uropathogenic *Escherichia coli* (UPEC) is the causative pathogen. The initial step in the pathogenesis of the infection is the adherence of UPEC to the human bladder epithelium, enabling the invasion into the host cells and the development of UTIs. This process is mediated by the lectin FimH located on type 1 pili and enables UPECs to attach to oligomannosides of the glycoprotein uroplakin Ia presented on uroepithelial cells. FimH antagonists such as  $\alpha$ -D-mannopyranosides have been shown to interfere with the attachment of UPEC to their host cells, thus providing a novel therapeutic opportunity for the treatment and prevention of UTIs. In this article, we report a flow cytometry-based assay to evaluate the potential of FimH antagonists for the prevention of the infection of the human urinary bladder cell line 5637 by UPEC strain UTI89. The assay was optimized and validated, and the inhibitory potency of different  $\alpha$ -D-mannopyranosides was determined. Finally, the  $IC_{50}$  values measured by the flow cytometry-based assay were compared with those reported for other assay formats.

## INTRODUCTION

Urinary tract infection (UTI) is one of the most common infections, affecting millions of people each year. Particularly affected are women, who have a 40%–50% risk to experience at least one symptomatic UTI episode at some time during their life.<sup>1</sup> In more than 80% of the reported cases, invasive uropathogenic *Escherichia coli* strains (UPEC) are the etiological agent. A nontreated UTI can lead to bladder (cystitis) and kidney infection (pyelonephritis).<sup>2</sup> The antibiotic treatment does not always eradicate UPEC and often results in the emergence of microbial resistance and consequently in recurrent infections.<sup>3</sup> Further, more than half of patients experience a relapse of the infection within 6 months.<sup>2,4</sup>

The initial step in the pathogenesis of UPEC infection is the adherence of bacteria to the bladder epithelium (urothelium), which thereby slows down their clearance from the urinary tract. At the same time, the attachment enables the pathogens to invade the host cells.<sup>5,6</sup> The attachment is mediated by 1–3  $\mu$ m long, filamentous, oligomeric organelles called type 1 pili,<sup>7,8</sup> which are helical rods with a diameter of 7 nm and composed of FimA, FimF, FimG, and FimH subunits. The adhesin FimH, which is located at the distal end of the linear fibrillum, contains an amino-terminal, mannose-specific carbohydrate recognition domain (FimH-CRD).<sup>9–11</sup> FimH-CRD binds to mannose residues provided by the glycoprotein uroplakin Ia (UPIa).<sup>12–14</sup> The adherence of UPEC to the urothelium activates the innate immune defense, triggering the exfoliation of infected bladder cells, the influx of neutrophils, and other inflammatory responses.<sup>15</sup> Nevertheless, UPEC can resist innate host defense mechanisms, invade deeper into the tissue, and adopt a quiescent state, probably the reason for the high incidence of recurrence of UTIs.<sup>15</sup>

Because of increasing antibiotic resistance, efforts are underway to identify new and inexpensive orally available therapeutics, which inhibit bacterial adhesion with a low potential for generating resistance. New studies are focusing on carbohydrate-based FimH antagonists.<sup>16–22</sup> For the evaluation of such antagonists, several *in vitro* assays have been reported, although most of them measure the effect of antagonists on the hemagglutination of erythrocytes<sup>18,23,24</sup> or the aggregation of yeast cells in the presence of UPEC.<sup>25–27</sup> In addition, FimH antagonists were evaluated with an enzyme-linked immunosorbent based assay<sup>20,27</sup> and with bacterial adhesion assays using green fluorescence protein (GFP)-tagged bacteria,<sup>28</sup> radiolabeled mannose,<sup>16</sup> or radiolabeled bacteria.<sup>29</sup> The inhibition of the binding of purified type 1 fimbriae to human granulocytes was investigated utilizing the flow cytometry technology.<sup>30</sup> In surface plasmon resonance experiments, the binding of FimH to an anti-FimH blocking antibody covalently linked to the sensor chip enabled the determination of the affinity of antagonists.<sup>16</sup> Depending on the applied assay format, the reported inhibitory potencies of the reference compounds D-mannose (1) and methyl  $\alpha$ -D-mannopyranoside (2) vary between millimolar<sup>18,26</sup> and micromolar.<sup>16,31</sup> The discrepancies noticed in aggregation and hemagglutination assays are mainly due to the variability in the levels of FimH expressed by different

**ABBREVIATIONS:** BSA, bovine serum albumin; CFSE, 5-(6)-carboxyfluorescein *N*-succinimidylester; CRD, carbohydrate recognition domain; DMSO, dimethylsulfoxide; FCS, fetal calf serum; GFP, green fluorescent protein; FSC, forward scatter; GPE, guinea pig erythrocytes; LB, Luria-Bertani; MFI, mean fluorescent intensity; MOI, multiplicity of infection; OD, optical density; PBS, phosphate-buffered saline; RPMI, Roswell Park Memorial Institute medium; SSC, side scatter; UPEC, uropathogenic *Escherichia coli*; UPIa, uroplakin Ia; UTI, urinary tract infection.

## SCHARENBERG ET AL.

bacterial strains<sup>25,26</sup> as well as significant differences in the sensitivity of erythrocytes to type 1 pili-mediated hemagglutination.<sup>23</sup> Further, FimH located at the tip of the pili mediates weak binding at low shear stress, but shifts to strong binding at high shear.<sup>32</sup> The isolated CRD, which is often used in target-based assays, always adopts the high-affinity state and therefore mediates strong binding to mannose even under static conditions.<sup>33</sup>

Recently, we reported two new assay formats for the evaluation of FimH antagonists, a cell-free target-based assay<sup>34</sup> and function-based aggregation assay.<sup>24</sup> Both formats are competitive assays, where the analytes compete with oligomannosides for the binding site. In the cell-free competitive binding assay, the competitors are polymer-bound trimannosides,<sup>34</sup> whereas in the aggregation assay, the antagonist competes with more potent oligo- and polysaccharide chains present on the surface of erythrocytes.<sup>24</sup>

In this article, we describe the development of a function-based flow cytometry assay that allows to quantify the effect of FimH antagonists on the adhesion of UPEC (UTI89) to human epithelial bladder cells 5637. The results are compared with those reported for the various assay formats mentioned earlier. The reproducibility, sensitivity, and assay conditions close to the physiological situation make this assay format suitable for the estimation of the minimal therapeutic concentration for *in vivo* UTI treatment studies.

## MATERIALS AND METHODS

### Cell Culture

The human epithelial bladder carcinoma cell line 5637 was obtained from the German Collection of Microorganisms and Cell Cultures (DSMZ). The cells were grown in Roswell Park Memorial Institute medium (RPMI) 1640 medium, supplemented with 10% fetal calf serum (FCS), 100 U/mL penicillin, and 100 µg/mL streptomycin, at 37°C under 5% CO<sub>2</sub>. All solutions were purchased from Invitrogen. The cells were subcultured 1:5 twice per week (using Trypsin/EDTA [Sigma] for the detachment) for six passages before using them in the infection assay. Two days before infection,  $1.8 \times 10^5$  cells were seeded in each well of a 24-well plate in RPMI 1640 containing 10% FCS without antibiotics. The cell density was approximately  $3\text{--}5 \times 10^5$  cells/well prior the infection.

### Bacterial Strains

The clinical *E. coli* isolate UTI89<sup>35</sup> (UTI89 *wt*) and the FimA-H knock-out strain UTI89  $\Delta$ *fimA-H* were kindly provided by Prof. Urs Jenal (Biocenter, University of Basel, Switzerland). The bacteria were frozen at  $-70^\circ\text{C}$  and, before the experiment, incubated for 24 h under static conditions at 37°C in 10 mL Luria-Bertani (LB) broth (Becton, Dickinson and Company). The bacterial suspension was washed twice and resuspended either in phosphate-buffered saline (PBS; Sigma) for staining and aggregometry measurements or in RPMI 1640 without supplements for infection experiments. The bacterial concentration was determined by plating serial 1:10 dilutions on blood agar plates (Becton, Dickinson and Company), followed by colony counting after overnight incubation at 37°C.

### GFP Staining

Plasmid pBR322GFP encoding GFP was transformed into bacterial strains (UTI89 *wt* and UTI89  $\Delta$ *fimA-H*) by electroporation. Briefly, purified DNA (10–100 ng) was mixed with bacterial suspension (80 µL), followed by electroporation in 1 mm cuvettes using a Gene Pulser (BioRad) set to 1.75 V, 25 µF, and 400 Ω. Electroporated cells were mixed with 1 mL superoptimal broth medium (2% bacto trypton, 0.5% yeast extract, 10 mM NaCl, and 2.5 mM KCl), incubated for 30 min at 37°C, and plated on LB agar plates containing 20 µg/mL ampicillin (AppliChem). Single clones were cultured and tested in the flow cytometer for the expression of GFP. Non-GFP-transformed cells were used as negative control.

### 5-(6)-Carboxyfluorescein *N*-succinimidylester Staining

5-(6)-Carboxyfluorescein *N*-succinimidylester (CFSE; Lubio Science) in PBS, 7.5 µM, was added to an equal volume of bacterial suspension (OD<sub>600</sub> of 0.5) and incubated for 30 min at 37°C, under constant shaking (80 rpm) and protected from light. The staining was blocked by the addition of 20 mL ice-cold 2.5% human serum albumin (CSL Behring). Subsequently, CFSE-labeled bacteria were washed four times with PBS prior to use. Unstained cells were used as negative control.

### FimH Antagonists

D-Mannoside (1), methyl  $\alpha$ -D-mannopyranoside (2), 4-nitrophenyl  $\alpha$ -D-mannopyranoside (4), and D-galactose (13) were purchased from Fluka Chemie GmbH. *n*-Heptyl  $\alpha$ -D-mannopyranoside (3) was synthesized as previously described.<sup>24,36</sup> 2-Chloro-4-nitrophenyl  $\alpha$ -D-mannopyranoside (5) and *o*-chloro-*p*-[*N*-(2-ethoxy-3,4-dioxocyclobut-1-enyl)amino]phenyl  $\alpha$ -D-mannopyranoside (6) were synthesized as previously described.<sup>20</sup> The biphenyl  $\alpha$ -D-mannopyranosides 7–12 were synthesized as described elsewhere<sup>21,37</sup> (see Fig. 1).

### Aggregometry Assay

The aggregometry assay was carried out as described by Abgottsson *et al.*<sup>24</sup> Briefly, the aggregation of *E. coli* with guinea pig erythrocytes (GPE) was quantitatively determined using an ARACT 4004 aggregometer (Endotell AG). Bacteria were cultivated as described earlier. GPE were isolated from guinea pig blood (Charles River Laboratories) using Histopaque (Sigma-Aldrich) (density of 1.077 g/mL at 24°C). Before the assay, the cell densities of *E. coli* and GPE were adjusted to an optical density (OD) at 600 nm of 4 ( $1.9 \times 10^8$  CFU/mL and  $2.2 \times 10^6$  cells/mL, respectively). To calibrate the instrument, the aggregation of protein-poor plasma in PBS was set at 100% and the aggregation of protein-rich plasma in the presence of GPE at 0%. After calibration, measurements were performed with 250 µL GPE and 50 µL bacterial suspension. After an aggregation phase of 600 s, 25 µL of a twofold serial dilution of the antagonist in PBS was added to each cuvette and disaggregation was monitored for 1,400 s (Fig. 2). UTI89  $\Delta$ *fimA-H* was used as negative control.

## CYTOMETRY-BASED ASSAY FOR FIMH ANTAGONISTS

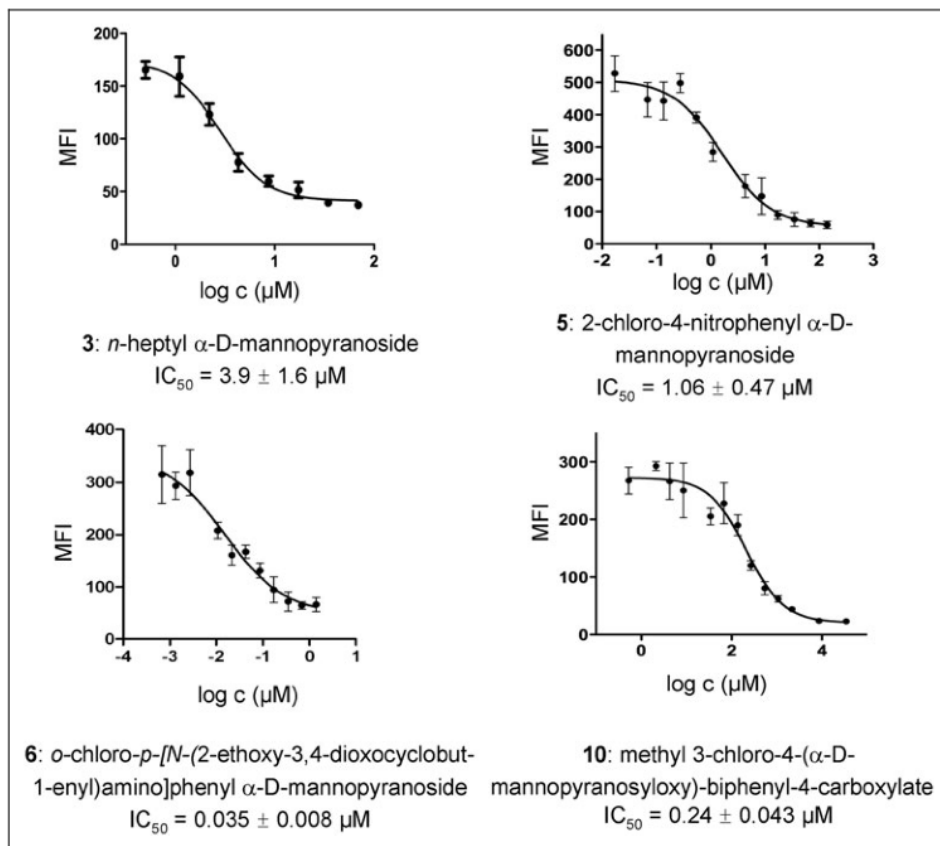


**Fig. 1.** Determination of the  $IC_{50}$  values for FimH antagonists (using an MOI of 1:50). Examples of sigmoidal inhibition curves obtained from the competitive flow cytometry assay for compound **3**, **5**, **6**, and **10**. Error bars represent standard error of  $n=2-3$  values. Assays were repeated at least twice.

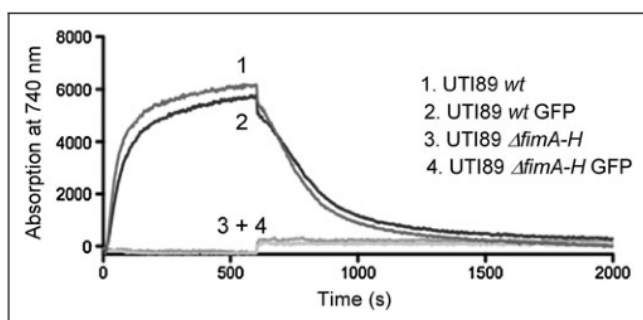


**Fig. 2.** The aggregation of guinea pig erythrocytes with GFP-expressing UTI89 strains (*wt* and  $\Delta$ *fimA-H*) and unlabeled strains was recorded at  $OD_{750}$ . After 600 s, the disaggregation was initiated by the addition of a single concentration of 5 mM *n*-heptyl  $\alpha$ -D-mannopyranoside (**3**).

## Competitive Binding Assay

The competitive binding assay was carried out as described by Rabbani *et al.*<sup>34</sup> A recombinant protein consisting of the CRD of FimH linked with a thrombin cleavage site to a 6His-tag (FimH-CRD-Th-6His) was expressed in *E. coli* strain HM125 and purified on a Ni-NTA column. Microtiter plates (F96 MaxiSorp; Nunc) were coated with 100  $\mu\text{L}$ /well of a 10  $\mu\text{g}/\text{mL}$  solution of FimH-CRD-Th-6His in assay buffer (20 mM HEPES, 150 mM NaCl, and 1 mM  $\text{CaCl}_2$  [pH 7.4]) overnight at 4°C. The coating solution was discarded and the wells were blocked with 150  $\mu\text{L}$ /well of 3% bovine serum albumin (BSA) in assay buffer for 2 h at 4°C. After three washing steps with assay buffer (150  $\mu\text{L}$ /well), a fourfold serial dilution of the test compound (50  $\mu\text{L}$ /well) in assay buffer containing 5% dimethylsulfoxide (DMSO) and streptavidin-peroxidase-coupled  $\text{Man}\alpha 1-3(\text{Man}\alpha 1-6)\text{Man}\beta 1-4\text{GlcNAc}\beta 1-4\text{GlcNAc}\beta$ -polymer (50  $\mu\text{L}$ /well of a 0.5  $\mu\text{g}/\text{mL}$  solution) were added. On each individual microtiter plate, *n*-heptyl  $\alpha$ -D-mannopyranoside (**3**) was tested in parallel. The plates were incubated for 3 h at 25°C and 350 rpm and then carefully washed four times with 150  $\mu\text{L}$ /well assay buffer. After the addition of 100  $\mu\text{L}$ /well of 2,2'-azino-bis-(3-ethylbenzthiazoline-6-sulfonic acid) substrate, the colorimetric reaction was allowed to develop for 4 min and then stopped by the addition of 2% aqueous oxalic acid before the OD was measured at 415 nm on a microplate reader (Spectramax 190; Molecular Devices).

## UPIa Immunoblotting

Human epithelial bladder 5637 cells from different passage numbers were grown at confluence and lysed with 1% Triton X-100 (Sigma). Cell lysates were resolved on a 12% sodium dodecyl sulfate-polyacrylamide gel electrophoresis under reducing conditions and transferred onto a nitrocellulose membrane (BioRad). The membrane was blocked with 3% BSA (Sigma) in PBS and incubated with a polyclonal goat anti-UPIa antibody (Santa Cruz Biotechnology). As secondary antibody an alkaline phosphatase-coupled donkey anti-goat IgG (Santa Cruz Biotechnology) was used. After three washing steps, the membrane was developed with the nitro blue tetrazolium chloride/5-bromo-4-chloro-3-indolylphosphate *p*-toluidine salt solution (Fluka).

## SCHARENBERG ET AL.

## Quantification of Bacterial Adhesion on 5637 Cells: Infection Assay

The 5637 cells, grown in 24-well plates, were infected with 200  $\mu$ L bacterial suspension at a multiplicity of infection (MOI) of 1:20, 1:50, and 1:100 (cell:bacteria). To homogenize the infection, plates were centrifuged at room temperature for 3 min at 600 *g*. After an incubation of 1.5 h at 37°C, infected cells were washed four times with RPMI 1640 medium and suspended in ice-cold PBS for 5–20 min (treatment with ice-cold PBS results in the detachment of the infected cells). The cells were then kept in the dark until analysis. All measurements were made within 1 h after the termination of the infection. Samples were measured with a CyAn ADP flow cytometer (Beckman-Coulter) and analyzed by gating on the eukaryotic cells based on forward (FSC) and side scatter (SSC), which excludes unbound labeled bacteria and debris from analysis. A total of  $10^4$  cells were measured per sample. Data were acquired in a linear mode for the SSC and in a logarithmic mode for FSC and the green fluorescent channel FL1-H (e.g., GFP, CFSE). The mean fluorescence intensity (MFI) of FL1-H was counted as a surrogate marker for the adherence of bacteria. Quantification of adhesion was evaluated with the FlowJo software 9.0.1 (Tree Star, Inc.).

## Inhibition Assay (Flow Cytometry Assay)

To evaluate FimH antagonists, a serial dilution in 5% DMSO was prepared. Before infection, bacterial suspension (200  $\mu$ L) and 25  $\mu$ L of the test compound were preincubated for 10 min at room temperature. The bacteria-antagonist mixture was then added to the monolayer of 5637 cells. Infection, measurement, and quantification of adhesive bacteria were performed as described earlier. IC<sub>50</sub> values were determined by plotting the concentration of the antagonist in a logarithmic mode versus the MFI and by fitting the curve with the prism software (GraphPad; inhibition curve, variable slope) ( $n = 2-3$ , in duplicates/triplicates). The protocol of the inhibition assay is summarized in Table 1.

## Internalization (Invasion) Assay

Invasion assays were performed essentially as described by Elsinghorst (gentamicin protection assay).<sup>38</sup> Briefly, the 5637 cells were grown in 24-well plates to confluence and infected with 200  $\mu$ L bacterial suspension at an MOI of 1:50. To homogenize the infection, plates were centrifuged at room temperature for 3 min at 600 *g*. After an incubation time of 1.5 h at 37°C, the infected cells were washed four times with PBS. To determine the total of extra- and intracellular bacteria, the cells were directly lysed by the addition of 0.2 mL lysis buffer (ddH<sub>2</sub>O and 0.1% Triton X-100 [Sigma]) and plated on blood agar plates in 1:10 dilutions. To determine only intracellular bacteria, infected cells were treated with gentamicin (100  $\mu$ g/mL; Essex Chemie AG) for 30 min after the initial washing step. Then, the cells were washed three times with PBS and lysed with 0.2 mL lysis buffer. The number of intracellular bacteria surviving the gentamicin treatment was determined by plating serial 1:10 dilutions on blood agar plates.

Table 1. Protocol Table of the Flow Cytometry Inhibition Assay

Step	Parameter	Value	Description
1	Plate cells	$1.8 \times 10^5$ cells/well	5637 cells
2	OD <sub>600</sub>	According to cells/well	UTI89 GFP density (MOI 1:50)
3	Antagonists	225 $\mu$ L	25 $\mu$ L antagonist (serial dilution) to 200 $\mu$ L UTI89 GFP
4	Preincubation time	10 min	UTI89 GFP with antagonist (serial dilution)
5	Infection	225 $\mu$ L	Bacteria-antagonist mixture to 5637 cells
6	Centrifugation	3 min	600 <i>g</i>
7	Incubation time	1.5 h	37°C
8	Wash step	200 $\mu$ L	4 $\times$ with PBS
9	Incubation time	200 $\mu$ L, 10 min	Ice-cold PBS
10	Read-out	$10^4$ cells	Flow cytometry measurements, MFI in green fluorescent channel

## Step Notes

- 24-well tissue culture plate.
  - OD<sub>600</sub> 1 equivalent to  $48 \times 10^6$  bacteria.
  - Serial dilution of antagonists (stock concentration 10 mM) in PBS, 5% DMSO.
  - 200  $\mu$ L bacterial solution with 25  $\mu$ L antagonist solution.
  - For homogenization of infection.
  - Clearance from nonadherent bacteria.
  - Leads to loosening of the cells from the culture tissue.
  - Gating on mammalian cells in FSC and SSC; IC<sub>50</sub> is obtained by plotting the MFI versus log[antagonist]; fit: inhibition curve with variable slope.
- OD, optical density; GFP, green fluorescent protein; MOI, multiplicity of infection; PBS, phosphate-buffered saline; MFI, mean fluorescent intensity; DMSO, dimethylsulfoxide; FSC, forward scatter; SSC, side scatter.

## RESULTS

## Analysis of UPIa Expression in 5637 Cells

The adhesion of *E. coli* UTI89 to bladder epithelial cells depends on the uroplakin receptor complex on the surface of the host cells, containing the protein UPIa.<sup>13</sup> To verify whether the human urinary bladder carcinoma cell line 5637 expresses UPIa, a western blot analysis was performed using cell lysates after different cell passage numbers and a polyclonal anti-UPIa antibody. The result clearly showed that the UPIa receptor on 5637 cells was efficiently expressed with the expected molecular weight (27 kDa), independent of the number of cell passages (Fig. 3). Weak additional signals were observed probably because of cross-reaction with other uroplakin family members.

## CYTOMETRY-BASED ASSAY FOR FIMH ANTAGONISTS

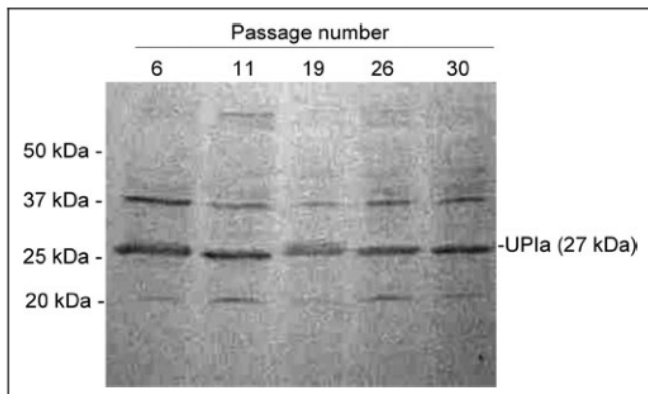


**Fig. 3.** Western blot analysis of UPIa. The expression of UPIa in 5637 cells from passage numbers 6 to 30 was analyzed by immunoblotting. The primary antibody was a polyclonal goat anti-UPIa (C-18) immunoglobulin G and secondary antibody a donkey anti-goat immunoglobulin G coupled to alkaline phosphatase. UPIa, uroplakin Ia.

#### Fluorescent Staining of UTI89 Bacteria

For visualization, UTI89 *wt* and the UTI89  $\Delta$ *fimA-H* strains were either transformed with a GFP-encoding plasmid or stained with CFSE directly before infection. Cell growth measurement and colony-plating assays demonstrated that the bacteria were not affected by labeling (data not shown). In the flow cytometry analysis, CFSE-treated bacteria

showed an inhomogeneous staining profile, with fluorescently active and inactive subpopulations, although a high concentration of the fluorescent agent was used (final concentration: 7.5  $\mu$ M) (Fig. 4A). In addition, we observed differences in fluorescent intensities between the UTI89 *wt* and UTI89  $\Delta$ *fimA-H* strains, that is, CFSE uptake into the wild-type strain was much more efficient than into the pilus-deficient strain.

In contrast to CFSE-labeled bacteria, GFP-expressing bacteria showed a uniform, intense fluorescence profile (Fig. 4B). Further, the stable expression of GFP by the bacteria made this labeling technique suitable for subsequent experiments. To test the binding ability of GFP-expressing bacteria to GPE, the aggregometry assay<sup>24</sup> using 384  $\mu$ M *n*-heptyl  $\alpha$ -D-mannopyranoside (3) was carried out, using GFP-labeled and nonlabeled strains. The result clearly indicated that the GFP expression did not alter the ability of the bacteria to interact with GPEs (Fig. 2), and thus, the expression of bacterial adhesins remains unaffected by GFP expression.

#### Infection Assay

For the optimization of the infection assay, three different MOI ratios (20:1, 50:1, and 100:1, bacteria:cell) were tested (Fig. 5). The fluorescence emitted from unbound bacteria was discriminated from fluorescence emitted from cell-bound bacteria by selecting the appropriate fluorescence-activated cell sorting size gate, which was determined by measuring uninfected cells and labeled bacteria alone. For the UTI89 *wt* strain, the fluorescence signal was proportional to the MOI ratio and was in the optimal range of MFI of >200. For all subsequent experiments, an MOI of 50:1 was used.

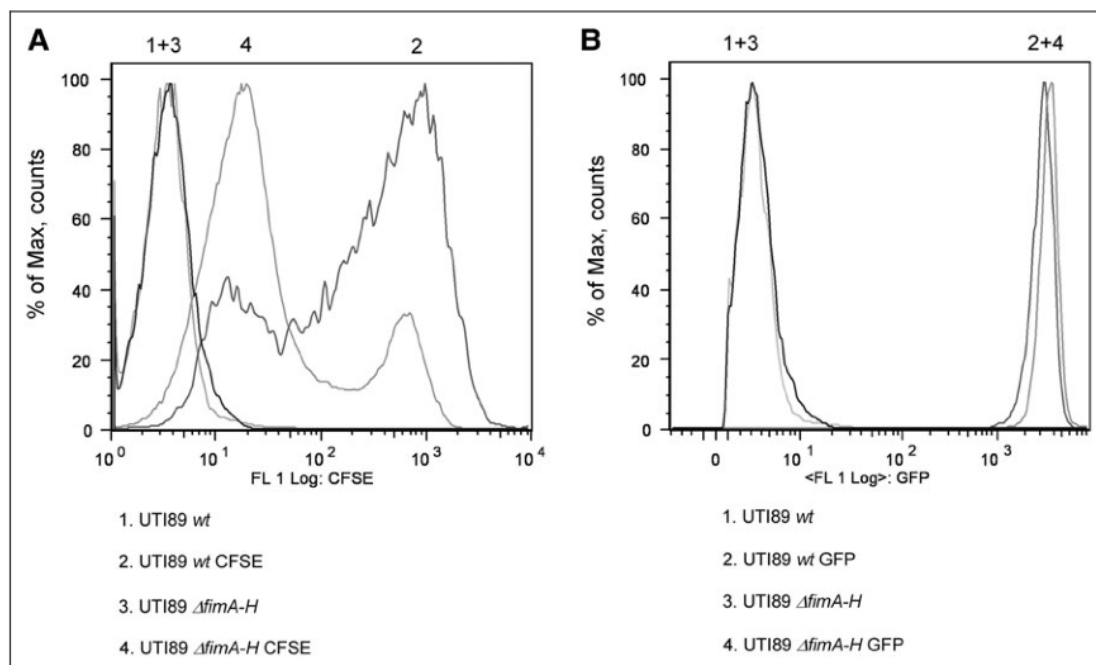


**Fig. 4.** Flow cytometry analysis of CFSE-stained (A) and GFP-expressing (B) UTI89 *wt* and UTI89  $\Delta$ *fimA-H* strains. The analysis was carried out as described in the Materials and Methods section. CFSE, 5-(6)-carboxyfluorescein *N*-succinimidylester; GFP, green fluorescent protein.

SCHARENBERG ET AL.

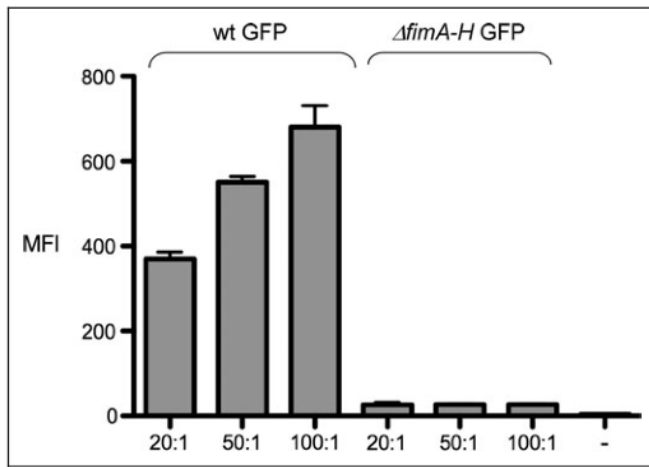


**Fig. 5.** Infection assay: MFI of 5637 cells infected with different ratios of GFP-expressing UTI89 strains (wt and  $\Delta fimA-H$  strain); MOIs: 20:1, 50:1, and 100:1 (bacteria:cell). (-) indicates uninfected 5637 cells. Assay and analysis were performed as described in the Materials and Methods section. Error bars represent standard error of  $n=3$  values. MFI, mean fluorescent intensity; MOI, multiplicity of infection.

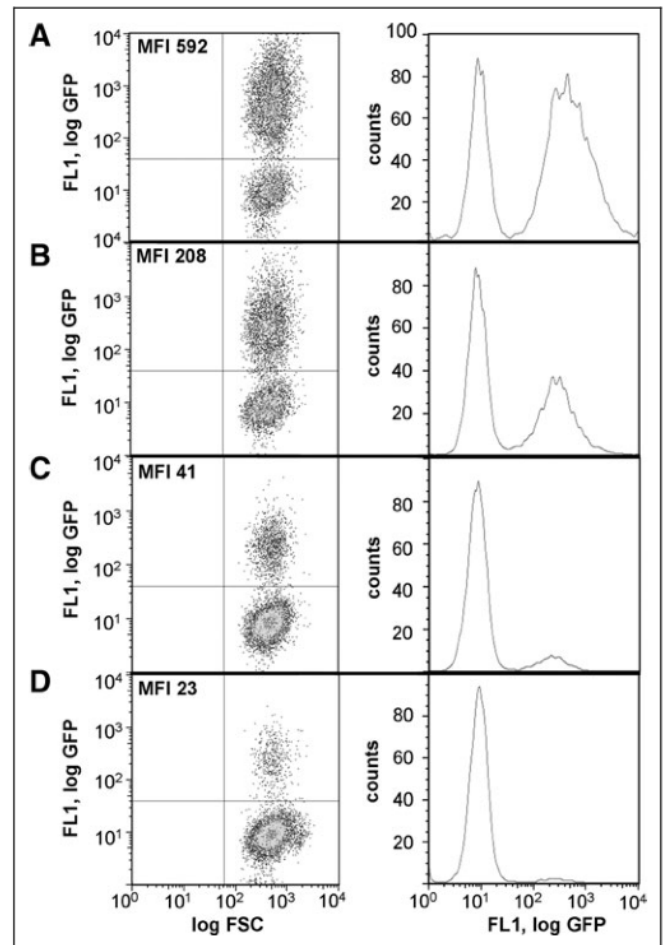
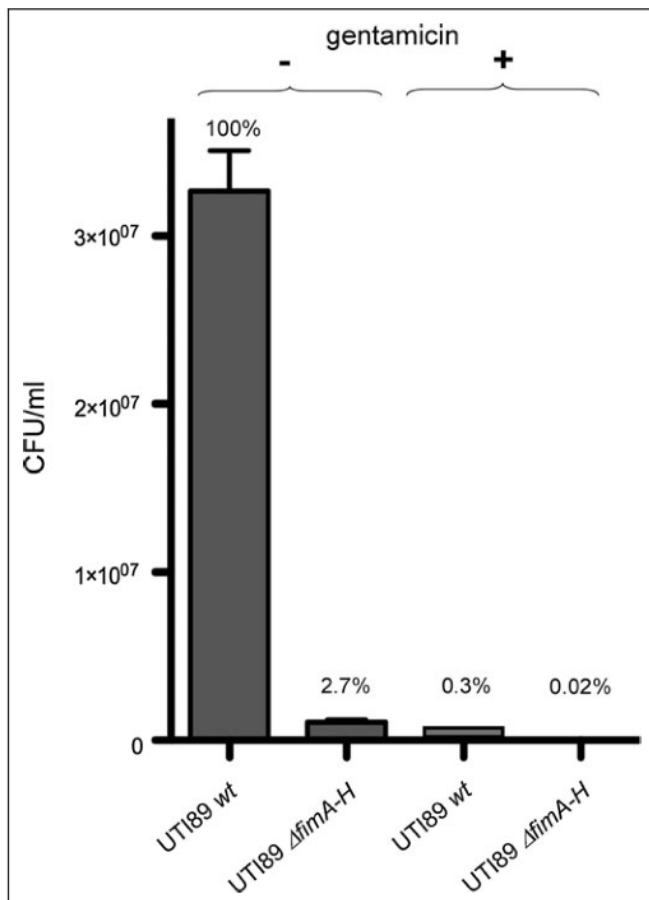


**Fig. 7.** Flow cytometry analysis of 5637 cells infected with GFP-expressing UTI89 strains (MOI 50:1, bacteria:cell). Histograms show the green fluorescence intensity of cells infected with UTI89 wt (A), pretreated UTI89 wt with 7  $\mu M$  (B) and 111  $\mu M$  (C) *n*-heptyl  $\alpha$ -D-mannopyranoside before infection, and UTI89  $\Delta fimA-H$  (D).

At this MOI, an intensive fluorescence profile without saturation, because of an excess of bacteria, was obtained. Bladder cells infected with the FimH-deficient strain UTI89  $\Delta fimA-H$  displayed a weak fluorescence signal, similar to that of uninfected cells (MFI below 30), confirming that the adhesion of UTI89 is exclusively type 1 pili dependent. Pils *et al.*<sup>39</sup> reported that trypan blue can be used to quench

**Fig. 6.** Internalization (invasion) assay: CFU/mL of UTI89 wt and UTI89  $\Delta fimA-H$  after infection (1.5 h) of 5637 cells with and without subsequent gentamicin (100  $\mu g/mL$ ) treatment. CFU/mL of the adhesive UTI89 wt was set to 100%. Assay and analysis were performed as described in the Material and Methods section. Error bars represent standard error of  $n=6$  values.



## CYTOMETRY-BASED ASSAY FOR FIMH ANTAGONISTS

extracellular fluorescence signals of CFSE-labeled bacteria. Therefore, infected cells treated with trypan blue emit light specifically from internalized bacteria. In our assay, the application of this method to GFP-labeled bacteria turned out to be not successful (data not shown), because the fluorescence emitted by GFP-labeled, extracellular bacteria could not be quenched. Consequently, GFP labeling could not be used to investigate the internalization of bacteria by flow cytometry via trypan blue treatment.

Therefore, the extent of internalization of bacteria within an incubation time of 1.5 h (Fig. 6) was determined according to the internalization assay published by Elsinghorst.<sup>38</sup> The observed CFU/mL of extra- and intracellular adhesive UTI89 *wt* before gentamicin treatment was set to 100%. As less than 1% of the adhesive UTI89 *wt* bacteria (representing internalized bacteria) survived the gentamicin

treatment, the internalization occurrence during 1.5 h of infection is negligible. As expected, the mutant UTI89  $\Delta$ *fimA-H* was nonadhesive and noninvasive under similar conditions.

## Inhibition Assay (Flow Cytometry Assay)

To evaluate the applicability of the assay for the evaluation of FimH antagonists, two different concentrations (7 and 111  $\mu$ M) of *n*-heptyl  $\alpha$ -D-mannopyranoside (3) were added to the bacterial suspension before infection. Figure 7 shows that compound 3 successfully antagonized the adhesion of bacteria to 5637 cells. The MFI of cells infected with the UTI89 *wt* strain in the absence of compound 3 was 592 (Fig. 7A) and decreased in the presence of compound 3 at 7 and 111  $\mu$ M to 208 and 41, respectively (Fig. 7B, C). Cells treated with the UTI89  $\Delta$ *fimA-H* mutant strain (Fig. 7D) exhibited only a low MFI

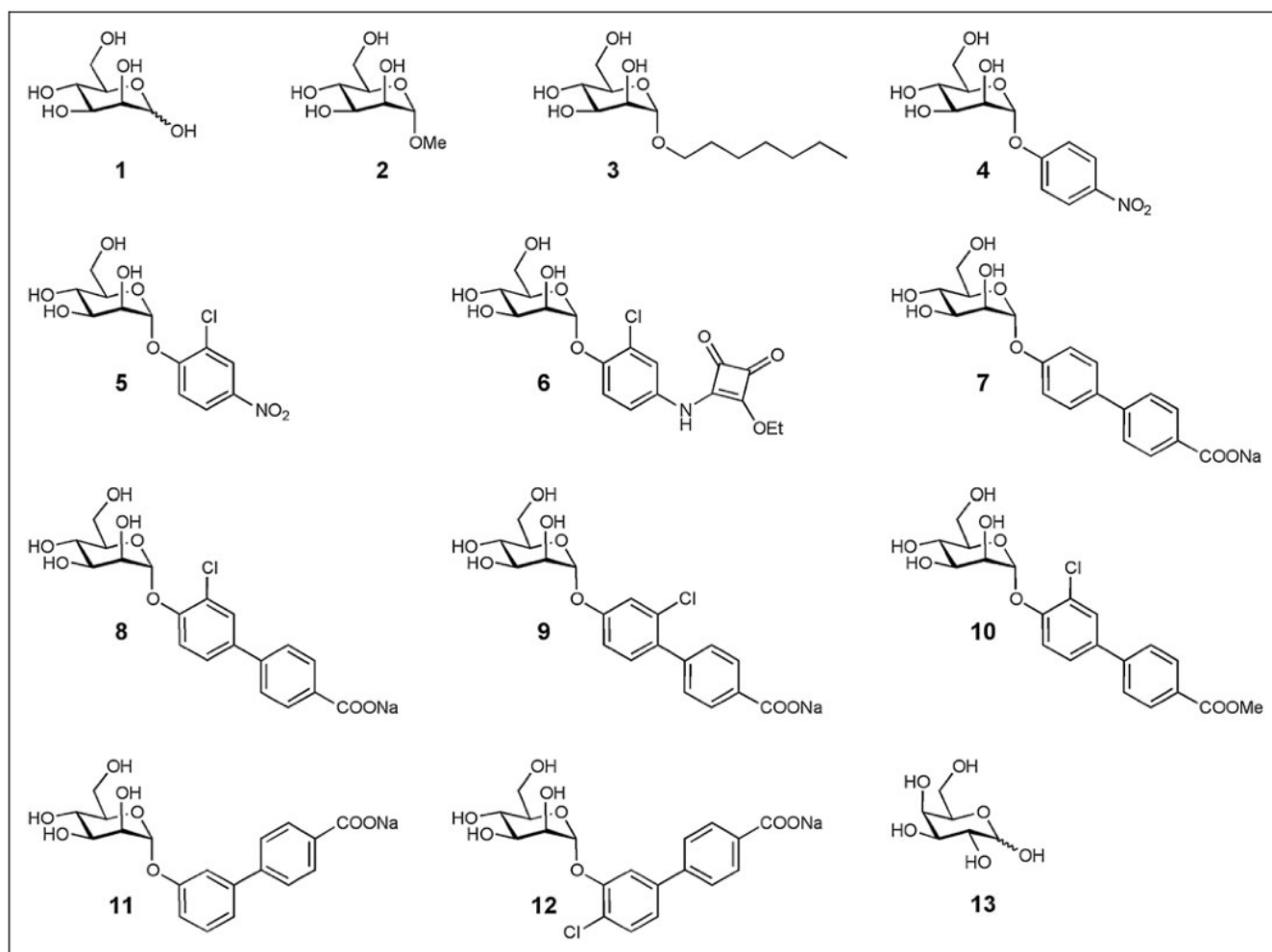


**Fig. 8.** Structures of FimH antagonists and the negative control D-galactose (13). D-Mannopyranoside (1), methyl  $\alpha$ -D-mannopyranoside (2), *n*-heptyl  $\alpha$ -D-mannopyranoside (3),<sup>24,36</sup> 4-nitrophenyl  $\alpha$ -D-manno-pyranoside (4), 2-chloro-4-nitrophenyl  $\alpha$ -D-mannopyranoside (5),<sup>20</sup> *o*-chloro-*p*-[*N*-(2-ethoxy-3,4-dioxocyclobut-1-enyl)amino]phenyl  $\alpha$ -D-mannopyranoside (6),<sup>20</sup> and the biphenyl  $\alpha$ -D-mannopyranoside derivatives 7–12.<sup>21,37</sup>

## SCHARENBERG ET AL.

Table 2. Inhibitory Potencies of FimH Antagonists

FimH Antagonist	Flow Cytometry Inhibition Assay		Aggregometry Assay <sup>24</sup>	Competitive Binding Assay <sup>34</sup>
	IC <sub>50</sub> [μM]	rIC <sub>50</sub>	rIC <sub>50</sub>	rIC <sub>50</sub>
2	249.2 ± 62.3	59.6	n.d.	29.2
3 (ref. compound)	3.9 ± 1.6	1	1	1
4	3.2 ± 0.69	0.76	0.84	1.57
5	1.06 ± 0.47	0.25	0.18	0.32
6	0.035 ± 0.008	0.008	0.01	0.15
7	0.86 ± 0.56	0.22	0.58	0.15
8	0.33 ± 0.05	0.08	0.13	0.09
9	0.53 ± 0.06	0.13	0.22	0.38
10	0.24 ± 0.043	0.06	0.12	0.06
11	4.45 ± 1.9	1.14	0.58	0.53
12	0.79 ± 0.16	0.2	n.d.	0.4
13	> 5500	–	n.d.	n.d.

IC<sub>50</sub> values (using an MOI of 1:50) were determined with the flow cytometry assay as described in the Materials and Methods section and compared with rIC<sub>50</sub> values obtained with the aggregometry and competition binding assays (values for compound 2–6 derive from literature<sup>24,34</sup> whereas compounds 7–13 were newly tested). rIC<sub>50</sub>s were calculated by dividing the IC<sub>50</sub> of the compound of interest by the IC<sub>50</sub> of the reference compound 3. This leads to rIC<sub>50</sub> values below 1.0 for derivatives with higher activity than 3 and rIC<sub>50</sub> values above 1.0 for compounds with lower activity than 3.  
n.d., not determined.

of 23. In a next step, the bacteria were treated with a serial dilution of inhibitor prior to infection. By measuring the MFI values, an IC<sub>50</sub> value could be derived from the sigmoid inhibition curve (MFI vs. log[antagonist]) (Fig. 1). The reproducible IC<sub>50</sub> value for the reference compound 3 was in the low μM range (3.9 ± 1.6 μM). To validate the assay, different FimH antagonists (Fig. 8) were evaluated. The assay was performed in duplicates/triplicates and repeated two or three times. Examples of inhibition curves of the antagonists 5, 6, and 10 are shown in Figure 1. Affinities were compared with affinity data obtained with the aggregometry assay<sup>24</sup> and competitive binding assay<sup>34</sup> (Table 2). Relative IC<sub>50</sub> values (rIC<sub>50</sub>) were calculated using *n*-heptyl α-D-mannopyranoside (3) as reference compound. As expected, methyl α-D-mannopyranoside (2) exhibited the weakest inhibitory potential, with an IC<sub>50</sub> value of 249.2 ± 62.3 μM. The best inhibitor turned out to be the squaric acid derivative compound 6, with an IC<sub>50</sub> value of 35 ± 8 nM. The other phenyl and biphenyl derivatives (4, 5, 7–12), except for compound 11, which had a similar

IC<sub>50</sub> value as 3, exhibited slightly higher inhibitory potentials than reference compound 3. D-Galactose (13), used as negative control, did not show any inhibitory effect up to a concentration of 5.5 mM.

## DISCUSSION

On epithelial bladder cells, α-mannosides are the primary ligands for UPEC. For their attachment, FimH lectins located at the tip of bacterial fimbriae are required. To prevent UTI, inhibition of this type 1 fimbriae-mediated bacterial adhesion to the bladder epithelium is a promising therapeutic approach.<sup>10</sup>

Various mannose derivatives<sup>16–18,20,21</sup> and oligomannosides<sup>19,40</sup> have been shown to antagonize FimH. For the evaluation of these antagonists, cell-based inhibition assays were mainly applied, using the properties of UPEC to agglutinate GPE<sup>18,23,24</sup> or to aggregate mannan-expressing yeast cells.<sup>25–27</sup> The results of these functional assays vary significantly because of the differential expression of FimH<sup>25,26</sup> and depend strongly on both source and batch of erythrocytes.<sup>23</sup> Further, GPE do not display the natural receptors for FimH, as the uroplakin proteins are exclusively expressed on bladder epithelial cells.<sup>14</sup>

Using GFP-labeled UPECs and human epithelial carcinoma bladder 5637 cells, a function-based flow cytometry assay was established. The assay allows a highly accurate analysis of bacterial adhesion, as more than 10,000 epithelial cells can be analyzed within a short time period. By investigating a large number of cells, variations caused by naturally occurring outliers are minimized. Further, easy handling reduces the effect of factors that influence reproducibility and reliability of the assay. In addition, the cumbersome fluorescent labeling prior to each experiment is not necessary when GFP-expressing bacteria are used.

It could be demonstrated with the UTI89 Δ*fimA-H* mutant strain that the adherence of the UPEC strain UTI89 to epithelial cells exclusively depends on type 1 pili. This result emphasizes the pivotal role of these pili for the pathogenesis of UPEC infection. Further, it validates FimH as a target for a therapeutic approach. The assay was first optimized with *n*-heptyl α-D-mannopyranoside (3), a potent FimH antagonist.<sup>16</sup> For the validation of the assay, the IC<sub>50</sub> values of different FimH antagonists were determined (Figs. 1 and 8) and compared with affinity data obtained by two other assay formats<sup>24,34</sup> (Table 2). As expected, methyl α-D-mannopyranoside (2) showed the lowest affinity (IC<sub>50</sub> = 249 ± 62.3 μM). For mannosides with aromatic aglycones such as *p*-nitrophenyl α-D-mannopyranoside (4) and 2-chloro-4-nitrophenyl α-D-mannopyranoside (5),<sup>20</sup> affinity was enhanced, thus confirming the beneficial effect of lipophilic interactions between the aromatic aglycone and the tyrosine gate of the binding site of the protein. The squaric acid derivative 6<sup>20</sup> showed the best inhibitory potential of all tested antagonists (IC<sub>50</sub> = 35 ± 8 nM), a more than 100-fold increased activity compared with 3. For the biphenyl mannosides 7–12,<sup>37</sup> the best activities were obtained with an *ortho*-chloro substituent on the aromatic ring adjacent to the anomeric oxygen and *para*-substitution of the biphenyl (8–10). Antagonists with a *meta*-substituted biphenyl aglycone exhibited a two- to fivefold lower activity (7 vs. 11, 8 vs. 12). A similar effect was found for an additional

chloro-substituent (11 vs. 12). Finally, for D-galactose (13), which was used as negative control, no inhibition of FimH-mediated adhesion at concentrations up to 5.5 mM was detected.

In Table 2, rIC<sub>50</sub> values obtained with the flow cytometry assay are compared with those obtained with the competitive binding assay<sup>34</sup> and the aggregometry assay.<sup>24</sup> However, a direct comparison of the IC<sub>50</sub> values is not possible, as the inhibition potencies were measured in different assay formats. For the competitive binding assay, we used the isolated CRD of FimH, which adopts the high-affinity state even under static conditions.<sup>33</sup> In contrast, in the cell-based aggregometry and flow cytometry assays, the bacteria display full-length fimbriae, representing the FimH low-affinity state under low shear stress.<sup>33</sup> However, when affinity data relative to a reference compound (rIC<sub>50</sub>) were compared, the rIC<sub>50</sub> values from the flow cytometry assay, in general, correlate well with values measured with the aggregometry assay<sup>24</sup> and the cell-free competitive binding assay<sup>34</sup> (Table 2). One exception is the squaric acid derivative 6, which gave similar results in the flow cytometry and aggregometry assays, but a much higher rIC<sub>50</sub> in the cell-free competitive binding assay. Further, the affinities of compounds 2, 4, and 5 agree very well with reported values.<sup>16,31</sup>

The assay was optimized for an infection time of 1.5 h. At this time point, the degree of internalization of bacteria by 5637 cells is below 1% and therefore negligible, as determined by an internalization assay<sup>38</sup> (Fig. 6). However, when the contact time between bacteria and cells is prolonged, internalization of bacteria may occur to a higher extent and will therefore falsify the readout of the assay.

In the target- and function-based assays published to date, the affinities of antagonists to purified lectin<sup>16,30,34</sup> or whole bacteria<sup>23,24,28</sup> are measured by competition assays with either immobilized/soluble D-mannose derivatives<sup>16,28,34</sup> or glycans present on cell surfaces of yeast,<sup>25–27</sup> erythrocytes,<sup>18,23,24</sup> or granulocytes.<sup>30</sup> In the presented flow cytometry assay, the antagonists compete with oligomannosides of the endogenously expressed physiological ligand UPIa on bladder epithelial cells for binding to type 1 fimbriae of the clinical isolate UTI89. Therefore, the new *in vitro* assay allows to estimate the inhibitory potential of antagonists *in vivo*.

In summary, we developed a reproducible and sensitive function-based assay that allows the quantitative analysis of FimH-mediated bacterial adhesion to mammalian cells and, further, the determination of the inhibitory potential of compounds that block the adhesion. Easy handling makes it a valuable tool for the evaluation of novel FimH antagonists. Moreover, the obtained IC<sub>50</sub> value can serve as a guidance value for the minimal therapeutic concentration in the bladder necessary for a successful treatment of UTI in *in vivo* studies.

## ACKNOWLEDGMENTS

The authors thank Prof. Urs Jenal, Biocenter of the University of Basel, for the clinical *E. coli* isolate UTI89 and the FimH knock-out strain UTI89Δ*fimA-H*. The financial support by the Swiss National Science Foundation (SNF interdisciplinary grant K-32K1-120904) is gratefully acknowledged.

## DISCLOSURE STATEMENT

No competing financial interests exist.

## REFERENCES

1. Foxman B, Barlow R, D'Arcy H, Gillespie B, Sobel JD: Urinary tract infection: self reported incidence and associated costs. *Ann Epidemiol* 2000;10:509–515.
2. Ronald A: The etiology of urinary tract infection: traditional and emerging pathogens. *Acad Med* 2002;113:145–195.
3. Foxman B, Brown P: Epidemiology of urinary tract infections—transmission and risk factors, incidence, and costs. *Infect Dis Clin North Am* 2003;17:227–241.
4. Foxman B: Recurring urinary tract infection: incidence and risk factors. *Am J Public Health* 1990;80:331–333.
5. Mulvey MA: Adhesion and entry of uropathogenic *Escherichia coli*. *Cell Microbiol* 2002;4:257–271.
6. Wiles TJ, Kulesus RR, Mulvey MA: Origins and virulence mechanisms of uropathogenic *Escherichia coli*. *Clin Mol Pathol* 2008;85:11–19.
7. Russell PW, Orndorff PE: Lesions in two *Escherichia coli* type 1 pilus genes alter pilus number and length without affecting receptor binding. *J Bacteriol* 1992; 174:5923–5935.
8. Jones CH, Pinkner JS, Roth R, Heuser J, Nicholes AV, Abraham SN, et al.: FimH adhesin of type 1 pili is assembled into a fibrillar tip structure in the Enterobacteriaceae. *Proc Natl Acad Sci U S A* 1995;92:2081–2085.
9. Hung C, Bouckaert J, Hung DL, Pinkner J, Widberg C, DeFusco A, et al.: Structural basis of tropism of *Escherichia coli* to the bladder during urinary tract infection. *Abstr Gen Meet Am Soc Microbiol* 2002;102:41.
10. Hanson MS, Brinton CC: Identification and characterization of *E. coli* type-1 pilus tip adhesion protein. *Nature* 1988;332:265–268.
11. Choudhury D, Thompson A, Stojanoff V, Langermann S, Pinkner J, Hultgren SJ, et al.: X-ray structure of the FimC-FimH chaperone-adhesin complex from uropathogenic *Escherichia coli*. *Science* 1999;285:1061–1066.
12. Xie B, Zhou G, Chan SY, Shapiro E, Kong XP, Wu XR, et al.: Distinct glycan structures of uroplakins Ia and Ib – Structural basis for the selective binding of FimH adhesin to uroplakin Ia. *J Biol Chem* 2006;281:14644–14653.
13. Zhou G, Mo WJ, Seibel P, Min GW, Neubert TA, Glockshuber R, et al.: Uroplakin Ia is the urothelial receptor for uropathogenic *Escherichia coli*: evidence from *in vitro* FimH binding. *J Cell Sci* 2001;114:4095–4103.
14. Wu XR, Sun TT, Medina JJ: *In vitro* binding of type 1-fimbriated *Escherichia coli* to uroplakins Ia and Ib: relation to urinary tract infections. *Proc Natl Acad Sci U S A* 1996;93:9630–9635.
15. Mulvey MA, Lopez-Boado YS, Wilson CL, Roth R, Parks WC, Heuser J, et al.: Induction and evasion of host defenses by type 1-piliated uropathogenic *Escherichia coli*. *Science* 1998;282:1494–1497.
16. Bouckaert J, Berglund J, Schembri M, De Genst E, Cools L, Wuhler M, et al.: Receptor binding studies disclose a novel class of high-affinity inhibitors of the *Escherichia coli* FimH adhesin. *Mol Microbiol* 2005;55:441–455.
17. Imberty A, Chabre YM, Roy R: Glycomimetics and glycodendrimers as high affinity microbial anti-adhesins. *Chemistry* 2008;14:7490–7499.
18. Lindhorst TK, Kieburg C, Krallmann-Wenzel U: Inhibition of the type 1 fimbriae-mediated adhesion of *Escherichia coli* to erythrocytes by multiantennary alpha-mannosyl clusters: the effect of multivalency. *Glycoconj J* 1998;15:605–613.
19. Dubber M, Sperling O, Lindhorst TK: Oligomannoside mimetics by glycosylation of 'octopus glycosides' and their investigation as inhibitors of type 1 fimbriae-mediated adhesion of *Escherichia coli*. *Org Biomol Chem* 2006;4:3901–3912.
20. Sperling O, Fuchs A, Lindhorst TK: Evaluation of the carbohydrate recognition domain of the bacterial adhesin FimH: design, synthesis and binding properties of mannoside ligands. *Org Biomol Chem* 2006;4:3913–3922.
21. Han Z, Pinker JS, Ford B, Obermann R, Nolan W, Wildman SA, Hobbs D, Ellenberger T, Cusumano CK, Hultgren SJ, Janetka JW: Structure-based drug design and optimization of mannoside bacterial FimH antagonists. *J Med Chem* 2010;53:4779–4792.

## **Part I: The lectin FimH**

---

**FimH Chapter 2: Results and discussion**

**Publication 2**

---

## FimH Antagonists for the Oral Treatment of Urinary Tract Infections: From Design and Synthesis to in Vitro and in Vivo Evaluation

Tobias Klein,<sup>†</sup> Daniela Abgottsporn,<sup>†</sup> Matthias Wittwer,<sup>†</sup> Said Rabbani,<sup>†</sup> Janno Herold,<sup>†</sup> Xiaohua Jiang, Simon Kleeb, Christine Lüthi, Meike Scharenberg, Jacqueline Bezençon, Erich Gubler, Lijuan Pang, Martin Smiesko, Brian Cutting, Oliver Schwardt, and Beat Ernst\*

*Institute of Molecular Pharmacy, Pharmacenter, University of Basel, Klingelbergstrasse 50, CH-4056 Basel, Switzerland.*

<sup>†</sup>These authors contributed equally to the project

Received August 4, 2010

Urinary tract infection (UTI) by uropathogenic *Escherichia coli* (UPEC) is one of the most common infections, particularly affecting women. The interaction of FimH, a lectin located at the tip of bacterial pili, with high mannose structures is critical for the ability of UPEC to colonize and invade the bladder epithelium. We describe the synthesis and the in vitro/in vivo evaluation of  $\alpha$ -D-mannosides with the ability to block the bacteria/host cell interaction. According to the pharmacokinetic properties, a prodrug approach for their evaluation in the UTI mouse model was explored. As a result, an orally available, low molecular weight FimH antagonist was identified with the potential to reduce the colony forming units (CFU) in the urine by 2 orders of magnitude and in the bladder by 4 orders of magnitude. With FimH antagonist **16b**, the great potential for the effective treatment of urinary tract infections with a new class of orally available antiinfectives could be demonstrated.

### Introduction

Urinary tract infection (UTI<sup>a</sup>) is one of the most common infections, affecting millions of people each year. Particularly affected are women, who have a 40–50% risk to experience at least one symptomatic UTI episode at some time during their life. In addition, more than half of them experience a relapse of the infection within 6 months.<sup>1,2</sup>

Although UTIs rarely cause severe diseases such as pyelonephritis or urosepsis, they are associated with high incidence rate and consume considerable healthcare resources.<sup>3</sup> Uropathogenic *Escherichia coli* (UPEC) are the primary cause of UTIs, accounting for 70–95% of the reported cases. Symptomatic UTIs require antimicrobial treatment, often resulting in the emergence of resistant microbial flora. As a consequence, treatment of consecutive infections becomes increasingly difficult because the number of antibiotics is limited and the resistance of *E. coli* is increasing, especially in patients with diabetes, urinary tract anomaly, paraplegy, and those with permanent urinary catheter. Therefore, a new approach for the prevention and treatment of UTI with inexpensive, orally

applicable therapeutics with a low potential for resistance would have a great impact on patient care, public health care, and medical expenses.

UPEC strains express a number of well-studied virulence factors used for a successful colonization of their host.<sup>3–5</sup> One important virulence factor is located on type 1 pili, allowing UPEC to adhere and invade host cells within the urinary tract. It enables UPEC to attach to oligomannosides, which are part of the glycoprotein uroplakin Ia on the urinary bladder mucosa. This initial step prevents the rapid clearance of *E. coli* from the urinary tract by the bulk flow of urine and at the same time enables the invasion of the host cells.<sup>3,6</sup>

Type 1 pili are the most prevalent fimbriae encoded by UPEC, consisting of the four subunits FimA, FimF, FimG, and FimH, the latter located at the tip of the pili.<sup>7</sup> As a part of the FimH subunit, a carbohydrate-recognizing domain (CRD) is responsible for bacterial interactions with the host cells within the urinary tract.<sup>6</sup> The crystal structure of the FimH-CRD was solved<sup>8</sup> and its complexes with *n*-butyl  $\alpha$ -D-mannopyranoside<sup>9</sup> and  $\text{Man}\alpha(1-3)[\text{Man}\alpha(1-6)]\text{Man}$ <sup>10</sup> recently became available.

Previous studies showed that vaccination with FimH adhesin inhibits colonization and subsequent *E. coli* infection of the urothelium in humans.<sup>11,12</sup> In addition, adherence and invasion of host cells by *E. coli* can also be prevented by  $\alpha$ -D-mannopyranosides, which are potent antagonists of interactions mediated by type 1 pili.<sup>13</sup> Whereas  $\alpha$ -D-mannopyranosides efficiently prevent adhesion of *E. coli* to human urothelium, they are not exhibiting a selection pressure to induce antimicrobial resistance. Furthermore, environmental contamination is less problematic compared to antibiotics.<sup>14</sup>

More than two decades ago, Sharon and co-workers have investigated various mannosides and oligomannosides as

\*To whom correspondence should be addressed. Phone: +41 61 267 1551. Fax: +41 61 267 1552. E-mail: beat.ernst@unibas.ch.

<sup>a</sup> Abbreviations: AUC, area under the curve; Caco-2 cells, Caucasian colon adenocarcinoma cells; CFU, colony forming units; CRD, carbohydrate recognition domain; DC-SIGN, dendritic cell-specific intercellular adhesion molecule-3-grabbing nonintegrin; CES, carboxylesterase; IC<sub>50</sub>, half maximal inhibitory concentration; iv, intravenous; D, distribution coefficient; GPE, guinea pig erythrocytes; LC-MS, liquid chromatography–mass spectrometry; MBP, mannose-binding protein; PAMPA, parallel artificial membrane permeation assay; *P*<sub>app</sub>, apparent permeability; *P*<sub>e</sub>, effective permeation; po, peroral; PPB, plasma protein binding; PSA, polar surface area; *S*, solubility; SAR, structure–activity relationship; sGF, simulated gastric fluid; sIF, simulated intestinal fluid; TEER, transepithelial resistance; UPEC, uropathogenic *E. coli*; UTI, urinary tract infection.

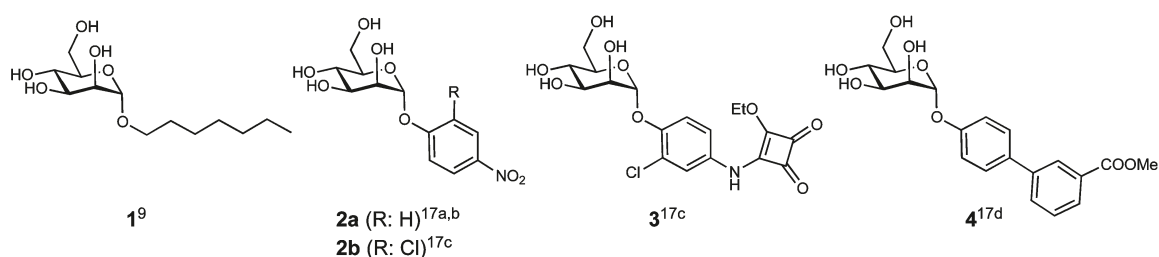
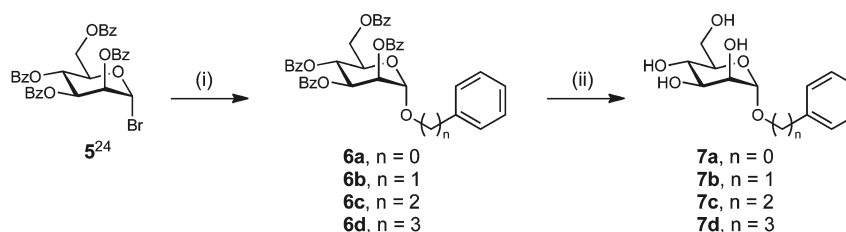


**Figure 1.** Known alkyl (**1**) and aryl (**2–4**)  $\alpha$ -D-mannosides exhibiting nanomolar affinities.

**Scheme 1.** Phenyl  $\alpha$ -D-Mannosides **7a–7d** with Spacers of Different Lengths between the Carbohydrate Moiety and the Phenyl Substituent<sup>a</sup>



<sup>a</sup> (i)  $\text{Ph}(\text{CH}_2)_n\text{OH}$ ,  $\text{Hg}(\text{CN})_2$ ,  $\text{HgBr}_2$ , DCM, 2 h to 7 d, rt, 57–99%; (ii) NaOMe, MeOH, 6–16 h, rt, 48–91%.

potential antagonists for type 1 fimbriae-mediated bacterial adhesion.<sup>15</sup> However, for these mannosides, only weak interactions in the milli- to micromolar range were observed. In contrast, numerous reports on glycoconjugate dendrimers with nanomolar affinities have been published.<sup>16</sup> However, on the basis of their large molecular weight and high polarity, they are predicted to exhibit only poor intestinal absorption and are therefore not amenable for oral dosing. Recently, some isolated reports on high affinity monovalent FimH antagonists were published<sup>17</sup> and, in one case, a systematic structure–activity relationship (SAR) profile was established.<sup>17d</sup> In summary,<sup>8,9,15–19</sup> long chain alkyl and aryl mannosides (selected examples are presented in Figure 1) displayed the highest affinity, likely due to hydrophobic interactions with two tyrosines and one isoleucine forming the entrance to the binding site, the so-called “tyrosine gate”.<sup>18</sup> Because binding affinities were obtained from diverse assay formats,<sup>9,17c,20</sup> a direct comparison of the affinities is difficult. On the basis of various crystal structures of methyl-<sup>8</sup> and *n*-butyl  $\alpha$ -D-mannoside<sup>18</sup> as well as oligomannose-3<sup>9</sup> bound to FimH, Han et al. recently presented a rationale for the design of arylmannosides with increased affinities.<sup>17d</sup>

To date, a few reports on the *in vivo* potential of methyl  $\alpha$ -D-mannoside<sup>10,21,22</sup> and *n*-heptyl  $\alpha$ -D-mannoside (**1**)<sup>10</sup> are available. In all cases, the FimH antagonists were directly instilled into the bladder concomitantly with uropathogenic *E. coli* (UPEC). In this communication, we present for the first time nanomolar FimH antagonists exhibiting appropriate pharmacokinetic properties for *iv* and oral treatment of urinary tract infections.

## Results and Discussion

**Identification of Lead Mannoside.** In most of the reported FimH antagonists, aromatic aglycones have been applied.<sup>17</sup> However, only limited information on the optimal spacer length between the mannose moiety and the aromatic substituent is available. Generally, the aromatic moiety is directly fused to the anomeric oxygen.<sup>17a–d</sup> Extended spacers containing one<sup>17b,d</sup> or two<sup>17e</sup> methylene moieties were also reported,

however, the corresponding antagonists are not really comparable to each other because different assay formats were used for their evaluation. For the identification of the optimal spacer length, we therefore synthesized mannosides **7a–d** (Scheme 1). In a competitive binding assay,<sup>23</sup> mannoside **7a** showed a slightly higher affinity (Table 1, entry 2) compared with **7b–7d** (see Table 1, entries 3–5), confirming recent data for **7a** and **7b**.<sup>17d</sup>

From the crystal structure of *n*-butyl  $\alpha$ -D-mannoside bound to FimH,<sup>18</sup> it becomes obvious that the hydrophobic rim formed by Tyr48, Tyr137, and Ile52 is not reached by an anomeric phenyl group. An extension by a second aromatic ring, i.e. a biphenyl  $\alpha$ -D-mannoside, however, should be compatible for  $\pi$ – $\pi$  stacking. Indeed, some recently published representatives of this compound class show excellent affinities.<sup>17d</sup>

To achieve an optimal fit with the hydrophobic binding site of FimH, the conformation of the biphenyl aglycone in **1** was modified by different substitution patterns on ring A (Figure 2). Because electron poor aromatic rings substantially improve the binding affinities of FimH antagonists (a 10-fold improvement is reported for **2B** vs **2A**<sup>17c</sup>), chloro substituents on ring A were used for the spatial exploration of the binding site. With substituents in *ortho*-position, only a minor change of the dihedral angle  $\Phi_1$  is observed ( $-3.3^\circ$  to  $-0.7^\circ$ ). However, by an increased rotational barrier, the conformational flexibility is limited. The dihedral angle  $\Phi_2$  between the conjugated aromatic rings results from an interplay between  $\pi$ -conjugation and steric effects.<sup>24,25</sup> By migrating the substituent to the *meta*-position, the torsion angle  $\Phi_2$  is substantially influenced. Whereas unsubstituted biphenyls show a global twisted minimum at a torsion angle  $\Phi_2$  of approximately  $39^\circ$ ,<sup>26</sup> substituents in the *meta*-position favor an increase of  $\Phi_2$  to  $60^\circ$ . Details of the conformational analyses are summarized in the Supporting Information.

**Design Strategy for Intestinal Absorption and Renal Elimination.** Besides high affinity, drug-like pharmacokinetic properties are a prerequisite for a successful *in vivo* application. In the present case, orally available FimH antagonists

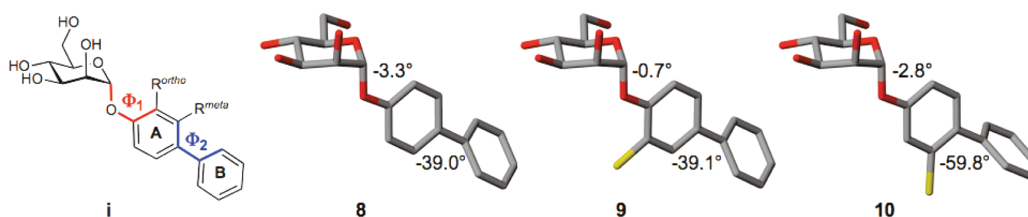


**Figure 2.** Conformational changes of the biphenyl aglycone by chloro substitutions in *ortho*- and *meta*-position of ring A.

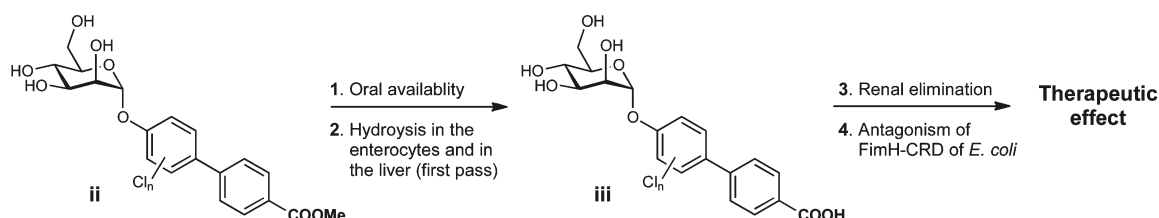


**Figure 3.** FimH antagonists with the pharmacodynamic and pharmacokinetic properties required for a therapeutic application. (1) For the prediction of oral availability, the PAMPA<sup>30</sup> and the Caco-2 cell assay<sup>31</sup> are applied. (2) The hydrolysis of ester **ii** to carboxylate **iii** is evaluated by mouse liver microsomes. (3) Renal excretion is estimated based on a positive correlation with polar descriptors (polar surface area, H-bond donors, H-bond acceptors, rotatable bonds).<sup>32</sup> (4) The potential of FimH antagonists is assessed with a target-based assay<sup>23</sup> and a function-based cellular assay.<sup>33</sup> For the evaluation of the therapeutic effect, a urinary tract infection mouse model (UTI mouse model in C3H/HeN mice) is applied.

that, once in circulation, are metabolically stable and undergo fast renal elimination, are required. This pharmacokinetic profile results from various serial and/or simultaneous processes that include dissolution, intestinal absorption, plasma protein binding, metabolic clearance, body distribution as well as renal and other clearance mechanisms. Because intestinal absorption and renal elimination are related to opposed properties, i.e. lipophilicity for intestinal absorption and hydrophilicity for renal elimination, a prodrug approach<sup>27</sup> was envisaged (Figure 3). Ester **ii** is expected to undergo intestinal absorption<sup>28</sup> and, later on, efficient hydrolysis to carboxylate **iii** by esterases<sup>29</sup> present in enterocytes lining the small intestine and in the liver.

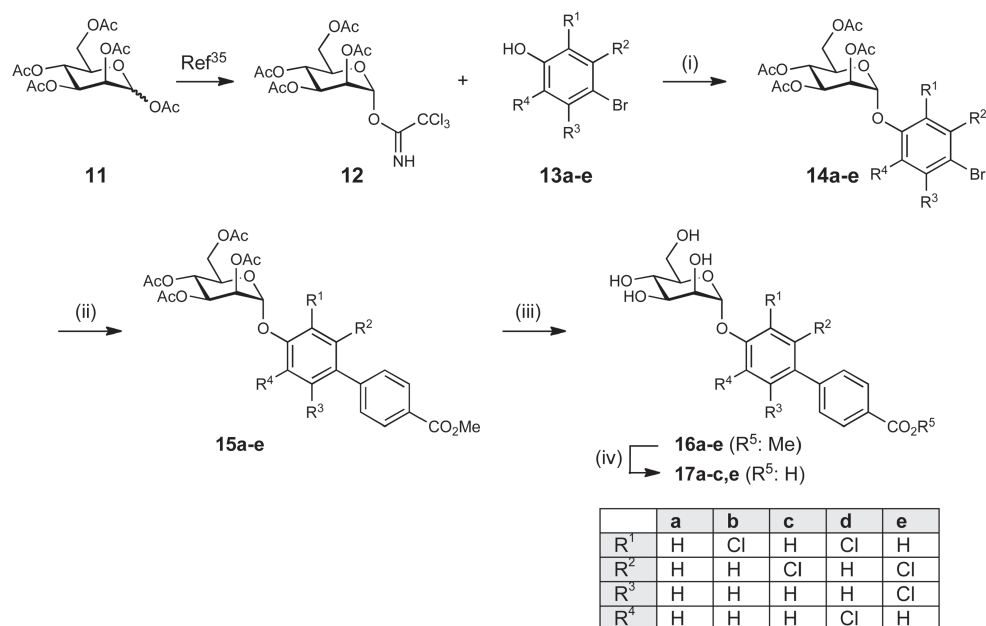
For renal clearance, the net result of glomerular filtration, active tubular secretion, and reabsorption, carboxylate **iii** should exhibit low lipophilicity ( $\log D_{7.4}$ ) and favorable polar descriptor values (polar surface area (PSA), H-bond capacity and rotatable bonds).<sup>32</sup> By contrast, lipophilic compounds are efficiently reabsorbed (as the passive reabsorption process occurs throughout the length of the nephron, whereas the secretion predominantly occurs at the proximal tubule). The estimated negative  $\log D_{7.4}$  for antagonists of type **iii** is expected to fulfill these specifications for an efficient renal elimination and a low reabsorption. Finally, once arrived at the site of action in the bladder, the antagonist binds to the carbohydrate recognition domain (CRD) located on the bacterial pili, thus interfering with the adhesion of *E. coli* to oligosaccharide structures on urothelial cells.<sup>34</sup> To identify antagonists with the pharmacokinetic properties required for oral absorption and fast renal elimination, it was planned to determine PK parameters such as  $\log D_{7.4}$ ,  $pK_a$ , solubility, plasma protein binding, metabolic stability, and oral availability using the parallel artificial membrane permeation assay (PAMPA)<sup>30</sup> and the Caco-2 cell assay.<sup>31</sup>

**Synthesis of FimH Antagonists.** The aglycone in the  $\alpha$ -1-position of D-mannose plays a ternary role, i.e. it mediates the lipophilic contact with the hydrophobic tyrosine gate, contains the elements required for intestinal absorption and, after metabolic cleavage of the prodrug, for a fast renal elimination.

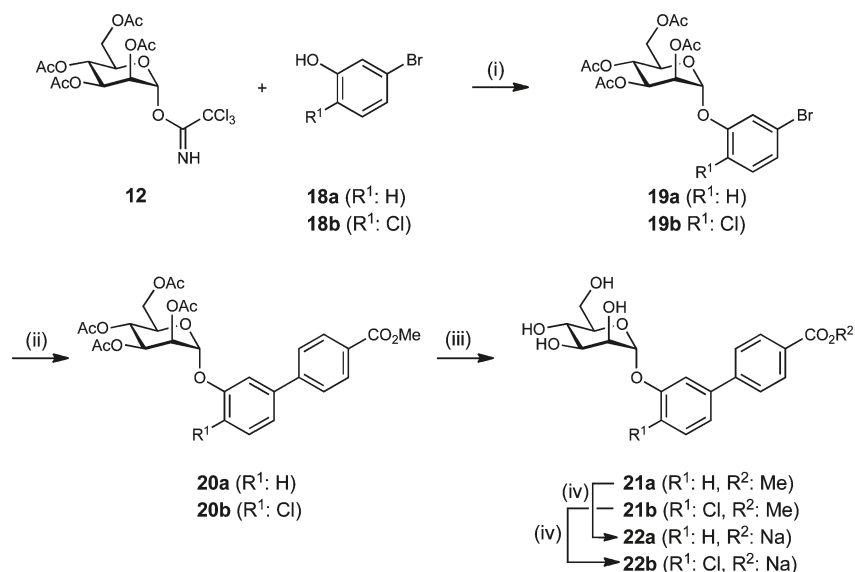
The syntheses of the *para*-substituted biphenyls **16a–e** and **17a–c,e** are outlined in Scheme 2. Lewis acid promoted glycosylation of the halogenated phenols **13a–e** with trichloroacetimidate **12**<sup>35</sup> yielded the phenyl  $\alpha$ -D-mannosides **14a–e**. In a palladium-catalyzed Suzuki coupling with 4-methoxycarbonylphenylboronic acid, the biphenyls **15a–e** were obtained. For the deprotection of the mannose moiety, Zemplén conditions were applied ( $\rightarrow$  **16a–e**). Finally, the methyl esters were saponified, yielding the sodium salts **17a–c,e**.

In a similar approach, two *meta*-substituted biphenyls in their ester form ( $\rightarrow$  **21a,b**) and as free acids ( $\rightarrow$  **22a,b**) were obtained (see Scheme 3).

**Binding Affinities and Activities.** For the biological in vitro evaluation of the FimH antagonists, two assay formats have been developed. For an initial characterization, a cell-free competitive binding assay<sup>23</sup> and, later on, a cell-based aggregation assay,<sup>33</sup> were applied. Whereas in the cell-free competitive binding assay only the CRD of the pili was used, the complete pili are present in the cell-based assay format. Furthermore, both formats are competitive assays, i.e. the analyzed antagonists compete with mannosides for the binding site. In the cell-free competitive binding assay, the competitors are polymer-bound trimannosides, whereas in the aggregation assay, the antagonist competes with more potent oligo- and polysaccharide chains present on the surface of erythrocytes.<sup>36</sup> Therefore, lower  $IC_{50}$  values are expected for the cell-free competitive binding assay. In addition, switching from the cell-free target-based assay to the function-based assay generally leads to a reduction of potency by several orders of magnitude. The interaction is further complicated by the existence of a high- and a low-affinity state of the CRD of FimH. Aprikian et al. experimentally demonstrated that in full-length fimbriae the pilin domain stabilizes the CRD domain in the low-affinity state, whereas the CRD domain alone adopts the high-affinity state.<sup>37</sup> It was recently shown that the pilin domain allosterically causes a twist in the  $\beta$ -sandwich fold of the CRD domain, resulting in a loosening of the binding pocket.<sup>38</sup> On

Scheme 2<sup>a</sup>

<sup>a</sup> (i) TMSOTf, toluene, rt, 5 h (42–77%); (ii) 4-methoxycarbonylphenylboronic acid, Cs<sub>2</sub>CO<sub>3</sub>, Pd(PPh<sub>3</sub>)<sub>4</sub>, dioxane, 120°C, 8 h (28–85%); (iii) NaOMe, MeOH, rt, 4–24 h (22–86%); (iv) NaOMe, MeOH, rt, then NaOH/H<sub>2</sub>O, rt, 16–24 h (63–94%).

Scheme 3<sup>a</sup>

<sup>a</sup> (i) TMSOTf, toluene, rt, 5 h (67–70%); (ii) 4-methoxycarbonylphenylboronic acid, Cs<sub>2</sub>CO<sub>3</sub>, Pd(PPh<sub>3</sub>)<sub>4</sub>, dioxane, 120°C, 8 h or Pd<sub>2</sub>(dba)<sub>3</sub>, S-Phos, dioxane, 80°C, overnight (46–56%); (iii) NaOMe, MeOH, rt, 24 h (52–67%); (iv) NaOMe, MeOH, rt, then NaOH/H<sub>2</sub>O, rt, 24 h (75–95%).

the basis of these findings, we expect a loss of affinity of our antagonists toward full-length fimbriae, when compared to the CRD domain alone.

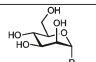
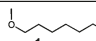
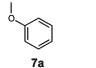
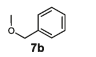
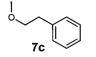
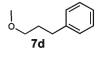
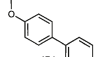
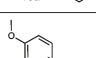
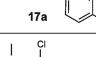
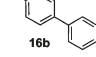
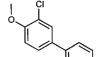
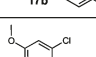
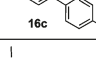
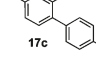
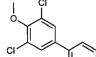
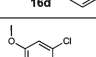
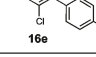
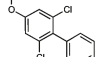
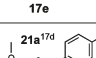
**Cell-Free Competitive Binding Assay.** The cell-free inhibition assay is based on the interaction of a biotinylated polyacrylamide glycopolymer with the FimH-CRD as previously reported.<sup>23</sup> A recombinant protein consisting of the carbohydrate recognition domain of FimH linked with a thrombin cleavage site to a 6His-tag (FimH-CRD-Th-6His) was expressed in *E. coli* strain HM125 and purified by affinity chromatography. The IC<sub>50</sub> values of the test compounds were determined in microtiter plates coated with

FimH-CRD-Th-6His. Complexation of the biotinylated glycopolymer with streptavidin coupled to horseradish peroxidase allowed the quantification of the binding properties of FimH antagonists (Figure 4a). To ensure comparability with different antagonists, the reference compound *n*-heptyl  $\alpha$ -D-mannopyranoside (**1**)<sup>33</sup> was tested in parallel in each individual microtiter plate. The affinities are reported relative to *n*-heptyl  $\alpha$ -D-mannopyranoside (**1**) as iC<sub>50</sub> in Table 1.

The most active representatives from the ester group are **16a** (Table 1, entry 6) and **16b** (entry 8) with affinities in the low nanomolar range, which is an approximately 10-fold improvement compared to reference compound **1**. The



**Table 1.** Pharmacodynamic and Pharmacokinetic Parameters of FimH Antagonists<sup>a,b</sup>

		IC <sub>50</sub> binding assay [nM]	rIC <sub>50</sub>	IC <sub>50</sub> Aggrego- metry assay [ $\mu$ M]	PAMPA log $P_e$ [log10 <sup>-6</sup> cm/s/ %Mm]	Caco-2 $P_{app}$ [10 <sup>-6</sup> cm/s]	log $D_{7.4}$	pK <sub>a</sub>	log $S$ [ $\mu$ g/mL]/ pH	PPB [%]
1		73±7.9	1.0	77.14±8.7	-4.89/21	nd	1.65	-	>3000	81
2		150±11.5	1.9	nd	nd/nd	nd	nd	-	>3000	nd
3		364±16.8	4.6	nd	nd/nd	nd	nd	-	nd	nd
4		210±11.2	2.6	nd	nd/nd	nd	nd	-	nd	nd
5		253±13.4	3.2	nd	nd/nd	nd	nd	-	nd	nd
6		10.4±1.2	0.14	42±7	-4.7/<20%	4.23	2.14	-	33.8/6.51	93
7		17.1±2.2	0.15	45±8	np	nd	<-1.5	3.88	>3000/6.61	73
8		4.8±1.2	0.06	9±2.7	-4.6/41.00	2.05	2.32	-	11.9/6.53	94
9		6.7±2.1	0.09	10±2.3	np/3.5	nd	-0.77	3.98	>3000/6.50	89
10		22.0±8.4	0.30	41 <sup>b)</sup>	-4.72/67.6	nd	2.42	-	11.5/6.50	95
11		27.6±3.9	0.38	17 <sup>b)</sup>	np	nd	-1.33	3.95	>3000/6.50	83
12		16.0±0.8	0.22	14 <sup>b)</sup>	-4.29/54.3	3.32	2.31	-	4.6/6.53	98
13		15.3±0.4	0.07	nd	-4.40/70.2	5.81	3.10	-	22.7/6.53	94
14		23.9±2.2	0.19	nd	nd/nd	nd	nd	nd	nd	nd
15		20.0±4.3	0.27	33 <sup>b)</sup>	-5.01/60.7	4.88	2.02	-	37.6/6.52	92
16		38.7±5.2	0.53	45 <sup>b)</sup>	np/9.7	nd	<-1.5	3.60	>3000/6.50	81
17		11.8±0.1	0.16	31 <sup>b)</sup>	-4.69/51.7	1.63	1.70	-	24.3/6.54	96
18		29.2±0.7	0.40	nd	np/nr	0.55	<-1.5	3.41	>3000/6.5	87

<sup>a</sup> Single determination;  $P_e$ , effective permeation;  $P_{app}$ , apparent permeability; np, no permeation; nr, no retention; nd, not determined. <sup>b</sup> The IC<sub>50</sub>s were determined with the cell-free competitive binding assay.<sup>23</sup> The rIC<sub>50</sub> of each substance was calculated by dividing the IC<sub>50</sub> of the compound of interest by the IC<sub>50</sub> of the reference compound **1** (entry 1). This leads to rIC<sub>50</sub> values below 1.00 for derivatives binding better than **1** and rIC<sub>50</sub> values above 1.00 for compounds with a lower affinity than **1**. The aggregation of *E. coli* and GPE were determined in the aggregometry assay.<sup>33</sup> Passive permeation through an artificial membrane and retention therein was determined by PAMPA (parallel artificial membrane permeation assay).<sup>30</sup> The permeation through cell monolayers was assessed by a Caco-2 assay.<sup>31</sup> Distribution coefficients (log  $D$  values) were measured by a miniaturized shake flask procedure.<sup>44</sup> pK<sub>a</sub> values were determined by NMR spectroscopy.<sup>45</sup> Plasma protein binding (PPB) was assessed by a miniaturized equilibrium dialysis protocol.<sup>46</sup> Thermodynamic solubility ( $S$ ) was measured by an equilibrium shake flask approach.<sup>47</sup>

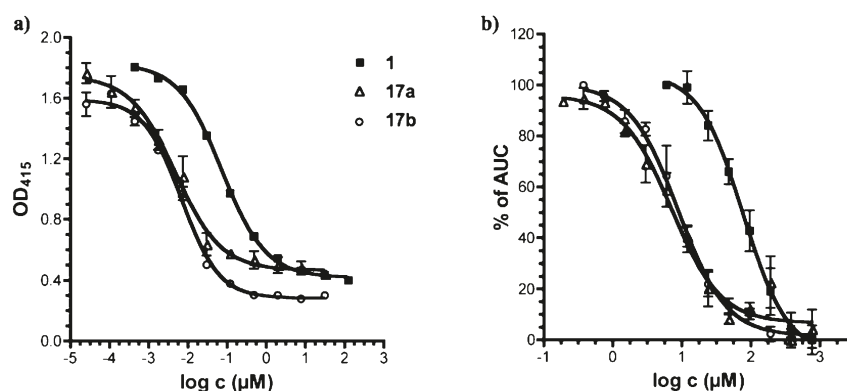


**Figure 4.** Affinities were determined in two different competitive assay formats. (a) a cell-free competitive binding assay<sup>23</sup> and (b) a cell-based aggregometry assay.<sup>33</sup> For antagonists **17a**, **17b**, and the reference compound **1**, IC<sub>50</sub> values in the nM and μM range, respectively, were obtained. The 1000-fold difference between the two assay formats is due to the different competitors used as well as the different affinity states present in FimH, i.e. the high-affinity state present in the CRD used in the cell-free competitive binding assay and the low-affinity state present in the pili of *E. coli* used in the aggregometry assay.

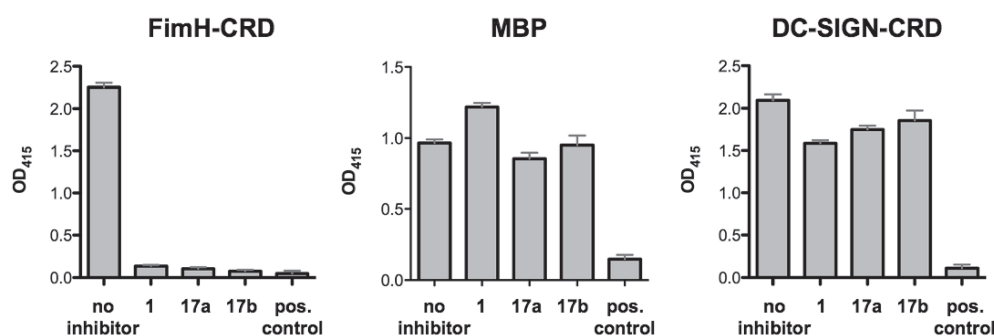


**Figure 5.** Competitive binding assay using FimH-CRD-Th-6His, DC-SIGN-CRD-IgG-Fc,<sup>43</sup> and MBP to evaluate the selectivity of compounds **1**, **17a**, and **17b**. Inhibitory capacities of the compounds were tested at a concentration of 1 mM. As positive control, D-mannose at a concentration of 50 mM was used.

corresponding carboxylic acids **17a** (entry 7) and **17b** (entry 9) exhibited a small reduction in affinity but are still 5-fold more active than reference compound **1**. All the remaining antagonists listed in Table 1 are slightly less active. For the in vivo examination, antagonists **17a** and **17b** were therefore foreseen for iv application and the prodrug **16b** for oral application.

Target selectivity is a further important issue. Mammalian mannose receptors are part of various biological processes, e.g. in cell–cell adhesion (DC-SIGN, dendritic cell-specific intercellular adhesion molecule-3-grabbing nonintegrin),<sup>39</sup> in the regulation of serum glycoprotein homeostasis (mannose receptor)<sup>40</sup> or in the innate and adaptive immune system by recognizing molecular patterns on pathogens (e.g., mannose-binding protein, mannose receptor, DC-SIGN).<sup>39,41,42</sup> Non-specific interactions to the various mannose receptors by FimH inhibitors would have a profound impact on these processes. We therefore determined the affinity of reference compound **1** and the two antagonists **17a** and **17b** for two additional mannose binding proteins, DC-SIGN,<sup>39,43</sup> and MBP (mannose-binding protein)<sup>42</sup> (Figure 5). In both cases, affinities above 1 mM, i.e. a decrease of more than 5 orders of magnitude, was detected.

**Aggregometry Assay.** The potential of the biphenyl mannosides to disaggregate *E. coli* from guinea pig erythrocytes (GPE) was determined by a function-based aggregometry assay.<sup>33</sup> Antagonists were measured in triplicates, and the corresponding IC<sub>50</sub> values were calculated by plotting the

area under the curve (AUC) of disaggregation against the concentration of the antagonists. *n*-Heptyl  $\alpha$ -D-mannopyranoside (**1**) was used again as reference compound and exhibits an IC<sub>50</sub> of  $77.14 \pm 8.7 \mu\text{M}$ . Antagonists **17a** and **17b** showed IC<sub>50</sub> values of  $45 \pm 8 \mu\text{M}$  and  $10 \pm 2.3 \mu\text{M}$ , respectively (Figure 4b). In general, the activities obtained from the aggregometry assay are approximately 1000-fold lower than the affinities determined in the target-based competitive assay (discussion see above).

**In Vitro Pharmacokinetic Characterization of FimH Antagonists.** For an application in the UTI mouse model, iv or po available FimH antagonists are required that, once absorbed to circulation, are metabolically stable and undergo fast renal elimination. Sufficient bioavailability requires a combination of high solubility and permeability to maximize absorption and low hepatic clearance to minimize first pass extraction. Furthermore, for efficient renal elimination, active and/or passive membrane permeability and low reabsorption in the renal tubuli is required. From the series of FimH antagonists with nanomolar in vitro activities (see Table 1), representatives with appropriate pharmacokinetic properties were selected for in vivo experiments based on the parameters shown below.

**Oral Absorption and Renal Excretion.** For the evaluation of oral absorption and renal excretion of the esters **16** and **21** as well as the acids **17** and **22** physicochemical parameters such as pK<sub>a</sub> values, lipophilicity (distribution coefficients, log *D*<sub>7,4</sub>), solubility, and permeability were determined

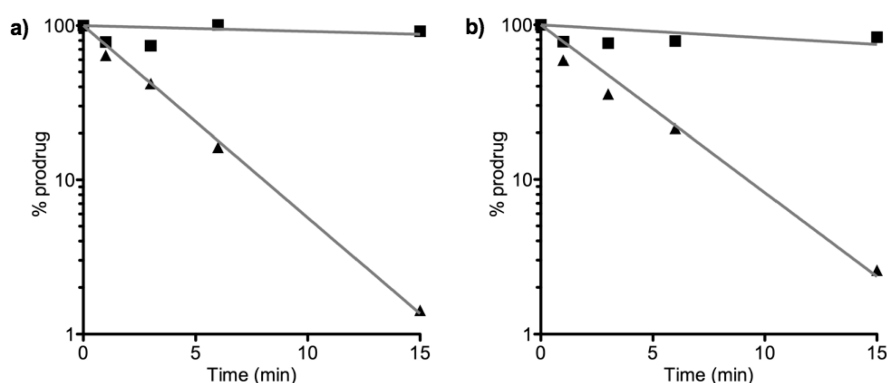


**Figure 6.** Incubation of (a) **16a** and (b) **16b** with pooled mouse liver microsomes (0.25 mg of protein/mL), in absence ( $\blacktriangle$ ) and in presence ( $\blacksquare$ ) of the specific carboxylesterase inhibitor bis(4-nitrophenyl) phosphate (BNPP).

(Table 1). Not surprisingly, the acids **17** and **22** showed  $\log D_{7.4}$  values in the range of  $-1$  to  $-2$  and  $pK_a$  values of approximately 4. While these parameters are beneficial for renal excretion,<sup>32</sup> oral absorption by passive diffusion seems unlikely. Indeed, when the permeation through an artificial membrane (PAMPA<sup>30</sup>) was studied, neither significant permeation ( $\log P_e$ ,  $P_e$ : effective permeation) nor membrane retention could be detected. Whereas for a successful oral absorption  $\log P_e$  should be above  $-5.7$  and/or the membrane retention above 80%,<sup>48</sup> the corresponding values for the carboxylic acids **17** and **22** are far from being in this range (see Table 1, e.g. entries 7 and 9). However,  $\log D_{7.4}$  values and PAMPA results were markedly improved for the esters **16** and **21** (Table 1, e.g. entries 6 and 8), suggesting that these FimH antagonists are orally absorbed. This assumption was fully confirmed in a cell-based permeation assay with Caco-2 cells.<sup>31</sup> For renal excretion, Varma et al.<sup>31</sup> correlated low lipophilicity and the presence of a charged state at physiological pH positively with enhanced elimination. On the basis of  $\log D_{7.4}$  and  $pK_a$  summarized in Table 1, the carboxylates **17** and **22** fulfill these requirements. Overall, these results support the prodrug approach: (i) oral application of the esters **16** and **21** and (ii) renal elimination of the corresponding acids **17** and **22**.

**Solubility.** A major problem of the antagonists **16** and **21** is their insufficient solubility, ranging from 4.6 to 37.6  $\mu\text{g}/\text{mL}$ . Even though the solubility issue can be addressed by appropriate formulations, further structural modifications to improve solubility are necessary. Opposite to the esters, the corresponding carboxylates **17** and **22** showed excellent solubility ( $> 3$  mg/mL). This enables their iv application in physiological solutions (PBS) in the UTI model without further needs to develop suitable formulations (see below).

**Stability in Simulated Gastrointestinal Fluids.** To exclude degradation in the gastrointestinal tract prior to absorption, the stability of **1**, **16b**, and **17b** in simulated gastric fluid (sGF) and simulated intestinal fluid (sIF) was determined. All three antagonists proved to be sufficiently stable with more than 80% of the initial concentrations found after two hours.

**Metabolic Stability.** Because the prodrug approach is only applicable when the esters **16a** and **16b** are rapidly metabolically cleaved into the corresponding acids, their propensity to enzymatic hydrolysis by carboxylesterase (CES) was studied. Mammalian CESs are localized in the endoplasmic reticulum of the liver and most other organs.<sup>29</sup> Because of the excellent affinity of the corresponding acids **17a** and

**17b** to FimH, we concentrated our metabolic studies on the ester prodrugs **16a** and **16b**, which were incubated with pooled male mouse liver microsomes to study the hydrolysis and the release of the metabolites. Preliminary experiments involving low substrate concentrations (2  $\mu\text{M}$ ) and a concentration of the microsomal protein of 0.25 mg/mL showed a fast degradation of the ester prodrugs (Figure 6). Addition of the specific CES inhibitor bis(4-nitrophenyl) phosphate (BNPP) prevented ester degradation, suggesting that the metabolic transformation can be attributed to CESs.<sup>49</sup>

On the basis of these *in vitro* results, we also expect fast hydrolysis of the esters *in vivo* at the first liver passage. Current studies are focusing on the kinetic parameters of the enzymatic ester cleavage.

To reach the minimal therapeutic concentration in the bladder (approximately 1  $\mu\text{g}/\text{mL}$ , as estimated from a cell-based infection assay<sup>50</sup>), the FimH antagonists **17a** and **17b** should be efficiently renally eliminated and not further metabolically processed. Therefore, the metabolic fate of the free carboxylic acids **17a** and **17b** was examined. A common method to predict a compound's propensity to phase I metabolism is its incubation with liver microsomes in presence of NADPH.<sup>51</sup> Under these conditions, *in vitro* incubations of the free carboxylic acids **17a** and **17b** with pooled male mouse liver microsomes (0.5 mg microsomal protein/mL) did not show significant compound depletion over a period of 30 min, suggesting a high stability against cytochrome P450 mediated metabolism *in vivo*. However, phase II metabolic pathways such as glucuronidation remain to be studied in details.

**Plasma Protein Binding (PPB).** Compared to the corresponding esters **16** and **21**, the antagonists **17** and **22** exhibit 5–20% lower plasma protein binding, typically in the range of 73–89%. This rather low PPB beneficially influences renal excretion because, in line with the free drug hypothesis,<sup>52</sup> molecules bound to plasma proteins evade metabolism and excretion. However, for a concluding statement, the kinetics of PPB, i.e. association and dissociation rate constants, have to be determined because PPB alone is not necessarily predictive for distribution, metabolism, and clearance.<sup>53,54</sup>

**In Vivo Pharmacokinetics and Treatment Studies.** The two mannose derivatives methyl  $\alpha$ -D-mannoside and *n*-heptyl  $\alpha$ -D-mannoside (**1**) were previously tested in the UTI mouse model.<sup>10,21,22</sup> In all three studies, the FimH antagonists were first preincubated with the bacterial suspension, followed by transurethral inoculation. To efficiently reduce infection,

Antagonist	Compartment	$C_{\max}$ ( $\mu\text{g/mL}$ )	$\text{AUC}_{0-24}$ ( $\mu\text{g} \times \text{h/mL}$ )	PPB
<b>1</b>	plasma	$35 \pm 14.1$	$34.3 \pm 33.3$	81%
	urine	$951.4 \pm 249.6$	$2469.3 \pm 636.4$	
<b>17a</b>	plasma	$34.4 \pm 11.8$	$19.3 \pm 6.2$	73%
	urine	$509.6 \pm 427.5$	$139.9 \pm 118.8$	
<b>17b</b>	plasma	$39.4 \pm 15.7$	$20.8 \pm 7.3$	89%
	urine	$588.4 \pm 218.2$	$209.6 \pm 72.3$	

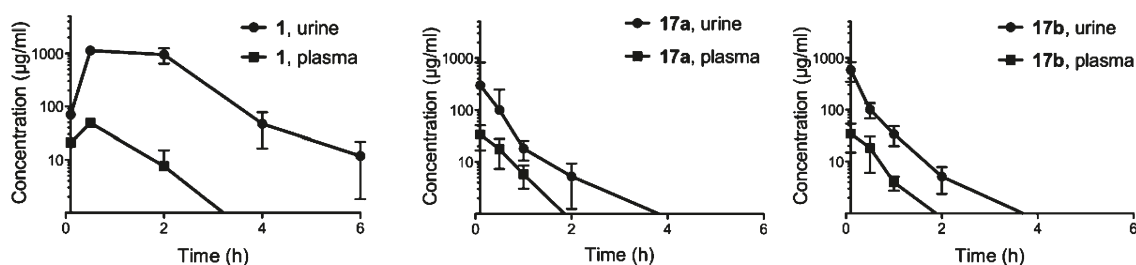


**Figure 7.** Determination of antagonist concentration in urine and plasma after a single iv application of 50 mg/kg. The data (table and graphs) show time-dependent urine and plasma concentrations of **1**, **17a**, and **17b**.

large amounts of methyl  $\alpha$ -D-mannoside had to be applied (up to 1 M).<sup>21</sup> For *n*-heptyl  $\alpha$ -D-mannoside (**1**), an approximately one  $\log_{10}$  unit reduction of bacterial counts in the bladder was reached with lower, but still millimolar, concentration.<sup>10</sup> In the previously presented studies, the FimH antagonists were exclusively instilled into the bladder, which is obviously not suitable for a therapeutic application. The aim of our project was therefore the identification of FimH antagonists suitable for iv or preferably po applications. Before infection studies in a mouse disease model could be performed, the in vivo pharmacokinetic parameters ( $C_{\max}$ , AUC) had to be determined to ensure the antagonists availability in the target organ (bladder).

**Pharmacokinetics of a Single iv Application in C3H/HeN Mice.** Plasma and urine concentrations of the FimH antagonists **1**, **17a**, and **17b** after iv application were determined. With a single dose of 50 mg/kg, the control compound **1** exhibited availability in the bladder over a period of 6 h after administration ( $n = 4$ ), whereas at similar doses, **17a** and **17b** showed lower urine concentrations over a reduced time period (max 2 h) ( $n = 6$ ). In Figure 7, the pharmacokinetic parameters are summarized. Overall, for all three compounds, higher availability of the antagonists in the urine was observed compared to the plasma. Because plasma protein binding is of comparable scale for the three compounds (see Table 1 and Figure 7), it similarly influences urine concentrations.

**Pharmacokinetics of a Single po Application in C3H/HeN Mice.** Aiming for an orally available FimH antagonist, the prodrug **16b** and its metabolite **17b** were tested. Because of the in vitro pharmacokinetic properties of **17b** (Table 1, entry 9), its low oral bioavailability after the administration of a single po dose (50 mg/kg) was not surprising. For the determination of the availability of a similar dose of **16b** at the target organ (bladder), plasma and urine concentrations were determined over a period of 24 h ( $n = 6$ ) (Figure 8). Because **16b** was designed as a prodrug expected to be rapidly

Antagonist applied	Antagonist detected	Compartment	$\text{AUC}_{0-24 \text{ p.o.}}$ ( $\mu\text{g} \times \text{h/mL}$ )
<b>17b</b>	<b>17b</b>	Plasma	n.d.
	<b>17b</b>	Urine	$2.7 \pm 3.2$
<b>16b</b>	<b>16b</b>	Plasma	$1.02 \pm 0.32$
		Urine	$1.89 \pm 0.37$
	<b>17b</b>	Urine	$21.69 \pm 3.88$

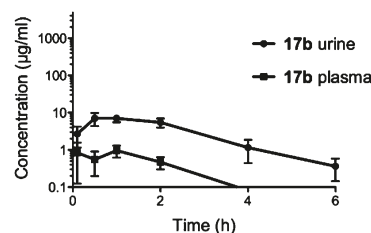


**Figure 8.** Determination of antagonist concentration in urine and plasma after a single po application of 50 mg/kg of antagonists **16b** and **17b**. The data (table and graph) show their time-dependent urine and plasma concentrations. When **17b** was orally applied, its plasma concentration was below the detection level, and only a small portion was present in the urine. However, after the application of the prodrug **16b**, metabolite **17b** was predominantly detected due to fast metabolic hydrolysis of **16b**. However, minor amounts of **16b** are still traceable in plasma as well as urine; nd, not detectable.

hydrolyzed, plasma and urine samples were analyzed not only for **16b** but also for its metabolite **17b**. **16b** was present only in minor concentrations in both plasma and urine. However, although the AUC of metabolite **17b** in urine is reduced by 90% compared to the iv application, its minimal therapeutic concentration can be maintained over a period of 2 to 3 h.

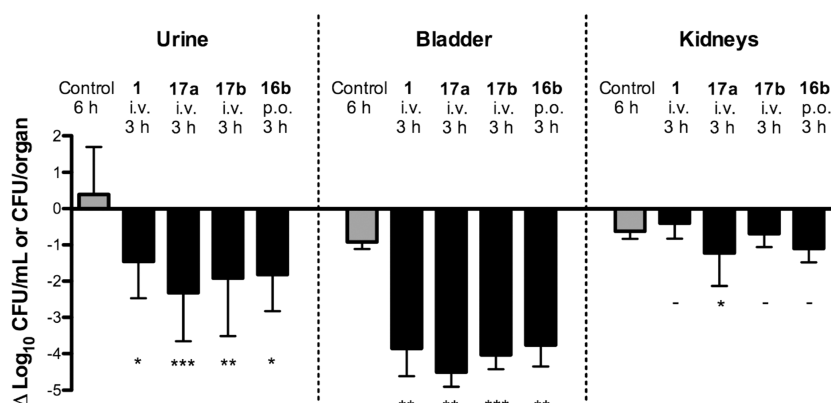


**Figure 9.** Treatment efficacy of the reference compound (**1**) and three FimH antagonists (**17a**, **17b**, **16b**) at a dosage of 50 mg/kg in the UTI mouse model after 3 h of infection, compared to a 6 h infection study ( $n = 6$ ). **1**, **17a**, and **17b** were applied iv into the tail vein, whereas **16b** was applied orally. As baseline (reference), the mean counts of the 3 h infection were subtracted from the results of the tested antagonists and the 6 h control group.  $P$  values were calculated by comparing the treatment groups with the 3 h control group. (\*)  $P < 0.05$ , (\*\*)  $P < 0.01$ , (\*\*\*)  $P < 0.001$ , (-) not significant (determined by Mann–Whitney test).

**UTI Mouse Model: Treatment Study.** Before treatment studies were started, the optimal infection profile was established. A 3 h infection exhibited the highest infection level in the C3H/HeN mouse strain. At longer infection times, e.g. 6 h, the control group showed indeed higher bacterial counts in the urine, however, the bladder and kidney counts already decreased due to self-clearance of the infection in the UTI mouse model.<sup>55</sup> For the in vivo UTI treatment studies (Figure 9), antagonists **1**, **17a**, **17b**, and **16b** were applied followed by infection with UPEC (UTI89). For each antagonist, a group of six animals was used. The animals were sacrificed 3 h after inoculation and urine and homogenized organs (bladder, kidneys) were examined for bacterial counts. The mean value in the untreated reference group ( $n = 6$ ) showed  $1.8 \times 10^6$  CFU/mL in the urine,  $1.4 \times 10^8$  CFU in the bladder and  $9.7 \times 10^6$  CFU in the kidneys. The bar diagram in Figure 9 summarizes the bacterial counts after iv (**1**, **17a**, and **17b**) and po (**16b**) treatment. The baseline represents the values obtained for the control group after 3 h and was used as reference for CFU reductions. **1** showed the lowest inhibition of growth in the urine with  $1.5 \log_{10}$  CFU reduction and an approximately  $4 \log_{10}$  reduction of bacterial counts in the bladder. After iv application of **17a**, a substantial decrease in the bacterial count was obtained ( $> 2 \log_{10}$  CFU reduction in the urine and  $4.5 \log_{10}$  reduction in the bladder). A slightly lower reduction was observed when **17b** was applied iv (a decrease of  $2 \log_{10}$  CFU in the urine and  $4 \log_{10}$  for bladder counts). Interestingly, almost the same reduction of the bacterial count was detected with orally applied **16b**.

In general, urine samples showed higher bacterial counts compared to the bladder. This could be due to the difficulties during urine sampling. We observed that infected C3H/HeN mice void considerably less urine (5–50  $\mu$ L) compared to healthy mice (50–100  $\mu$ L). As a consequence, the lower urine volume leads to a higher concentration of bacteria in the collected urine and therefore to higher bacterial counts compared to the bladder.

In all treated animals, bacterial counts were only marginally reduced in the kidneys. This lower response to the treatment with FimH antagonists is probably due to different bacterial adhesion mechanisms in bladder and kidney. Whereas in the bladder adhesion is mediated by type I pili (via the CRD of FimH), P pili-dependent interactions are crucial for the adhesion in the kidneys.<sup>6</sup>

## Summary and Conclusions

With the objective to develop an oral treatment of urinary tract infections, we have synthesized a series of potent small molecular weight FimH antagonists. Starting from the known antagonist phenyl  $\alpha$ -D-mannopyranoside (**7a**), two equally potent classes of biphenyl  $\alpha$ -D-mannopyranoside, those with an ester function (**16** and **21**) and those with a carboxylate (**17** and **22**) on the terminal aromatic ring, were synthesized. According to their pharmacokinetic properties, the acids **17** and **22** were not expected to be orally absorbed, a prediction that was also confirmed by an in vivo PK study. Therefore, a prodrug approach was envisaged. On the basis of permeation assays (PAMPA and Caco-2), the esters **16** and **22** were expected to exhibit oral availability. Moreover, metabolic studies with mouse liver microsomes proposed fast in vivo hydrolysis of orally applied **16b** to the corresponding carboxylate **17b**. In vivo PK studies in mice finally confirmed the in vitro prediction of a fast renal elimination of **17b** to the target organ, the bladder. When orally applied **16b** was tested in the UTI mouse model, it reduced the colony forming units (CFU) in the urine by 2 orders of magnitude and in the bladder by 4 orders of magnitude. As a result, a low molecular weight FimH antagonist suitable for the oral treatment of urinary tract infections was identified.

However, a number of parameters remain to be improved. Because the solubilities of the esters **16** and **22** are in the low  $\mu$ g/mL range, an iv application was impossible and the suspension in DMSO/1% Tween 80 used for oral dosing is not optimal. In addition, due to fast renal elimination, the minimal therapeutic concentration of **17b** in the bladder could only be maintained for 2–3 h. Because high plasma protein binding was observed, an unfavorable kinetic of dissociation of the active principle from plasma proteins followed by fast renal elimination might be the reason for these findings. An improvement of the corresponding pharmacokinetic parameters should positively influence the duration of action. Furthermore, a detailed analysis of the metabolic pathway of **16b** and its metabolite **17b** will elucidate their overall metabolic fate. Finally, a detailed PK/PD profile in the mouse model will elucidate the full potential of FimH antagonists for the therapy of urinary tract infections (UTI).

## Experimental Section

**General Methods.** NMR spectra were recorded on a Bruker Avance DMX-500 (500 MHz) spectrometer. Assignment of  $^1\text{H}$

and  $^{13}\text{C}$  NMR spectra was achieved using 2D methods (COSY, HSQC, TOCSY). Chemical shifts are expressed in ppm using residual  $\text{CHCl}_3$ ,  $\text{CHD}_2\text{OD}$ , and  $\text{H}_2\text{O}$  as references. Optical rotations were measured using Perkin-Elmer polarimeter 341. Electron spray ionization mass spectra (ESI-MS) were obtained on a Waters micromass ZQ. HRMS analysis were carried out using a Bruker Daltonics microTOF spectrometer equipped with a TOF hexapole detector. Microanalyses were performed at the Department of Chemistry, University of Basel, Switzerland. Microwave-assisted reactions were carried out with a CEM Discover and Explorer. Reactions were monitored by TLC using glass plates coated with silica gel 60 F<sub>254</sub> (Merck) and visualized by using UV light and/or by heating to 140 °C for 5 min with a molybdate solution (a 0.02 M solution of ammonium cerium sulfate dihydrate and ammonium molybdate tetrahydrate in aqueous 10%  $\text{H}_2\text{SO}_4$ ). Column chromatography was performed on a CombiFlash Companion (Teledyne-ISCO, Inc.) using RediSep normal phase disposable flash columns (silica gel). Reversed phase chromatography was performed on LiChroprepRP-18 (Merck, 40–63  $\mu\text{m}$ ). Commercially available reagents were purchased from Fluka, Aldrich, Merck, AKSci, ASDI, or Alfa Aesar. Methanol (MeOH) was dried by refluxing with sodium methoxide and distilled immediately before use. Toluene was dried by filtration over  $\text{Al}_2\text{O}_3$  (Fluka, type 5016 A basic). Dioxane was dried by distillation from sodium/benzophenone.

**4-Bromophenyl 2,3,4,6-Tetra-O-acetyl- $\alpha$ -D-mannopyranoside (14a).** To a stirred solution of **12** (1.17 g, 3.00 mmol) and 4-bromophenol (**13a**, 623 mg, 3.60 mmol) in toluene (12 mL), TMSOTf (65  $\mu\text{L}$ , 0.36 mmol) was added dropwise under argon. The mixture was stirred at rt for 5 h and then diluted with toluene (15 mL) and washed with satd aq  $\text{NaHCO}_3$ . The organic layer was separated, and the aqueous layer was extracted three times with toluene. The combined organic layers were dried over  $\text{Na}_2\text{SO}_4$  and concentrated in vacuo. The residue was purified by flash chromatography on silica (petroleum ether/EtOAc, 19:1 to 1.5:1) to yield **14a** (1.17 g, 74%) as a white solid.

$^1\text{H}$  NMR (500 MHz,  $\text{CDCl}_3$ ):  $\delta$  2.06 (s, 9H, 3 COCH<sub>3</sub>), 2.19 (s, 3H, COCH<sub>3</sub>), 4.06 (m, 2H, H-5, H-6a), 4.27 (dd,  $J$  = 5.6, 12.4 Hz, 1H, H-6b), 5.36 (t,  $J$  = 10.2 Hz, 1H, H-4), 5.43 (dd,  $J$  = 1.8, 3.5 Hz, 1H, H-2), 5.48 (d,  $J$  = 1.7 Hz, 1H, H-1), 5.53 (dd,  $J$  = 3.5, 10.1 Hz, 1H, H-3), 6.98, 7.41 (AA', BB' of AA'BB',  $J$  = 9.0 Hz, 4H, C<sub>6</sub>H<sub>4</sub>).  $^{13}\text{C}$  NMR (125 MHz,  $\text{CDCl}_3$ ):  $\delta$  20.71, 20.73, 20.74, 20.9 (4 COCH<sub>3</sub>), 62.1 (C-6), 65.9 (C-4), 68.8 (C-3), 69.2 (C-2), 69.3 (C-5), 95.9 (C-1), 115.6, 118.3, 132.6, 154.7 (6C, C<sub>6</sub>H<sub>4</sub>), 170.0 (4C, 4 CO).

**4-Bromo-2-chlorophenyl 2,3,4,6-tetra-O-acetyl- $\alpha$ -D-mannopyranoside (14b).** According to the procedure described for **14a**, compound **12** (2.38 g, 4.84 mmol) and 4-bromo-2-chlorophenol (**13b**, 1.20 g, 5.80 mmol) were treated with TMSOTf (107 mg, 0.484 mmol) to yield **14b** (1.54 g, 59%) as a white solid.

$[\alpha]_{\text{D}} +60.6$  (c 0.40,  $\text{CHCl}_3$ ).  $^1\text{H}$  NMR (500 MHz,  $\text{CDCl}_3$ ):  $\delta$  2.02, 2.04, 2.18 (3s, 12H, 4 COCH<sub>3</sub>), 4.05 (dd,  $J$  = 2.3, 12.2 Hz, 1H, H-6a), 4.10 (ddd,  $J$  = 2.7, 5.3, 9.6 Hz, 1H, H-5), 4.24 (dd,  $J$  = 5.4, 12.2 Hz, 1H, H-6b), 5.35 (t,  $J$  = 10.1 Hz, 1H, H-4), 5.48 (m, 2H, H-1, H-2), 5.56 (dd,  $J$  = 3.2, 10.1 Hz, 1H, H-3), 7.03 (d,  $J$  = 8.8 Hz, 1H, C<sub>6</sub>H<sub>3</sub>), 7.30 (dd,  $J$  = 2.4, 8.8 Hz, 1H, C<sub>6</sub>H<sub>3</sub>), 7.53 (d,  $J$  = 2.4 Hz, 1H, C<sub>6</sub>H<sub>3</sub>).  $^{13}\text{C}$  NMR (125 MHz,  $\text{CDCl}_3$ ):  $\delta$  20.9, 21.1 (4C, 4 COCH<sub>3</sub>), 62.3 (C-6), 65.9 (C-4), 68.9 (C-3), 69.4 (C-2), 70.1 (C-5), 96.9 (C-1), 115.9, 118.4, 125.7, 130.8, 133.3, 150.6 (C<sub>6</sub>H<sub>3</sub>), 169.9, 170.0, 170.1, 170.7 (4 CO). ESI-MS calcd for  $\text{C}_{20}\text{H}_{22}\text{BrClNaO}_{10} [\text{M} + \text{Na}]^+$  559.0; found 559.0; Anal. Calcd for  $\text{C}_{20}\text{H}_{22}\text{BrClO}_{10}$ : C 44.67, H 4.12, Found: C 45.08, H 4.14.

**Methyl 4'-(2,3,4,6-Tetra-O-acetyl- $\alpha$ -D-mannopyranosyloxy)-biphenyl-4-carboxylate (15a).** A Schlenk tube was charged with **14a** (503 mg, 1.00 mmol), 4-methoxycarbonylphenylboronic acid (224 mg, 1.24 mmol), S-Phos (20.5 mg, 0.05 mmol), cesium carbonate (1.17 g, 3.6 mmol),  $\text{Pd}_2(\text{dba})_3$  (10.4 mg, 0.01 mmol), and a stirring bar. The tube was closed with a rubber septum and was evacuated and flushed with argon. This procedure was

repeated once, and then freshly degassed dioxane (5 mL) was added under a stream of argon. The reaction tube was quickly sealed and the contents were stirred at 80 °C overnight. The reaction mixture was cooled to rt, diluted with EtOAc (10 mL), washed with satd aq  $\text{NaHCO}_3$  (5 mL) and brine (5 mL), and dried over  $\text{Na}_2\text{SO}_4$ . The solvents were removed in vacuo, and the residue was purified by flash chromatography on silica (petroleum ether/EtOAc, 3:1 to 3:2) to give **15a** (474 mg, 85%) as a white solid.

$[\alpha]_{\text{D}} +80.8$  (c 1.00,  $\text{CHCl}_3$ ).  $^1\text{H}$  NMR (500 MHz,  $\text{CDCl}_3$ ):  $\delta$  2.02, 2.03, 2.04, 2.19 (4s, 12H, COCH<sub>3</sub>), 3.91 (s, 3H, OCH<sub>3</sub>), 4.08 (m, 2H, H-6a, H-5), 4.27 (dd,  $J$  = 5.2, 12.2 Hz, 1H, H-6b), 5.37 (t,  $J$  = 10.1 Hz, 1H, H-4), 5.45 (dd,  $J$  = 1.8, 3.4 Hz, 1H, H-2), 5.56 (m, 2H, H-1, H-3), 7.16 (AA' of AA'BB',  $J$  = 8.7 Hz, 2H, C<sub>6</sub>H<sub>4</sub>), 7.57 (m, 4H, C<sub>6</sub>H<sub>4</sub>), 8.07 (BB' of AA'BB',  $J$  = 8.4 Hz, 2H, C<sub>6</sub>H<sub>4</sub>).  $^{13}\text{C}$  NMR (125 MHz,  $\text{CDCl}_3$ ):  $\delta$  20.74, 20.75, 20.77, 21.0 (4 COCH<sub>3</sub>), 52.2 (OCH<sub>3</sub>), 62.1 (C-6), 65.9 (C-4), 68.9 (C-3), 69.3, 69.4 (C-2, C-5), 95.8 (C-1), 116.9, 126.7, 128.5, 128.7, 130.2, 134.8, 144.8, 155.7 (12C, 2 C<sub>6</sub>H<sub>4</sub>), 167.0, 169.8, 170.0, 170.1, 170.6 (5 CO). ESI-MS calcd for  $\text{C}_{28}\text{H}_{30}\text{NaO}_{12} [\text{M} + \text{Na}]^+$  581.2; found 581.0.

**Methyl 4'-(2,3,4,6-Tetra-O-acetyl- $\alpha$ -D-mannopyranosyloxy)-3'-chlorobiphenyl-4-carboxylate (15b).** A microwave tube was charged with bromide **14b** (720 mg, 1.34 mmol), 4-methoxycarbonylphenylboronic acid (289 mg, 1.61 mmol), cesium carbonate (1.31 g, 4.02 mmol), and  $\text{Pd}(\text{PPh}_3)_4$  (77.4 mg, 0.067 mmol). The tube was sealed with a Teflon septum, evacuated through a needle, and flushed with argon. Degassed dioxane (1.5 mL) was added and the closed tube was degassed in an ultrasonic bath for 15 min, flushed again with argon for 20 min, and exposed to microwave irradiation at 120 °C for 500 min. The solvent was evaporated in vacuo. The residue was dissolved in DCM (10 mL), washed with brine (2  $\times$  10 mL), dried over  $\text{Na}_2\text{SO}_4$ , and concentrated in vacuo. The residue was purified by flash chromatography on silica (petroleum ether/EtOAc, 5:1 to 0.5:1) to yield **15b** (333 mg, 42%) as a white foam.

$[\alpha]_{\text{D}} +66.3$  (c 1.06,  $\text{CHCl}_3$ ).  $^1\text{H}$  NMR (500 MHz,  $\text{CDCl}_3$ ):  $\delta$  2.03, 2.06, 2.20 (3s, 12H, COCH<sub>3</sub>), 3.92 (s, 3H, OCH<sub>3</sub>), 4.08 (dd,  $J$  = 2.4, 12.3 Hz, 1H, H-6a), 4.17 (m, 1H, H-5), 4.28 (dd,  $J$  = 5.4, 12.3 Hz, 1H, H-6b), 5.39 (t,  $J$  = 10.6 Hz, 1H, H-4), 5.54 (dd,  $J$  = 1.9, 3.4 Hz, 1H, H-2), 5.59 (d,  $J$  = 1.8 Hz, 1H, H-1), 5.62 (dd,  $J$  = 3.5, 10.1 Hz, 1H, H-3), 7.24 (s, 1H, C<sub>6</sub>H<sub>3</sub>), 7.44 (dd,  $J$  = 2.2, 8.5 Hz, 1H, C<sub>6</sub>H<sub>3</sub>), 7.57 (AA' of AA'BB',  $J$  = 8.5 Hz, 2H, C<sub>6</sub>H<sub>4</sub>), 7.65 (d,  $J$  = 2.2 Hz, 1H, C<sub>6</sub>H<sub>3</sub>), 8.08 (BB' of AA'BB',  $J$  = 8.5 Hz, 2H, C<sub>6</sub>H<sub>4</sub>).  $^{13}\text{C}$  NMR (125 MHz,  $\text{CDCl}_3$ ):  $\delta$  20.9, 21.0, 21.1 (4C, 4 COCH<sub>3</sub>), 52.5 (OCH<sub>3</sub>), 62.3 (C-6), 66.0 (C-4), 69.0 (C-3), 69.5 (C-2), 70.0 (C-5), 96.8 (C-1), 117.4, 126.7, 126.9, 129.5, 130.5, 136.4, 143.6, 151.3 (12C, C<sub>6</sub>H<sub>3</sub>, C<sub>6</sub>H<sub>4</sub>), 167.0, 169.9, 170.0, 170.2, 170.7 (5 CO). ESI-MS calcd for  $\text{C}_{28}\text{H}_{29}\text{ClNaO}_{12} [\text{M} + \text{Na}]^+$  615.1; found 615.2. Anal. Calcd for  $\text{C}_{28}\text{H}_{29}\text{ClO}_{12}$ : C 56.71, H 4.93. Found: C 56.79, H 4.92.

**Methyl 4'-( $\alpha$ -D-Mannopyranosyloxy)-biphenyl-4-carboxylate (16a).**<sup>17d</sup> To a solution of **15a** (170 mg, 0.304 mmol) in MeOH (3 mL) was added freshly prepared 1 M NaOMe in MeOH (100  $\mu\text{L}$ ) under argon. The mixture was stirred at rt until the reaction was complete (monitored by TLC), then neutralized with Amberlyst-15 ( $\text{H}^+$ ) ion-exchange resin, filtered, and concentrated in vacuo. The residue was purified by reversed-phase chromatography (RP-18,  $\text{H}_2\text{O}/\text{MeOH}$ , 1:0–1:1) to give **16a** (90 mg, 76%) as white solid.

$[\alpha]_{\text{D}} +82.8$  (c 0.2, MeOH).  $^1\text{H}$  NMR (500 MHz,  $\text{CD}_3\text{OD}$ ):  $\delta$  3.62 (m, 1H, H-5), 3.72 (m, 3H, H-4, H-6a, H-6b), 3.92 (m, 4H, H-3, OCH<sub>3</sub>), 4.03 (s, 1H, H-2), 5.55 (s, 1H, H-1), 7.24 (AA' of AA'BB',  $J$  = 8.0 Hz, 2H, C<sub>6</sub>H<sub>4</sub>), 7.64 (AA' of AA'BB',  $J$  = 7.5 Hz, 2H, C<sub>6</sub>H<sub>4</sub>), 7.71 (BB' of AA'BB',  $J$  = 8.0 Hz, 2H, C<sub>6</sub>H<sub>4</sub>), 8.07 (BB' of AA'BB',  $J$  = 7.5 Hz, 2H, C<sub>6</sub>H<sub>4</sub>).  $^{13}\text{C}$  NMR (125 MHz,  $\text{CD}_3\text{OD}$ ):  $\delta$  52.6 (OCH<sub>3</sub>), 62.7 (C-6), 68.3 (C-4), 72.0 (C-2), 72.4 (C-3), 75.5 (C-5), 100.1 (C-1), 118.2, 127.7, 131.1, 135.1, 146.6, 158.2, 160.3 (12C, 2 C<sub>6</sub>H<sub>4</sub>), 166.1 (CO). HR-MS calcd for  $\text{C}_{20}\text{H}_{22}\text{NaO}_8 [\text{M} + \text{Na}]^+$  413.1212; found 413.1218.

**Methyl 3'-Chloro-4'-( $\alpha$ -D-mannopyranosyloxy)-biphenyl-4-carboxylate (16b).** According to the procedure described for **16a**, compound **16b** was prepared from **15b** (764 mg, 1.29 mmol). Yield: 69 mg, 12%.

$[\alpha]_D +97.4$  (*c* 1.01, MeOH).  $^1\text{H NMR}$  (500 MHz,  $\text{CD}_3\text{OD}$ ):  $\delta$  3.64 (m, 1H, H-5), 3.72 (m, 1H, H-6a), 3.78 (m, 2H, H-4, H-6b), 3.91 (s, 3H,  $\text{OCH}_3$ ), 4.00 (dd,  $J=3.4, 9.5$  Hz, 1H, H-3), 4.11 (dd,  $J=1.8, 3.1$  Hz, 1H, H-2), 5.60 (d,  $J=1.1$  Hz, 1H, H-1), 7.46 (d,  $J=8.6$  Hz, 1H,  $\text{C}_6\text{H}_3$ ), 7.58 (dd,  $J=2.2, 8.6$  Hz, 1H,  $\text{C}_6\text{H}_3$ ), 7.69 (AA' of AA'BB',  $J=8.4$  Hz, 2H,  $\text{C}_6\text{H}_4$ ), 7.72 (d,  $J=2.2$  Hz, 1H,  $\text{C}_6\text{H}_3$ ), 8.08 (BB' of AA'BB',  $J=8.4$  Hz, 2H,  $\text{C}_6\text{H}_4$ ).  $^{13}\text{C NMR}$  (125 MHz,  $\text{CD}_3\text{OD}$ ):  $\delta$  52.7 ( $\text{OCH}_3$ ), 62.8 (C-6), 68.3 (C-4), 71.9 (C-2), 72.5 (C-3), 76.2 (C-5), 100.8 (C-1), 118.7, 125.58, 127.8, 127.9, 129.9, 130.3, 131.3, 136.4, 145.3, 153.5 (12C,  $\text{C}_6\text{H}_3$ ,  $\text{C}_6\text{H}_4$ ), 168.4 (CO). HR-MS calcd for  $\text{C}_{20}\text{H}_{21}\text{ClNaO}_8$  [ $\text{M} + \text{Na}$ ] $^+$  447.0823; found 447.082.

**Sodium 4'-( $\alpha$ -D-Mannopyranosyloxy)-biphenyl-4-carboxylate (17a).** To a solution of **15a** (228 mg, 0.408 mmol) in MeOH (6.0 mL) was added 1 M NaOMe in MeOH (60  $\mu\text{L}$ ) at rt. The reaction mixture was stirred at rt for 4 h, and then NaOH (82 mg) in water (6 mL) was added and stirring was continued at rt overnight. The reaction mixture was concentrated in vacuo, and the residue was purified by reversed-phase chromatography (RP-18,  $\text{H}_2\text{O}/\text{MeOH}$ , 1:0–1:1) to afford **17a** (96 mg, 63%) as a white solid.

$[\alpha]_D +103$  (*c* 0.10, MeOH).  $^1\text{H NMR}$  (500 MHz,  $\text{CD}_3\text{OD}$ ):  $\delta$  3.60 (m, 1H, H-5), 3.72 (m, 3H, H-6a, H-6b, H-4), 3.89 (dd,  $J=3.4, 9.5$  Hz, 1H, H-3), 4.00 (dd,  $J=1.8, 3.3$  Hz, 1H, H-2), 5.51 (s, 1H, H-1), 7.19, 7.60 (AA', BB' of AA'BB',  $J=8.7$  Hz, 4H,  $\text{C}_6\text{H}_4$ ), 8.01 (d,  $J=8.2$  Hz, 2H,  $\text{C}_6\text{H}_4$ ), 8.46 (s, 2H,  $\text{C}_6\text{H}_4$ ).  $^{13}\text{C NMR}$  (125 MHz,  $\text{CD}_3\text{OD}$ ):  $\delta$  63.2 (C-6), 68.9 (C-4), 72.6 (C-2), 73.0 (C-3), 76.1 (C-5), 100.7 (C-1), 118.7, 128.0, 129.9, 131.8 (12C, 2  $\text{C}_6\text{H}_4$ ). HR-MS calcd for  $\text{C}_{19}\text{H}_{20}\text{NaO}_8$  [ $\text{M} + \text{H}$ ] $^+$  399.1056; found 399.1052.

**Sodium 3'-Chloro-4'-( $\alpha$ -D-mannopyranosyloxy)-biphenyl-4-carboxylate (17b).** To a solution of **15b** (380 mg, 0.641 mmol) in MeOH (10 mL) was added 1 M NaOMe in MeOH (300  $\mu\text{L}$ ). After stirring at rt for 24 h, 0.5 M aq NaOH (18 mL) was added and stirring continued for another 24 h. The solution was concentrated in vacuo and the residue was purified by reversed-phase chromatography (RP-18,  $\text{H}_2\text{O}/\text{MeOH}$ , 1:0–1:1) to yield **17b** (222 mg, 80%) as a white solid.

$[\alpha]_D +61.6$  (*c* 1.00,  $\text{H}_2\text{O}$ ).  $^1\text{H NMR}$  (500 MHz,  $\text{D}_2\text{O}$ ):  $\delta$  3.66 (m, 1H, H-5), 3.73 (m, 2H, H-6a, H-6b), 3.79 (t,  $J=9.8$  Hz, 1H, H-4), 4.07 (dd,  $J=3.4, 9.8$  Hz, 1H, H-3), 4.14 (d,  $J=1.4$  Hz, 1H, H-2), 5.47 (bs, 1H, H-1), 7.04 (d,  $J=8.6$  Hz, 1H,  $\text{C}_6\text{H}_3$ ), 7.24 (d,  $J=8.6$  Hz, 1H,  $\text{C}_6\text{H}_3$ ), 7.37 (AA' of AA'BB',  $J=8.1$  Hz, 2H,  $\text{C}_6\text{H}_4$ ), 7.41 (bs, 1H,  $\text{C}_6\text{H}_3$ ), 7.86 (BB' of AA'BB',  $J=8.1$  Hz, 2H,  $\text{C}_6\text{H}_4$ ).  $^{13}\text{C NMR}$  (125 MHz,  $\text{D}_2\text{O}$ ):  $\delta$  60.6 (C-6), 66.5 (C-4), 69.0 (C-2), 70.5 (C-3), 73.9 (C-5), 98.6 (C-1), 117.5, 123.9, 126.2, 126.4, 128.4, 129.6, 135.2, 135.3, 141.0, 150.4 (12C,  $\text{C}_6\text{H}_3$ ,  $\text{C}_6\text{H}_4$ ), 175.0 (CO). HR-MS calcd for  $\text{C}_{19}\text{H}_{18}\text{ClNaO}_8$  [ $\text{M} + \text{H}$ ] $^+$  433.0666; found 433.0670.

**Competitive Binding Assay.** A recombinant protein consisting of the CRD of FimH linked with a thrombin cleavage site to a 6His-tag (FimH-CRD-Th-6His) was expressed in *E. coli* strain HM125 and purified by affinity chromatography.<sup>23</sup> To determine the affinity of the various FimH antagonists, a competitive binding assay described previously<sup>23</sup> was applied. Microtiter plates (F96 MaxiSorp, Nunc) were coated with 100  $\mu\text{L}/\text{well}$  of a 10  $\mu\text{g}/\text{mL}$  solution of FimH-CRD-Th-6His in 20 mM HEPES, 150 mM NaCl, and 1 mM  $\text{CaCl}_2$ , pH 7.4 (assay buffer) overnight at 4  $^\circ\text{C}$ . The coating solution was discarded and the wells were blocked with 150  $\mu\text{L}/\text{well}$  of 3% BSA in assay buffer for 2 h at 4  $^\circ\text{C}$ . After three washing steps with assay buffer (150  $\mu\text{L}/\text{well}$ ), a 4-fold serial dilution of the test compound (50  $\mu\text{L}/\text{well}$  in assay buffer containing 5% DMSO and streptavidin-peroxidase coupled Man- $\alpha$ (1-3)-[Man- $\alpha$ (1-6)]-Man- $\beta$ (1-4)-GlcNAc- $\beta$ (1-4)-GlcNAc $\beta$  polyacrylamide (TM-PAA) polymer (50  $\mu\text{L}/\text{well}$  of a 0.5  $\mu\text{g}/\text{mL}$  solution) were added. On each individual microtiter plate, *n*-heptyl  $\alpha$ -D-mannopyranoside (**1**) was tested in parallel.

The plates were incubated for 3 h at 25  $^\circ\text{C}$  and 350 rpm and then carefully washed four times with 150  $\mu\text{L}/\text{well}$  assay buffer. After the addition of 100  $\mu\text{L}/\text{well}$  of 2,2'-azino-di-(3-ethylbenzthiazoline-6-sulfonic acid) (ABTS)-substrate, the colorimetric reaction was allowed to develop for 4 min and then stopped by the addition of 2% aqueous oxalic acid before the optical density (OD) was measured at 415 nm on a microplate-reader (Spectramax 190, Molecular Devices, California, USA). The  $\text{IC}_{50}$  values of the compounds tested in duplicates were calculated with prism software (GraphPad Software, Inc., La Jolla, California, USA). The  $\text{IC}_{50}$  defines the molar concentration of the test compound that reduces the maximal specific binding of TM-PAA polymer to FimH-CRD by 50%. The relative  $\text{IC}_{50}$  ( $\text{rIC}_{50}$ ) is the ratio of the  $\text{IC}_{50}$  of the test compound to the  $\text{IC}_{50}$  of *n*-heptyl  $\alpha$ -D-mannopyranoside (**1**).

**Selectivity for FimH vs Mannose-Binding Protein and DC-SIGN.** Recombinant FimH-CRD-Th-6His (10  $\mu\text{g}/\text{mL}$ ), DC-SIGN-CRD-Fc-IgG<sup>39</sup> (2.5  $\mu\text{g}/\text{mL}$ ), and mannose-binding protein<sup>42</sup> (MBP, 10  $\mu\text{g}/\text{mL}$ , R&D Systems, Minneapolis, MN) were each diluted in assay buffer (20 mM HEPES, pH 7.4, 150 mM NaCl, and 10 mM  $\text{CaCl}_2$ ) and were coated on microtiter plates (F96 MaxiSorp, Nunc) with 100  $\mu\text{L}/\text{well}$  overnight at 4  $^\circ\text{C}$ . The further steps were performed as described above.

**Aggregometry Assay.** The aggregometry assay was carried out as previously described.<sup>33</sup> In short, the percentage of aggregation of *E. coli* UTI89 with guinea pig erythrocytes (GPE) was quantitatively determined by measuring the optical density at 740 nm and 37  $^\circ\text{C}$  under stirring at 1000 rpm using an APACT 4004 aggregometer (Endotell AG, Allschwil, Switzerland). Bacteria were cultivated as described below (see in vivo models). GPE were separated from guinea pig blood (Charles River Laboratories, Sulzfeld, Germany) using Histopaque (density of 1.077 g/mL at 24  $^\circ\text{C}$ , Sigma-Aldrich, Buchs, Switzerland). Prior to the measurements, the cell densities of *E. coli* and GPE were adjusted to an  $\text{OD}_{600}$  of 4, corresponding to  $1.9 \times 10^8$  CFU/mL and  $2.2 \times 10^6$  cells/mL, respectively. For the calibration of the instrument, the aggregation of protein-poor plasma (PPP) using PBS alone was set as 100% and the aggregation of protein-rich plasma (PRP) using GPE as 0%. After calibration, measurements were performed with 250  $\mu\text{L}$  of GPE and 50  $\mu\text{L}$  of bacterial suspension and the aggregation monitored over 600 s. After the aggregation phase of 600 s, 25  $\mu\text{L}$  of antagonist in PBS was added to each cuvette and disaggregation was monitored for 1400 s. UTI89  $\Delta\text{fimA-H}$  was used as negative control.

**Determination of the Pharmacokinetic Parameters. Materials.** Dimethyl sulfoxide (DMSO), 1-octanol, pepsin, pancreatin, reduced nicotinamide adenine dinucleotide phosphate (NADPH), Dulbecco's Modified Eagle's Medium (DMEM) high glucose, and bis(4-nitrophenyl) phosphate (BNPP) were purchased from Sigma-Aldrich (Sigma-Aldrich, St. Louis MO, USA). PAMPA System Solution, GIT-0 Lipid Solution, and Acceptor Sink Buffer were ordered from plon (plon, Woburn MA, USA). L-Glutamine-200 mM (100 $\times$ ) solution, MEM nonessential amino acid (MEM-NEAA) solution, fetal bovine serum (FBS), and DMEM without sodium pyruvate and phenol red were bought from Invitrogen (Invitrogen, Carlsbad CA, USA). Human plasma was bought from Biopredic (Biopredic, Rennes, France) and acetonitrile (MeCN) from Acros (Acros Organics, Geel, Belgium). Pooled male mouse liver microsomes were purchased from BD Bioscience (BD Bioscience, Woburn, MA, USA). Magnesium chloride was bought from Fluka (Fluka Chemie GmbH, Buchs, Switzerland). Tris(hydroxymethyl)-aminomethane (TRIS) was obtained from AppliChem (AppliChem, Darmstadt, Germany). The Caco-2 cells were kindly provided by Prof G. Imanidis, FHNW, Muttentz, and originated from the American Type Culture Collection (Rockville, MD, USA).

**log  $D_{7.4}$  Determination.** The in silico prediction tool ALOGPS 2.1<sup>56</sup> was used to estimate the log *P* values of the compounds. Depending on these values, the compounds were classified into three categories: hydrophilic compounds (log *P*

**Table 2**

compound type	log <i>P</i>	ratios (1-octanol:buffer)
hydrophilic	< 0	30:140, 40:130
moderately lipophilic	0–1	70:110, 110:70
lipophilic	> 1	3:180, 4:180

below zero), moderately lipophilic compounds (log *P* between zero and one) and lipophilic compounds (log *P* above one). For each category, two different ratios (volume of 1-octanol to volume of buffer) were defined as experimental parameters (Table 2):

Equal amounts of phosphate buffer (0.1 M, pH 7.4) and 1-octanol were mixed and shaken vigorously for 5 min to saturate the phases. The mixture was left until separation of the two phases occurred, and the buffer was retrieved. Stock solutions of the test compounds were diluted with buffer to a concentration of 1 μM. For each compound, six determinations, i.e., three determinations per 1-octanol:buffer ratio, were performed in different wells of a 96-well plate. The respective volumes of buffer containing analyte (1 μM) were pipetted to the wells and covered by saturated 1-octanol according to the chosen volume ratio. The plate was sealed with aluminum foil, shaken (1350 rpm, 25 °C, 2 h) on a Heidolph Titramax 1000 plate-shaker (Heidolph Instruments GmbH & Co. KG, Schwabach, Germany) and centrifuged (2000 rpm, 25 °C, 5 min, 5804 R Eppendorf centrifuge, Hamburg, Germany). The aqueous phase was transferred to a 96-well plate for analysis by liquid chromatography–mass spectrometry (LC-MS).

log *D*<sub>7.4</sub> was calculated from the 1-octanol:buffer ratio (*o:b*), the initial concentration of the analyte in buffer (1 μM), and the concentration of the analyte in buffer (*c*<sub>B</sub>) with equilibration:

$$\log D_{7.4} = \log \left( \frac{1 \mu\text{M} - c_B}{c_B} \times \frac{1}{o:b} \right)$$

The average of the three log *D*<sub>7.4</sub> values per 1-octanol:buffer ratio was calculated. If the two mean values obtained for a compound did not differ by more than 0.1 unit, the results were accepted.

**Parallel Artificial Membrane Permeation Assay (PAMPA).** log *P*<sub>e</sub> was determined in a 96-well format with the PAMPA<sup>30</sup> permeation assay. For each compound, measurements were performed at three pH values (5.0, 6.2, 7.4) in quadruplicates. For this purpose, 12 wells of a deep well plate, i.e., four wells per pH value, were filled with 650 μL of System Solution. Samples (150 μL) were withdrawn from each well to determine the blank spectra by UV-spectroscopy (SpectraMax 190, Molecular Devices, Silicon Valley CAa, USA). Then, analyte dissolved in DMSO was added to the remaining System Solution to yield 50 μM solutions. To exclude precipitation, the optical density was measured at 650 nm, with 0.01 being the threshold value. Solutions exceeding this threshold were filtrated. Afterward, samples (150 μL) were withdrawn to determine the reference spectra. A further 200 μL were transferred to each well of the donor plate of the PAMPA sandwich (pIon, Woburn MA, USA, P/N 110 163). The filter membranes at the bottom of the acceptor plate were impregnated with 5 μL of GIT-0 Lipid Solution and 200 μL of Acceptor Sink Buffer were filled into each acceptor well. The sandwich was assembled, placed in the GutBox, and left undisturbed for 16 h. Then, it was disassembled and samples (150 μL) were transferred from each donor and acceptor well to UV-plates. Quantification was performed by both UV-spectroscopy and LC-MS. log *P*<sub>e</sub> values were calculated with the aid of the PAMPA Explorer Software (pIon, version 3.5).

**Colorectal Adenocarcinoma Cells (Caco-2 Cells) Permeation Assay.** The cells were cultivated in tissue culture flasks (BD Biosciences, Franklin Lakes NJ, USA) with DMEM high glucose medium, containing 1% L-glutamine solution, 1% MEM-NEAA solution, and 10% FBS. The cells were kept at

37 °C in humidified air containing 8% CO<sub>2</sub>, and the medium was changed every second to third day. When approximately 90% confluence was reached, the cells were split in a 1:10 ratio and distributed to new tissue culture flasks. At passage numbers between 60 and 65, they were seeded at a density of 5.33 × 10<sup>5</sup> cells per well to Transwell 6-well plates (Corning Inc., Corning NY, USA) with 2.5 mL of culture medium in the basolateral compartment and 1.5 mL (days 1–10) or 1.8 mL (from day 10 on) in the basolateral compartment. The medium was renewed on alternate days. Experiments were performed between days 19 and 21 postseeding. DMEM without sodium pyruvate and phenol red was used as transport medium for experiments. Previous to the experiment, the integrity of the Caco-2 monolayers was evaluated by measuring the transepithelial resistance (TEER) in transport medium (37 °C) with an Endohm tissue resistance instrument (World Precision Instruments Inc., Sarasota, FL, USA). Only wells with TEER values higher than 300 Ωcm<sup>2</sup> were used. Experiments were performed in triplicates. Transport medium (10 μL) from the apical compartments of three wells were replaced by the same volume of compound stock solutions (10 mM). The Transwell plate was then shaken (250 rpm) in the incubator. Samples (100 μL) were withdrawn after 5, 15, 30, 60, and 120 min from the basolateral compartment and concentrations were analyzed by HPLC. Apparent permeability coefficients (*P*<sub>app</sub>) were calculated according to the following equation

$$P_{\text{app}} = \frac{dQ}{dt} \times \frac{1}{A \times c_0}$$

where *dQ/dt* is the permeability rate, *A* the surface area of the monolayer, and *c*<sub>0</sub> the initial concentration in the donor compartment.<sup>31</sup> After the experiment, TEER values were assessed again for every well and results from wells with values below 300 Ωcm<sup>2</sup> were discarded.

**p*K*<sub>a</sub> Values.** The p*K*<sub>a</sub> values were determined as described elsewhere.<sup>45</sup> Briefly, the pH of a sample solution was gradually changed and the chemical shift of protons adjacent to ionizable centers was monitored by <sup>1</sup>H nuclear magnetic resonance (NMR) spectroscopy. The shift was plotted against the pH of the respective sample, and the p*K*<sub>a</sub> was read out from the inflection point of the resulting sigmoidal curve.

**Plasma Protein Binding (PPB).** The dialysis membranes (HTDialysis LCC, Gales Ferry, CT, USA; MWCO 12–14 K) were prepared according to company instructions. The human plasma was centrifuged (5800 rpm, 25 °C, 10 min), the pH of the centrifugate (without floating plasma lipids) was adjusted to 7.5, and analyte was added to yield 10 μM solutions. Equal volumes (150 μL) of phosphate buffer (0.1 M, pH 7.5) and analyte-containing plasma were transferred to the separated compartments of the assembled 96-well high throughput dialysis block (HTDialysis LCC, Gales Ferry, CT, USA). Measurements were performed in triplicates. The plate was covered with a sealing film and incubated (5 h, 37 °C). Buffer and plasma compartment were processed separately. From the buffer compartments, 90 μL were withdrawn and 10 μL of blank plasma were added. From the plasma compartments, 10 μL were withdrawn and 90 μL of blank buffer were added. After protein precipitation with 300 μL ice-cooled MeCN, the solutions were mixed, centrifuged (3600 rpm, 4 °C, 11 min), and 50 μL of the supernatant were retrieved. Analyte concentrations were determined by LC-MS. The fraction bound (*f*<sub>b</sub>) was calculated as follows:

$$f_b = 1 - \frac{c_b}{c_p}$$

where *c*<sub>b</sub> is the concentration in the buffer and *c*<sub>p</sub> the concentration in the plasma compartment. Values were accepted if the recovery of analyte was between 80 and 120%.

**Thermodynamic Solubility.** Microanalysis tubes (Labo-Tech J. Stofer LTS AG, Muttenz, Switzerland) were charged with



1 mg of solid substance and 250  $\mu\text{L}$  of phosphate buffer (50 mM, pH 6.5). The samples were briefly shaken by hand and then sonicated for 15 min and vigorously shaken (600 rpm, 25 °C, 2 h) on a Eppendorf Thermomixer Comfort. Afterward, the samples were left undisturbed for 24 h. After measuring the pH, the saturated solutions were filtered through a filtration plate (MultiScreen HTS, Millipore, Billerica MA, USA) by centrifugation (1500 rpm, 25 °C, 3 min). Prior to concentration determination by LC-MS, the filtrates were diluted (1:1, 1:10 and 1:100 or, if the results were outside of the calibration range, 1:1000 and 1:10000). The calibration was based on six values ranging from 0.1 to 10  $\mu\text{g}/\text{mL}$ .

**Stability in Simulated Gastrointestinal Fluids.** Simulated gastric fluid (sGF) and simulated intestinal fluid (sIF) were prepared according to the United States Pharmacopeia (USP 28). sGF contained sodium chloride (200 mg), pepsin (320 mg), and 37% aq HCl (0.7 mL) in bidistilled water (100 mL). sIF consisted of monopotassium phosphate (680 mg), 0.2 M NaOH (7.7 mL), and pancreatin (1 g) in bidistilled water (100 mL). sIF was adjusted to pH 6 by adding 0.2 M NaOH. sGF and sIF were preheated (37 °C), and the compounds were added to yield 10  $\mu\text{M}$  solutions. Incubations were performed on a Eppendorf Thermomixer Comfort (500 rpm, 37 °C). Before starting the experiment ( $t = 0$  min) and after an incubation time of 15, 30, 60, and 120 min, samples (20  $\mu\text{L}$ ) were withdrawn, precipitated with ice-cooled MeCN, and centrifuged (3600 rpm, 4 °C, 10 min). The concentrations of analyte in the supernatant were analyzed by LC-MS. Stability was expressed as percentage remaining compound relative to the initial concentration.

**In Vitro Metabolism: Ester Hydrolysis.** Incubations were performed in a 96-well format on a Eppendorf Thermomixer Comfort. Each compound was incubated with a reaction mixture (270  $\mu\text{L}$ ) consisting of pooled male mouse liver microsomes in the presence of TRIS buffer (0.1 M, pH 7.4) and  $\text{MgCl}_2$  (2 mM). After preheating (37 °C, 500 rpm, 10 min), the incubation was initiated by adding 30  $\mu\text{L}$  of compound solution (20  $\mu\text{M}$ ) in TRIS buffer. The final concentration of the compounds was 2  $\mu\text{M}$ , and the microsomal concentration was 0.25 mg/mL. At the beginning of the experiment ( $t = 0$  min) and after an incubation time of 1, 3, 6, and 15 min, samples (50  $\mu\text{L}$ ) were transferred to 150  $\mu\text{L}$  of ice-cooled MeCN, centrifuged (3600 rpm, 4 °C, 10 min), and 80  $\mu\text{L}$  of supernatant were transferred to a 96-well plate for LC-MS analysis. Metabolic degradation was assessed as percentage remaining compound versus incubation time. Control experiments were performed in parallel by preincubating the microsomes with the specific carboxylesterase inhibitor BNPP (1 mM) for 5 min before addition of the antagonists.

**In Vitro Metabolism: Cytochrome P450-Mediated Metabolism.** Incubations consisted of pooled male mouse liver microsomes (0.5 mg microsomal protein/mL), compounds (2  $\mu\text{M}$ ),  $\text{MgCl}_2$  (2 mM), and NADPH (1 mM) in a total volume of 300  $\mu\text{L}$  TRIS buffer (0.1 M, pH 7.4) and were performed in a 96-well plate on a Thermomixer Comfort. Compounds and microsomes were preincubated (37 °C, 700 rpm, 10 min) before NADPH was added. Samples (50  $\mu\text{L}$ ) at  $t = 0$  min and after an incubation time of 5, 10, 20, and 30 min were quenched with 150  $\mu\text{L}$  of ice-cooled acetonitrile, centrifuged (3600 rpm, 4 °C, 10 min), and 80  $\mu\text{L}$  of each supernatant were transferred to a 96-well plate for LC-MS analysis. Control experiments without NADPH were performed in parallel.

**LC-MS Measurements.** Analyses were performed using a 1100/1200 series HPLC system coupled to a 6410 triple quadrupole mass detector (Agilent Technologies, Inc., Santa Clara, CA, USA) equipped with electrospray ionization. The system was controlled with the Agilent MassHunter Workstation Data Acquisition software (version B.01.04). The column used was an Atlantis T3 C18 column (2.1 mm  $\times$  50 mm) with a 3  $\mu\text{m}$  particle size (Waters Corp., Milford, MA, USA). The mobile phase consisted of two eluents: solvent A ( $\text{H}_2\text{O}$ , containing 0.1%

formic acid, v/v) and solvent B (acetonitrile, containing 0.1% formic acid, v/v), both delivered at 0.6 mL/min. The gradient was ramped from 95% A/5% B to 5% A/95% B over 1 min, and then held at 5% A/95% B for 0.1 min. The system was then brought back to 95% A/5% B, resulting in a total duration of 4 min. MS parameters such as fragmentor voltage, collision energy, polarity were optimized individually for each drug, and the molecular ion was followed for each compound in the multiple reaction monitoring mode. The concentrations of the analytes were quantified by the Agilent Mass Hunter Quantitative Analysis software (version B.01.04).

**In Vivo Pharmacokinetic and Disease Model. Bacteria.** The clinical *E. coli* isolate UTI89<sup>55</sup> (UTI89wt) were kindly provided by the group of Prof. Urs Jenal, Biocenter, University of Basel. Microorganisms were stored at -70 °C and before experiment incubated for 24 h under static conditions at 37 °C in 10 mL of Luria-Bertani broth (Becton, Dickinson and Company, Le Pont de Claix, France) using 50 mL tubes. Prior to each experiment, the microorganisms were washed twice and resuspended in phosphate buffered saline (PBS, Hospital Pharmacy at the University Hospital Basel, Switzerland). Bacterial concentrations were determined by plating serial 1:10 dilutions on blood agar, followed by colony counting with 20–200 colonies after overnight incubation at 37 °C.

**Animals.** Female C3H/HeN mice weighting between 19 and 25 g were obtained from Charles River (Sulzfeld, Germany) and were housed four to a cage. Mice were kept under specific-pathogen-free conditions in the Animal House of the Department of Biomedicine, University Hospital Basel, and animal experimentation guidelines according to the regulations of Swiss veterinary law were followed. After seven days of acclimatization, 9- to 10-week old mice were used for the PK and infection studies. During the studies, animals were allowed free access to chow and water. Three days before infection studies and during infection, 5% D-(+)-glucose (AppliChem, Baden-Dättwil, Switzerland) was added to the drinking water to increase the number of bacterial counts in the urine and kidneys.<sup>57</sup>

**Pharmacokinetic Studies.** Single-dose pharmacokinetic studies were performed by iv and po application of the FimH antagonists at a concentration of 50 mg/kg followed by urine and plasma sampling. For iv application, the antagonists (**1**, **17a**, **17b**) were diluted in 100  $\mu\text{L}$  of PBS and injected into the tail vein. For po application, antagonist **1** was diluted in 200  $\mu\text{L}$  of PBS and antagonists **17b** and **16b** were first dissolved in DMSO (20 $\times$ ) and then slowly diluted to the final concentration (1 $\times$ ) in 1% Tween-80/PBS to obtain a suspension. Antagonists were applied iv by injection into the tail vein and po using a gavage followed by blood and urine sampling (10  $\mu\text{L}$ ) after 6 min, 30 min, 1 h, 2 h, 4 h, 6 h, 8 h, and 24 h. Before analysis, proteins in blood and urine samples were precipitated using methanol (Acros Organics, Basel, Switzerland) and centrifuged for 11 min at 13000 rpm. The supernatant was transferred into a 96-well plate (0.5 mL, polypropylene, Agilent Technologies, Basel, Switzerland) and analyzed by LC-MS as described above.

**UTI Mouse Model.** Mice were infected as previously described.<sup>57</sup> In brief, before infection, all remaining urine was depleted from the bladder by gentle pressure on the abdomen. Mice were anesthetized with 2.5 vol% isoflurane/oxygen mixture (Attane, Minrad Inc., Buffalo, NY, USA) and placed on their back. Anesthetized mice were inoculated transurethrally with the bacterial suspension by use of a 2 cm polyethylene catheter (Intramedic polyethylene tubing, inner diameter 0.28 mm, outer diameter 0.61 mm, Becton Dickinson, Allschwil, Switzerland), which was placed on a syringe (Hamilton Gastight Syringe 50  $\mu\text{L}$ , removable 30G needle, BGB Analytik AG, Boeckten, Switzerland). The catheter was gently inserted through the urethra until it reached the top of the bladder, followed by slow injection of 50  $\mu\text{L}$  of bacterial suspension at a concentration of approximately  $10^9$  to  $10^{10}$  CFU/mL.

**Antagonist Treatment Studies.** FimH antagonists were applied iv in 100  $\mu\text{L}$  of PBS into the tail vein or po as a suspension by the help

of a gavage, 10 min (**17a**, **17b**, **16b**) or 1 h before infection (**1**). Three h after the onset of infection, urine was collected by gentle pressure on the abdomen and then the mouse was sacrificed with CO<sub>2</sub>. Organs were removed aseptically and homogenized in 1 mL of PBS by using a tissue lyser (Retsch, Haan, Germany). Serial dilutions of urine, bladder, and kidneys were plated on Levine Eosin Methylene Blue Agar plates (Beckton Dickinson, Le Pont de Claix, France). CFU counts were determined after overnight incubation at 37 °C and expressed as CFU/mL for the urine and CFU/bladder and CFU/2 kidneys for the organs.

**Acknowledgment.** We thank Professor Rudi Glockshuber (ETH Zürich, Switzerland) for gratefully providing the plasmid pNT-FimH used for the cloning of the FimH CRD and *E. coli* strain HM 125. We thank Dr. Manfred Kansy and Dr. Christoph Funk, F. Hoffmann-La Roche AG, Basel, Switzerland, for supporting us with their expertise when we established the PADMET platform, and to Prof. Angelo Vedani, University of Basel, Switzerland, for fruitful discussions on conformational issues. We further appreciate the support by Prof. Dr. med. Radek Skoda, Department of Biomedicine, University Hospital Basel, Switzerland, for giving us access to the animal facility and Prof. Niels Frimodt-Møller, Statens Serum Institut, Copenhagen, Denmark for the introduction to the in vivo model. We thank Prof G. Imanidis, FHNW, Muttentz, Switzerland, for providing the Caco-2 cells, and Dr. M. Schneider, Department of Pharmaceutical Sciences, University of Basel, Switzerland, for his help during the assay build-up. We are grateful to Prof. Urs Jenal, Biocenter of the University of Basel, Switzerland, for the clinical *E. coli* isolate UTI89 and the FimH knock out strain UTI89Δ*fimA-H*. Finally, we thank the Swiss National Science Foundation (project K-32K1-120904) for their financial support.

**Supporting Information Available:** <sup>1</sup>H NMR spectra and HPLC traces for the target compounds **16a–e**, **17a–c,e**, **21a,b**, and **22a,b** and experimental and spectroscopic details for compounds **6a–d**, **7a–d**, **14c–e**, **15c–e**, **16c–e**, **17c,e**, **19a,b**, **20a,b**, and **21a,b**. This material is available free of charge via the Internet at <http://pubs.acs.org>.

## References

- Fihn, S. D. Clinical practice. Acute uncomplicated urinary tract infection in women. *N. Engl. J. Med.* **2003**, *349*, 259–266.
- Hooton, T. M. Recurrent urinary tract infection in women. *Int. J. Antimicrob. Agents* **2001**, *17*, 259–268.
- Wiles, T. J.; Kulesus, R. R.; Mulvey, M. A. Origins and virulence mechanisms of uropathogenic *Escherichia coli*. *Exp. Mol. Pathol.* **2008**, *85*, 11–19.
- Gouin, S. G.; Wellens, A.; Bouckaert, J.; Kovensky, J. Synthetic Multimeric Heptyl Mannosides as Potent Antiadhesives of Uropathogenic *Escherichia coli*. *ChemMedChem* **2009**, *4*, 749–755.
- Rosen, D. A.; Hung, C. S.; Kline, K. A.; Hultgren, S. J. Streptozocin-induced diabetic mouse model of urinary tract infection. *Infect. Immun.* **2008**, *76*, 4290–4298.
- Mulvey, M. A. Adhesion and entry of uropathogenic *Escherichia coli*. *Cell Microbiol.* **2002**, *4*, 257–271.
- Capitani, G.; Eidam, O.; Glockshuber, R.; Grutter, M. G. Structural and functional insights into the assembly of type 1 pili from *Escherichia coli*. *Microbes Infect.* **2006**, *8*, 2284–2290.
- Choudhury, D.; Thompson, A.; Stojanoff, V.; Langermann, S.; Pinkner, J.; Hultgren, S. J.; Knight, S. D. X-ray structure of the FimC–FimH chaperone–adhesin complex from uropathogenic *Escherichia coli*. *Science* **1999**, *285*, 1061–1066.
- Bouckaert, J.; Berglund, J.; Schembri, M.; Genst, E. D.; Cools, L.; Wuhrer, M.; Hung, C. S.; Pinkner, J.; Slättergard, R.; Zavialov, A.; Choudhury, D.; Langermann, S.; Hultgren, S. J.; Wyns, L.; Klemm, P.; Oscarson, S.; Knight, S. D.; Greve, H. D. Receptor binding studies disclose a novel class of high-affinity inhibitors of the *Escherichia coli* FimH adhesin. *Mol. Microbiol.* **2005**, *55*, 441–455.
- Wellens, A.; Garofalo, C.; Nguyen, H.; Van Gerven, N.; Slättergard, R.; Hernalsteens, J.-P.; Wyns, L.; Oscarson, S.; De Greve, H.; Hultgren, S.; Bouckaert, J. Intervening with urinary tract infections using anti-adhesives based on the crystal structure of the FimH–oligomannose-3 complex. *PLoS ONE* **2008**, *3*, 4–13.
- Langermann, S.; Mollby, R.; Burlein, J. E.; Palaszynski, S. R.; Auguste, C. G.; DeFusco, A.; Strouse, R.; Schenerman, M. A.; Hultgren, S. J.; Pinkner, J. S.; Winberg, J.; Guldevall, L.; Soderhall, M.; Ishikawa, K.; Normark, S.; Koenig, S. Vaccination with FimH adhesin protects cynomolgus monkeys from colonization and infection by uropathogenic *Escherichia coli*. *J. Infect. Dis.* **2000**, *181*, 774–778.
- Langermann, S.; Palaszynski, S.; Barnhart, M.; Auguste, G.; Pinkner, J. S.; Burlein, J.; Barren, P.; Koenig, S.; Leath, S.; Jones, C. H.; Hultgren, S. J. Prevention of mucosal *Escherichia coli* infection by FimH-adhesin-based systemic vaccination. *Science* **1997**, *276*, 607–611.
- Bouckaert, J.; Mackenzie, J.; de Paz, J. L.; Chipwaza, B.; Choudhury, D.; Zavialov, A.; Mannerstedt, K.; Anderson, J.; Pierard, D.; Wyns, L.; Seeburger, P. H.; Oscarson, S.; De Greve, H.; Knight, S. D. The affinity of the FimH fimbrial adhesin is receptor-driven and quasi-independent of *Escherichia coli* pathotypes. *Mol. Microbiol.* **2006**, *61*, 1556–1568.
- Sharon, N. Carbohydrates as future anti-adhesion drugs for infectious diseases. *Biochim. Biophys. Acta* **2006**, *1760*, 527–537.
- (a) Firon, N.; Ofek, I.; Sharon, N. Interaction of mannose-containing oligosaccharides with the fimbrial lectin of *Escherichia coli*. *Biochem. Biophys. Res. Commun.* **1982**, *105*, 1426–1432. (b) Firon, N.; Ofek, I.; Sharon, N. Carbohydrate specificity of the surface lectins of *Escherichia coli*, *Klebsiella pneumoniae* and *Salmonella typhimurium*. *Carbohydr. Res.* **1983**, *120*, 235–249. (c) Sharon, N. Bacterial lectins, cell–cell recognition and infectious disease. *FEBS Lett.* **1987**, *217*, 145–157.
- (a) Neeser, J.-R.; Koellreutter, B.; Wuersch, P. Oligomannoside-type glycopeptides inhibiting adhesion of *Escherichia coli* strains mediated by type 1 pili: preparation of potent inhibitors from plant glycoproteins. *Infect. Immun.* **1986**, *52*, 428–436. (b) Lindhorst, T. K. Artificial multivalent sugar ligands to understand and manipulate carbohydrate–protein interactions. *Top. Curr. Chem.* **2002**, *218*, 201–235 (review); (c) Patel, A.; Lindhorst, T. K. A modular approach for the synthesis of oligosaccharide mimetics. *Carbohydr. Res.* **2006**, *341*, 1657–1668. (d) Nagahori, N.; Lee, R. T.; Nishimura, S.-L.; Pagé, S.; Roy, R.; Lee, Y. C. Inhibition of adhesion of type 1 fimbriated *Escherichia coli* to highly mannosylated ligands. *ChemBioChem* **2002**, *3*, 836–844. (e) Appeldoorn, C. C. M.; Joosten, J. A. F.; Maate, F. A.; Dobrindt, U.; Hacker, J.; Liskamp, R. M. J.; Khan, A. S.; Pieters, R. J. Novel multivalent mannose compounds and their inhibition of the adhesion of type 1 fimbriated uropathogenic *E. coli*. *Tetrahedron Asymmetry* **2005**, *16*, 361–372. (f) Touaibia, M.; Wellens, A.; Shiao, T. C.; Wang, Q.; Sirois, S.; Bouckaert, J.; Roy, R. Mannosylated G(0) dendrimers with nanomolar affinities to *Escherichia coli* FimH. *ChemMedChem* **2007**, *2*, 1190–1201.
- (a) Firon, N.; Ashkenazi, S.; Mirelman, D.; Ofek, I.; Sharon, N. Aromatic alpha-glycosides of mannose are powerful inhibitors of the adherence of type 1 fimbriated *Escherichia coli* to yeast and intestinal epithelial cells. *Infect. Immun.* **1987**, *55*, 472–476. (b) Lindhorst, T. K.; Kötter, S.; Kubisch, J.; Krallmann-Wenzel, U.; Ehlers, S.; Kren, V. Effect of p-substitution of aryl α-D-mannosides on inhibiting mannose-sensitive adhesion of *Escherichia coli*—synthesis and testing. *Eur. J. Org. Chem.* **1998**, 1669–1674. (c) Sperling, O.; Fuchs, A.; Lindhorst, T. K. Evaluation of the carbohydrate recognition domain of the bacterial adhesin FimH: design, synthesis and binding properties of mannose ligands. *Org. Biomol. Chem.* **2006**, *4*, 3913–3922. (d) Han, Z.; Pinker, J. S.; Ford, B.; Obermann, R.; Nolan, W.; Wildman, S. A.; Hobbs, D.; Ellenberger, T.; Cusumano, C. K.; Hultgren, S. J.; Janetka, J. W. Structure-Based Drug Design and Optimization of Mannoside Bacterial FimH Antagonists. *J. Med. Chem.* **2010**, *53*, 4779–4792. (e) Berglund, J.; Bouckaert, J.; De Greve, H.; Knight, S. Anti-adhesive compounds to prevent and treat bacterial infections. International Patent Application PCT/US 2005/089733, 2005.
- Hung, C. S.; Bouckaert, J.; Hung, D.; Pinkner, J.; Widberg, C.; DeFusco, A.; Auguste, C. G.; Strouse, R.; Langermann, S.; Waksman, G.; Hultgren, S. J. Structural basis of tropism of *Escherichia coli* to the bladder during urinary tract infection. *Mol. Microbiol.* **2002**, *44*, 903–918.
- Ernst, B.; Magnani, J. L. From carbohydrate leads to glycomimetic drugs. *Nature Rev. Drug Discovery* **2009**, *8*, 661–677.
- (a) Lindhorst, T. K.; Kieburg, C.; Krallmann-Wenzel, U. Inhibition of the type 1 fimbriae-mediated adhesion of *Escherichia coli* to erythrocytes by multiantennary α-mannosyl clusters: the effect of multivalency. *Glycoconjugate J.* **1998**, *15*, 605–613. (b) Dubber, M.; Sperling, O.; Lindhorst, T. K. Oligomannoside mimetics by glycosylation of 'octopus glycosides' and their investigation as inhibitors of type 1

- fimbriae-mediated adhesion of *Escherichia coli*. *Org. Biomol. Chem.* **2006**, *4*, 3901–3912. (c) Touaibia, M.; Wellens, A.; Shiao, T. C.; Wang, Q.; Sirois, S.; Bouckaert, J.; Roy, R. Mannosylated G0 dendrimers with nanomolar affinities to *Escherichia coli* FimH. *ChemMedChem* **2007**, *2*, 1190–1201.
- (21) Aronson, M.; Medalia, O.; Schori, L.; Mirelman, D.; Sharon, N.; Ofek, I. Prevention of colonization of the urinary tract of mice with *Escherichia coli* by blocking of bacterial adherence with methyl  $\alpha$ -D-mannopyranoside. *J. Infect. Dis.* **1979**, *139*, 329–332.
- (22) Svanborg Eden, C.; Freter, R.; Hagberg, L.; Hull, R.; Leffer, H.; Schoolnik, G. Inhibition of experimental ascending urinary tract infection by an epithelial cell-surface receptor analog. *Nature* **1982**, *298*, 560–562.
- (23) Rabbani, S.; Jiang, X.; Schwardt, O.; Ernst, B. Expression of the carbohydrate recognition domain of FimH and development of a competitive binding assay. *Anal. Biochem.* **2010**, *407*, 188–195.
- (24) Ness, R. K.; Fletcher, H. G.; Hudson, C. S. Reaction of 2,3,4,6-tetrabenzoyl- $\alpha$ -D-glucopyranosyl bromide and 2,3,4,6-tetrabenzoyl- $\alpha$ -D-mannopyranosyl bromide with methanol. Certain benzoylated derivatives of D-glucose and D-mannose. *J. Am. Chem. Soc.* **1950**, *72*, 2200–2205.
- (25) Sancho-Garcia, J. C.; Cornil, J. Anchoring the Torsional Potential of Biphenyl at the ab Initio Level: The Role of Basis Set versus Correlation Effects. *J. Chem. Theory Comput.* **2005**, *1*, 581–589.
- (26) Eaton, V. J.; Steele, D. Dihedral angle of biphenyl in solution and the molecular force field. *J. Chem. Soc., Faraday Trans. 2* **1973**, *1601*–1608.
- (27) Albert, A. Chemical aspects of selective toxicity. *Nature* **1958**, *182*, 421–422.
- (28) Winiwarter, S.; Bonham, N. M.; Ax, F.; Hallberg, A.; Lennernäs, H.; Karlén, A. Correlation of Human Jejunal Permeability (in Vivo) of Drugs with Experimentally and Theoretically Derived Parameters. A Multivariate Data Analysis Approach. *J. Med. Chem.* **1998**, *41*, 4939–4949.
- (29) Taketani, M.; Shii, M.; Ohura, K.; Ninomiya, S.; Imai, T. Carboxylesterase in the liver and small intestine of experimental animals and human. *Life Sci.* **2007**, *81*, 924–932.
- (30) Kansy, M.; Senner, F.; Gubernator, K. Physicochemical High Throughput Screening: Parallel Artificial Membrane Permeation Assay in the Description of Passive Absorption Processes. *J. Med. Chem.* **1998**, *41*, 1007–1010.
- (31) Artursson, P.; Karlsson, J. Correlation between oral drug absorption in humans and apparent drug permeability coefficients in human intestinal epithelial (Caco-2) cells. *Biochem. Biophys. Res. Com.* **1991**, *175*, 880–885.
- (32) Varma, M. V. S.; Feng, B.; Obach, R. S.; Troutman, M. D.; Chupka, J.; Miller, H. R.; El-Kattan, A. Physicochemical Determinants of Human Renal Clearance. *J. Med. Chem.* **2009**, *52*, 4844–4852.
- (33) Abgottsporn, D.; Rölli, G.; Hosch, L.; Steinhuber, A.; Jiang, X.; Schwardt, O.; Cutting, B.; Smiesko, M.; Jenal, U.; Ernst, B.; Trampuz, A. Development of an Aggregation Assay to Screen FimH Antagonists. *J. Microbiol. Methods* **2010**, *82*, 249–255.
- (34) Zhou, G.; Mo, W.-J.; Sebbel, P.; Min, G.; Neubert, T. A.; Glockshuber, R.; Wu, X.-R.; Sun, T.-T.; Kong, X.-P. Uroplakin Ia is the urothelial receptor for uropathogenic *Escherichia coli*: evidence from in vitro FimH binding. *J. Cell Sci.* **2001**, *114*, 4095–4103.
- (35) (a) Kartha, K. P. R.; Field, R. A. Iodine: a versatile reagent in carbohydrate chemistry. IV. Per-O-acetylation, regioselective acylation and acetolysis. *Tetrahedron* **1997**, *53*, 11753–11766. (b) Chittaboina, S.; Hodges, B.; Wang, Q. A facile route for the regioselective deacetylation of peracetylated carbohydrates at anomeric position. *Lett. Org. Chem.* **2006**, *3*, 35–38. (c) Mori, M.; Ito, Y.; Ogawa, T. Total synthesis of the mollu-series glycosyl ceramides  $\alpha$ -D-Manp-(1 $\rightarrow$ 3)- $\beta$ -D-Manp-(1 $\rightarrow$ 4)- $\beta$ -D-Glcp-(1 $\rightarrow$ 1)-Cer and  $\alpha$ -D-Manp-(1 $\rightarrow$ 3)-[ $\beta$ -D-Xylp-(1 $\rightarrow$ 2)]- $\beta$ -D-Manp-(1 $\rightarrow$ 4)- $\beta$ -D-Glcp-(1 $\rightarrow$ 1)-Cer. *Carbohydr. Res.* **1990**, *195*, 199–224. (d) Egusa, K.; Kusumoto, S.; Fukase, K. Solid-phase synthesis of a phytoalexin elicitor pentasaccharide using a 4-azido-3-chlorobenzyl group as the key for temporary protection and catch-and-release purification. *Eur. J. Org. Chem.* **2003**, 3435–3445.
- (36) Giampapa, C. S.; Abraham, S. N.; Chiang, T. M.; Beachey, E. H. Isolation and characterization of a receptor for type 1 fimbriae of *Escherichia coli* from guinea pig erythrocytes. *J. Biol. Chem.* **1988**, *263*, 5362–5367.
- (37) Aprikian, P.; Tchesnokova, V.; Kidd, B.; Yakovenko, O.; Yarov-Yarovoy, V.; Trinchina, E.; Vogel, V.; Thomas, W.; Sokurenko, E. Interdomain interaction in the FimH adhesin of *Escherichia coli* regulates the affinity to mannose. *J. Biol. Chem.* **2007**, *282*, 23437–23446.
- (38) Trong, I. L.; Aprikian, P.; Kidd, B. A.; Forero-Shelton, M.; Tchesnokova, V.; Rajagopal, P.; Rodriguez, V.; Interlandi, G.; Klevit, R.; Vogel, V.; Stenkamp, R. E.; Sokurenko, E. V.; Thomas, W. E. Structural basis for mechanical force regulation of the adhesin FimH via finger trap-like beta sheet twisting. *Cell* **2010**, *141*, 645–655.
- (39) Khoo, U. S.; Chan, K. Y. K.; Chan, V. S. F.; Lin, C. L. S. DC-SIGN and L-SIGN: the SIGNs for infection. *J. Mol. Med.* **2008**, *86*, 861–874.
- (40) Lee, S. J.; Evers, S.; Roeder, D.; Parlow, A. F.; Risteli, J.; Risteli, L.; Lee, Y. C.; Feizi, T.; Langen, H.; Nussenzweig, M. C. Mannose receptor-mediated regulation of serum glycoprotein homeostasis. *Science* **2002**, *295*, 1898–1901.
- (41) East, L.; Isacke, C. M. The mannose receptor family. *Biochim. Biophys. Acta* **2002**, *1572*, 364–386.
- (42) Dommert, R. M.; Klein, N.; Turner, M. W. Mannose-binding lectin in innate immunity: past, present and future. *Tissue Antigens* **2006**, *68*, 193–209.
- (43) Scharenberg, M. Expression and purification of DC-SIGN-CRD-Fc-IgG. Unpublished results.
- (44) Dearden, J. C.; Bresnen, J. G. M. The measurement of partition coefficients. *QSAR Comb. Sci.* **1988**, *7*, 133–144.
- (45) Wittwer, M.; Bezençon, J.; Cutting, B.; Wagner, B.; Kansy, M.; Ernst, B.  $pK_a$  determination by  $^1\text{H-NMR}$  spectroscopy—an old methodology revisited. Unpublished results.
- (46) Banker, M. J.; Clark, T. H.; Williams, J. A. Development and validation of a 96-well equilibrium dialysis apparatus for measuring plasma protein binding. *J. Pharm. Sci.* **2003**, *92*, 967–974.
- (47) Kerns, E. H. High throughput physicochemical profiling for drug discovery. *J. Pharm. Sci.* **2001**, *90*, 1838–1858.
- (48) Avdeef, A.; Bendels, S.; Di, L.; Faller, B.; Kansy, M.; Sugano, K.; Yamauchi, Y. Parallel artificial membrane permeability assay (PAMPA)-critical factors for better predictions of absorption. *J. Pharm. Sci.* **2007**, *96*, 2893–2909.
- (49) Brandt, E.; Heymann, E.; Mentlein, R. Selective inhibition of rat liver carboxylesterases by various organophosphorus diesters in vivo and in vitro. *Biochem. Pharmacol.* **1980**, *29*, 1927–1931.
- (50) Scharenberg, M.; Abgottsporn, D. Personal communication.
- (51) Obach, R. S. Prediction of human clearance of twenty-nine drugs from hepatic microsomal intrinsic clearance data: an examination of in vitro half-life approach and nonspecific binding to microsomes. *Drug Metab. Dispos.* **1999**, *27*, 1350–1359.
- (52) Trainor, G. L. The importance of plasma protein binding in drug discovery. *Expert Opin. Drug Discovery* **2007**, *2*, 51–64.
- (53) Weisiger, R. A. Dissociation from albumin: a potentially rate-limiting step in the clearance of substances by the liver. *Proc. Natl. Acad. Sci. U.S.A.* **1985**, *82*, 1563–1567.
- (54) Urien, S.; Tillement, J.-P.; Barre, J. The significance of plasma protein binding in drug research. In *Pharmacokinetic Optimization in Drug Research: Biological, Physicochemical, and Computational Strategies*; Wiley-VCH: Weinheim, Germany, 2001; pp 189–197.
- (55) Mulvey, M. A.; Schilling, J. D.; Hultgren, S. J. Establishment of a persistent *Escherichia coli* reservoir during the acute phase of a bladder infection. *Infect. Immun.* **2001**, *69*, 4572–4579.
- (56) (a) VCCLAB, Virtual Computational Chemistry Laboratory; <http://www.vcclab.org>, 2005; (b) Tetko, I. V.; Gasteiger, J.; Todeschini, R.; Mauri, A.; Livingstone, D.; Ertl, P.; Palyulin, V. A.; Radchenko, E. V.; Zefirov, N. S.; Makarenko, A. S.; Tanchuk, V. Y.; Prokopenko, V. V. Virtual computational chemistry laboratory—design and description. *J. Comput.-Aided Mol. Des.* **2005**, *19*, 453–463.
- (57) Kern, M. B.; Frimodt-Møller, N.; Espersen, F. Effects of Sulfo-methizole and Amdinocillin against *Escherichia coli* Strains (with Various Susceptibilities) in an Ascending Urinary Tract Infection Model. *Antimicrob. Agents Chemother.* **2003**, *47*, 1002–1009.

## **Part I: The lectin FimH**

---

**FimH Chapter 2: Results and discussion**

**Publication 3**

---

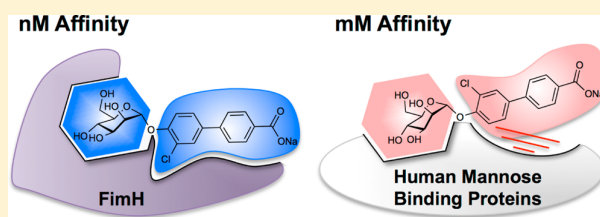
## Target Selectivity of FimH Antagonists

Meike Scharenberg, Oliver Schwardt, Said Rabbani, and Beat Ernst\*

Institute of Molecular Pharmacy, Pharmacenter, University of Basel, Klingelbergstrasse 50, CH-4056 Basel, Switzerland

## Supporting Information

**ABSTRACT:** Mannose-based FimH antagonists are considered new therapeutics for the treatment of urinary tract infections (UTIs). They prevent the adhesion of uropathogenic *Escherichia coli* (UPEC) to urothelial cell surfaces triggered by the lectin FimH, which is located at the tip of bacterial type 1 pili. Because all reported FimH antagonists are  $\alpha$ -D-mannosides, they are also potential ligands of mannose receptors of the human host system. We therefore investigated the selectivity range of five FimH antagonists belonging to different compound families by comparing their affinities for FimH and eight human mannose receptors. On the basis of the detected selectivity range of approximately 5 orders of magnitude, no adverse side effects resulting from nonselective binding to the human receptors have to be expected. FimH antagonists can therefore be further considered as potential therapeutics for the treatment of UTI.



## INTRODUCTION

Urinary tract infections (UTIs) are primarily caused by uropathogenic *Escherichia coli* (UPEC) (70–95% of cases) expressing type 1 pili.<sup>1</sup> At the tip of these pili, the lectin FimH is located. It enables the bacteria to adhere to oligomannosides of the glycoprotein uroplakin Ia (UPIa), which is located on uroepithelial cells.<sup>2</sup> This initial adhesion is a prerequisite for the infection to take place, because it prevents the rapid clearance of *E. coli* from the urinary tract by the bulk flow of urine and at the same time enables the invasion of the host cells.<sup>2a,b</sup> FimH antagonists, such as  $\alpha$ -D-mannopyranosides, have been shown to interfere with the attachment of UPEC to their host cells, thus providing a novel therapeutic opportunity for prevention and treatment of UTIs as an alternative to antibiotics.<sup>3</sup> To date, several FimH antagonists have been investigated in vitro.<sup>4</sup> Furthermore, in vivo studies with methyl  $\alpha$ -D-mannopyranoside,<sup>5a</sup> *n*-heptyl  $\alpha$ -D-mannopyranoside (**1**, Figure 1),<sup>5b,d</sup> biphenyl  $\alpha$ -D-mannopyranosides such as **2** and **3**,<sup>5c–f</sup> and indolinylphenyl  $\alpha$ -D-mannopyranosides like **5**<sup>5g</sup> exhibited a considerable potential to reduce bacterial infections.

Target selectivity is of great concern in drug development and should be evaluated in the early stages of preclinical development.<sup>6</sup> Because all reported FimH antagonists are  $\alpha$ -D-mannopyranosides and therefore also potential ligands for mannose receptors of the human host system, target selectivity of these FimH antagonists is a pivotal concern. Although various antagonists were already tested in vivo,<sup>5</sup> their target selectivity was not verified so far. Mammalian mannose receptors are present on many tissues throughout the whole body and are involved in numerous biological processes, such as cell–cell adhesion<sup>7</sup> and serum glycoprotein homeostasis.<sup>8</sup> They also intervene in the innate and the adaptive immune response by recognizing molecular patterns on pathogens.<sup>7,9</sup> Consequently, nonselective interactions of FimH antagonists

with these various mannose receptors would have a profound impact on these processes and could cause severe side effects. A high selectivity of FimH antagonists is therefore of importance for a clinical application and should be evaluated in the early stages of preclinical development.

The majority of human mannose-binding lectins belong to the group of pathogen-recognition receptors (PRRs). Most PRRs are members of the C-type lectin superfamily.<sup>10</sup> They are either secreted as soluble plasma proteins or expressed as membrane-bound proteins on the surface of cells of the immune system such as macrophages, dendritic cells, or Langerhans cells. Secreted PRRs, such as the mannose binding protein (MBL)<sup>11</sup> and the lung surfactant protein D (SP-D),<sup>12</sup> bind to pathogens and simultaneously associate with cell surface receptors, triggering signaling pathways such as the lectin complement activation pathway, which results in enhanced phagocytosis of the pathogens as well as activation of the host defense system.<sup>13</sup> MBL and SP-D belong to the collectin family and share a similar collagen-like domain connected to the C-terminal C-type lectin domain, which contains the carbohydrate recognition domain (CRD). They consist of homotrimers, which oligomerize with 2–6 other trimers, forming high molecular weight complexes.<sup>14</sup> Transmembrane PRRs, which are classified into type I and type II C-type lectins, are also involved in the phagocytosis of pathogens, leading to their elimination or their processing for antigen presentation.<sup>15</sup> The type I C-type lectins such as the macrophage mannose receptor (MMR)<sup>9</sup> contain multiple CRDs within a single polypeptide backbone. In contrast, the type II C-type lectins such as langerin,<sup>16</sup> DC-specific ICAM-3-grabbing nonintegrin (DC-SIGN),<sup>17</sup> DC-specific ICAM-3-

Received: July 14, 2012

Published: October 22, 2012

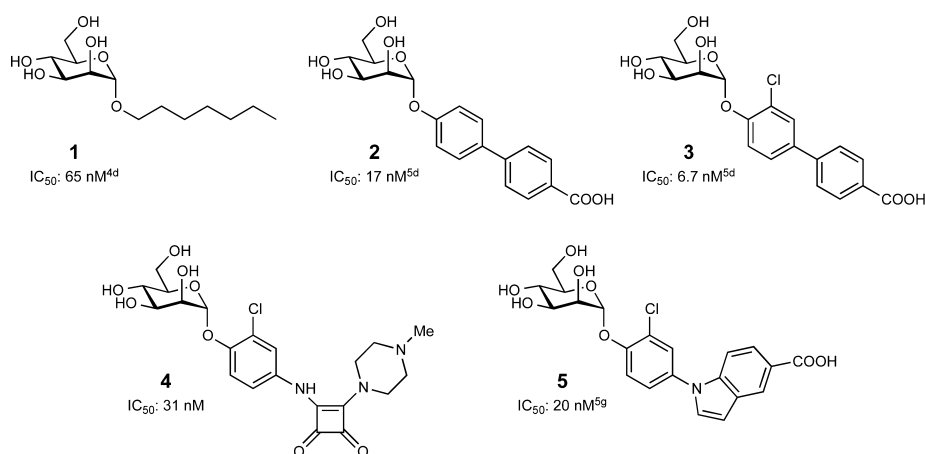


**Figure 1.** FimH antagonists tested for their selectivities for various human mannose-binding lectins: *n*-heptyl  $\alpha$ -D-mannopyranoside (**1**),<sup>4d</sup> biphenyl  $\alpha$ -D-mannopyranoside derivatives **2** and **3**,<sup>5d</sup> squaric acid derivative **4**, and indolylphenyl derivative **5**.<sup>5g</sup> IC<sub>50</sub> values for FimH were obtained by a competitive binding assay.<sup>4d</sup>

grabbing nonintegrin related (DC-SIGNR),<sup>18</sup> dectin-2,<sup>19</sup> and dendritic cell lectin (DLEC)<sup>20</sup> exhibit only a single CRD. However, by formation of homomultimers, type II C-type lectins can greatly enhance their binding affinity. This was shown for the trimeric langerin<sup>21</sup> and tetrameric DC-SIGN and DC-SIGNR.<sup>19</sup> The multimeric arrangement of the CRDs further supports the discrimination between innate and extrinsic carbohydrate epitopes.<sup>22</sup>

For defense mechanisms against a broad range of microorganisms, human mannose-binding receptors require highly specific binding. Thus, MMR exhibits a preference for branched sugars with terminal D-mannose, L-fucose, or N-acetyl-D-glucosamine moieties that are specifically expressed on mycobacteria and fungi.<sup>9a</sup> Dectin-2 selectively binds to high mannose structures predominantly expressed on the surfaces of yeast and fungi,<sup>23</sup> whereas DC-SIGN recognizes high mannose oligosaccharides and Lewis blood group antigens such as Lewis<sup>x</sup> or Lewis<sup>a</sup>, found on mycobacteria, some viruses (e.g., HIV), and fungi.<sup>18,24</sup>

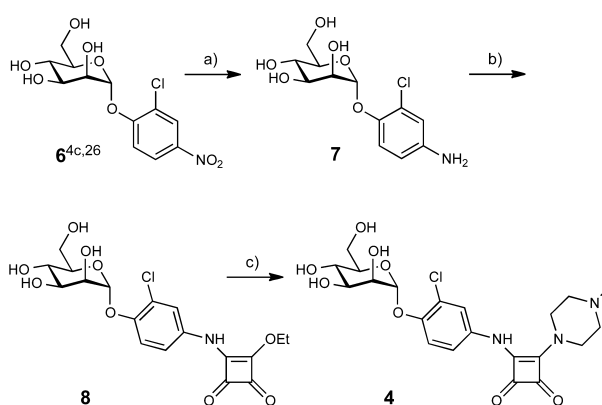
To ensure that FimH antagonists do not cause any adverse side effects due to nonselective binding to human mannose receptors, their selectivity profile to eight different PRRs was established. Nonselective binding may also have a profound impact on the serum half-life of FimH antagonists, since binding to PRRs often triggers endocytosis and would result in their elimination from circulation. To address this selectivity issue, we tested five mannose-based FimH antagonists with diverse aglycones (alkyl, biphenyl, squaric acid, and indolylphenyl derivatives) for their binding affinity to various mannose-binding lectins (MBL, SP-D, MMR, DC-SIGN, DC-SIGNR, langerin, dectin-2, and DLEC).

## RESULTS AND DISCUSSION

With a competitive binding assay,<sup>4d</sup> five high-affinity FimH antagonists belonging to different compound families (Figure 1, **1**–**5**<sup>4d,5d,5g</sup>) were tested for their selectivity for eight human mannose receptors.

**Synthesis of FimH Antagonists.** *n*-Heptyl  $\alpha$ -D-mannopyranoside (**1**),<sup>25</sup> the biphenyl  $\alpha$ -D-mannopyranosides **2**<sup>5d</sup> and **3**,<sup>5d</sup> and the indolylphenyl  $\alpha$ -D-mannopyranoside **5**<sup>5g</sup> were synthesized as previously reported. The synthesis of FimH antagonist **4** (Scheme 1) started from nitrophenyl mannoside **6**, which is

### Scheme 1<sup>4c</sup>



<sup>4c</sup>Reagents and conditions: (a) H<sub>2</sub> (1 atm), cat. PtO<sub>2</sub>, morpholine, MeOH, 45 min. (b) Diethyl squarate, MeOH, 1 day, 61% (2 steps).<sup>4c</sup> (c) *N*-Methylpiperazine, DIPEA, MeOH, 18 h, 90%.

easily available from peracetylated D-mannose.<sup>4c,26</sup> Because the reported procedure<sup>4c</sup> for the hydrogenation to aniline **7** using palladium on charcoal as a catalyst resulted in a substantial loss of the chloro substituent, platinum dioxide in the presence of morpholine was applied.<sup>27</sup> The mannosylated ethyl squarate **8** was then obtained in analogy to Sperling et al.<sup>4c</sup> Finally, treatment of ester **8** with *N*-methylpiperazine yielded amide **4** in 90%, which was ready for biological testing.

**Binding Assays.** The cell-free competitive binding assay<sup>4d</sup> is based on the interactions of a biotinylated polyacrylamide (PAA) glycopolymer [Man $\alpha$ 1–3(Man $\alpha$ 1–6)Man $\beta$ 1–4GlcNAc $\beta$ 1–4GlcNAc $\beta$ -PAA, TM-PAA] with the mannose receptors. Complexation of the biotinylated glycopolymer with streptavidin coupled to horseradish peroxidase allows for the quantification of the binding potencies of the tested FimH antagonists.

For our selectivity study, two parameters, the protein concentration and the TM-PAA concentration, were optimized to obtain comparable optical densities (ODs) for the different lectins in the competitive binding assay (Figure 2 and Table 1). Because of distinctive coating properties of the proteins, different protein concentrations (2.5–20  $\mu$ g/mL) were

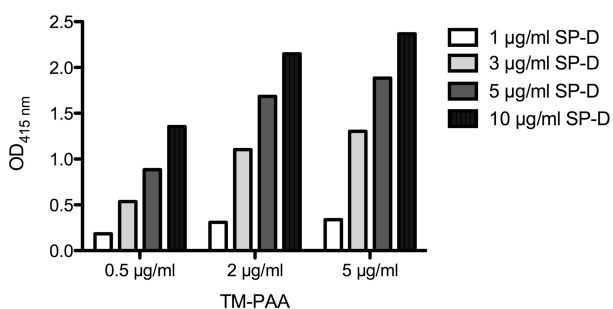


**Figure 2.** Assay development and optimization on the example of the human lectin SP-D. Different concentrations of coated SP-D (1–10 µg/mL) in combination with various TM-PAA concentrations (0.5–5 µg/mL) were tested.

**Table 1. Optimized Protein and TM-PAA Concentrations Used in the Competition Assays for Each Individual Lectin**

protein	µg/mL		OD <sub>415 nm</sub>
	[protein]	[TM-PAA]	
FimH	20	0.25	2.20
MBP	10	5	1.82
SP-D	5	5	1.88
MMR	5	2	2.03
langerin	10	2	2.12
dectin-2	10	5	1.92
DLEC	10	5	1.93
DC-SIGN	2.5	1	2.15
DC-SIGNR	10	5	2.10

necessary to obtain comparable levels of immobilization. The TM-PAA concentration in turn required adaptation due to different affinities of the various lectins. Because of the multivalent oligosaccharide presentation, the affinity of the polymer is expected to be higher than the affinity of the corresponding free oligosaccharide. We therefore used low TM-PAA concentrations between 0.5 and 5 µg/mL, which correspond to 16–160 µM TM-PAA assuming a molecular mass of approximately 30 kDa. As a representative example, the results of this optimization process for the lectin SP-D are summarized in Figure 2. Briefly, when 5 µg/mL SP-D was used for the immobilization step, an OD<sub>415nm</sub> of approximately 2 was obtained with 5 µg/mL TM-PAA. The protein and polymer concentrations leading to comparable ODs for the other investigated lectins are summarized in Table 1.

For the competitive binding assays, concentrations of 1 mM antagonists and 50 mM D-mannose (positive control) were used. The results are summarized in Figure 3. The ODs obtained in the absence of an antagonist were set to 100% TM-PAA binding, the background in the absence of the polymer to 0% TM-PAA binding. D-Mannose showed a strong inhibition of binding for all proteins at a concentration of 50 mM (more than 90% inhibition). As expected, at a concentration of 1 mM, the antagonists 1–5 strongly inhibited binding of the polymer to FimH, whereas none of the antagonists showed relevant inhibition potencies for the tested human lectins. The highest inhibition of TM-PAA binding was observed for the antagonists 3 (54%) and 5 (58%) to MMR, for compound 3 (63%) to langerin, and for compound 2 (50%) to DLEC (indicated by asterisks, Figure 3). On the basis of their ODs, the IC<sub>50</sub> value (concentration at 50% inhibition) of these antagonists can be estimated to be in the order of 1 mM. As compared to the low

nanomolar FimH affinities of the five investigated antagonists (Figure 1), the affinities for the human lectins are at least 5 orders of magnitude lower, indicating an excellent selectivity margin for a therapeutic application of these FimH antagonists.

Infection studies in a mouse disease model, using compounds 1–3, were previously reported.<sup>5d</sup> In these studies, a high dose of 50 mg/kg was applied, resulting in a substantial reduction of the bacterial infection caused by UPEC UTI89 [reduction of the colony-forming units (CFU) in the urine by 2 orders of magnitude and in the bladder by 4 orders of magnitude]. Furthermore, the in vivo pharmacokinetic parameters were determined, including the maximal plasma concentrations (C<sub>max</sub>) of the FimH antagonists after iv application. Maximal concentrations of 39 µg/mL for 1, 35 µg/mL for 2, and 39 µg/mL for 3 were detected in blood samples, which correspond to C<sub>max</sub> values of 144, 80, and 97 µM, respectively. Low binding to mammalian mannose receptors is expected even at these concentrations, since the IC<sub>50</sub> values of the antagonists 1–3 for the eight tested human mannose receptors are approximately 10-fold higher than the detected maximal blood concentrations in treated mice. Furthermore, with improved antagonists like indolylphenyl derivative 5,<sup>5g</sup> the dose of 50 mg/kg could be reduced to 1 mg/kg, thus additionally increasing the selectivity margin.

Binding affinities of various human mannose receptors to monosaccharides, such as D-mannose, L-fucose, and D-galactose, have already been characterized in previous studies. Monovalent sugars showed only weak binding affinities in the millimolar range toward DC-SIGN,<sup>18</sup> DC-SIGNR,<sup>28</sup> dectin-2,<sup>23</sup> langerin,<sup>21</sup> or MMR.<sup>29</sup> The functional affinity to carbohydrates necessary for pathogen capturing is predominantly an effect of avidity, caused by the combined strength of multiple interactions with ligands. The presentation of multivalent carbohydrates on the pathogen surface and the multimerization and/or clustering of the receptors on the host cells greatly support binding between the interaction partners. Therefore, multivalent presentations of α-D-mannosidic antagonists<sup>4a,30</sup> might be prone to cause severe side effects due to strong binding to human mannose receptors.

## CONCLUSION

On the basis of the presented data, adverse side effects resulting from nonselective binding of monovalent FimH antagonists to the investigated mannose-binding lectins are not considered to be a critical issue for their potential therapeutic application to treat UTI. Although this selection does not cover the entire mammalian mannose-binding proteins, it represents the most abundant and best-characterized receptors expressed in various tissues. The 10<sup>5</sup>-fold lower affinity for the tested human receptors as compared to the bacterial FimH lectin confirms a high selectivity safety range. This primarily results from the fact that the investigated FimH antagonists were optimized by introducing hydrophobic substituents at their reducing end, enabling the interaction with the tyrosine gate, the entrance to the ligand-binding site, which is a unique feature of FimH.<sup>31</sup> Furthermore, because of the importance of multivalent ligand presentation in nature, monovalent α-D-mannopyranosides in general can be considered to exhibit only low affinities to human mannose receptors.

## EXPERIMENTAL SECTION

**General Methods.** Commercially available reagents were purchased from Sigma-Aldrich or Acros. Methanol (MeOH) was

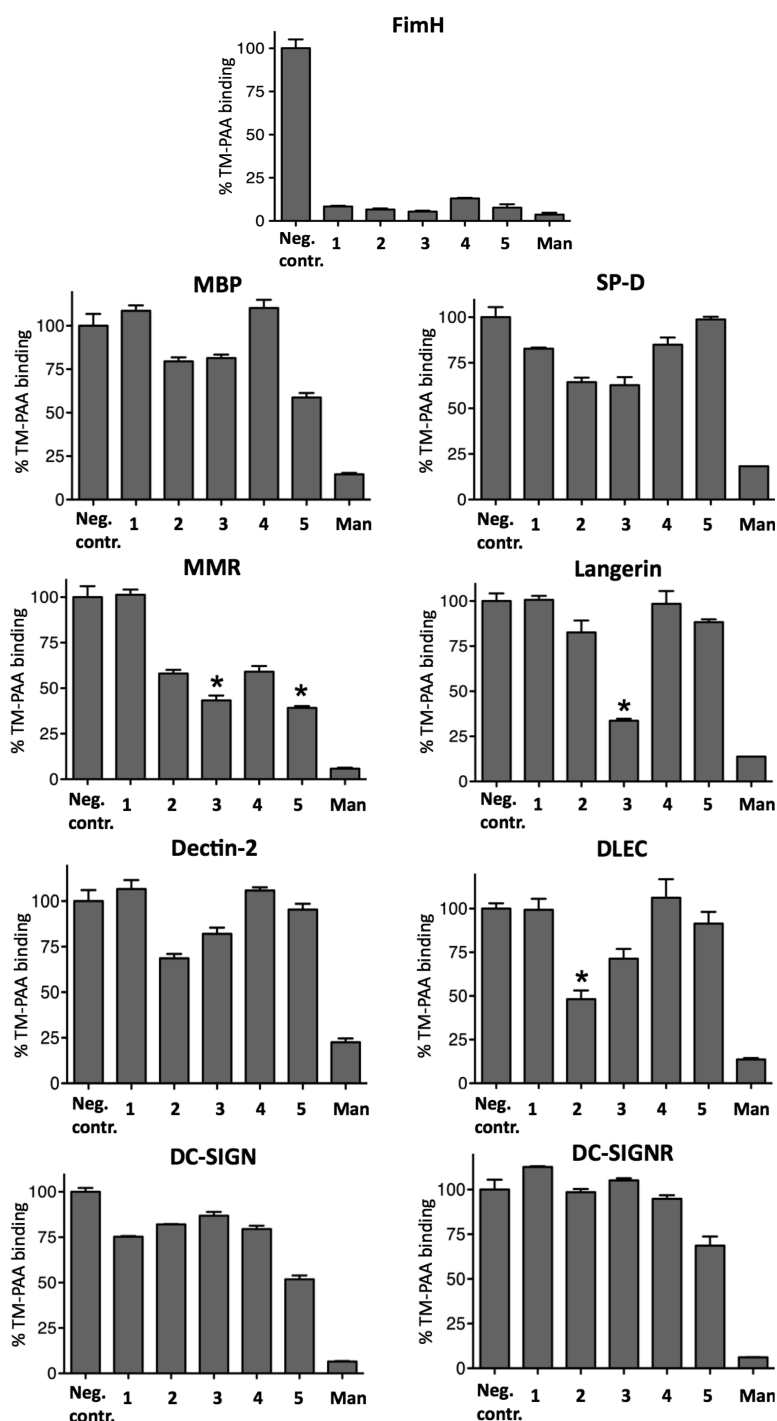


**Figure 3.** Selectivity profile of FimH antagonists 1–5. Competitive binding assays with FimH, MBP, SP-D, MMR, langerin, dectin-2, DLEC, DC-SIGN, and DC-SIGNR to evaluate the selectivity of compounds 1–5. Inhibitory capacities of the compounds were tested at a concentration of 1 mM. D-Mannose (Man) served as a positive control (50 mM). The binding signals of TM-PAA to the proteins in absence of antagonists were set to 100%, and background signals were set to 0%. Asterisks indicate inhibition of TM-PAA binding by 50% or more. The assays were performed in triplicate.

dried by distillation from sodium methoxide. Optical rotation was measured at 20 °C on a Perkin-Elmer 341 polarimeter. Nuclear magnetic resonance (NMR) spectra were obtained on a Bruker Avance 500 UltraShield spectrometer at 500.13 MHz ( $^1\text{H}$ ) or 125.76 MHz ( $^{13}\text{C}$ ). Chemical shifts are given in ppm and were calibrated on residual solvent peaks. Assignment of the  $^1\text{H}$  and  $^{13}\text{C}$  NMR spectra

was achieved using 2D methods (COSY and HSQC). Electron spray ionization mass spectra (ESI-MS) were recorded on a Waters micromass ZQ instrument. High-resolution mass spectra (HR-MS) were obtained on an ESI Bruker Daltonics micrOTOF spectrometer equipped with a TOF hexapole detector. Reactions were monitored by TLC using glass plates coated with silica gel 60 F<sub>254</sub> and visualized by



using UV light and/or by charring with a molybdate solution (a 0.02 M solution of ammonium cerium sulfate dihydrate and ammonium molybdate tetrahydrate in aqueous 10% H<sub>2</sub>SO<sub>4</sub>) with heating to 150 °C for 5 min. MPLC separations were carried out on a CombiFlash Rf from Teledyne Isco equipped with RP-18 reversed-phase flash columns. LC-MS separations were done on a Waters system equipped with a Waters SunFire C<sub>18</sub> OBD (5 μm, 19 mm × 150 mm) column, sample manager 2767, pump 2525, PDA 2525, and micromass ZQ mass spectrometer.

**Compound Purity.** The test compounds 1–3 and 5 were purified by reversed-phase chromatography (RP-18 column, gradient of MeOH in H<sub>2</sub>O, compound 1–3<sup>5d,25</sup>) or chromatography on silica (DCM/MeOH/H<sub>2</sub>O, compound 5<sup>58</sup>) followed by Bio-Gel P2 (exclusion limit 1800 Da, Bio-Rad Laboratories) size exclusion chromatography (elution with water containing up to 20% MeOH at 0.25 mL/min) prior to HPLC, HR-MS, NMR, and activity testing. Compound 4 was purified by preparative LC-MS (Waters SunFire C<sub>18</sub> OBD column, H<sub>2</sub>O/MeCN + 0.2% HCO<sub>2</sub>H). The purity of all test compounds was determined by NMR and HPLC to be ≥95% [method A (compounds 2, 3, and 5): Beckman Coulter Gold, consisting of pump 126, DAD 168 (190–410 nm), and autosampler 508; column, Waters Atlantis T3 (3 μm, 2.1 mm × 100 mm); A, H<sub>2</sub>O + 0.1% TFA; B, MeCN + 0.1% TFA; detection, 254 or 270 nm; gradient, 5% B → 95% B (22 min); and flow rate, 0.5 mL/min. Method B (compounds 1 and 4): Agilent 1100/1200 with UV detector (190–410 nm) and ELSD; column, Waters Atlantis T3 (3 μm, 2.1 mm × 100 mm); A, H<sub>2</sub>O + 0.1% TFA; B, H<sub>2</sub>O/MeCN (90:10) + 0.1% TFA; gradient, 5% B (1 min), 5% B → 70% B (15 min), 70% B (1 min), 70% B → 5% B (3 min); flow rate, 0.5 mL/min; and detection, 254 nm or ELSD]. For the <sup>1</sup>H NMR spectrum and HPLC trace of compound 4, see the Supporting Information.

**4-Amino-2-chlorophenyl α-D-Mannopyranoside (7).** A suspension of 6<sup>4c,26</sup> (430 mg, 1.28 mmol), morpholine (30 μL), and PtO<sub>2</sub> (50 mg) in MeOH (20 mL) was hydrogenated (1 atm H<sub>2</sub>) for 45 min. Then, the mixture was filtered and concentrated in vacuo to give crude 7 (443 mg) as a colorless oil, which contained approximately 15% morpholine and was used in the next step without further purification. <sup>1</sup>H NMR (500 MHz, CD<sub>3</sub>OD): δ 3.71–3.81 (m, 3H, H-4, H-5, H-6a), 3.83 (dd, *J* = 1.7, 12.7 Hz, 1H, H-6b), 3.95 (dd, *J* = 3.4, 9.1 Hz, 1H, H-3), 4.11 (dd, *J* = 1.8, 3.4 Hz, 1H, H-2), 5.27 (d, *J* = 1.7 Hz, 1H, H-1), 6.61 (dd, *J* = 2.7, 8.7 Hz, 1H, C<sub>6</sub>H<sub>3</sub>), 6.78 (d, *J* = 2.7 Hz, 1H, C<sub>6</sub>H<sub>3</sub>), 7.09 (d, *J* = 8.7 Hz, 1H, C<sub>6</sub>H<sub>3</sub>). <sup>13</sup>C NMR (125 MHz, CD<sub>3</sub>OD): δ 62.6 (C-6), 68.4 (C-4), 71.9 (C-2), 72.3 (C-3), 75.7 (C-5), 102.1 (C-1), 115.7, 117.4, 121.2, 153.2 (6C, C<sub>6</sub>H<sub>3</sub>). ESI-MS: *m/z* calcd for C<sub>12</sub>H<sub>17</sub>ClNO<sub>6</sub> [M + H]<sup>+</sup>, 306.1; found, 306.0.

**2-Chloro-4-[(2-ethoxy-3,4-dioxocyclobuten-1-yl)amino]phenyl α-D-Mannopyranoside (8).**<sup>4c</sup> To a solution of 7 (443 mg) in MeOH (15 mL) was added diethyl squarate (379 μL, 2.56 mmol) under argon, and the reaction mixture was stirred at rt for 1 d. Then, the solvent was removed in vacuo, and the residue was purified by MPLC on RP-18 (H<sub>2</sub>O/MeOH) to yield 8 (337 mg, 61% from 6) as a yellow solid. <sup>1</sup>H NMR (500 MHz, CD<sub>3</sub>OD): δ 1.47 (t, *J* = 7.1 Hz, 3H, OCH<sub>2</sub>CH<sub>3</sub>), 3.66 (dt, *J* = 3.7, 9.9 Hz, 1H, H-5), 3.75 (d, *J* = 3.7 Hz, 2H, H-6), 3.79 (t, *J* = 9.8 Hz, 1H, H-4), 4.00 (dd, *J* = 3.4, 9.6 Hz, 1H, H-3), 4.16 (dd, *J* = 1.8, 3.3 Hz, 1H, H-2), 4.81 (q, *J* = 7.1 Hz, 2H, OCH<sub>2</sub>CH<sub>3</sub>), 5.56 (d, *J* = 1.5 Hz, 1H, H-1), 7.23 (m, 1H, C<sub>6</sub>H<sub>3</sub>), 7.32 (d, *J* = 9.0 Hz, 1H, C<sub>6</sub>H<sub>3</sub>), 7.47 (s, 1H, C<sub>6</sub>H<sub>3</sub>). <sup>13</sup>C NMR (125 MHz, CD<sub>3</sub>OD): δ 15.7 (OCH<sub>2</sub>CH<sub>3</sub>), 61.4 (C-6), 67.2 (C-4), 70.8 (C-2), 71.4 (C-3), 71.6 (OCH<sub>2</sub>CH<sub>3</sub>), 74.9 (C-5), 100.0 (C-1), 119.2, 120.2, 122.4, 124.7, 134.6, 152.5 (C<sub>6</sub>H<sub>3</sub>), 168.9, 176.2 (C=C), 183.3, 186.9 (2 CO). ESI-MS: *m/z* calcd for C<sub>18</sub>H<sub>21</sub>ClNO<sub>9</sub> [M + H]<sup>+</sup>, 430.1; found, 430.1.

**2-Chloro-4-[(2-(4-methylpiperazin-1-yl)-3,4-dioxocyclobuten-1-yl)amino]phenyl α-D-Mannopyranoside (4).** Compound 8 (72.5 mg, 0.169 mmol) was dissolved in MeOH (7.5 mL) at 50 °C. After it was cooled to rt, *N*-methylpiperazine (28.0 μL, 0.252 mmol) and diisopropyl-ethylamine (DIPEA) (145 μL) were added, and the reaction mixture was stirred for 18 h at rt. Then, the solvent was removed in vacuo, and the residue was purified by LC-MS (RP-18, H<sub>2</sub>O/MeCN + 0.2% HCO<sub>2</sub>H) to give 4 (73.9 mg, 90%) as a white

powder after a final lyophilization from H<sub>2</sub>O/dioxane. [α]<sub>D</sub><sup>25</sup> +74.5 (c 1.00, MeOH). <sup>1</sup>H NMR (500 MHz, CD<sub>3</sub>OD): δ 2.47 (s, 3H, NCH<sub>3</sub>), 2.76 (m, 4H, 2 CH<sub>2</sub>), 3.66 (ddd, *J* = 2.1, 5.6, 9.8 Hz, 1H, H-5), 3.71 (dd, *J* = 5.6, 11.8 Hz, 2H, H-6a), 3.74 (t, *J* = 9.7 Hz, 1H, H-4), 3.79 (dd, *J* = 2.1, 11.8 Hz, 2H, H-6b), 3.88 (m, 4H, 2 CH<sub>2</sub>), 3.96 (dd, *J* = 3.4, 9.4 Hz, 1H, H-3), 4.09 (dd, *J* = 1.8, 3.3 Hz, 1H, H-2), 5.48 (d, *J* = 1.4 Hz, 1H, H-1), 7.15 (dd, *J* = 2.7, 8.9 Hz, 1H, C<sub>6</sub>H<sub>3</sub>), 7.33 (d, *J* = 8.9 Hz, 1H, C<sub>6</sub>H<sub>3</sub>), 7.35 (d, *J* = 2.7 Hz, 1H, C<sub>6</sub>H<sub>3</sub>). <sup>13</sup>C NMR (125 MHz, CD<sub>3</sub>OD): δ 45.4 (NCH<sub>3</sub>), 47.4 (2C, 2 CH<sub>2</sub>), 55.0 (2C, 2 CH<sub>2</sub>), 62.7 (C-6), 68.2 (C-4), 71.8 (C-2), 72.3 (C-3), 76.0 (C-5), 101.2 (C-1), 119.0, 121.6, 123.8, 125.0, 135.1, 150.2 (C<sub>6</sub>H<sub>3</sub>), 164.9, 169.2 (C=C), 183.3, 185.9 (2 CO). HR-MS: *m/z* calcd for C<sub>21</sub>H<sub>26</sub>ClN<sub>2</sub>NaO<sub>8</sub> [M + Na]<sup>+</sup>, 506.1306; found, 506.1303.

**Expression and Purification of DC-SIGN CRD-Fc and DC-SIGNR CRD-Fc.** Plasmids containing the full-length cDNA of DC-SIGN and DC-SIGNR were kindly provided by Daniel A. Mitchell, Clinical Sciences Research Institute, Warwick Medical School (Coventry, United Kingdom). Standard molecular techniques<sup>32</sup> were used for the cloning of the CRD of DC-SIGN (DC-SIGN CRD; aa residues 250–404, GenBank accession no. M98457) and DC-SIGNR (DC-SIGNR CRD; aa residue 262–398, GenBank accession no. Q9H2x3). The DC-SIGN/DC-SIGNR CRD encoding inserts were amplified by PCR using primers containing the restriction sites *Eco*RI and *Nco*I, respectively. The insert was ligated into the corresponding cloning site of the pFUSE-hIgG2-Fc2 expression vector (Invivogen, Toulouse, France). The constructs were amplified in chemocompetent DH5α *E. coli* (Novagen, Lucerne, Switzerland), and their correctness was confirmed by DNA sequencing.

CHO-K1 cells (American Type Culture Collection No. CCL-61) were cultivated in Ham's Nutrient Mixture F-12 supplemented with 2 mM L-glutamate (Invitrogen, Paisley, United Kingdom), 10% fetal calf serum (FCS, Invitrogen), 100 U/mL penicillin, and 100 μg/mL streptomycin (both Sigma-Aldrich, Basel, Switzerland). The CHO-K1 cells were transfected with the DC-SIGN CRD or DC-SIGNR CRD expression vector using the FuGENE HD transfection reagent (Roche Applied Science, Rotkreuz, Switzerland). Stably transfected CHO-K1 cells were selected by treatment with Zeocin (0.5 μg/mL, Invitrogen), and single clones were obtained by limiting dilution. For protein production, the cells were cultivated as described above, and the culture medium containing the secreted DC-SIGN CRD-Fc and DC-SIGN CRD-Fc chimera was harvested weekly. Purification of the recombinant protein was achieved by applying conditioned medium on a protein A-sepharose column (BioVision, Mountain View, CA) attached to a fast protein liquid chromatography apparatus [BioLogic (FPLC) system, BioRad, Reinach BL, Switzerland], with loading buffer I [20 mM Tris/HCl, pH 7.6, 150 mM NaCl, and 0.05% (v/v) Tween-20]. The protein was eluted with elution buffer I (0.5 M acetic acid/ammonium acetate, pH 3.4). The collected protein was further purified on a L-fucose-sepharose column (prepared in house) using loading buffer II (20 mM Tris/HCl, pH 7.8, 0.5 M NaCl, and 25 mM CaCl<sub>2</sub>) and elution buffer II (20 mM Tris/HCl, pH 7.8, 0.5 M NaCl, and 2 mM EDTA). For long-term storage, the protein was stored at –80 °C.

**FimH, Human Langerin, DLEC, SP-D, Mannose Binding Protein (MBP), Dectin-2, and MMR.** The FimH CRD linked with a thrombin cleavage site to a 6His-tag (FimH-CRD-Th-6His) was expressed in *E. coli* strain HM125 and purified by affinity chromatography as described in Rabbani et al.<sup>4d</sup> Human langerin, DLEC, SP-D, MBP, dectin-2, and MMR were purchased from R&D systems (Minneapolis, MN).

**Competitive Binding Assay.** Biotinylated trimannose (TM)-PAA polymer (20 μL, 1 mg/mL, Lectinity, Moscow) was mixed with 80 μL of assay buffer (20 mM HEPES, 150 mM NaCl, and 10 mM CaCl<sub>2</sub>, pH 7.4), 20 μL of FCS, and 80 μL of streptavidin–horseradish peroxidase conjugate (500 U/mL, Roche, Mannheim, Germany) and incubated for 2 h at 37 °C. The complex was stable for several weeks when stored at 4 °C.

For assay development FimH, DC-SIGN, DC-SIGNR, MBP, langerin, DLEC, SP-D, dectin-2, and MMR were each diluted in assay buffer (20 mM HEPES, pH 7.4, 150 mM NaCl, and 10 mM

CaCl<sub>2</sub>) at concentrations of 1, 3, 5, and 10 µg/mL and were coated on microtiter plates (F96 MaxiSorp, Nunc, Langensfeld, Germany) with 100 µL/well overnight at 4 °C. The coating solution was discarded, and the wells were blocked with 200 µL/well of a 3% bovine serum albumin (BSA) solution in assay buffer for 2 h at 4 °C. After three washing steps with assay buffer, the streptavidin–peroxidase-coupled TM-PAA polymer (0.5–5 µg/mL) in assay buffer (50 µL/well) was added to the wells. The plates were incubated for 3 h at 25 °C and 350 rpm and then washed four times with assay buffer. After the addition of 100 µL/well of 2,2'-azino-bis-(3-ethylbenzthiazoline-6-sulfonic acid) (ABTS) substrate (Invitrogen), the colorimetric reaction was allowed to develop for 4 min and then stopped by adding 100 µL/well of 2% aqueous oxalic acid. The OD was measured at 415 nm on a microplate reader (Spectramax 190, Molecular Devices, CA).

For measuring the binding properties of FimH antagonists to the mannose binding receptors, a mix (total volume 100 µL/well) of the test compounds 1–5 (final concentration 1 mM) or  $\alpha$ -D-mannose (final concentration 50 mM) and the streptavidin–peroxidase-coupled TM-PAA polymer in assay buffer (final concentration see Table 1) was added to the protein-coated wells and developed as described above.

## ■ ASSOCIATED CONTENT

### ● Supporting Information

HPLC trace and <sup>1</sup>H NMR spectrum for compound 4. This material is available free of charge via the Internet at <http://pubs.acs.org>.

## ■ AUTHOR INFORMATION

### Corresponding Author

\*Tel: +41 61 267 1551. Fax: +41 61 267 1552. E-mail: [beat.ernst@unibas.ch](mailto:beat.ernst@unibas.ch).

### Notes

The authors declare no competing financial interest.

## ■ ACKNOWLEDGMENTS

Plasmids containing the full-length cDNA of DC-SIGN and DC-SIGNR were kindly provided by Dr. Daniel Mitchell, Clinical Sciences Research Institute, Warwick Medical School (Coventry, United Kingdom). The financial support by the Swiss National Science Foundation (SNF interdisciplinary grant K-32K1-120904) is gratefully acknowledged.

## ■ ABBREVIATIONS USED

ABTS, 2,2'-azino-bis-(3-ethylbenzthiazoline-6-sulfonic acid); BSA, bovine serum albumin; CFU, colony-forming units; CRD, carbohydrate recognition domain; DC-SIGN, DC-specific ICAM-3-grabbing nonintegrin; DC-SIGNR, DC-specific ICAM-3-grabbing nonintegrin related; DLEC, dendritic cell lectin; DIPEA, diisopropyl-ethylamine; FCS, fetal calf serum; MBP, mannose binding protein; MMR, macrophage mannose receptor; OD, optical density; PAA, polyacrylamide; TM-PAA, Man $\alpha$ 1–3(Man $\alpha$ 1–6)Man $\beta$ 1–4GlcNAc $\beta$ 1–4GlcNAc $\beta$ -PAA; PRR, pathogen-recognition receptors; SP-D, lung surfactant protein D; UPEC, uropathogenic *Escherichia coli*; UPIa, uroplakin Ia; UTI, urinary tract infection

## ■ REFERENCES

- (1) Ronald, A. The etiology of urinary tract infection: Traditional and emerging pathogens. *Am. J. Med.* **2002**, *113*, 14S–19S.
- (2) (a) Mulvey, M. A. Adhesion and entry of uropathogenic *Escherichia coli*. *Cell. Microbiol.* **2002**, *4*, 257–271. (b) Wiles, T. J.; Kulesus, R. R.; Mulvey, M. A. Origins and virulence mechanisms of uropathogenic *Escherichia coli*. *Exp. Mol. Pathol.* **2008**, *85*, 11–19. (c) Xie, B.; Zhou, G.; Chan, S. Y.; Shapiro, E.; Kong, X. P.; Wu, X. R.; Sun, T. T.; Costello, C. E. Distinct glycan structures of uroplakins Ia

and Ib—Structural basis for the selective binding of FimH adhesion to uroplakin Ia. *J. Biol. Chem.* **2006**, *281*, 14644–14653. (d) Zhou, G.; Mo, W. J.; Sebbel, P.; Min, G. W.; Neubert, T. A.; Glockshuber, R.; Wu, X. R.; Sun, T. T.; Kong, X. P. Uroplakin Ia is the urothelial receptor for uropathogenic *Escherichia coli*: evidence from in vitro FimH binding. *J. Cell Sci.* **2001**, *114*, 4095–4103.

(3) (a) Ofek, I.; Hasy, D. L.; Sharon, N. Anti-adhesion therapy of bacterial diseases: Prospects and problems. *FEMS Immunol. Med. Microbiol.* **2003**, *38*, 181–191. (b) Sharon, N. Carbohydrates as future anti-adhesion drugs for infectious diseases. *Biochim. Biophys. Acta, Gen. Subj.* **2006**, *1760*, 527–537. (c) Ernst, B.; Magnani, J. L. From carbohydrate leads to glycomimetic drugs. *Nat. Rev. Drug Discovery* **2009**, *8*, 661–677.

(4) (a) Lindhorst, T. K.; Kieburg, C.; Krallmann-Wenzel, U. Inhibition of the type 1 fimbriae-mediated adhesion of *Escherichia coli* to erythrocytes by multiantennary alpha-mannosyl clusters: The effect of multivalency. *Glycoconjugate J.* **1998**, *15*, 605–613. (b) Bouckaert, J.; Berglund, J.; Schembri, M.; De Genst, E.; Cools, L.; Wuhler, M.; Hung, C. S.; Pinkner, J.; Slattegard, R.; Zavalov, A.; Choudhury, D.; Langermann, S.; Hultgren, S. J.; Wyns, L.; Klemm, P.; Oscarson, S.; Knight, S. D.; De Greve, H. Receptor binding studies disclose a novel class of high-affinity inhibitors of the *Escherichia coli* FimH adhesion. *Mol. Microbiol.* **2005**, *55*, 441–455. (c) Sperling, O.; Fuchs, A.; Lindhorst, T. K. Evaluation of the carbohydrate recognition domain of the bacterial adhesin FimH: design, synthesis and binding properties of mannoside ligands. *Org. Biomol. Chem.* **2006**, *4*, 3913–3922. (d) Rabbani, S.; Jiang, X.; Schwardt, O.; Ernst, B. Expression of the carbohydrate recognition domain of FimH and development of a competitive binding assay. *Anal. Biochem.* **2010**, *407*, 188–195. (e) Pang, L.; Kleeb, S.; Lemme, K.; Rabbani, S.; Scharenberg, M.; Zalewski, A.; Schädler, F.; Schwardt, O.; Ernst, B. FimH antagonists: Structure-activity and structure-property relationships for biphenyl  $\alpha$ -D-mannopyranosides. *ChemMedChem* **2012**, *7*, 1404–1422.

(5) (a) Aronson, M.; Medalia, O.; Schori, L.; Mirelman, D.; Sharon, N.; Ofek, I. Preventing of colonization of the urinary tract of mice with *Escherichia coli* by blocking of bacterial adherence with methyl alpha-D-mannopyranoside. *J. Infect. Dis.* **1979**, *139*, 329–332. (b) Wellens, A.; Garofalo, C.; Nguyen, H.; Van Gerven, N.; Slattegard, R.; Hernalsteens, J.-P.; Wyns, L.; Oscarson, S.; De Greve, H.; Hultgren, S.; Bouckaert, J. Intervening with urinary tract infections using anti-adhesives based on the crystal structure of the FimH-oligomannose-3 complex. *PLoS One* **2008**, *3*, e2040. (c) Han, Z.; Pinkner, J. S.; Ford, B.; Obermann, R.; Nolan, W.; Wildman, S. A.; Hobbs, D.; Ellenberger, T.; Cusumano, C. K.; Hultgren, S. J.; Janetka, J. W. Structure-based drug design and optimization of mannose bacterial FimH antagonists. *J. Med. Chem.* **2010**, *53*, 4779–4792. (d) Klein, T.; Abgottspon, D.; Wittwer, M.; Rabbani, S.; Herold, J.; Jiang, X.; Kleeb, S.; Luethi, C.; Scharenberg, M.; Bezençon, J.; Gubler, E.; Pang, L.; Smiesko, M.; Cutting, B.; Schwardt, O.; Ernst, B. FimH antagonists for the oral treatment of urinary tract infections: From design and synthesis to in vitro and in vivo evaluation. *J. Med. Chem.* **2010**, *53*, 8627–8641. (e) Han, Z.; Pinkner, J. S.; Ford, B.; Chorell, E.; Crowley, J. M.; Cusumano, C. K.; Campbell, S.; Henderson, J. P.; Hultgren, S. J.; Janetka, J. W. Lead optimization studies on FimH antagonists: Discovery of potent and orally bioavailable ortho-substituted biphenyl mannosides. *J. Med. Chem.* **2012**, *55*, 3945–3959. (f) Cusumano, C. K.; Pinkner, J. S.; Han, Z.; Greene, S. E.; Ford, B. A.; Crowley, J. R.; Henderson, J. P.; Janetka, J. W.; Hultgren, S. J. Treatment and prevention of urinary tract infection with orally active FimH inhibitors. *Sci. Transl. Med.* **2011**, *3*, 1–10. (g) Jiang, X.; Abgottspon, D.; Kleeb, S.; Rabbani, S.; Scharenberg, M.; Wittwer, M.; Haug, M.; Schwardt, O.; Ernst, B. Anti-adhesion therapy for urinary tract infections—A balanced PK/PD-profile proved to be key for success. *J. Med. Chem.* **2012**, *55*, 4700–4713.

(6) Huggins, D. J.; Sherman, W.; Tidor, B. Rational approaches to improving selectivity in drug design. *J. Med. Chem.* **2012**, *55*, 1424–1444.

- (7) Khoo, U. S.; Chan, K. Y. K.; Chan, V. S. F.; Lin, C. L. S. DC-SIGN and L-SIGN: The SIGNs for infection. *J. Mol. Med.* **2008**, *86*, 861–874.
- (8) Lee, S. J.; Evers, S.; Roeder, D.; Parlow, A. F.; Risteli, J.; Risteli, L.; Lee, Y. C.; Feizi, T.; Langen, H.; Nussenzweig, M. C. Mannose receptor-mediated regulation of serum glycoprotein homeostasis. *Science* **2002**, *295*, 1898–1901.
- (9) (a) East, L.; Isacke, C. M. The mannose receptor family. *Biochim. Biophys. Acta, Gen. Subj.* **2002**, *1572*, 364–386. (b) Dommett, R. M.; Klein, N.; Turner, M. W. Mannose-binding lectin in innate immunity: Past, present and future. *Tissue Antigens* **2006**, *68*, 193–209.
- (10) Weis, W. I.; Taylor, M. E.; Drickamer, K. The C-type lectin superfamily in the immune system. *Immunol. Rev.* **1998**, *163*, 19–34.
- (11) Mori, K.; Kawasaki, T.; Yamashina, I. Isolation and characterization of endogenous ligands for liver mannan-binding protein. *Arch. Biochem. Biophys.* **1988**, *264*, 647–656.
- (12) Kishore, U.; Greenhough, T. J.; Waters, P.; Shrive, A. K.; Ghai, R.; Kamran, M. F.; Bernal, A. L.; Reid, K. B. M.; Madan, T.; Chakraborty, T. Surfactant proteins SP-A and SP-D: Structure, function and receptors. *Mol. Immunol.* **2006**, *43*, 1293–1315.
- (13) Wallis, R.; Mitchell, D. A.; Schmid, R.; Schwaeble, W. J.; Keeble, A. H. Paths reunited: Initiation of the classical and lectin pathways of complement activation. *Immunobiology* **2010**, *215*, 1–11.
- (14) (a) Jensen, P. H.; Weilguny, D.; Matthiesen, F.; McGuire, K. A.; Shi, L.; Hojrup, P. Characterization of the oligomer structure of recombinant human mannan-binding lectin. *J. Biol. Chem.* **2005**, *280*, 11043–11051. (b) Teillet, F.; Dublet, B.; Andrieu, J. P.; Gaboriaud, C.; Arland, G. J.; Thielens, N. M. The two major oligomeric forms of human mannan-binding lectin: Chemical characterization, carbohydrate-binding properties, and interaction with MBL-associated serine proteases. *J. Immunol.* **2005**, *174*, 2870–2877. (c) Sim, R. B.; Clark, H.; Hajela, K.; Mayilyan, K. R. Collectins and host defence. *Novartis Found. Symp.* **2006**, *279*, 170–181. (d) Ohya, M.; Nishitani, C.; Sano, H.; Yamada, C.; Mitsuzawa, H.; Shimizu, T.; Saito, T.; Smith, K.; Crouch, E.; Kuroki, Y. Human pulmonary surfactant protein D binds the extracellular domains of toll-like receptors 2 and 4 through the carbohydrate recognition domain by a mechanism different from its binding to phosphatidylinositol and lipopolysaccharide. *Biochemistry* **2006**, *45*, 8657–8664.
- (15) Kerrigan, A. M.; Brown, G. D. C-type lectins and phagocytosis. *Immunobiology* **2009**, *214*, 562–575.
- (16) Valladeau, J.; Ravel, O.; Dezutter-Dambuyant, C.; Moore, K.; Kleijmeer, M.; Liu, Y.; Duvert-Frances, V.; Vincent, C.; Schmitt, D.; Davoust, J.; Caux, C.; Lebecque, S.; Saeland, S. Langerin, a novel C-type lectin specific to Langerhans cells, is an endocytic receptor that induces the formation of Birbeck granules. *Immunity* **2000**, *12*, 71–81.
- (17) Geijtenbeek, T. B. H.; Torensma, R.; van Vliet, S. J.; van Duijnhoven, G. C. F.; Adema, G. J.; van Kooyk, Y.; Figdor, C. G. Identification of DC-SIGN, a novel dendritic cell-specific ICAM-3 receptor that supports primary immune responses. *Cell* **2000**, *100*, 575–585.
- (18) Feinberg, H.; Mitchell, D. A.; Drickamer, K.; Weis, W. I. Structural basis for selective recognition of oligosaccharides by DC-SIGN and DC-SIGNR. *Science* **2001**, *294*, 2163–2166.
- (19) Kanazawa, N. Dendritic cell immunoreceptors: C-type lectin receptors for pattern-recognition and signaling on antigen-presenting cells. *J. Dermatol. Sci.* **2007**, *45*, 77–86.
- (20) Kanazawa, N.; Tashiro, K.; Miyachi, Y. Signaling and immune regulatory role of the dendritic cell immunoreceptor (DCIR) family lectins: DCIR, DCAR, dectin-2 and BDCA-2. *Immunobiology* **2004**, *209*, 179–190.
- (21) Stambach, N. S.; Taylor, M. E. Characterization of carbohydrate recognition by langerin, a C-type lectin of Langerhans cells. *Glycobiology* **2003**, *13*, 401–410.
- (22) Crouch, E. C.; Smith, K.; McDonald, B.; Briner, D.; Linders, B.; McDonald, J.; Holmskov, U.; Head, J.; Hartshorn, K. Species differences in the carbohydrate binding preferences of surfactant protein D. *J. Dermatol. Sci.* **2006**, *35*, 84–94.
- (23) McGreal, E. P.; Rosas, M.; Brown, G. D.; Zamze, S.; Wong, S. Y. C.; Gordon, S.; Martinez-Pomares, L.; Taylor, P. R. The carbohydrate-recognition domain of Dectin-2 is a C-type lectin with specificity for high mannose. *Glycobiology* **2006**, *16*, 422–430.
- (24) Appelmelk, B. J.; van Die, I.; van Vliet, S. J.; Vandenbroucke-Grauls, C.; Geijtenbeek, T. B. H.; van Kooyk, Y. Cutting edge: Carbohydrate profiling identifies new pathogens that interact with dendritic cell-specific ICAM-3-grabbing nonintegrin on dendritic cells. *J. Immunol.* **2003**, *170*, 1635–1639.
- (25) Abgottspon, D.; Roelli, G.; Hosch, L.; Steinhuber, A.; Jiang, X.; Schwardt, O.; Cutting, B.; Smiesko, M.; Jenal, U.; Ernst, B.; Trampuz, A. Development of an aggregation assay to screen FimH antagonists. *J. Microbiol. Methods* **2010**, *82*, 249–255.
- (26) (a) Vervoort, A.; De Bruyne, C. K. Enzymatic hydrolysis of substituted phenyl- $\alpha$ -D-mannopyranosides. *Carbohydr. Res.* **1970**, *12*, 277–280. (b) De Priecker, J.; De Bock, A.; De Bruyne, C. K.  $\alpha$ -D-mannosidase-catalyzed hydrolysis of substituted phenyl  $\alpha$ -D-mannopyranosides. *Carbohydr. Res.* **1978**, *60*, 141–153.
- (27) Kosak, J. R. Catalytic hydrogenation of aromatic halonitro compounds. *Ann. N.Y. Acad. Sci.* **1970**, *172*, 175–185.
- (28) Guo, P.; Feinberg, H.; Conroy, E.; Mitchell, D. A.; Alvarez, R.; Blixt, O.; Taylor, M. E.; Weis, W. I.; Drickamer, K. Structural basis for distinct ligand-binding and targeting properties of the receptors DC-SIGN and DC-SIGNR. *Nat. Struct. Mol. Biol.* **2004**, *11*, 591–598.
- (29) Linehan, S. A.; Martinez-Pomares, L.; da Silva, R. P.; Gordon, S. Endogenous ligands of carbohydrate recognition domains of the mannose receptor in murine macrophages, endothelial cells and secretory cells; potential relevance to inflammation and immunity. *Eur. J. Immunol.* **2001**, *31*, 1857–1866.
- (30) (a) Imberthy, A.; Chabre, Y. M.; Roy, R. Glycomimetics and glycodendrimers as high affinity microbial anti-adhesins. *Chemistry* **2008**, *14*, 7490–7499. (b) Hartmann, M.; Lindhorst, T. K. The bacterial lectin FimH, a target for drug discovery—Carbohydrate inhibitors of type 1 fimbriae-mediated bacterial adhesion. *Eur. J. Org. Chem.* **2011**, 3583–3609.
- (31) Hung, C. S.; Bouckaert, J.; Hung, D.; Pinkner, J.; Widberg, C.; DeFusco, A.; Auguste, C. G.; Strouse, R.; Langermann, S.; Waksman, G.; Hultgren, S. J. Structural basis of tropism of *Escherichia coli* to the bladder during urinary tract infection. *Mol. Microbiol.* **2002**, *44*, 903–915.
- (32) Sambrook, J.; Fritsch, E. F.; Maniatis, T. *Molecular Cloning. A Laboratory Manual*, 2nd ed.; Cold Spring Harbor Laboratory Press: Cold Spring Harbor, NY, 1989; Vols. 1–3.

## **Part I: The lectin FimH**

---

**FimH Chapter 2: Results and discussion**

**Publication 4**

---

DOI: 10.1002/cmdc.200((will be filled in by the editorial staff))

## Kinetic Properties of Carbohydrate-Lectin Interactions: FimH Antagonists

Meike Scharenberg, Xiaohua Jiang, Lijuan Pang, Giulio Navarra, Said Rabbani, Florian Binder, Oliver Schwardt, Beat Ernst\*<sup>[a]</sup>

Urinary tract infections (UTIs) are among the most prevalent infections and affect millions of people each year. In 70 - 95% of all cases, UTI is caused by uropathogenic *Escherichia coli* (UPEC).<sup>[1]</sup> These bacteria express type 1 pili with a terminally located adhesive protein called FimH. FimH-mediated adhesion to the surface of urothelial cells by binding to oligomannoside residues of the glycoprotein uroplakin Ia (UPIa)<sup>[2-5]</sup> is a prerequisite for the invasion of the host cells leading to UTI.<sup>[2,3]</sup> Therefore, efforts are made to identify orally available FimH antagonists to interfere with the attachment of UPEC to urothelial cells. From these studies  $\alpha$ -D-mannopyranosides have emerged providing a novel therapeutic opportunity for prevention and treatment of UTI as an alternative to antibiotics.<sup>[6-8]</sup> To date, several mannose-based FimH antagonists have been validated in various *in vitro* and *in vivo* studies.<sup>[9-20]</sup>

As part of their pharmacodynamic characterization, not only equilibrium dissociation constants ( $K_D$ ) or half-maximal inhibitory concentrations ( $IC_{50}$ ) but also the kinetics of the binding process are studied.<sup>[21-23]</sup> One crucial factor for a sustained *in vivo* efficacy is the half-life ( $t_{1/2}$ ) of the drug-receptor complex, especially when drugs compete with endogenous ligands.

The  $t_{1/2}$  of a drug-receptor complex depends on the dissociation rate ( $k_{off}$ ). Slow off-rates are beneficial for the *in vivo* efficacy, as prolonged occupancy of the target by the drug results in an extended duration of the pharmacological effect. Consequently, lower drug concentrations are required to obtain high efficacy, reducing the risk of off-target toxicity.<sup>[21-23]</sup> The importance of long target occupancy is reflected in the long half-lives of many drugs reaching the market, such as the HIV-1 protease inhibitor Darunavir ( $t_{1/2} > 240$  h),<sup>[24]</sup> the CCR5 receptor antagonist Maraviroc ( $t_{1/2} = 10.5$  h),<sup>[25]</sup> or the viral neuraminidase inhibitor Zanamivir, which was developed from a carbohydrate-based lead structure ( $t_{1/2} > 33$  min).<sup>[26]</sup>

For carbohydrate-lectin interactions, only a few studies describing the kinetic properties are available. For the lectins myelin-associated glycoprotein (MAG),<sup>[27,28]</sup> E-, L- and P-selectin,<sup>[29-31]</sup> galectin-1 and -3,<sup>[32]</sup> mannose-binding protein (MBP),<sup>[33]</sup> concanavalin A (ConA)<sup>[34]</sup> and calreticulin<sup>[35]</sup> surface plasmon resonance (SPR) experiments revealed fast association and dissociation kinetics with  $k_{off}$  rates between  $2.6 \times 10^{-3}$  and  $> 10$  s<sup>-1</sup>, resulting in short half-lives ranging from 266 to 0.07 seconds (Table 1). This fast binding kinetics typical for carbohydrate-lectin interactions strongly hamper the development of carbohydrate derived drugs. The determination of the kinetic parameters of FimH antagonists is therefore of utmost importance for a successful lead optimization.

**Table 1.** Typical kinetic binding parameters of carbohydrate-protein interactions.

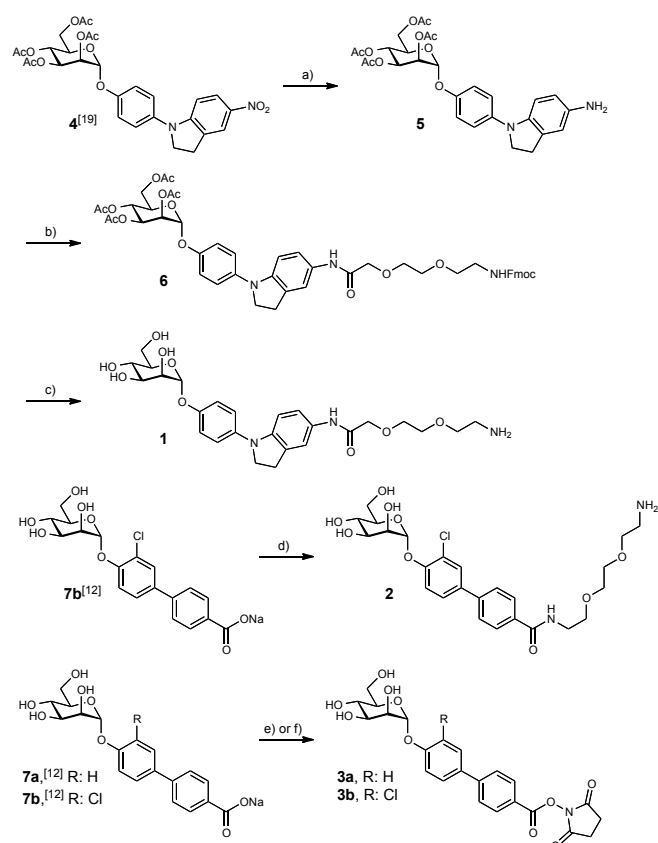
Protein	Ligand	$K_D$ [ $\mu$ M]	$k_{on}$ [ $M^{-1}/s^{-1}$ ]	$k_{off}$ [ $s^{-1}$ ]	$t_{1/2}$ [s]	Ref.
L-selectin	GlyCAM1	108	$>10^5$	$>10$	0.07	[30]
E-selectin	ESL 1	62	$4 \times 10^4$	3.0	0.2	[29]
P-selectin	PSGL 1	0.3	$4 \times 10^6$	1.4	0.5	[31]
GSLA-2 mAB	sialyl Lewis <sup>a</sup>	4.3	$1.1 \times 10^5$	$8 \times 10^{-1}$	0.9	[36]
Myelin-associated glycoprotein (MAG)	D-Neu5Ac derivative	2.8	$3.5 \times 10^5$	$0.8 \times 10^{-1}$	0.9	[27]
Galectin-1	D-Lactose derivative	1010	$1.9 \times 10^2$	$2.1 \times 10^{-1}$	3.3	[32]
Galectin-3	D-Lactose derivative	280	$7.3 \times 10^2$	$2.0 \times 10^{-1}$	3.4	[32]
CG-1A (avian galectin)	D-Lactose derivative	83.5	$2.5 \times 10^3$	$2.1 \times 10^{-1}$	3.3	[32]
Calreticulin	Glc <sub>1</sub> Man <sub>9</sub> -GlcNAc <sub>2</sub>	2	$3.9 \times 10^4$	$8 \times 10^{-2}$	8.6	[35]
Concanavalin A	D-Man derivative	65	$1.43 \times 10^2$	$9.4 \times 10^{-3}$	73.7	[34]
Mannose-binding protein (MBP)	D-Man <sub>16</sub> /BSA	13.3	$3.47 \times 10^4$	$2.6 \times 10^{-3}$	266.6	[33]

Beside  $K_D$  values, dissociation rates ( $k_{off}$ ) of the complex of FimH-antagonist with the target protein FimH are of special interest. To study these parameters, SPR is widely applied, including for carbohydrate-lectin<sup>[37]</sup> and carbohydrate-antibody<sup>[36]</sup> interactions. For the lectin domain of FimH different affinity states are known.<sup>[38]</sup> In this study, the lectin domain in the high-affinity state was used.<sup>[39]</sup> Immobilization attempts by standard amine coupling failed, presumably due to accessible amino groups in and close to the ligand-binding site. Thus, the *N*-terminal phenylalanine is part of the binding site. Immobilization *via* a C-terminal His-tag onto a Ni-NTA chip or indirect coupling *via* an anti-His-tag antibody failed due to instability of the base line, resulting from a slow detachment of the non-covalently

[a] Dr. M. Scharenberg, Dr. F. Binder, L. Pang, Dr. S. Rabbani, G. Navarra, Dr. X. Jiang, Dr. O. Schwardt, Prof. Dr. B. Ernst  
Institute of Molecular Pharmacy  
Pharmazentrum, University of Basel  
Klingelbergstrasse 50, CH-4056 Basel (Switzerland)  
Fax: (+41) 61 267 1552  
E-mail: beat.ernst@unibas.ch

Supporting information for this article is available on the WWW under <http://www.chemmedchem.org> or from the author.

immobilized FimH. Furthermore, harsh regenerating conditions (50 mM NaOH), necessary for the dissociation of the antagonist-lectin complex, caused the inactivation of the protein. Consequently, we immobilized FimH antagonists functionalized with an amino- (**1** & **2**, Scheme 1) or *N*-hydroxy-succinimide (**3a,b**, Scheme 1) via an amine-coupling procedure on CM4 dextran sensor surface chips.

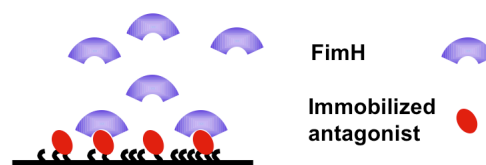


**Scheme 1.** Synthesis of the amino- or *N*-hydroxyl-succinimide functionalized FimH antagonists **1**, **2**, **3a** and **3b**. a)  $H_2$  (1 atm),  $PtO_2$ , morpholine, EtOAc/MeOH (1:1) (97%); b) 8-(Fmoc-amino)-3,6-dioxo-octanoic acid, PyBOP, DIPEA, DMF, rt; c) NaOMe, MeOH, rt (47% over two steps); d) EBE, COMU, DIPEA, DMF, 0 °C to rt (20%); e) EDC, NHS,  $H_2O$ , rt (**3a**: 98%); f) EDC, NHS, MES buffer (pH 5.6), rt (**3b**: 99%).

**Direct binding assay - Kinetics of FimH antagonists.** To determine the kinetic parameters of the FimH-antagonist interaction, FimH was passed at concentrations between 0-200 nM over the flow cells (CM4 chip) equipped with covalently linked antagonists (Figure 1a). A reference cell without antagonist but treated with NHS/EDC and ethanolamine (EA) was used to account for nonspecific binding of the protein to the dextran matrix.

The kinetic parameters  $k_{on}$  and  $k_{off}$  were obtained by applying a global fit to the sensorgrams, using a 1:1 (Langmuir-type) binding-model (Scrubber 2.0c). The fitted sensorgrams of compounds **1**, **2**, **3a** and **3b** are shown in Figure 1b.

### a) Direct binding assay



### b) Binding sensorgrams

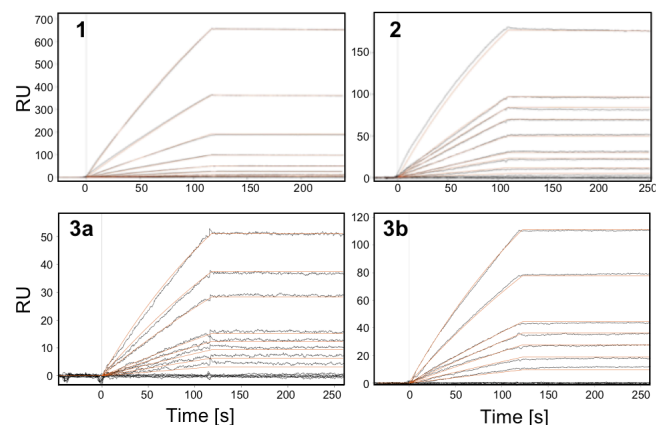


**Figure 1.** a) Schematic representation of a direct binding assay format. FimH binds to **1**, **2**, **3a** and **3b**, which are immobilized on the chip. b) Sensorgrams obtained by kinetic fits of FimH binding to the immobilized antagonists **1**, **2**, **3a** and **3b**. FimH concentrations between 0-200 nM were passed over the surface. For the fitting of the sensorgrams Scrubber 2.0c was applied.

Mass transfer limitations, which might occur when using proteins as analytes (MW of FimH: 18.6 kD), can falsify the measured kinetic parameters. They depend on the cell dimension, the flow rate, and the diffusion coefficient of the analyte. Proteins having smaller diffusion coefficients than low molecular weight compounds are prone to show mass transfer limitations. To rule out these limitations, we used high flow rates (20-30  $\mu\text{L}/\text{min}$ ) and a low surface antagonist density (usage of CM4 chips instead of CM5 chips). Furthermore, we immobilized antagonist **1** at three different immobilization levels (different ratios between **1** and EA used for the immobilization) on the same sensor chip. FimH was screened simultaneously on all three surfaces and the kinetic parameters and affinities were evaluated. Since all three surfaces showed similar kinetic rates and affinities, mass transfer effects are negligible. The obtained kinetic parameters are summarized in Table 2.

Table 2. Kinetic binding parameters for the interaction of FimH with antagonists <b>1</b> , <b>2</b> and <b>3a,b</b> .					
Antagonist	Molar ratio Ligand : EA <sup>[a]</sup>	$K_D$ [nM]	$k_{on}$ [ $10^4 \text{ M}^{-1}\text{s}^{-1}$ ]	$k_{off}$ [ $10^{-5} \text{ s}^{-1}$ ]	$t_{1/2}$ [h]
<b>1</b>	1:0 (high density)	3.5	1.4	5.2	3.7
	1:10 (middle density)	2.5	2.0	5.1	3.8
	1:100 (low density)	2.0	2.6	5.3	3.6
<b>2</b>	1:0	0.7	4.8	3.5	5.5

<b>3a</b>	1:0	2.3	1.1	2.0	9.6
<b>3b</b>	1:0	n.d. <sup>[b]</sup>	1.4	$\leq 10^{-6}$ (out of limit)	>19
[a] EA: ethanolamine [b] n.d.: not determinable due to $k_{\text{off}} \leq 10^{-6} \text{ s}^{-1}$ .					

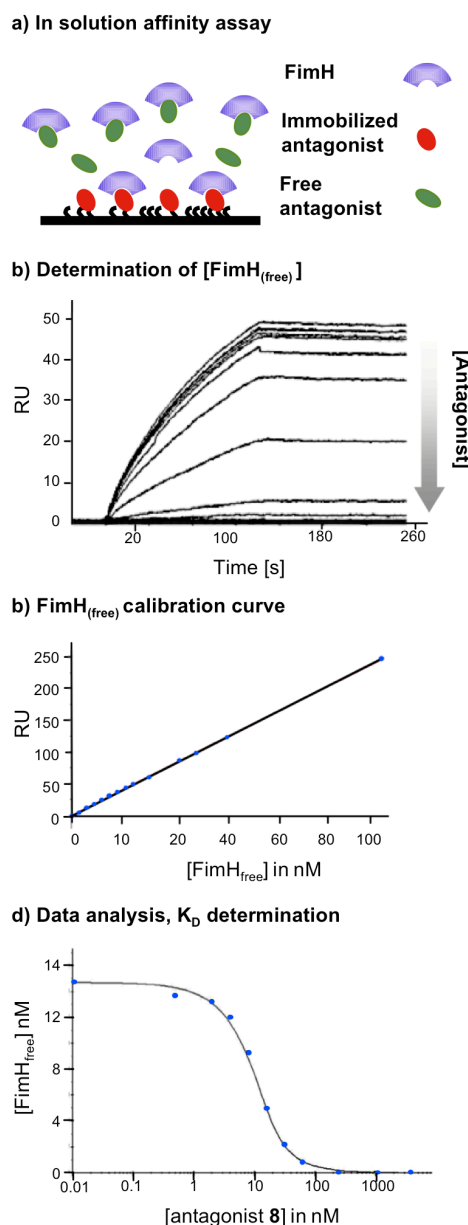
Association rates ( $k_{\text{on}}$ ) between  $1.4 \times 10^4$  and  $4.8 \times 10^4 \text{ M}^{-1}\text{s}^{-1}$  were obtained and are in the expected range for low molecular weight compounds. The dissociation rates ( $k_{\text{off}}$ ) were  $5.2 \times 10^{-5} \text{ s}^{-1}$  for **1**,  $3.5 \times 10^{-5} \text{ s}^{-1}$  for **2**, and  $2.0 \times 10^{-5} \text{ s}^{-1}$  for **3a**. For compound **3b** the detection limit of  $k_{\text{off}}$  (below  $10^{-6} \text{ s}^{-1}$ ) was reached and consequently the  $K_D$  value not determinable. The small dissociation constants resulted in half-lives between 3.6 h and > 19 h, representing extraordinary long half-lives for carbohydrate-lectin interactions, which are usually in the range of seconds (see Table 1). Consistent with the long half-lives, the equilibrium state of the interactions can only be reached after an extended period of time, conditions, which were not applicable to our SPR experiments. The affinity ( $K_D$ ) of the antagonists was therefore calculated from the kinetic parameters ( $K_D = k_{\text{off}}/k_{\text{on}}$ ) and not determined from steady state measurements. As expected,<sup>[12,19]</sup> affinities in the low nanomolar range (0.7 to 3.5 nM) were obtained. Furthermore, the three-fold higher affinity of compound **2** compared to compound **3a** is consistent with published data, confirming that a chloro-substituent in *ortho*-position of the aromatic ring adjacent to the anomeric center enhances binding affinity to FimH.<sup>[12]</sup> The off-rate of compound **2** was already close to the detection limit of the used method. Compound **3b**, which differs from **2** only by a shorter linker length, did not reveal reliable kinetic data, due to its immeasurable  $k_{\text{off}}$  value ( $\leq 10^{-6} \text{ s}^{-1}$ ), indicating that the linker length presumably has a small effect on the binding affinity.

FimH can exhibit two conformations, a low-affinity conformation and a high-affinity conformation. The switch from the low-affinity state to the high-affinity state can be triggered by applying a mechanical force along the molecule. This behaviour is characteristic for the catch-bond mechanism found for the FimH-ligand interaction.<sup>[38]</sup> It enables the bacteria to firmly attach to oligomannosides on bladder epithelial cells, even under the harsh conditions of the urinary tract (flow of urine). In the high-affinity state, the binding site of FimH forms a deep, narrow, and negatively charged pocket, unlike mammalian lectins, often characterized by shallow and water accessible binding sites (see e.g. selectins,<sup>[40]</sup> galectins,<sup>[41]</sup> mannose-binding protein<sup>[42]</sup> or DC-SIGN<sup>[43]</sup>). Hydrophilic side chains of the amino acids lining the FimH binding pocket, establish a perfect network of hydrogen bonds with the hydroxyl groups of  $\alpha$ -D-mannopyranosides.<sup>[44]</sup> Consequently, the slow dissociation of the carbohydrate-FimH complex found in this study, can be explained by the binding mode of FimH ligands to the high-affinity FimH conformation. As the pathogenicity of the bacteria depends on the interaction between FimH and its physiological ligand on the urothelial surface, a long half-life of FimH antagonists is of utmost importance for a successful treatment.

#### In solution affinity assay – $K_D$ values of FimH antagonists.

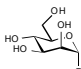
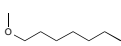
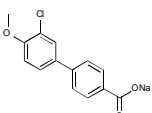
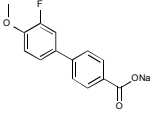
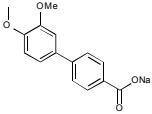
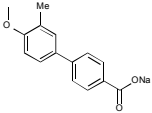
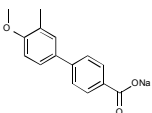
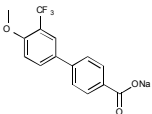
Due to the high affinity of FimH antagonists and their small dissociation rate, in solution affinity experiments (as described in Durka *et al.*<sup>[45]</sup>) can be applied to determine  $K_D$  values of antagonists. For these experiments we used the CM4 sensor chip coated with compound **1** (Chip 1). For an accurate determination

of  $K_D$  values, a constant concentration of FimH (10-15 nM) in the range of the  $K_D$  value to prevent stoichiometric titration conditions was equilibrated with a dilution series of the antagonists **7b-13**<sup>[46]</sup>. After equilibration, the unbound FimH,  $[\text{FimH}_{\text{free}}]$  binds to the immobilized antagonist **1** (Figure 2a) and can therefore be determined by SPR (Figure 2b) using a calibration curve (Figure 2c). Finally,  $[\text{FimH}_{\text{free}}]$  was plotted versus the antagonist concentration and the curve was fitted with the in-solution-affinity-fit-algorithm of the BiaEvaluation software (Figure 2d). The obtained  $K_D$  values are summarized in Table 3.



**Figure 2.** Results from the in solution affinity assay with *n*-heptyl  $\alpha$ -D-mannopyranoside **8** (see Table 3, entry 1). a) Schematic representation of the in solution affinity assay.  $\text{FimH}_{\text{free}}$  after equilibration binds to **1**, which is immobilized on the chip; b) Sensorgrams obtained after passing over the equilibrated mixtures of compound **8** and FimH; c) FimH calibration curve (FimH 0-120 nM) and d)  $K_D$  determination by in-solution-affinity-fit-algorithm of the BiaEvaluation software.

**Table 3.**  $K_D$  values of FimH antagonists<sup>[46]</sup> determined by the in solution affinity assay.

Entry		$K_D$ [nM] <sup>[a]</sup>	$rK_D$ <sup>[b]</sup>
1		5.21 ± 1.6	1
2		0.71 ± 0.01 0.5 ± 0.05 <sup>[c]</sup>	0.13 0.10 <sup>[c]</sup>
3		1.63 ± 0.9	0.32
4		1.08 ± 0.18	0.21
5		0.44 ± 0.22	0.09
6		2.19 ± 0.1	0.42
7		1.1 ± 0.34	0.21

[a] Determined on Chip 1 (CM4 chip functionalized with compound 1). [b] The relative  $K_D$ s ( $rK_D$ ) were calculated by dividing the  $K_D$  of the antagonist of interest by the  $K_D$  of *n*-heptyl  $\alpha$ -D-mannopyranoside (**8**). [c] Determined on Chip 2 (CM4 chip functionalized with compound 2,  $n = 3$ .)

*n*-Heptyl  $\alpha$ -D-mannopyranoside **8** and the biphenyl-substituted mannose antagonists **7b** and **9-13** with different substitutions in *ortho*-position of the aromatic ring adjacent to the anomeric position showed affinities in the low nanomolar range, which is in good agreement with data obtained from isothermal titration calorimetry (ITC).<sup>[46]</sup> To further validate the assay, we additionally tested compound **7b** on a chip functionalized with compound **2** (Chip 2), and obtained a similar  $K_D$  value (0.5 vs. 0.7 nM). Furthermore, the  $K_D$  value of **7b** determined by the in solution affinity approach is equal to the  $K_D$  value of **2** found by the direct binding assay (Table 2) ( $K_D = 0.7$  nM). Compounds **2** and **7b** share identical structure with the only difference that **2** was immobilized on the chip *via* a linker (for the direct binding approach) whereas the  $K_D$  for **7b** was determined by the in solution affinity assay. The comparable affinities of the two approaches confirm that the attachment of a linker and the immobilization process do not significantly influence the affinity of the antagonist.

In conclusion, for most medical applications, half-lives ( $t_{1/2}$ ) of the drug/target complex of several tens of minutes or even hours are of utmost importance, since long half-lives translate into higher *in vivo* efficacies and reduced adverse side effects resulting from off-target toxicity.<sup>[21,22]</sup> However, carbohydrate-lectin interactions often exhibit low affinities and fast off-rates, properties that hamper the development of carbohydrate-derived drugs. Therefore, as part of the preclinical development process of FimH antagonists, we examined their kinetic characteristics by surface plasmon resonance (SPR). In this study, the lectin domain of FimH in the high-affinity state was used. The surprisingly small dissociation rates for FimH-antagonist complexes resulting in long half-lives in the range of several hours (> 3.6 h) are indicators for high *in vivo* efficacy. This is a further indication that the corresponding ester prodrugs not only have a beneficial pharmacokinetic profile<sup>[46]</sup> but also fulfil the pharmacodynamic requirement for a therapeutic application, i.e. high affinity and long residence time. However, whether the investigated high-affinity state of FimH investigated in our study<sup>[39]</sup> is the only pathophysiologically relevant state remains to be demonstrated. Therefore, studies with FimH lectin in other affinity states are planned.

## Experimental Section

**Synthesis.** For synthesis and spectroscopic details of antagonists **1**, **2** and **3a,b** see Supporting Information. The synthesis and characterization of compounds **9-13** is described in ref.<sup>[46]</sup>

**FimH-CRD-6His protein expression.** The FimH carbohydrate recognition domain (CRD) with a thrombin cleavage site linked to a 6His-tag (FimH-CRD-Th-6His) was expressed in *E. coli* strain HM125 and purified by affinity chromatography as described in Rabbani *et al.*<sup>[39]</sup>

**Surface plasmon resonance (SPR) analysis.** The SPR measurements were performed on a Biacore 3000 surface plasmon resonance based optical biosensor (Biacore<sup>TM</sup>, GE Healthcare, Uppsala). Sensor chips (CM4), immobilization kits, maintenance supply and HBS-P buffer were purchased from GE Healthcare (Uppsala). The amino-functionalized monovalent compounds **1** and **2** were covalently attached to the activated dextrane matrix on CM4 chips by the standard amine-coupling method (GE Healthcare, Uppsala). The surface was activated by *N*-hydroxysuccinimide (NHS) and *N*-(3-dimethylaminopropyl)-*N*-ethylcarbodiimide hydrochloride (EDC). To obtain different ligand densities on the chip, compound **1** (1 mM in borate buffer) was mixed with ethanolamine (EA, 1 M) in different molar ratios prior to the coupling process (1:EA ratios: 1:0, 1:10, and 1:100). Pure compound **2** (1 mM in borate buffer) was coupled to the chip. After coupling, the matrix was capped with ethanolamine. For the coupling of the *N*-hydroxy-succinimide-functionalized compounds **3** and **4** the free carboxyl groups on the chip were activated with NHS and EDC and reacted with 1,2-diaminoethane (0.1 M in borate buffer, pH 8.5) to give free amino groups. The next steps were followed as described above. A reference cell without immobilized ligand was prepared and the system equilibrated with HBS-P buffer (10 mM HEPES, 150 mM NaCl, 0.005% P20, pH 7.4). The activity of the chips was confirmed by FimH binding at a constant concentration of 50 nM in HBS-P buffer. All binding experiments were performed at 25 °C at a flow rate of 20 or 30  $\mu$ L/min using HBS-P buffer. For kinetic studies a dilution series of FimH with concentrations ranging from 0-200 nM in HBS-P buffer was used. Contact time was 120 s and the dissociation time 1200 s. The surface was regenerated with a single injection of 50 mM NaOH for 120 s. Data processing as well as  $k_{on}$ ,  $k_{off}$ , and  $K_D$  determination were accomplished with the Scrubber software (BioLogic Software, Version 2.0c, Campbell, Australia). Double referencing (subtraction of



reference and blank injection) was applied to correct for bulk effects and other systematic artefacts.

**In solution affinity inhibition experiments.** FimH (10-15 nM in HBS-P buffer) was inhibited with a series of increasing concentrations of test compounds (0-1  $\mu$ M) over night at rt to allow the equilibration of the system. The mixtures were run over a sensor surface coated with compound 1 and the resonance units (RU) after an association time of 110 s were detected. The non-inhibited FimH concentration ( $[FimH]_{free}$ ) in the protein-compound mixtures was determined by means of a FimH calibration curve using free FimH concentrations ranging from 0 to 120 nM. The  $K_D$  values of the compounds were calculated by plotting  $[FimH]_{free}$  versus [compound] and fitting the curve with the in solution affinity fit.

## Acknowledgements

We gratefully acknowledge the financial support for GN by Nano-Tera (grant no. NT.ch 611\_61).

**Keywords:** Kinetics of carbohydrate-lectin interactions · FimH · FimH antagonists · Uropathogenic *Escherichia coli* · urinary tract infections

- [1] A. Ronald, *Am. J. Med.* **2002**, *113*, 14S-19S.
- [2] M. A. Mulvey, *Cell Microbiol.* **2002**, *4*, 257-271.
- [3] T. J. Wiles, R. R. Kulesus, M. A. Mulvey, *Exp. Mol. Pathol.* **2008**, *85*, 11-19.
- [4] B. Xie, G. Zhou, S. Y. Chan, E. Shapiro, X. P. Kong, X. R. Wu, T. T. Sun, C. E. Costello, *J. Biol. Chem.* **2006**, *281*, 14644-14653.
- [5] G. Zhou, W. J. Mo, P. Sebbel, G. W. Min, T. A. Neubert, R. Glockshuber, X. R. Wu, T. T. Sun, X. P. Kong, *Cell Sci.* **2001**, *114*, 4095-4103.
- [6] I. Ofek, D. L. Hasy, N. Sharon, *FEMS Immunology and Medical Microbiology* **2003**, *38*, 181-191.
- [7] N. Sharon, *Biochim. Biophys. Acta* **2006**, *1760*, 527-537.
- [8] B. Ernst, J. L. Magnani, *Nat. Rev. Drug Discov.* **2009**, *8*, 661-677.
- [9] J. Bouckaert, J. Berglund, M. Schembri, E. De Genst, L. Cools, M. Wührer, C. S. Hung, J. Pinkner, R. Slättegård, A. Zavialov, D. Choudhury, S. Langermann, S. J. Hultgren, L. Wyns, P. Klemm, S. Oscarson, S. D. Knight, H. De Greve, *Mol. Microbiol.* **2005**, *55*, 441-455.
- [10] T. K. Lindhorst, C. Kieburg, U. Krallmann-Wenzel, *Glycoconj. J.* **1998**, *15*, 605-613.
- [11] O. Sperling, A. Fuchs, T. K. Lindhorst, *Org. Biomol. Chem.* **2006**, *4*, 3913-3922.
- [12] T. Klein, D. Abgottspon, M. Wittwer, S. Rabbani, J. Herold, X. Jiang, S. Kleeb, C. Lüthi, M. Scharenberg, J. Bezençon, E. Gubler, L. Pang, M. Smiesko, B. Cutting, O. Schwardt, B. Ernst, *J. Med. Chem.* **2010**, *53*, 8627-8641.
- [13] D. Abgottspon, G. Roelli, L. Hosch, A. Steinhuber, X. Jiang, O. Schwardt, B. Cutting, M. Smiesko, U. Jenal, B. Ernst, A. Trampuz, *J. Microbiol. Methods.* **2010**, *82*, 249-255.
- [14] Z. Han, J. S. Pinkner, B. Ford, R. Obermann, W. Nolan, S. A. Wildman, D. Hobbs, T. Ellenberger, C. K. Cusumano, S. J. Hultgren, J. W. Janetka, *J. Med. Chem.* **2010**, *53*, 4779-4792.
- [15] A. Wellens, C. Garofalo, H. Nguyen, N. Van Gerven, R. Slättegård, J.-P. Hernalsteens, L. Wyns, S. Oscarson, H. De Greve, S. Hultgren, J. Bouckaert, *Plos One* **2008**, *3*, 1-13.
- [16] C. S. Eden, R. Freter, L. Hagberg, R. Hull, S. Hull, H. Leffler, G. Schoolnik, *Nature* **1982**, *298*, 560-562.
- [17] M. Aronson, O. Medalia, L. Schori, D. Mirelman, N. Sharon, I. Ofek, *J. Infect. Dis.* **1979**, *139*, 329-332.
- [18] M. Scharenberg, D. Abgottspon, E. Cicek, X. Jiang, O. Schwardt, S. Rabbani, B. Ernst, *Assay Drug. Dev. Technol.* **2011**, *9*, 455-464.
- [19] X. Jiang, D. Abgottspon, S. Kleeb, S. Rabbani, M. Scharenberg, M. Wittwer, M. Haug, O. Schwardt, B. Ernst, *J. Med. Chem.* **2012**, *55*, 4700-4713.
- [20] M. Hartmann, T.K. Lindhorst, *Eur. J. Org. Chem.* **2011**, 3583-3609.
- [21] R. A. Copeland, D. L. Pompliano, T. D. Meek, *Nat. Rev. Drug Discov.* **2006**, *5*, 730-739.
- [22] D. C. Swinney, *Nat. Rev. Drug Discov.* **2004**, *3*, 801-808.
- [23] H. Lu, P. J. Tonge, *Curr. Opin. Chem. Biol.* **2010**, *14*, 467-474.
- [24] C. Napier, H. Sale, M. Mosley, G. Rickett, P. Dorr, R. Mansfield, M. Holbrook, *Pharmacol.* **2005**, *71*, 163-172.
- [25] I. Dierynck, M. De Wit, E. Gustin, I. Keuleers, J. Vandersmissen, S. Hallenberger, K. Hertogs, *J. Virol.* **2007**, *81*, 13845-13851.
- [26] W. M. Kati, D. Montgomery, R. Carrick, L. Gubareva, C. Maring, K. McDaniel, K. Steffy, A. Molla, F. Hayden, D. Kempf, W. Kohlbrenner, *Antimicrob. Agents Chemother.* **2002**, *46*, 1014-1021.
- [27] O. Schwardt, H. Gätthje, A. Vedani, S. Mesch, G.-P. Gao, M. Spreafico, J. von Orelli, S. Kelm, B. Ernst, *J. Med. Chem.* **2009**, *52*, 989-1004.
- [28] S. Mesch, K. Lemme, H. Koliwer-Brandl, D. S. Strasser, O. Schwardt, S. Kelm, B. Ernst, *Carbohydr. Res.* **2010**, *345*, 1348-1359.
- [29] M. K. Wild, M. C. Huang, U. Schulze-Horsel, P. A. van der Merwe, D. Vestweber, *J. Biol. Chem.* **2001**, *276*, 31602-31612.
- [30] M. W. Nicholson, A. N. Barclay, M. S. Singer, S. D. Rosen, P. A. van der Merwe, *J. Biol. Chem.* **1998**, *273*, 763-770.
- [31] P. Mehta, R. D. Cummings, R. P. McEver, *J. Biol. Chem.* **1998**, *273*, 32506-32513.
- [32] G. Javier Munoz, J. Ignacio Santos, A. Arda, S. Andre, H.-J. Gabius, J. V. Sinisterra, J. Jimenez-Barbero, M. J. Hernaiz, *Org. Biomol. Chem.* **2010**, *8*, 2986-2992.
- [33] T. Terada, M. Nishikawa, F. Yamashita, M. Hashida, *Int. J. Pharmaceut.* **2006**, *316*, 117-123.
- [34] B. N. Murthy, S. Sinha, A. Surolia, S. S. Indi, N. Jayaraman, *Glycoconj. J.* **2008**, *25*, 313-321.
- [35] A. R. Patil, C. J. Thomas, A. Surolia, *J. Biol. Chem.* **2000**, *275*, 24348-24356.
- [36] L. Herfurth, B. Ernst, B. Wagner, D. Ricklin, D. S. Strasser, J. L. Magnani, A. J. Benie, T. Peters, *J. Med. Chem.* **2005**, *48*, 6879-6886.
- [37] E. Duverger, N. Frison, A. C. Roche, M. Monsigny, *Biochimie* **2003**, *85*, 167-179.
- [38] I. Le Trong, P. Aprikian, B. A. Kidd, M. Forero-Shelton, V. Tchesnokova, P. Rajagopal, V. Rodriguez, G. Interlandi, R. Klevit, V. Vogel, R. E. Stenkamp, E. V. Sokurenko, W. E. Thomas, *Cell* **2010**, *141*, 645-655.
- [39] S. Rabbani, X. Jiang, O. Schwardt, B. Ernst, *Anal. Biochem.* **2010**, *407*, 188-195.
- [40] a) W. S. Somers, J. Tang, G. D. Shaw, R. T. Camphausen, *Cell* **2000**, *103*, 467-479; b) B. J. Graves, R. L. Crowther, C. Chandran, J. M. Rumberger, S. Li, K. S. Huang, D. H. Presky, P. C. Famillett, B. A. Wolitzky, D. K. Burns, *Nature* **1994**, *367*, 532-538.
- [41] P. M. Collins, C. T. Öberg, H. Leffler, U. J. Nilsson, H. Blanchard, *Chem. Biol. Drug Des.* **2012**, *79*, 339-346.
- [42] K. S. Kenneth, K. Drickamer, W. I. Weis, *J. Biol. Chem.* **1996**, *271*, 663-674.
- [43] Y. Guo, H. Feinberg, E. Conroy, D. Mitchell, R. Alvarez, O. Blixt, M. Taylor, W. I. Weis, K. Drickamer, *Nat. Struct. Mol. Biol.* **2004**, *11*, 591-598.
- [44] C. Hung, J. Bouckaert, D. L. Hung, J. Pinkner, C. Widberg, A. DeFusco, G. Auguste, R. Strouse, S. Langermann, S. J. Hultgren, *Abstracts of the General Meeting of the American Society for Microbiology* **2002**, *102*, 41.
- [45] M. Durka, K. Buffet, J. Iehl, M. Holler, J. F. Nierengarten, J. Taganna, J. Bouckaert, S. P. Vincent, *Chem. Commun.* **2011**, *47*, 1321-1323.
- [46] L. Pang, S. Kleeb, K. Lemme, S. Rabbani, M. Scharenberg, A. Zalewski, F. Schädler, O. Schwardt, B. Ernst, *ChemMedChem* **2012**, *7*, 1404-1422.

Received: ((will be filled in by the editorial staff))

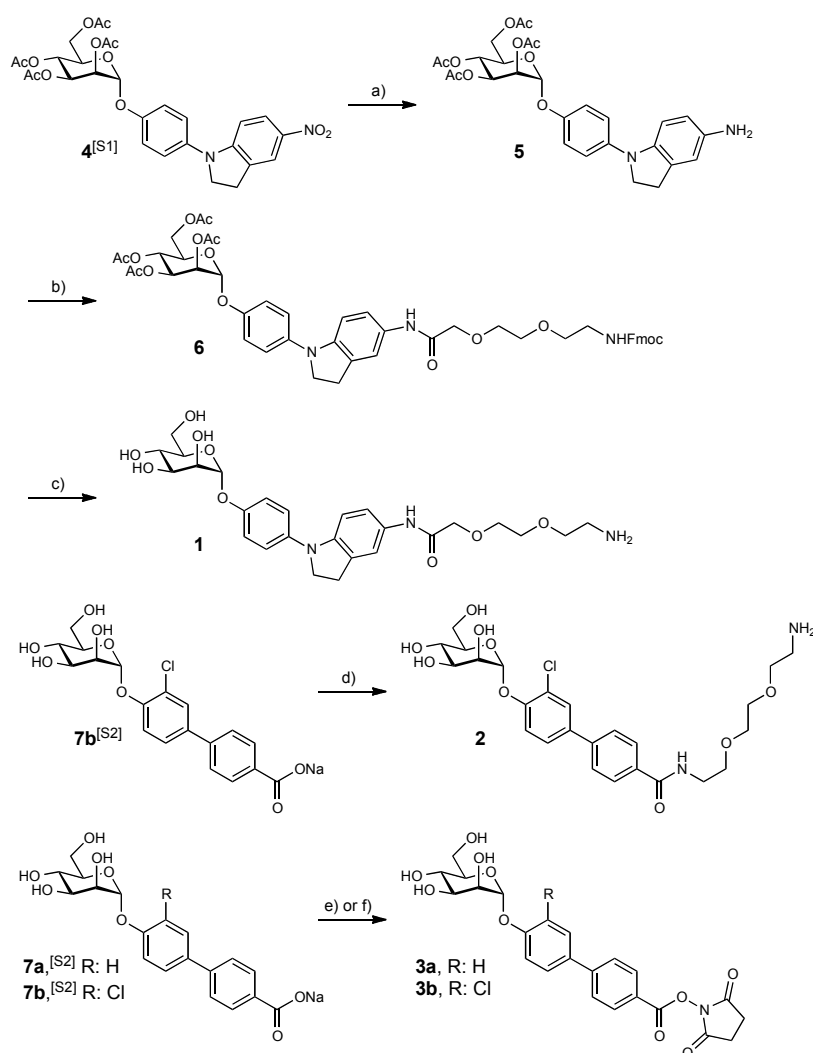
Published online: ((will be filled in by the editorial staff))

## Supporting Information

## Kinetic Properties of Carbohydrate-Lectin Interactions: FimH Antagonists

Meike Scharenberg, Xiaohua Jiang, Lijuan Pang, Giulio Navarra, Said Rabbani, Florian Binder, Oliver Schwardt, Beat Ernst\*

Institute of Molecular Pharmacy, Pharmacenter, University of Basel, Switzerland

Synthesis and spectroscopic details of antagonists **1**, **2** and **3a,b**

**Scheme S1.** Synthesis of the amino- or *N*-hydroxyl-succinimide functionalized FimH antagonists **1**, **2**, **3a** and **3b**. a) H<sub>2</sub> (1 atm), PtO<sub>2</sub>, morpholine, EtOAc/MeOH (1:1) (97%); b) 8-(Fmoc-amino)-3,6-dioxa-octanoic acid, PyBOP, DIPEA, DMF, rt; c) NaOMe, MeOH, rt (47% over two steps); d) EBE, COMU, DIPEA, DMF, 0 °C to rt (20%); e) EDC, NHS, H<sub>2</sub>O, rt (**3a**: 98%); f) EDC, NHS, MES buffer (pH 5.6), rt (**3b**: 99%).

**General methods.** NMR spectra were recorded on a Bruker Avance DMX-500 (500 MHz) spectrometer. Assignment of  $^1\text{H}$  and  $^{13}\text{C}$  NMR spectra was achieved using 2D methods (COSY, HSQC, TOCSY). Chemical shifts are expressed in ppm using residual  $\text{CHCl}_3$ ,  $\text{CHD}_2\text{OD}$  and HDO as references. Optical rotations were measured using Perkin-Elmer Polarimeter 341. Electron spray ionization mass spectra (ESI-MS) were obtained on a Waters micromass ZQ. HRMS analysis was carried out using a Bruker Daltonics micrOTOF spectrometer equipped with a TOF hexapole detector. Reactions were monitored by TLC using glass plates coated with silica gel 60  $\text{F}_{254}$  (Merck) and visualized by using UV light and/or by heating to 150 °C for 5 min with a molybdate solution (a 0.02 M solution of ammonium cerium sulfate dihydrate and ammonium molybdate tetrahydrate in aqueous 10%  $\text{H}_2\text{SO}_4$ ). Column chromatography was performed on a CombiFlash Companion (Teledyne-ISCO, Inc.) using RediSep® normal phase disposable flash columns (silica gel). Reversed phase chromatography was performed on LiChroprep®RP-18 (Merck, 40-63  $\mu\text{m}$ ). Commercially available reagents were purchased from Fluka, Aldrich or Acros. Methanol (MeOH) was dried by refluxing with sodium methoxide and distilled immediately before use. Dichloromethane (DCM) and ethyl acetate (EtOAc) were dried by filtration over  $\text{Al}_2\text{O}_3$  (Fluka, type 5016 A basic).

**4-(5-Aminoindolin-1-yl)phenyl 2,3,4,6-tetra-*O*-acetyl- $\alpha$ -D-mannopyranoside (5).** To a solution of **4**<sup>[S1]</sup> (47.8 mg, 0.08 mmol) in MeOH/EtOAc (1:1, 5 mL)  $\text{PtO}_2$  (5 mg) and morpholine (10  $\mu\text{L}$ ) were added. The reaction mixture was stirred at rt under hydrogen (1 atm) for 1 h, then filtrated through a pad of celite and the celite was washed thoroughly with EtOAc. The filtrate was concentrated in vacuo to give **5** (44 mg, 97%) as off-white foam, which was used in the next step without further purification.

**2-(2-(2-Fmoc-aminoethoxy)ethoxy)-*N*-(4-(2,3,4,6-tetra-*O*-acetyl- $\alpha$ -D-mannopyranosyloxy)phenyl)-indolin-5-yl)-acetamide (6).** To a mixture of **5** (45 mg, 0.08 mmol), PyBoP (50 mg, 0.096 mmol) and 8-(Fmoc-amino)-3,6-dioxo-octanoic acid (39 mg, 0.1 mmol) in dry DMF (1.5 mL) was added DIPEA (32  $\mu\text{L}$ , 0.19 mmol) at rt. The reaction mixture was stirred at rt overnight, then diluted with EtOAc, and washed with water and brine. The organic layer was dried over  $\text{Na}_2\text{SO}_4$  and the solvent was removed under reduced pressure. The residue was purified by silica gel chromatography (DCM/MeOH 24:1) to provide crude **6** as black oil, which contained some DMF.  $^1\text{H}$  NMR (500 MHz,  $\text{CDCl}_3$ ):  $\delta$  = 2.05, 2.06, 2.08, 2.21 (4s, 12H, 4 OAc), 3.19 (t,  $J$  = 8.4 Hz, 2H,  $\text{CH}_2$ ), 3.42 (dd,  $J$  = 5.2, 10.4 Hz, 2H,  $\text{CH}_2$ ), 3.62 (t,  $J$  = 5.0 Hz, 2H,  $\text{CH}_2$ ), 3.70 (m, 2H,  $\text{CH}_2$ ), 3.80 (m, 2H,  $\text{CH}_2$ ), 4.08-4.16 (m, 4H, H-5, H-6a,  $\text{CH}_2$ ), 4.33 (d,  $J$  = 7.1 Hz, 2H,  $\text{CH}_2$ ), 4.29 (dd,  $J$  = 5.2, 12.2 Hz, 1H, H-6b), 5.15 (t,  $J$  = 5.3 Hz, 1H, NH), 5.37 (t,  $J$  = 10.0 Hz, 1H, H-4), 5.44 (m, 2H, H-1, H-2), 5.56 (dd,  $J$  = 3.0, 10.0 Hz, 1H, H-3), 6.88 (d,  $J$  = 8.5 Hz, 1H), 7.01-7.07 (m, 4H, Ar-H), 7.27 (m, 1H, Ar-H), 7.36 (m, 2H, Ar-H), 7.46 (s, 1H, Ar-H), 7.52 (d,  $J$  = 7.0 Hz, 2H, Ar-H), 7.74 (d,  $J$  = 8.0 Hz, 2H, Ar-H), 8.47 (s, 1H, Ar-H);  $^{13}\text{C}$  NMR (125 MHz,  $\text{CDCl}_3$ ):  $\delta$  20.52, 20.71, 20.89 (4C, 4 OAc), 28.12, 40.74, 47.12, 52.70 (4  $\text{CH}_2$ ), 62.14 (C-6), 65.96 (C-4), 66.72 ( $\text{CH}_2$ ), 68.90 (C-3), 68.99 (C-5), 69.43 (C-2), 70.02, 70.23, 70.61, 71.06 ( $\text{CH}_2$ , CH), 96.35 (C-1), 107.29, 117.44, 118.47, 119.15, 119.43, 119.93, 124.85, 125.01, 126.99, 127.65, 128.44, 131.83, 139.72, 141.23, 144.82, 150.04, 156.40 (Ar-C), 167.63, 169.76, 169.97, 170.02, 170.57, 174.43 (6 CO); ESI-MS:  $m/z$ : Calcd for  $\text{C}_{28}\text{H}_{31}\text{N}_2\text{O}_{12}$  [ $\text{M}+\text{Na}$ ] $^+$ : 946.34, found 946.30.

**2-(2-(2-Aminoethoxy)ethoxy)-*N*-(4-( $\alpha$ -D-mannopyranosyloxy)phenyl)-indolin-5-yl)-acetamide (1).** Crude **6** was dissolved in dry MeOH and treated at rt with 0.5 M NaOMe/MeOH (0.2 mL) until completion of the reaction. The reaction mixture was neutralized with Amberlyst-15 ( $\text{H}^+$ ) ion-exchange resin and filtered. The filtrate was concentrated and the residue was purified by silica gel chromatography

(DCM/MeOH/H<sub>2</sub>O 50:50:6) to afford amine **1** (20 mg, 47% over two steps from **5**) as an off-white solid.  $[\alpha]_D^{20} +70.7$  (*c* 0.095, MeOH); <sup>1</sup>H NMR (500 MHz, CD<sub>3</sub>OD):  $\delta$  = 2.84 (t, *J* = 5.5 Hz, 2H, CH<sub>2</sub>), 3.10 (t, *J* = 8.0 Hz, 2H, CH<sub>2</sub>), 3.59 (t, *J* = 5.5 Hz, 2H, CH<sub>2</sub>), 3.67 (m, 3H, H-5, CH<sub>2</sub>), 3.73 (m, 4H, H-4, H-6a, CH<sub>2</sub>), 3.78 (m, 3H, H-6b, CH<sub>2</sub>), 3.89 (m, 3H, H-3, CH<sub>2</sub>), 4.01 (dd, *J* = 2.0, 3.5 Hz, 1H, H-2), 5.41 (d, *J* = 2.0 Hz, 1H, H-1), 6.88 (d, *J* = 8.5 Hz, 1H, Ar-H), 7.12-7.18 (m, 5H, Ar-h), 7.39 (d, *J* = 1.5 Hz, 1H, Ar-H); <sup>13</sup>C NMR (125 MHz, CD<sub>3</sub>OD):  $\delta$  = 29.09, 41.87, 54.10 (3 CH<sub>2</sub>), 62.73 (C-6), 68.39 (C-4), 71.28 (C-2), 71.53, 72.10 (2 CH<sub>2</sub>), 72.42 (C-3), 73.03 (CH<sub>2</sub>), 75.33 (C-5), 100.84 (C-1), 108.11, 118.90, 119.96, 120.88, 121.28, 129.79, 132.90, 140.76, 146.81, 152.86 (Ar-C), 170.56 (CO); ESI-MS: *m/z*: Calcd for C<sub>21</sub>H<sub>20</sub>ClNO<sub>8</sub> [M+H]<sup>+</sup>: 534.24, found 534.20.

***N*-(2-(2-(2-Aminoethoxy)ethoxy)ethyl)-3'-chloro-4'-( $\alpha$ -D-mannopyranosyloxy)-biphenyl-4-carboxamide (2).** COMU was added at 0 °C to a mixture of **7b**<sup>[S21]</sup> (20 mg, 0.05 mmol) and DIPEA (9  $\mu$ L, 0.05 mmol) in dry DMF (0.5 mL). The reaction mixture was activated for 5 min, then EBE (14  $\mu$ L, 0.1 mmol) and DIPEA (9  $\mu$ L, 0.05 mmol) were added. The reaction mixture was stirred at 0 °C for 1 h and at rt overnight. Water (0.5 mL) was added to the mixture and stirring continued for 5 min. The reaction was concentrated under reduced pressure, then the yellow residue was loaded onto a RP-18 chromatography column and eluted with MeOH (0 to 100%) in 0.01 N aqueous ammonia to give **2** (5.0 mg, 20%). <sup>1</sup>H NMR (500 MHz, CD<sub>3</sub>OD):  $\delta$  = 3.42-3.68 (m, 16H, H-4, H-5, H-6a, H-6b, 6 CH<sub>2</sub>), 3.90 (dd, *J* = 3.4, 9.5 Hz, 1H, H-3), 4.02 (dd, *J* = 1.8, 3.4 Hz, 1H, H-2), 5.50 (d, *J* = 1.6 Hz, 1H, H-1), 7.37 (d, *J* = 8.7 Hz, 1H, Ar-H), 7.49 (dd, *J* = 2.3, 8.6, Hz, 1H, Ar-H), 7.58-7.63 (m, 3H, Ar-H), 7.76-7.85 (m, 2H, Ar-H); ESI-MS: *m/z*: Calcd for C<sub>25</sub>H<sub>34</sub>ClN<sub>2</sub>O<sub>9</sub><sup>+</sup>[M+H]<sup>+</sup>: 541.19, found: 541.24.

**2,5-Dioxopyrrolidin-1-yl 4'-( $\alpha$ -D-mannopyranosyloxy)-biphenyl-4-carboxylate (3a).** Compound **7a**<sup>[S21]</sup> (3.0 mg, 7.5  $\mu$ mol) was added to a stirred solution of NHS (4.3 mg, 37  $\mu$ mol) and EDC (538 mg, 2.8 mmol) in water (37.5 mL) resulting in the formation of a white precipitate. After stirring for 30 min, the reaction mixture was diluted with satd aq. NH<sub>4</sub>Cl, filtered (syringe filter) and the filter was washed with DCM (2 x 3 mL). The product was recovered from the filter by washing with MeOH several times. Evaporation of the volatiles under reduced pressure gave the activated acid **3a** (3.5 mg, 98%) as a white solid. <sup>1</sup>H NMR (500 MHz, CD<sub>3</sub>OD):  $\delta$  = 2.92 (s, 4H, 2 CH<sub>2</sub>), 3.61 (ddd, *J* = 2.7, 5.0, 9.8 Hz, 1H, H-5), 3.71-3.80 (m, 3H, H-4, H-6a, H-6b), 3.93 (dd, *J* = 3.4, 9.5 Hz, 1H, H-3), 4.04 (dd, *J* = 1.8, 3.4 Hz, 1H, H-2), 5.57 (d, *J* = 1.6 Hz, 1H, H-1), 7.26 (d, *J* = 8.8 Hz, 2H, Ar-H), 7.70 (d, *J* = 8.8 Hz, 2H, Ar-H), 7.83 (d, *J* = 8.5 Hz, 2H, Ar-H), 8.18 (d, *J* = 8.5 Hz, 2H, Ar-H); <sup>13</sup>C NMR (125 MHz, CD<sub>3</sub>OD):  $\delta$  = 26.55 (2 CH<sub>2</sub>), 62.16 (C-6), 67.69 (C-4), 71.44 (C-2), 72.01 (C-3), 75.00 (C-5), 99.56 (C-1), 117.64, 127.64, 128.95, 131.17 (Ar-C); ESI-MS: *m/z*: Calcd for C<sub>23</sub>H<sub>23</sub>NNaO<sub>10</sub> [M+Na]<sup>+</sup>: 496.12, found: 496.16 [M+Na]<sup>+</sup>.

**2,5-Dioxopyrrolidin-1-yl 3'-chloro-4'-( $\alpha$ -D-mannopyranosyloxy)-biphenyl-4-carboxylate (3b).** NHS (160 mg, 1.38 mmol) and EDC (532 mg, 2.77 mmol) were dissolved in 0.1 M MES buffer (pH 5.6, 10 mL). After stirring for 10 min **7b**<sup>[S21]</sup> (300 mg, 0.693 mmol) was added. The solution became turbid, then clear, and then a precipitate started to form. After 20 min the solid was collected by filtration on a frittered-glass G4 filter, and washed with satd aq. NH<sub>4</sub>Cl and DCM. The solid was recovered with MeOH, the solvent was evaporated, and the residue dried under high vacuum to yield **3b** (350 mg, 99%) as a white solid. <sup>1</sup>H NMR (500 MHz, CD<sub>3</sub>OD):  $\delta$  = 2.94 (s, 4H, 2 CH<sub>2</sub>), 3.68-3.82 (m, 4H, H-4, H-5, H-6a, H-6b), 4.03 (dd, *J* = 3.3, 9.3 Hz, 1H, H-3), 4.15 (dd, *J* = 1.3, 3.3 Hz, 1H, H-2), 5.66 (d, *J* = 1.6 Hz, 1H, H-1), 7.53 (d, *J* = 10.0 Hz, 1H, Ar-H), 7.68 (dd, *J* = 10.5 Hz, 1H, Ar-H), 7.83-7.87 (m, 3H, Ar-H), 7.76 (m, 1H, Ar-H), 8.21 (m, 1H, Ar-H); <sup>13</sup>C NMR (125 MHz, CD<sub>3</sub>OD):  $\delta$  = 26.63 (2 CH<sub>2</sub>), 62.64 (C-6), 68.21 (C-4),

71.83 (C-2), 72.41 (C-3), 76.06 (C-5), 100.70 (C-1), 118.61, 128.01, 128.30, 129.96, 132.03 (Ar-C), 171.88 (CO); ESI-MS: *m/z*: Calcd for C<sub>23</sub>H<sub>22</sub>ClNNaO<sub>10</sub> [M+Na<sup>+</sup>]: 530.09, found: 530.00 [M+Na<sup>+</sup>].

#### **References**

- [S1] X. Jiang, D. Abgottspon, S. Kleeb, S. Rabbani, M. Scharenberg, M. Wittwer, M. Haug, O. Schwardt, B. Ernst, *J. Med. Chem.* **2012**, *55*, 4700-4713.
- [S2] T. Klein, D. Abgottspon, M. Wittwer, S. Rabbani, J. Herold, X. Jiang, S. Kleeb, C. Lüthi, M. Scharenberg, J. Bezençon, E. Gubler, L. Pang, M. Smiesko, B. Cutting, O. Schwardt, B. Ernst, *J. Med. Chem.* **2010**, *53*, 8627-8641.

## **Part I: The lectin FimH**

---

**FimH Chapter 2: Results and discussion**

**Publication 5**

---

DOI: 10.1002/cmdc.201200125

# FimH Antagonists: Structure–Activity and Structure–Property Relationships for Biphenyl $\alpha$ -D-Mannopyranosides

Lijuan Pang, Simon Kleeb, Katrin Lemme, Said Rabbani, Meike Scharenberg, Adam Zalewski, Florentina Schädler, Oliver Schwardt, and Beat Ernst<sup>\*,[a]</sup>

Urinary tract infections (UTIs) are caused primarily by uropathogenic *Escherichia coli* (UPEC), which encode filamentous surface-adhesive organelles called type 1 pili. FimH is located at the tips of these pili. The initial attachment of UPEC to host cells is mediated by the interaction of the carbohydrate recognition domain (CRD) of FimH with oligomannosides on urothelial cells. Blocking these lectins with carbohydrates or analogues thereof prevents bacterial adhesion to host cells and therefore offers a potential therapeutic approach for prevention and/or treatment of UTIs. Although numerous FimH antagonists have been developed so far, few of them meet the requirement for clinical application due to poor pharmacokinetics. Additionally, the binding mode of an antagonist to the

CRD of FimH can switch from an in-docking mode to an out-docking mode, depending on the structure of the antagonist. In this communication, biphenyl  $\alpha$ -D-mannosides were modified to improve their binding affinity, to explore their binding mode, and to optimize their pharmacokinetic properties. The inhibitory potential of the FimH antagonists was measured in a cell-free competitive binding assay, a cell-based flow cytometry assay, and by isothermal titration calorimetry. Furthermore, pharmacokinetic properties such as  $\log D$ , solubility, and membrane permeation were analyzed. As a result, a structure–activity and structure–property relationships were established for a series of biphenyl  $\alpha$ -D-mannosides.

## Introduction

Urinary tract infections (UTIs), the most prevalent series of infectious diseases worldwide, affect millions of people and account for significant morbidity as well as high medical costs.<sup>[1]</sup> The primary cause of UTIs are strains of uropathogenic *Escherichia coli* (UPEC), which make up 70–95% of reported cases.<sup>[1a,2]</sup> UTIs are treated with antibiotics; however, recurrent infections by UPEC with subsequent antibiotic exposure can lead to the emergence of antimicrobial resistance.<sup>[3]</sup>

Adhesion to host cells is the initial step of microbial infection. To gain an initial foothold within the bladder, UPEC strains encode filamentous surface-adhesive organelles called type 1 pili (fimbriae).<sup>[4]</sup> They mediate bacterial attachment to uroplakin Ia, a glycoprotein located on urothelial cells. This initial step prevents the clearance of *E. coli* by the bulk flow of urine and facilitates the invasion of host cells.<sup>[1b,5]</sup> A bacterial lectin known as FimH is located at the tips of type 1 pili. The carbohydrate recognition domain (CRD) of this lectin is responsible for binding to the complementary carbohydrate epitope of the host tissue. Blocking this lectin by a carbohydrate or a glycomimetic thereof offers a potential therapeutic approach for prevention and/or treatment of UTIs.<sup>[6]</sup>

More than two decades ago, Sharon and co-workers explored various mannosides and oligomannosides as potential antagonists for type 1 pili-mediated bacterial adhesion and observed interactions in the micro- to millimolar range.<sup>[7]</sup> The first crystal structure of FimH was solved in 1999,<sup>[8]</sup> and since then, numerous crystallographic studies have been reported, greatly facilitating the design of high-affinity ligands.<sup>[9]</sup> In summary,

the reported affinities can be rationalized on the basis of the structure of FimH: First, the binding pocket accommodates the mannose with the hydroxy groups forming an extended hydrogen bond network. Second, the entrance to the binding site, referred to as the “tyrosine gate”, is formed by three hydrophobic amino acids (Tyr48, Tyr137, and Ile52)<sup>[9a]</sup> and can host aliphatic and aromatic aglycones.

As a consequence of hydrophobic contacts of the alkyl aglycone, *n*-heptyl  $\alpha$ -D-mannopyranoside (**1**) exhibits nanomolar affinity.<sup>[9b]</sup> With aromatic aglycones such as **2–5** (Figure 1), further improvements in affinity were observed.<sup>[10]</sup> To explore the binding mode and to improve affinity as well as ADME properties, a series of biphenyl FimH antagonists were synthesized.

## Results and Discussion

An unexpected docking mode was discovered upon co-crystallization of biphenyl mannoside **3** with the FimH CRD.<sup>[10d]</sup> Whereas the alkyl aglycone of *n*-butyl  $\alpha$ -D-mannopyranoside<sup>[9b]</sup>

[a] L. Pang,<sup>+</sup> S. Kleeb,<sup>+</sup> Dr. K. Lemme,<sup>+</sup> Dr. S. Rabbani,<sup>+</sup> Dr. M. Scharenberg, A. Zalewski, F. Schädler, Dr. O. Schwardt, Prof. Dr. B. Ernst  
Institute of Molecular Pharmacy, Pharmazentrum, University of Basel  
Klingelbergstrasse 50, 4056 Basel (Switzerland)  
E-mail: beat.ernst@unibas.ch

[\*] These authors contributed equally to this work.

Supporting information for this article is available on the WWW under <http://dx.doi.org/10.1002/cmdc.201200125>.

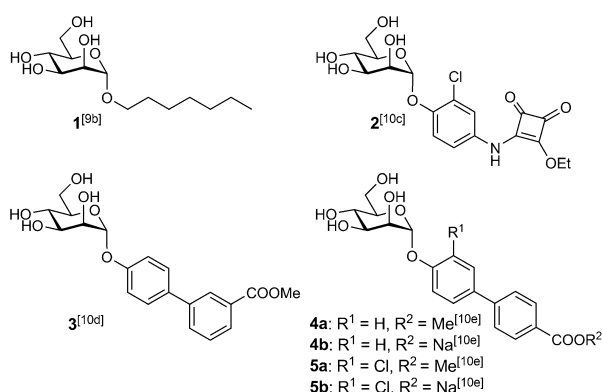


**Figure 1.** FimH antagonists: *n*-heptyl  $\alpha$ -D-mannopyranoside (**1**) is used as reference compound; the squaric acid derivative **2** and biphenyl derivatives **3–5** exhibit nanomolar affinities.

interacts with both Tyr48 and Tyr137 of the tyrosine gate (in-docking mode),<sup>[10f]</sup> the biphenyl aglycone adopts the out-docking mode; that is, it interacts only with Tyr48 (Figure 2A), probably due to insufficient flexibility;  $\pi$ - $\pi$  stacking of the outer aromatic ring of the biphenyl aglycone (ring B) with Tyr48 is effected by induced fit: a substantial move of Tyr48. Moreover, further stabilization of the protein–ligand complex by polar interaction between the ester in the *meta* position of **3** and the side chain of Arg98 was proposed.<sup>[10d]</sup>

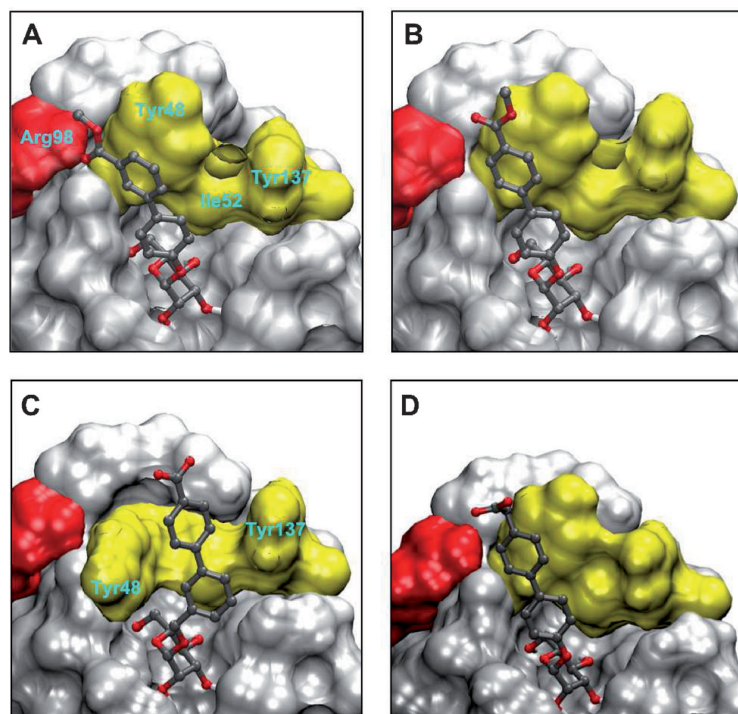


**Figure 2.** A) Crystal structure of biphenyl **3** (PDB ID: 3MCY)<sup>[10d]</sup> bound to the FimH CRD. B–D) In silico docking studies obtained with flexible docking (Glide software package)<sup>[111]</sup> to the same FimH CRD structure; top-scored binding mode of B) **4a**, C) **6**, and D) **7**.

In silico docking studies with biphenyl derivative **4a**<sup>[10e]</sup> suggested a similar out-docking mode (Figure 2B). A close inspection revealed empty space between the *ortho* position of the aromatic ring adjacent to the anomeric center (ring A) and the protein surface. Indeed, with an *ortho*-chloro substituent ( $\rightarrow$  **5a**, Figure 1), affinity was substantially improved. Further studies with FimH antagonists that exhibit enhanced flexibility (e.g., compound **6**; Figure 2C and Figure 3) indicated a switch from the out-docking mode to the in-docking mode. However, whether an optimal  $\pi$ - $\pi$  stacking within the tyrosine gate can be realized remains to be determined. Finally, docking studies also indicated that elongation of the carboxylate-bearing *para* substituent enables a polar interaction between the carboxylate and Arg98 (e.g., compound **7**; Figure 2D and Figure 3).

Starting from antagonist **4**, we explored three types of modifications (Figure 3):

- 1) For optimizing the van der Waals contact between the *ortho* position of ring A and the binding pocket, a series of substituents — F, CH<sub>3</sub>, CF<sub>3</sub>, OCH<sub>3</sub>, cyclopropyl, and CN — were introduced as depicted in Scheme 1.
- 2) To determine whether the out-docking mode reported for **3**<sup>[10d]</sup> results from insufficient flexibility, we increased the aglycone flexibility by introducing a methylene spacer between the anomeric oxygen and ring A of the biphenyl moiety (Scheme 2). This should decrease the conformational constraints to allow an optimized spatial arrangement of the aglycone in the tyrosine gate ( $\rightarrow$  **6**, Figure 2C); at the same time, water solubility should be improved as a result of the decreased stacking tendency derived from disruption of the symmetry of the aglycone.<sup>[15]</sup>
- 3) To enable a polar interaction between the carboxylate substituent on ring B with Arg98 of FimH, we extended the *para* substituent of **4**, that is, we replaced it with either a flexible methyl ethanolate or a rigid methyl cyclopropanecarboxylate (Scheme 3). Biphenyl  $\alpha$ -D-mannoside **24**<sup>[10d]</sup> shows a three- to eightfold lower affinity for FimH than its counterparts with a methoxycarbonyl substituent at the *meta* ( $\rightarrow$  **3**)<sup>[10d]</sup> or *para* positions ( $\rightarrow$  **4**)<sup>[10e]</sup> of ring B (Table 1). Han et al. assigned the increased affinity of compound **3** to a polar interaction of the ester with Arg98 of FimH.<sup>[10d]</sup> Because for spatial reasons the ester in the



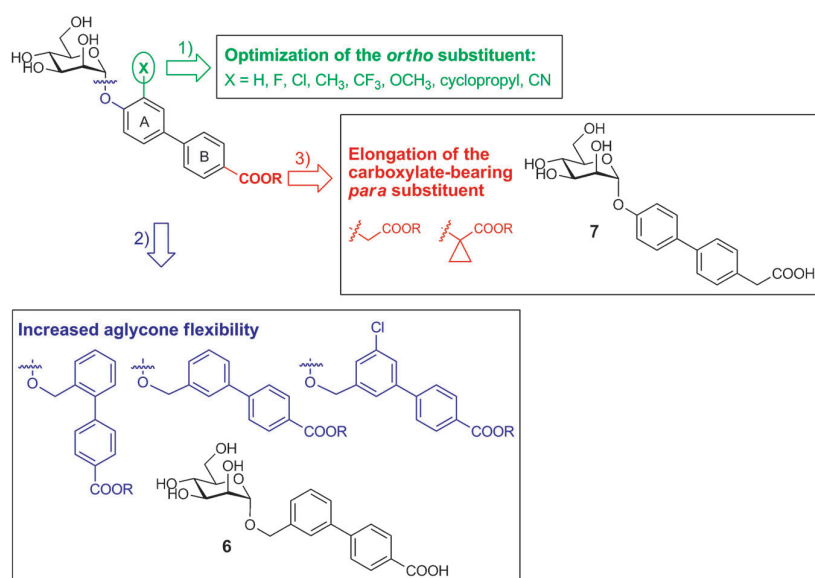


**Figure 3.** Modifications to the aglycone of FimH antagonists by 1) optimization of the ortho substituent, 2) an increase in the flexibility of the aglycone, and 3) elongation of the carboxylate-bearing para substituent.

para-substituted derivative **4** cannot establish a similar interaction with Arg98, the substantial improvement in affinity may result from solvation effects.

## Synthesis

### Optimization of ortho substituents (Scheme 1)

Mannosylation of phenols **9a–f** with mannosyl fluoride **8** and BF<sub>3</sub>·OEt<sub>2</sub> as promoter yielded α-mannosides **10a–f** stereospecifically.<sup>[12]</sup> Whereas the phenols **9a–d** and **9f** are commercially available, the cyclopropyl derivative **9e** was prepared via tandem carbolithiation/1,3-elimination according to Ocasio and Scanlan.<sup>[13]</sup> In a palladium-catalyzed Miyaura–Suzuki coupling<sup>[14]</sup> of **10a–f** with 4-methoxycarbonylphenylboronic acid (**11**), biphenyls **12a–f** were obtained in good to excellent yields. Deacetylation using Zemplén conditions (→**13a–f**) followed by saponification of the methyl esters gave the test compounds **14a–e**. Owing to the instability of the cyano group under aqueous basic conditions, **14f** was synthesized by coupling **10f** with 4-carboxyphenylboronic acid pinacol ester (**15**) followed by transesterification under Zemplén conditions to avoid the final saponification with aqueous sodium hydroxide.

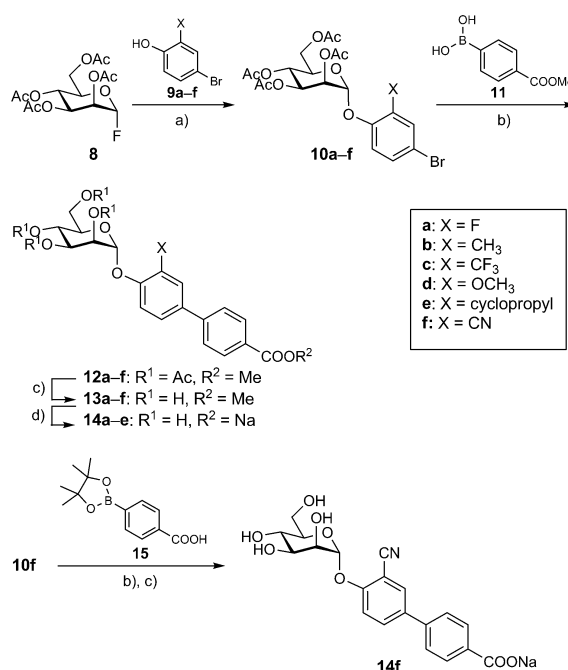
### Increase in aglycone flexibility (Scheme 2)

Benzyl alcohols **16a–c** were first mannosylated with donor **8**<sup>[12]</sup> to yield the benzyl mannosides **17a–c**. Subsequent cross-coupling with 4-methoxycarbonylphenylboronic acid (**11**) afforded acetates **18a,b** and **21**. Deacetylation of the mannose moiety

(→**19a,b** and **22**) followed by saponification of the methyl esters gave compounds **6**, **20**, and **23**.

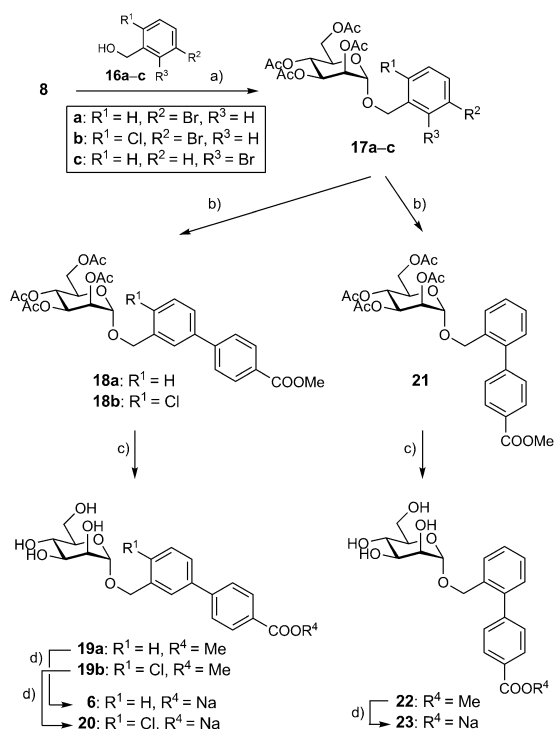
### Elongation of the carboxylate-bearing para substituent (Scheme 3)

Peracetylated mannose **25** was treated with 4-iodophenol in the presence of BF<sub>3</sub>·Et<sub>2</sub>O. The resulting iodide **26** was transformed into boronic acid pinacol ester **27**, which was coupled with 4-bromophenylacetic acid methyl ester (**28**) and 4-bromophenylcyclopropylcarboxylic acid methyl ester (**32**) under Miyaura–Suzuki coupling conditions<sup>[14]</sup> to yield biphenyls **29** and **33**. Deacetylation with sodium methoxide (→

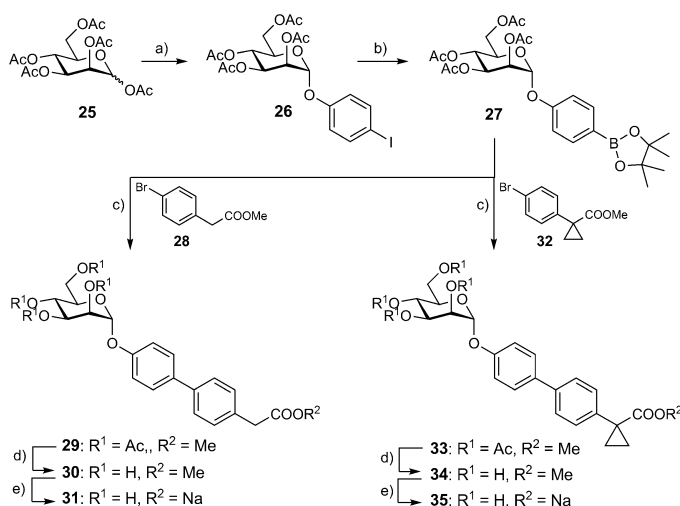


**Scheme 1.** Reagents and conditions: a) BF<sub>3</sub>·Et<sub>2</sub>O, CH<sub>2</sub>Cl<sub>2</sub>, 0 °C, 3 h (**10a–f**, 73–86%); b) Pd(Cl<sub>2</sub>)dppf·CH<sub>2</sub>Cl<sub>2</sub>, K<sub>3</sub>PO<sub>4</sub>, DMF, 80 °C, overnight (**12a–f**, 55–91%); c) NaOMe, MeOH, RT, 4 h (**13a–e**, **14f**, 52–73%); d) 1. 0.2 N NaOH<sub>(aq)</sub>, MeOH, RT, overnight; 2. Dowex (Na<sup>+</sup>), size-exclusion chromatography (P-2 gel) (**14a–e**, 15–74%).

**30** and **34**) followed by saponification of the methyl ester yielded the sodium salts **31** and **35**.



**Scheme 2.** Reagents and conditions: a) BF<sub>3</sub>·Et<sub>2</sub>O, CH<sub>2</sub>Cl<sub>2</sub>, 0 °C, 3 h (17a–c, 34–48 %); b) 4-methoxycarbonylphenylboronic acid (11), Pd(Cl<sub>2</sub>)dppf·CH<sub>2</sub>Cl<sub>2</sub>, K<sub>3</sub>PO<sub>4</sub>, DMF, 80 °C, overnight (18a,b and 21, 73–94 %); c) NaOMe, MeOH, RT, 4 h (19a,b and 22, 47–90 %); d) 1. 0.2 N NaOH<sub>(aq)</sub>, MeOH, RT, overnight; 2. Dowex (Na<sup>+</sup>), size-exclusion chromatography (P-2 gel) (6, 20 and 23, 10–96 %).



**Scheme 3.** Reagents and conditions: a) 4-iodophenol, BF<sub>3</sub>·Et<sub>2</sub>O, CH<sub>2</sub>Cl<sub>2</sub>, 40 °C, overnight (70 %); b) bis(pinacolato)diboron, Pd(Cl<sub>2</sub>)dppf·CH<sub>2</sub>Cl<sub>2</sub>, KOAc, DMF, MW 120 °C, 2 h (50 %); c) Pd(Cl<sub>2</sub>)dppf·CH<sub>2</sub>Cl<sub>2</sub>, K<sub>3</sub>PO<sub>4</sub>, DMF, 80 °C, overnight (34–56 %); d) NaOMe, MeOH, RT, 4 h (33–95 %); e) 1. 0.2 N NaOH<sub>(aq)</sub>, MeOH, RT, overnight; 2. Dowex (Na<sup>+</sup>), size-exclusion chromatography (P-2 gel) (31: 40%; 35: 23 %).

### Binding affinity and activity

The biphenyl  $\alpha$ -D-mannosides with varying *ortho* substituents (5a–b, 13a–f, 14a–f), increased aglycone flexibility (6, 19, 20, 22, 23), and elongated carboxylate-bearing *para* substituents (30, 31, 34, 35) were evaluated in vitro by two competitive assay formats (Table 1). All antagonists were tested in a cell-free competitive binding assay.<sup>[16]</sup> Subsequently, the best candidates were investigated in a cell-based flow cytometry assay.<sup>[17]</sup>

The cell-free competitive binding assay is based on the interaction of a biotinylated polyacrylamide glycopolymer as competitor with the isolated CRD of FimH. In contrast, the cell-based flow cytometry assay involves the infection of human urinary bladder epithelial carcinoma cells with GFP-labeled UPECs expressing the complete type 1 pili (see the Experimental Section below for details). The competitors in the former assay are thus polymer-bound trimannosides, whereas in the latter the antagonists compete with more potent high-mannose oligosaccharides present on uroplakin Ia, which is located on the surface of human urinary bladder cells.<sup>[18,19]</sup> The interaction is further affected by the presence of high- and low-affinity states of the CRD of FimH. Aprikian et al. experimentally demonstrated that in full-length fimbriae, the pilin domain stabilizes the CRD domain in the low-affinity state, whereas the CRD domain alone adopts the high-affinity state.<sup>[20]</sup> Furthermore, it was recently shown that shear stress can induce a conformational switch (twist in the  $\beta$ -sandwich fold of the CRD domain), resulting in improved affinity.<sup>[21]</sup> Therefore, differing affinities were expected in the cell-based flow cytometry assay, in which full-length fimbriae are present, relative to the cell-free competitive binding assay.

### Cell-free competitive binding assays<sup>[16]</sup>

These assays were performed twice for every compound with each concentration in duplicate. To ensure comparability between various antagonists, the reference compound *n*-heptyl  $\alpha$ -D-mannopyranoside 1<sup>[22]</sup> was tested each time in parallel. The affinities are reported relative to 1 as rIC<sub>50</sub> in Table 1. A comparison of the affinities of compounds 4a and 4b with the *ortho*-substituted analogues 5a, 13a–f and 5b, 14a–f clearly demonstrates that *ortho* substituents on ring A indeed improve binding. However, the differences between the various substituted FimH antagonists are small. For a better understanding of these results, a more detailed analysis of the thermodynamic profile by isothermal titration calorimetry (ITC) was performed (see below). By increasing the flexibility of the aglycone, we expected a switch from the out-docking mode as present for antagonists 3 and 4 (Figure 2A,B) to the in-docking mode (represented by antagonist 6 in Figure 2C).<sup>[10]</sup> However, affinities for all six representatives with increased spacer length between carbohydrate and aglycone (Table 1: 6, 19, 20, 22, and 23) were dramatically decreased. A similar tendency was observed

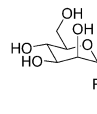
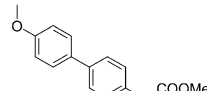
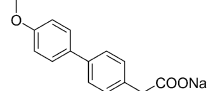
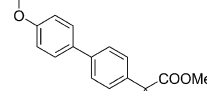
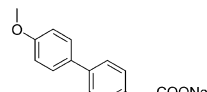
**Table 1.** Pharmacodynamic parameters of FimH antagonists.

Compd		Binding assay		Flow cytometry
		IC <sub>50</sub> [nM] <sup>[a]</sup>	rIC <sub>50</sub> <sup>[b]</sup>	IC <sub>50</sub> [μM] <sup>[a,c]</sup>
<b>1</b> <sup>[10e]</sup>		73 ± 7.9	1	3.9 ± 1.6
<b>24</b> <sup>[10d]</sup>		84.9	1.47	n.d.
<b>3</b> <sup>[10d]</sup>		28.6	0.55	n.d.
<b>4a</b> <sup>[10e]</sup>		10.4 ± 1.2	0.14	n.d.
<b>4b</b> <sup>[10e]</sup>		17.1 ± 2.2	0.15	n.d.
<b>5a</b>		4.8 ± 1.2	0.06	n.d.
<b>5b</b>		6.7 ± 2.1	0.09	0.33 ± 0.05
<b>13a</b>		8.0	0.14	n.d.
<b>14a</b>		33.5	0.58	1.54 ± 0.31
<b>13b</b>		23.3	0.40	n.d.
<b>14b</b>		9.2	0.16	1.83 ± 0.14
<b>13c</b>		2.6	0.04	n.d.
<b>14c</b>		8.9	0.15	0.89 ± 0.10

**Table 1.** (Continued)

Compd		Binding assay		Flow cytometry
		IC <sub>50</sub> [nM] <sup>[a]</sup>	rIC <sub>50</sub> <sup>[b]</sup>	IC <sub>50</sub> [μM] <sup>[a,c]</sup>
<b>13d</b>		3.5	0.06	n.d.
<b>14d</b>		4.8	0.08	1.95 ± 0.36
<b>13e</b>		31.7	0.55	n.d.
<b>14e</b>		63.0	1.09	4.85 ± 0.79
<b>13f</b>		22.5	0.39	n.d.
<b>14f</b>		33.9	0.58	n.d.
<b>19a</b>		56.1	0.97	n.d.
<b>6</b>		107.9	1.87	n.d.
<b>19b</b>		98.9	1.7	n.d.
<b>20</b>		142.2	2.44	n.d.
<b>22</b>		85.8	1.49	n.d.
<b>23</b>		642.0	11.14	n.d.

**Table 1.** (Continued)

Compd		Binding assay		Flow cytometry
		IC <sub>50</sub> [nM] <sup>[a]</sup>	rIC <sub>50</sub> <sup>[b]</sup>	IC <sub>50</sub> [μM] <sup>[a,c]</sup>
30		63.2	1.09	n.d.
31		70.5	1.21	n.d.
34		49.5	0.85	n.d.
35		62.5	1.07	n.d.

[a] IC<sub>50</sub> values were determined in a cell-free competitive binding assay.<sup>[16]</sup>  
 [b] The rIC<sub>50</sub> values were calculated by dividing the IC<sub>50</sub> of the compound of interest by that of reference compound **1**; this leads to rIC<sub>50</sub> values < 1 for derivatives that bind better than reference **1**, and rIC<sub>50</sub> values > 1 for compounds with lower affinity than **1**. [c] The anti-adhesion potential to human epithelial bladder cells was determined in the flow cytometry assay;<sup>[17]</sup> n.d. = not determined.

for the biphenyls with an elongated carboxylate-bearing *para* substituent (Table 1: **30**, **31**, **34**, and **35**). It was previously described that the ester of **3** is placed within hydrogen bonding distance to form a polar interaction with Arg98 and Glu50.<sup>[10d]</sup> However, an improvement of affinity provided by a similar polar interaction between Arg98 and the antagonists **31** and **35** could not be achieved, probably due to the high desolvation penalty of Arg98. Finally, it is important to note that the free acids (sodium salt) of the antagonists in general showed slightly lower affinities than their methyl ester counterparts, with the only exceptions of **13b** and **14b** (Table 1). However, because the esters are thought to act as prodrugs and to be rapidly cleaved after oral application,<sup>[10e]</sup> the affinities of the carboxylates are relevant with regard to the therapeutic potential of the present FimH antagonists.

#### Cell-based flow cytometry assay<sup>[17]</sup>

These assays were performed in duplicate/triplicate, and *n*-heptyl  $\alpha$ -D-mannopyranoside **1** was used as reference compound with an IC<sub>50</sub> value of 3.9 ± 1.6 μM. The most potent antagonists **5b** and **14c** (Table 1) showed respective IC<sub>50</sub> values of 0.33 ± 0.05 and 0.89 ± 0.10 μM. In general, the activities obtained from the flow cytometry assay were ~50-fold lower than the affinities determined in the target-based competitive assay (see above).

#### Isothermal titration calorimetry

Because the biological *in vitro* evaluation only revealed small differences between affinities, ITC experiments were carried out to study the thermodynamic profile of the variously *ortho*-substituted biphenyl compounds **5b** and **14a–f** in binding to FimH. ITC directly measures the heat of interaction (change in enthalpy,  $\Delta H$ ) at a constant temperature on titrating two compounds of known concentration that form an equilibrium complex.<sup>[23]</sup> It includes contributions from all equilibria that occur as the interacting molecules go from the free to the bound state, including those associated with solvent interactions and macromolecular conformational changes. The noncovalent interaction between a protein and a ligand can be quantified by the change in free energy ( $\Delta G$ ), consisting of the change in enthalpy ( $\Delta H$ ) and change in entropy ( $\Delta S$ ) [Eq. (1)].<sup>[24]</sup> The binding energy under standard conditions ( $\Delta G^\circ$ ), in which all reactants and products are at a concentration of 1 M, can be calculated from the dissociation constant,  $K_D$  [Eq. (2)]. With ITC,  $K_D$  and  $\Delta H$  can be measured directly, whereas  $\Delta G$  and the entropy term  $T\Delta S$  are calculated according to Equations (1) and (2).

$$\Delta G = \Delta H - T\Delta S \quad (1)$$

$$\Delta G = RT \ln K_D \quad (2)$$

A favorable enthalpy term  $\Delta H$  is associated with hydrogen bond formation, electrostatic, and dipole–dipole interactions at the overcompensation of the desolvation penalty.<sup>[25]</sup> The entropy term  $\Delta S$  reflects the overall change in the degrees of freedom of a system. It can be dissected into translational and rigid body rotational entropy,<sup>[26]</sup> solvation entropy,<sup>[27]</sup> and entropy costs related to conformational changes of protein and ligand [Eq. (3)].<sup>[28]</sup> Whereas the formation of a protein–ligand complex is always associated with a decrease in translational and rotational freedom and therefore with entropy costs, the entropic contribution involving changes in solvation ( $\Delta S_{\text{solv}}$ ) and changes in rotational and vibrational entropy due to the loss of conformational flexibility ( $\Delta S_{\text{conf}}$ ) can differ both in sign and magnitude.<sup>[29]</sup>

$$\Delta S = \Delta S_{\text{solv}} + \Delta S_{\text{trans/rot}} + \Delta S_{\text{conf}} \quad (3)$$

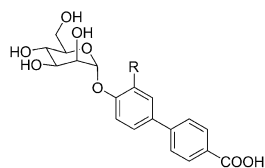
The FimH CRD was used for the ITC experiments. It was prepared from FimH-CRD-Th-His<sub>6</sub> (see *Competitive binding assay*, Experimental Section below) by incubation with thrombin, as described earlier.<sup>[16]</sup>

The thermodynamic fingerprints of the various biphenyl derivatives (Table 2, Figure 4) reveal a significant improvement in the enthalpic term ( $\Delta\Delta H$  –4.3 to –11.2 kJ mol<sup>–1</sup>) for all substituted biphenyls (**5b**, **14a–f**) in comparison with the unsubstituted derivative **4b**. The largest enthalpy improvement was observed for the trifluoromethyl group (**14c**; Table 2). Interestingly, these largely improved enthalpic contributions are mostly compensated by entropic penalties ( $-T\Delta\Delta S$  +3.2 to +7.5 kJ mol<sup>–1</sup>), resulting in only marginally improved  $K_D$  values. In the best case, the trifluoromethyl derivative **14c**, a fourfold improvement in  $K_D$  was measured. Similar, but less pronounced

**Table 2.** Binding thermodynamics of FimH antagonists determined by ITC.

Compd	R	$K_D$ [nM]	$\Delta G^\circ$ [kJ mol <sup>-1</sup> ]	$\Delta H^\circ$ [kJ mol <sup>-1</sup> ]	$-T\Delta S^\circ$ [kJ mol <sup>-1</sup> ]	$N^{[a]}$	$V_{vdW}$ [Å <sup>3</sup> ] <sup>[b]</sup>
<b>4b</b>	H	14.1	-44.8	-47.3	+2.5	1.00	7.2
<b>5b</b>	Cl	3.7	-48.1	-55.5	+7.4	1.01	22.4
<b>14a</b>	F	9.2	-45.9	-51.6	+5.7	1.00	13.3
<b>14b</b>	Me	4.8	-47.5	-56.2	+8.7	1.01	26.7
<b>14c</b>	CF <sub>3</sub>	3.2	-48.5	-58.5	+10.0	1.02	41.4
<b>14d</b>	OMe	7.7	-46.3	-52.5	+6.2	1.02	34.8
<b>14e</b>	cPr	6.9	-46.6	-46.7	+0.1	1.01	52.5
<b>14f</b>	CN	7.4	-46.4	-55.0	+8.6	1.01	29.7

[a] Molar ratio of protein/ligand. [b] van der Waals volumes ( $V_{vdW}$ ) of the *ortho* substituent were calculated with the Phase volCalc utility.<sup>[30]</sup>



cific *ortho* substituent and varies between  $-2.39$  kJ mol<sup>-1</sup> for CH<sub>3</sub> and  $19.31$  kJ mol<sup>-1</sup> for CN.<sup>[25]</sup> Finally, depending on the surface area of the *ortho* substituent, the entropy of solvation may change. In summary, the various effects are superimposed and of opposing contributions to the free binding energy  $\Delta G$ .

### Physicochemical and in vitro pharmacokinetic characterization

To estimate the oral bioavailability and renal elimination of acids **4b**, **5b**, **6**, **14a–f**, **20**, **23**, **31**, **35**, and the methyl esters **4a**, **5a**,

effects were observed for most other *ortho* substituents. This trend was broken only by the cyclopropyl derivative **14e** ( $\Delta\Delta H$  +0.7 kJ mol<sup>-1</sup>,  $-T\Delta\Delta S$  -2.4 kJ mol<sup>-1</sup>; Table 2).

The influence of the *ortho* substituent on binding can be attributed to three factors. First, *ortho* substituents of appropriate volume establish an improved shape complementarity within the binding pocket, leading to a better van der Waals (vdW) contact and therefore an improvement in the enthalpy term  $\Delta H$ . The improvement in enthalpy ( $\Delta\Delta H$ ) correlates well with increasing vdW volumes of spherical *ortho* substituents (**5b**, **14a–c**; Figure 5). For non-spherical substituents (OMe, **14d**; cyclopropyl, **14e**; and CN, **14f**), the shape complementarity is not optimal, leading to only a decreased enthalpy contribution. However, better vdW contacts also lead to decreased conformational flexibility and therefore an entropic compensation by a less favorable  $\Delta S_{conf}$  value. A second parameter is the desolvation enthalpy, which depends on the polarity of a spe-

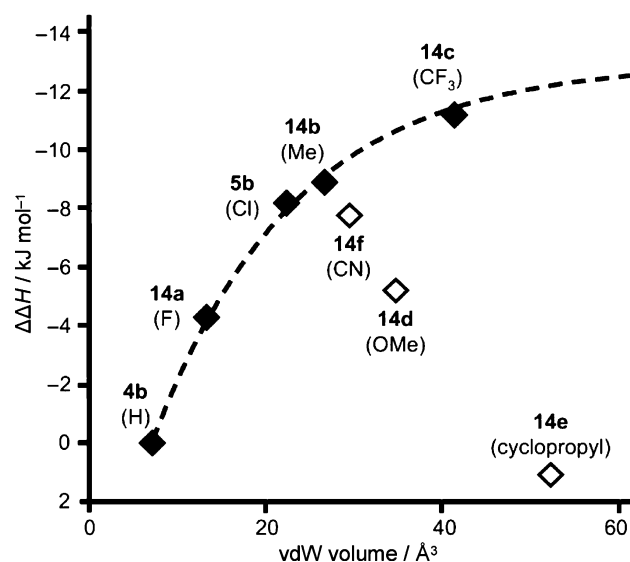


**Figure 5.** Correlation of  $\Delta\Delta H$  (relative to antagonist **4b**) with the van der Waals volumes<sup>[30]</sup> of *ortho* substituents.

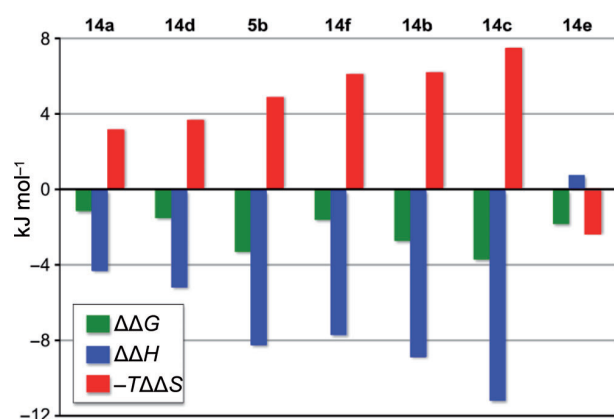


**Figure 4.** Enthalpy–entropy compensation, a property often reported for carbohydrate–lectin interactions,<sup>[31]</sup> for *ortho*-substituted biphenyl  $\alpha$ -D-mannopyranosides;  $\Delta\Delta G$ ,  $\Delta\Delta H$ , and  $T\Delta\Delta S$  values for **5b** and **14a–f** are plotted relative to the unsubstituted derivative **4b**.

**13a–f**, **19a–b**, **22**, **30** and **34**, several physicochemical parameters (lipophilicity, solubility) as well as permeability through an artificial membrane and a cell monolayer were determined (Table 3). The free acids of the antagonists assessed in this study (**4b**, **5b**, **6**, **14a–f**, **20**, **23**, **31**, and **35**) are generally hydrophilic and soluble at pH values  $>5$ . All acids showed  $\log D_{7,4}$  values below zero and are therefore thought to undergo considerable renal clearance,<sup>[32]</sup> a prerequisite for FimH antagonists to reach their target in the urinary bladder. Permeation studies through an artificial membrane (PAMPA<sup>[33]</sup>) indicated for all acids except **14a** effective permeation values ( $\log P_e$ ) below  $-6.7$ , suggesting low absorption in the small intestine by passive permeation.<sup>[34]</sup> However, the high absorption potential of the fluoro-substituted biphenyl **14a** predicted by

**Table 3.** Physicochemical and in vitro pharmacokinetic parameters of FimH antagonists.

Compd	PAMPA $\log P_e$ [ $\log 10^{-6} \text{ cm s}^{-1}$ ]/pH <sup>[a]</sup>	Caco-2 $P_{app}$ [ $10^{-6} \text{ cm s}^{-1}$ ] <sup>[b]</sup>			$\log D_{7.4}$ <sup>[c]</sup>	Solubility [ $\mu\text{g mL}^{-1}$ ]/pH <sup>[d]</sup>
		a→b	b→a	(b→a)/(a→b)		
<b>1</b>	-4.9	7.0±0.6	9.4±0.2	1.3	1.7	>3000/6.5
<b>24</b>	-5.0±0.1/5.0	10.0±0.9	19.0±1.2	1.9	2.1±0.1	22±0/3.0
	-4.9±0.1/6.2					22±1/5.0
	-4.7±0.1/7.4					21±1/7.4
<b>3</b>	-4.9±0.0/5.0	2.2±0.2	17.6±0.4	8.0	2.0±0.0	>150/3.0
	-4.9±0.0/6.2					>150/5.0
	-4.9±0.0/7.4					>150/7.4
<b>4a</b>	-4.7	1.5±0.0	6.4±0.4	4.3	2.1	14±1/3.0
						13±1/5.0
						12±1/7.4
<b>4b</b>	n.p.	n.d.	n.d.	n.d.	<-1.5	>3000/6.6
<b>5a</b>	-4.6	5.3±0.6	17.5±1.3	3.3	2.3	16±2/3.0
						15±0/5.0
						17±2/7.4
<b>5b</b>	n.p.	0.2±0.0	0.4±0.0	1.6	-0.8	>3000/6.5
<b>13a</b>	-4.8±0.0/5.0	5.6±0.7	22.0±0.6	4.0	2.7±0.1	22±1/3.0
	-4.8±0.0/6.2					24±3/5.0
	-4.8±0.0/7.4					17±6/7.4
<b>14a</b>	-5.8±0.1/5.0	0.2±0.1	0.2±0.0	0.8	<-1.5	30±3/3.0
	-6.3±0.1/6.2					>100/5.0
	-7.4±0.1/7.4					>100/7.4
<b>13b</b>	-4.5±0.1/5.0	6.2±1.3	22.7±1.2	3.6	2.4±0.2	7±0/3.0
	-4.5±0.0/6.2					7±0/5.0
	-4.6±0.1/7.4					7±0/7.4
<b>14b</b>	-8.6±1.7/5.0	n.d.	n.d.	n.d.	-0.6±0.1	34±3/3.0
	-8.8±1.4/6.2					>200/5.0
	-8.7±1.5/7.4					>200/7.4
<b>13c</b>	-4.4±0.0/5.0	9.2±0.1	16.9±1.5	1.8	2.8±0.1	17±1/3.0
	-4.4±0.0/6.2					15±1/5.0
	-4.5±0.1/7.4					16±1/7.4
<b>14c</b>	-8.4±1.3/5.0	n.d.	n.d.	n.d.	-0.8±0.1	15±1/3.0
	-9.3±1.4/6.2					140±6/5.0
	-8.6±1.6/7.4					>200/7.4
<b>13d</b>	-5.4±0.0/5.0	4.2±0.7	16.4±1.2	3.9	1.8±0.1	24±0/3.0
	-5.4±0.0/6.2					24±1/5.0
	-5.4±0.0/7.4					26±1/7.4
<b>14d</b>	-8.5±0.6/5.0	n.d.	n.d.	n.d.	<-1.5	127±4/3.0
	-9.1±0.2/6.2					>200/5.0
	-9.2±0.4/7.4					>200/7.4
<b>13e</b>	-4.5±0.2/5.0	6.1±0.6	17.9±1.2	3.0	2.9±0.1	14±2/3.0
	-4.4±0.0/6.2					13±0/5.0
	-4.4±0.1/7.4					14±1/7.4
<b>14e</b>	-9.3±1.3/5.0	n.d.	n.d.	n.d.	-0.8±0.1	31±2/3.0
	-8.7±1.5/6.2					>200/5.0
	-8.7±1.5/7.4					>200/7.4
<b>13f</b>	-6.5±0.0/5.0	0.9±0.7	18.1±0.6	19.7	1.7±0.0	22±2/3.0
	-6.5±0.1/6.2					24±1/5.0
	-6.3±0.1/7.4					23±1/7.4
<b>14f</b>	-8.5±1.7/5.0	n.d.	n.d.	n.d.	<-1.5	35±11/3.0
	-7.3±0.3/6.2					>200/5.0
	-7.8±1.5/7.4					>200/7.4
<b>19a</b>	-4.9±0.0/5.0	4.4±0.1	18.8±1.7	4.3	1.9±0.1	103±8/3.0
	-4.9±0.0/6.2					100±6/5.0
	-4.9±0.1/7.4					95±5/7.4
<b>6</b>	-8.6±1.6/5.0	n.d.	n.d.	n.d.	<-1.5	>130/3.0
	-9.3±1.4/6.2					>130/5.0
	-8.7±1.5/7.4					>130/7.4
<b>19b</b>	-5.3±0.1/5.0	n.d.	n.d.	n.d.	2.4±0.1	30±0/3.0
	-5.6±0.1/6.2					29±1/5.0
	-5.1±0.2/7.4					31±1/7.4
<b>20</b>	-8.6±1.6/5.0	n.d.	n.d.	n.d.	-1.2±0.2	>130/3.0
	-9.3±1.4/6.2					>130/5.0
	-10/7.4					>130/7.4

**Table 3.** (Continued)

Compd	PAMPA $\log P_e$ [ $\log 10^{-6} \text{ cm s}^{-1}$ ]/pH <sup>[a]</sup>	Caco-2 $P_{app}$ [ $10^{-6} \text{ cm s}^{-1}$ ] <sup>[b]</sup>			$\log D_{7.4}$ <sup>[c]</sup>	Solubility [ $\mu\text{g mL}^{-1}$ ]/pH <sup>[d]</sup>
		a→b	b→a	(b→a)/(a→b)		
<b>22</b>	-5.1 ± 0.0/5.0	n.d.	n.d.	n.d.	1.7 ± 0.1	> 130/3.0
	-5.1 ± 0.0/6.2					> 130/5.0
	-5.1 ± 0.0/7.4					> 130/7.4
<b>23</b>	-7.3 ± 1.8/5.0	n.d.	n.d.	n.d.	< -1.5	> 130/3.0
	-8.1 ± 2.2/6.2					> 130/5.0
	-10/7.4					> 130/7.4
<b>30</b>	-5.5 ± 0.0/5.0	n.d.	n.d.	n.d.	1.6 ± 0.1	> 130/3.0
	-5.5 ± 0.0/6.2					> 130/5.0
	-5.4 ± 0.1/7.4					> 130/7.4
<b>31</b>	-7.7 ± 1.6/5.0	n.d.	n.d.	n.d.	< -1.5	> 130/3.0
	-8.1 ± 1.3/6.2					> 130/5.0
	-10/7.4					> 130/7.4
<b>34</b>	-5.3 ± 0.1/5.0	n.d.	n.d.	n.d.	2.2 ± 0.1	> 130/3.0
	-5.6 ± 0.0/6.2					> 130/5.0
	-5.3 ± 0.2/7.4					> 130/7.4
<b>35</b>	-8.0 ± 1.3/5.0	n.d.	n.d.	n.d.	n.d.	63 ± 8/3.0
	-8.6 ± 1.6/6.2					> 130/5.0
	-10/7.4					> 130/7.4

[a]  $P_e$  = effective permeation: passive permeation through an artificial membrane was determined by parallel artificial membrane permeation assay (PAMPA); values represent the mean ± SD of quadruplicate measurements taken at three pH values (pH 5.0, 6.2, and 7.4).<sup>[33]</sup> [b]  $P_{app}$  = apparent permeability: permeation through cell monolayers was assessed by a Caco-2 assay in the absorptive (a→b) and secretory (b→a) directions in triplicate;<sup>[42]</sup> n.p. = no permeation, n.d. = not determined. [c] Distribution coefficients ( $\log D$ ) were measured by a miniaturized shake-flask procedure at pH 7.4. [d] Kinetic solubility was measured in a 96-well format using the  $\mu\text{SOL}$  Explorer solubility analyzer at three pH values (pH 3.0, 5.0, and 7.4) in triplicate.

PAMPA could not be confirmed by the colorectal adenocarcinoma (Caco-2) cell permeation assay. In contrast, the methyl esters (**3**, **4a**, **5a**, **13a–f**, **19a–b**, **22**, **30**, and **34**) showed  $\log D_{7.4}$  values > 1.5, that is, they are more lipophilic and hence more permeable than the corresponding acids, as shown by the PAMPA and Caco-2 permeation assay. Despite this high absorption potential, the ratios between the apparent permeability coefficients ( $P_{app}$ ) in the basolateral-to-apical (b→a, secretory) and apical-to-basolateral (a→b, absorptive) directions revealed active efflux processes as an additional issue of all the assessed compounds. Moreover, the methyl esters must be readily hydrolyzed after absorption to become more polar and to be renally eliminated. Rapid metabolic turnover by the enzyme carboxylesterase was previously shown for the methyl esters **4a** and **5a**.<sup>[10e]</sup>

The different substituents at the *ortho* position of ring A (**5a**, **5b**, **13a–f**, **14a–f**; Table 3) only have a minor influence on the physicochemical properties. The addition of chloro, fluoro, methyl, trifluoromethyl, or cyclopropyl substituents slightly increases the lipophilicity of the respective acids and methyl esters, whereas methoxy and cyano substituents render the compounds more hydrophilic and less permeable. Moreover, the substituents at the *ortho* position have negligible effects on the low aqueous solubility, which is a major drawback of all methyl esters.<sup>[35]</sup> In contrast, the modifications with increased spacer length between carbohydrate and aglycone (**6**, **19a–b**, **20**, **22**, and **23**; Table 3) show higher aqueous solubility. Extending the spacer and linking it at the *ortho* or *meta* positions of the biaryl moiety disrupts the symmetry of the molecular structure, leading to increased solubility.<sup>[15,36]</sup> However, an additional chloro substituent at the 4-position (**19b**, **20**; Table 3) restores the symmetrical character of the structure, which in turn

lowers the solubility of the compound. Disrupted structural symmetry might also hold true for the enhanced solubility of the biphenyls with an elongated carboxylate-bearing *para* substituent (**30**, **31**, **34**, and **35**; Table 3). The introduction of a methylene or cyclopropylene group between the biphenyl and the carboxylate moiety markedly improved the aqueous solubility of the methyl esters, whereas the absorption potential was only slightly decreased.

## Summary and Conclusions

In this study, we investigated the structure–affinity relationship for *ortho* substituents on ring A of the biphenyl aglycone of the FimH antagonists **13** and **14**. The correlation between vdW volumes of these substituents and the enthalpy term clearly indicates the importance of shape complementarity. This interpretation is further supported by the fact that the electronic character of the substituent [Cl in **5a** (Table 2), CF<sub>3</sub> in **14c** versus CH<sub>3</sub> in **14b**] is less important. The correlation of enthalpic improvements ( $\Delta\Delta H$ ) with vdW volumes offers a potent tool for guiding further structural optimization.

The successful oral application using a prodrug approach was recently demonstrated with the ester **5a**.<sup>[10e]</sup> A major drawback of the biphenyl methyl esters is their insufficient solubility, which is mostly in the range of 15–35  $\mu\text{g mL}^{-1}$ . As expected,<sup>[15]</sup> solubility could be substantially improved when the symmetry of the aglycone was disrupted. Thus, the solubility of **3** (> 150  $\mu\text{g mL}^{-1}$ ; Table 3), **19a** (100  $\mu\text{g mL}^{-1}$ ), and **22** (> 130  $\mu\text{g mL}^{-1}$ ) was improved by a factor of ~10. However, for these more flexible derivatives, the expected optimized fit leading to improved affinities in the in-docking mode could not be observed. In fact, the affinities for the members of this

family of compounds are drastically decreased, for example, compounds **20** or **23** (Table 1).

Finally, the elongation of the ester-bearing *para* substituent (Table 1; compounds **31** and **35**) did not lead to the expected additional polar interaction with Arg98. Instead, a five- to sevenfold decrease in affinity was observed. Clearly, the desolvation penalty for the guanidinium group could not be matched by the geometrically possible salt bridge with the carboxylate of the antagonists **31** and **35**.

In summary, our study confirms the earlier selection of the FimH antagonists **5a** for oral and **5b** for intravenous application. However, the methoxy derivative **13d** (Table 1) shows slightly improved pharmacokinetic properties and therefore represents an additional candidate for future in vivo studies.

## Experimental Section

**General methods:** NMR spectra were recorded on a Bruker Avance DMX-500 (500.1 MHz) spectrometer. Assignment of  $^1\text{H}$  and  $^{13}\text{C}$  NMR spectra was achieved using 2D methods (COSY, HSQC, HMBC). Chemical shifts are expressed in ppm using residual  $\text{CHCl}_3$ ,  $\text{CHD}_2\text{OD}$ , or  $\text{H}_2\text{O}$  as references. Optical rotations were measured with a PerkinElmer Polarimeter 341. Electrospray ionization mass spectrometry (ESI-MS) data were obtained on a Waters Micromass ZQ instrument. LC–HRMS analyses were carried out using an Agilent 1100 LC equipped with a photodiode array detector and a Micromass QTOF I equipped with a 4 GHz digital time converter. Microwave-assisted reactions were carried out with a CEM Discover and Explorer. Reactions were monitored by TLC using glass plates coated with silica gel 60  $F_{254}$  (Merck) and visualized by UV light and/or by charring with a molybdate solution (0.02 M solution of ammonium cerium sulfate dihydrate and ammonium molybdate tetrahydrate in aqueous 10%  $\text{H}_2\text{SO}_4$ ). MPLC separations were carried out on a CombiFlash Companion or  $R_f$  from Teledyne Isco equipped with RediSep normal-phase or RP-18 reversed-phase flash columns. LC–MS separations were carried out on a Waters system equipped with sample manager 2767, pump 2525, PDA 2525, and Micromass ZQ. Size-exclusion chromatography was performed on Bio-Gel P-2 Gel (45–90 mm) from Bio-Rad (Reinach, Switzerland). All compounds used for biological assays are at least of 98% purity based on analytical HPLC results. Commercially available reagents were purchased from Fluka, Aldrich, Alfa Aesar or Iris Biotech (Germany). Solvents were purchased from Sigma–Aldrich (Buchs, Switzerland) or Acros Organics (Geel, Belgium) and were dried prior to use where indicated. MeOH was dried by reflux with sodium methoxide and distilled immediately before use.  $\text{CH}_2\text{Cl}_2$  was dried by filtration over  $\text{Al}_2\text{O}_3$  (Fluka, type 5016 A basic). Molecular sieves (4 Å) were activated in vacuo at 500 °C for 1 h immediately before use.

**General procedure A for the synthesis of mannosides 10a–f and 17a–c:** To an ice-cold suspension of **8**<sup>[12]</sup> (200 mg, 0.57 mmol, 1.1 equiv), phenol **9a–f** or benzyl alcohol **16a–c** (0.52 mmol, 1.0 equiv), and molecular sieves (4 Å, 600 mg) in dry  $\text{CH}_2\text{Cl}_2$  (5 mL),  $\text{BF}_3 \cdot \text{Et}_2\text{O}$  (0.3 mL, 2.44 mmol, 4.7 equiv) was added dropwise under argon. The mixture was stirred at 0 °C for 3 h, and then at RT overnight. The reaction mixture was filtered over Celite, and the filtrate was diluted with  $\text{CH}_2\text{Cl}_2$  (50 mL), extracted with 0.5 N  $\text{NaOH}_{(\text{aq})}$  (50 mL),  $\text{H}_2\text{O}$  (50 mL), and brine (50 mL). The organic layer was dried over  $\text{Na}_2\text{SO}_4$  and concentrated in vacuo. The residue was purified by MPLC on silica gel (petroleum ether (PE)/EtOAc) to yield **10a–f** or **17a–c**.

**General procedure B for the synthesis of mannosylated biphenyls:** A Schlenk tube was charged with aryl bromide (1.0 equiv), boronic acid or boronate (1.1 equiv),  $\text{Pd}(\text{dppf})\text{Cl}_2 \cdot \text{CH}_2\text{Cl}_2$  (0.03 equiv),  $\text{K}_3\text{PO}_4$  (1.5 equiv) and a stirring bar. The tube was closed with a rubber septum and was evacuated and flushed with argon. This procedure was repeated once, then anhydrous DMF (2 mL) was added under a stream of argon. The mixture was degassed in an ultrasonic bath and flushed with argon for 5 min, and then stirred at 80 °C overnight. The reaction mixture was cooled to RT, diluted with EtOAc (50 mL), and washed with  $\text{H}_2\text{O}$  (50 mL) and brine (50 mL). The organic layer was dried over  $\text{Na}_2\text{SO}_4$  and concentrated in vacuo. The residue was purified by MPLC on silica gel (PE/EtOAc) to afford biphenyls **12a–f**, **18a,b**, **21**, **29** or **33**.

**General procedure C for deacetylation:** To a solution of **12a–f**, **18a,b**, **21**, **29** or **33** (1.0 equiv) in dry MeOH (5 mL) was added freshly prepared 1 M NaOMe/MeOH (0.1 equiv) under argon. The mixture was stirred at RT until the reaction was complete (monitored by TLC), then neutralized with Amberlyst-15 ( $\text{H}^+$ ) ion-exchange resin, filtered and concentrated in vacuo. The residue was purified by MPLC on silica gel ( $\text{CH}_2\text{Cl}_2/\text{MeOH}$ , 10:1–8:1) to afford **13a–f**, **19a,b**, **22**, **30** or **34** as white solids.

**General procedure D for saponification:** To a solution of **12a–e**, **18a,b**, **21**, **29** or **33** (1.0 equiv) in MeOH (5 mL) was added 1 M NaOMe/MeOH (0.1 equiv) at RT. The reaction mixture was stirred at RT for 4 h and concentrated. The residue was treated with 0.5 M  $\text{NaOH}_{(\text{aq})}$  (1 mL) for 24 h at RT. The solution was then adjusted to pH 3–4 with Amberlyst-15 ( $\text{H}^+$ ), and the mixture was filtered and concentrated. The crude product was transformed into the sodium salt by passing through a small column of Dowex 50X8 ( $\text{Na}^+$  form) ion-exchange resin. After concentration, the residue was purified by MPLC (RP-18,  $\text{H}_2\text{O}/\text{MeOH}$ , 1:0–2:1) followed by size-exclusion chromatography (P-2 gel,  $\text{H}_2\text{O}$ ) to give **14a–e**, **6**, **20**, **23**, **31** or **35** as white solids after final lyophilization from  $\text{H}_2\text{O}$ .

**4-Bromo-2-fluorophenyl 2,3,4,6-tetra-O-acetyl- $\alpha$ -D-mannopyranoside (10a):** Prepared according to general procedure A from **8**<sup>[12]</sup> and 4-bromo-2-fluorophenol (**9a**). Yield: 220 mg (74%) as white solid.  $R_f=0.48$  (PE/EtOAc, 2:1);  $[\alpha]_D^{20}+83.0$  ( $c=0.70$ , EtOAc);  $^1\text{H}$  NMR (500 MHz,  $\text{CDCl}_3$ ):  $\delta=7.30$  (dd,  $J=2.3$ , 10.1 Hz, 1H, Ar-H), 7.21 (dt,  $J=1.7$ , 8.8 Hz, 1H, Ar-H), 7.08 (t,  $J=8.6$  Hz, 1H, Ar-H), 5.54 (dd,  $J=3.5$ , 10.0 Hz, 1H, H-3), 5.50 (dd,  $J=1.8$ , 3.4 Hz, 1H, H-2), 5.46 (d,  $J=1.5$  Hz, 1H, H-1), 5.36 (t,  $J=10.0$  Hz, 1H, H-4), 4.26 (dd,  $J=5.5$ , 12.2 Hz, 1H, H-6a), 4.17 (ddd,  $J=2.1$ , 5.5, 10.0 Hz, 1H, H-5), 4.10 (dd,  $J=2.2$ , 12.2 Hz, 1H, H-6b), 2.20, 2.07, 2.05, 2.04 ppm (4 s, 12H, 4 OAc);  $^{13}\text{C}$  NMR (125 MHz,  $\text{CDCl}_3$ ):  $\delta=170.51$ , 169.95, 169.82, 169.76 (4 CO), 153.28 (d,  $J=251.4$  Hz, Ar-C), 142.64 (d,  $J=11.1$  Hz, Ar-C), 127.58 (d,  $J=4.0$  Hz, Ar-C), 120.4 (d,  $J=21.5$  Hz, Ar-C), 120.28 (d,  $J=0.9$  Hz, Ar-C), 115.73 (d,  $J=8.1$  Hz, Ar-C), 97.49 (C-1), 69.76 (C-5), 69.15 (C-2), 68.60 (C-3), 65.76 (C-4), 62.09 (C-6), 20.87, 20.71, 20.69, 20.67 ppm (4  $\text{COCH}_3$ ); elemental analysis calcd (%) for  $\text{C}_{20}\text{H}_{22}\text{BrFO}_{10}$ : C 46.08, H 4.25, found: C 46.11, H 4.26.

**4-Bromo-2-methylphenyl 2,3,4,6-tetra-O-acetyl- $\alpha$ -D-mannopyranoside (10b):** Prepared according to general procedure A from **8**<sup>[12]</sup> and 4-bromo-2-methylphenol (**9b**). Yield: 254 mg (86%) as white solid.  $R_f=0.60$  (PE/EtOAc, 2:1);  $[\alpha]_D^{20}+61.8$  ( $c=1.00$ , EtOAc);  $^1\text{H}$  NMR (500 MHz,  $\text{CDCl}_3$ ):  $\delta=7.31$  (d,  $J=1.9$  Hz, 1H, Ar-H), 7.24 (dd,  $J=2.3$ , 8.7 Hz, 1H, Ar-H), 6.97 (d,  $J=8.8$  Hz, 1H, Ar-H), 5.53 (dd,  $J=3.4$ , 10.0 Hz, 1H, H-3), 5.47 (d,  $J=1.7$  Hz, 1H, H-1), 5.45 (dd,  $J=2.0$ , 3.4 Hz, 1H, H-2), 5.37 (t,  $J=10.0$  Hz, 1H, H-4), 4.28 (dd,  $J=5.6$ , 12.3 Hz, 1H, H-6a), 4.10–4.03 (m, 2H, H-5, H-6b), 2.27 (s, 3H,  $\text{CH}_3$ ), 2.20, 2.06, 2.05, 2.04 ppm (4 s, 12H, 4 OAc);  $^{13}\text{C}$  NMR (125 MHz,  $\text{CDCl}_3$ ):  $\delta=170.53$ , 170.04, 169.96, 169.73 (4 CO), 152.96, 133.78,



129.88, 129.61, 115.81, 115.23 (Ar-C), 95.91 (C-1), 69.39 (C-5), 69.38 (C-2), 68.88 (C-3), 65.76 (C-4), 62.12 (C-6), 20.88, 20.70, 20.68 (4C, 4 COCH<sub>3</sub>), 16.07 ppm (CH<sub>3</sub>); elemental analysis calcd (%) for C<sub>21</sub>H<sub>25</sub>BrO<sub>10</sub>: C 48.76, H 4.87, found: C 48.84, H 4.91.

**4-Bromo-2-trifluoromethyl-phenyl 2,3,4,6-tetra-O-acetyl- $\alpha$ -D-mannopyranoside (10c):** Prepared according to general procedure A from **8**<sup>[12]</sup> and 4-bromo-2-trifluoromethylphenol (**9c**). Yield: 260 mg (80%) as white solid.  $R_f$ =0.50 (PE/EtOAc, 2:1);  $[\alpha]_D^{20}$ +64.6 ( $c$ =1.00, EtOAc); <sup>1</sup>H NMR (500 MHz, CDCl<sub>3</sub>):  $\delta$ =7.74 (d,  $J$ =2.3 Hz, 1H, Ar-H), 7.61 (dd,  $J$ =2.4, 8.9 Hz, 1H, Ar-H), 7.15 (d,  $J$ =8.9 Hz, 1H, Ar-H), 5.60 (d,  $J$ =1.6 Hz, 1H, H-1), 5.51 (dd,  $J$ =3.5, 10.1 Hz, 1H, H-3), 5.45 (dd,  $J$ =2.0, 3.3 Hz, 1H, H-2), 5.39 (t,  $J$ =10.1 Hz, 1H, H-4), 4.27 (dd,  $J$ =5.3, 12.4 Hz, 1H, H-6a), 4.08–4.00 (m, 2H, H-5, H-6b), 2.21, 2.06, 2.05, 2.04 ppm (4 s, 12H, 4 OAc); <sup>13</sup>C NMR (125 MHz, CDCl<sub>3</sub>):  $\delta$ =170.41, 169.91, 169.74, 169.62 (4 CO), 152.16 (d,  $J$ =1.7 Hz, Ar-C), 136.07 (Ar-C), 130.35 (t,  $J$ =5.3 Hz, Ar-C), 122.30 (d,  $J$ =271.4 Hz, CF<sub>3</sub>), 121.72 (d,  $J$ =31.7 Hz, Ar-C), 117.08, 114.88 (Ar-C), 95.75 (C-1), 69.96 (C-5), 69.02 (C-2), 68.45 (C-3), 65.44 (C-4), 61.95 (C-6), 20.84, 20.70, 20.67, 20.63 ppm (4 COCH<sub>3</sub>); elemental analysis calcd (%) for C<sub>21</sub>H<sub>22</sub>BrF<sub>3</sub>O<sub>10</sub>: C 44.15, H 3.88, found: C 44.10, H 3.88.

**4-Bromo-2-methoxyphenyl 2,3,4,6-tetra-O-acetyl- $\alpha$ -D-mannopyranoside (10d):** Prepared according to general procedure A from **8**<sup>[12]</sup> and 4-bromo-2-methoxyphenol (**9d**). Yield: 234 mg (77%) as white solid.  $R_f$ =0.32 (PE/acetone, 4:1);  $[\alpha]_D^{20}$ +70.3 ( $c$ =0.70, EtOAc); <sup>1</sup>H NMR (500 MHz, CDCl<sub>3</sub>):  $\delta$ =7.03–6.95 (m, 3H, Ar-H), 5.58 (dd,  $J$ =3.5, 10.0 Hz, 1H, H-3), 5.52 (dd,  $J$ =1.8, 3.4 Hz, 1H, H-2), 5.42 (d,  $J$ =1.8 Hz, 1H, H-1), 5.34 (t,  $J$ =10.0 Hz, 1H, H-4), 4.28–4.24 (m, 2H, H-5, H-6a), 4.10 (m, 1H, H-6b), 3.84 (s, 3H, OCH<sub>3</sub>), 2.19, 2.07, 2.05, 2.04 ppm (4 s, 12H, 4 OAc); <sup>13</sup>C NMR (125 MHz, CDCl<sub>3</sub>):  $\delta$ =170.58, 169.98, 169.89, 169.80 (4 CO), 151.52, 143.91, 123.49, 120.37, 116.69, 115.94 (Ar-C), 97.52 (C-1), 69.45 (C-5), 69.36 (C-2), 68.80 (C-3), 66.06 (C-4), 62.27 (C-6), 56.04 (OCH<sub>3</sub>), 20.91, 20.73, 20.71, 20.69 ppm (4 COCH<sub>3</sub>); elemental analysis calcd (%) for C<sub>21</sub>H<sub>25</sub>BrO<sub>11</sub>: C 47.29, H 4.72, found: C 47.20, H 4.70.

**4-Bromo-2-cyclopropylphenyl 2,3,4,6-tetra-O-acetyl- $\alpha$ -D-mannopyranoside (10e):** Prepared according to general procedure A from **8**<sup>[12]</sup> and 4-bromo-2-cyclopropylphenol (**9e**). Yield: 235 mg (76%) as white solid.  $R_f$ =0.30 (PE/EtOAc, 3:1);  $[\alpha]_D^{20}$ +64.7 ( $c$ =0.40, EtOAc); <sup>1</sup>H NMR (500 MHz, CDCl<sub>3</sub>):  $\delta$ =7.20 (d,  $J$ =8.7 Hz, 1H, Ar-H), 7.00–6.69 (m, 2H, Ar-H), 5.58 (d,  $J$ =10.1 Hz, 1H, H-3), 5.50 (s, 2H, H-1, H-2), 5.39 (t,  $J$ =10.1 Hz, 1H, H-4), 4.28 (dd,  $J$ =5.4, 12.2 Hz, 1H, H-6a), 4.14–4.08 (m, 2H, H-5, H-6b), 2.21, 2.09, 2.04 (3 s, 12H, 4 OAc), 1.02 (d,  $J$ =8.1 Hz, 2H, CH<sub>2</sub>-cPr), 0.65 ppm (d,  $J$ =4.6 Hz, 2H, CH<sub>2</sub>-cPr); <sup>13</sup>C NMR (125 MHz, CDCl<sub>3</sub>):  $\delta$ =170.54, 170.03, 170.15, 169.75 (4 CO), 153.64, 135.64, 129.11, 128.94, 116.29, 115.79 (Ar-C), 96.15 (C-1), 69.46 (C-5), 69.39 (C-2), 68.93 (C-3), 65.78 (C-4), 62.16 (C-6), 21.07, 20.89, 20.70 (4C, 4COCH<sub>3</sub>), 9.73, 7.88, 7.82 ppm (cPr); elemental analysis calcd (%) for C<sub>23</sub>H<sub>27</sub>BrFO<sub>10</sub>: C 50.84, H 5.01, found: C 50.82, H 5.00.

**4-Bromo-2-cyanophenyl 2,3,4,6-tetra-O-acetyl- $\alpha$ -D-mannopyranoside (10f):** Prepared according to general procedure A from **8**<sup>[12]</sup> and 4-bromo-2-cyanophenol (**9f**). Yield: 220 mg (73%) as white solid.  $R_f$ =0.51 (PE/EtOAc, 2:3);  $[\alpha]_D^{20}$ +54.3 ( $c$ =0.60, EtOAc); IR (KBr):  $\tilde{\nu}$ =2232 (s, C≡N), 1749 cm<sup>-1</sup> (vs, C=O); <sup>1</sup>H NMR (500 MHz, CDCl<sub>3</sub>):  $\delta$ =7.73 (d,  $J$ =2.5 Hz, 1H, Ar-H), 7.66 (dd,  $J$ =2.5, 9.0 Hz, 1H, Ar-H), 7.15 (d,  $J$ =9.0 Hz, 1H, Ar-H), 5.62 (d,  $J$ =1.7 Hz, 1H, H-1), 5.56 (dd,  $J$ =3.5, 10.0 Hz, 1H, H-3), 5.51 (dd,  $J$ =2.0, 3.4 Hz, 1H, H-2), 5.41 (t,  $J$ =10.0 Hz, 1H, H-4), 4.28 (dd,  $J$ =4.9, 12.1 Hz, 1H, H-6a), 4.13–4.08 (m, 2H, H-5, H-6b), 2.21, 2.07, 2.05, 2.04 ppm (4 s, 12H, 4 OAc); <sup>13</sup>C NMR (125 MHz, CDCl<sub>3</sub>):  $\delta$ =169.37, 168.93, 168.71, 168.48 (4CO), 155.18, 136.28, 135.00, 116.12, 114.41, 112.97, 104.62 (Ar-C,

CN), 95.68 (C-1), 69.26 (C-5), 68.02 (C-2), 67.35 (C-3), 64.38 (C-4), 60.85 (C-6), 19.81, 19.67, 19.64, 19.58 ppm (4 COCH<sub>3</sub>); elemental analysis calcd (%) for C<sub>21</sub>H<sub>22</sub>BrNO<sub>10</sub>: C 47.74, H 4.02, N 2.65, found: C 47.78, H 4.29, N 2.67.

**Methyl 4'-(2,3,4,6-tetra-O-acetyl- $\alpha$ -D-mannopyranosyloxy)-3'-fluorobiphenyl-4-carboxylate (12a):** Prepared according to general procedure B from **10a** (100 mg, 0.192 mmol), 4-methoxycarbonylphenylboronic acid (**11**, 38.0 mg, 0.211 mmol), Pd(dppf)Cl<sub>2</sub>·CH<sub>2</sub>Cl<sub>2</sub> (4.7 mg, 5.8  $\mu$ mol) and K<sub>3</sub>PO<sub>4</sub> (61.1 mg, 0.288 mmol). Yield: 83 mg (75%) as white solid.  $R_f$ =0.26 (PE/EtOAc, 2:1);  $[\alpha]_D^{20}$ +93.0 ( $c$ =0.60, EtOAc); <sup>1</sup>H NMR (500 MHz, CDCl<sub>3</sub>):  $\delta$ =8.03–8.02 (m, 2H, Ar-H), 7.53–7.52 (m, 2H, Ar-H), 7.33 (dd,  $J$ =2.1, 11.8 Hz, 1H, Ar-H), 7.27 (dd,  $J$ =1.5, 8.9 Hz, 1H, Ar-H), 7.20 (t,  $J$ =8.3 Hz, 1H, Ar-H), 5.53 (dd,  $J$ =3.4, 10.0 Hz, 1H, H-3), 5.49–5.47 (m, 2H, H-1, H-2), 5.32 (t,  $J$ =10.0 Hz, 1H, H-4), 4.22 (dd,  $J$ =5.4, 12.1 Hz, 1H, H-6a), 4.17 (m, 1H, H-5), 4.05 (dd,  $J$ =1.8, 12.1 Hz, 1H, H-6b), 3.87 (s, 3H, OCH<sub>3</sub>), 2.15, 2.01, 1.98, 1.97 ppm (4 s, 12H, 4OAc); <sup>13</sup>C NMR (125 MHz, CDCl<sub>3</sub>):  $\delta$ =170.54, 170.00, 169.86, 169.79, 166.82 (5 CO), 153.50 (d,  $J$ =247.0 Hz, Ar-C), 143.56 (d,  $J$ =1.8 Hz, Ar-C), 143.22 (d,  $J$ =11.2 Hz, Ar-C), 136.48 (d,  $J$ =6.7 Hz, Ar-C), 130.27, 129.29, 126.75 (5C, Ar-C), 123.16 (d,  $J$ =3.4 Hz, Ar-C), 119.32 (Ar-C), 115.64 (d,  $J$ =19.4 Hz, Ar-C), 97.42 (C-1), 69.71 (C-5), 69.26 (C-2), 68.70 (C-3), 65.83 (C-4), 62.10 (C-6), 52.24 (OMe), 20.91, 20.74, 20.72, 20.70 ppm (4 COCH<sub>3</sub>); HRMS:  $m/z$ : calcd for C<sub>28</sub>H<sub>29</sub>FN<sub>2</sub>O<sub>12</sub> [M+Na]<sup>+</sup>: 599.1535, found: 599.1536.

**Methyl 4'-(2,3,4,6-tetra-O-acetyl- $\alpha$ -D-mannopyranosyloxy)-3'-methylbiphenyl-4-carboxylate (12b):** Prepared according to general procedure B from **10b** (100 mg, 0.193 mmol), **11** (38.2 mg, 0.212 mmol), Pd(dppf)Cl<sub>2</sub>·CH<sub>2</sub>Cl<sub>2</sub> (4.7 mg, 5.8  $\mu$ mol) and K<sub>3</sub>PO<sub>4</sub> (61.5 mg, 0.290 mmol). Yield: 87 mg (79%) as white solid.  $R_f$ =0.41 (PE/EtOAc, 1:0.9);  $[\alpha]_D^{20}$ +85.4 ( $c$ =0.80, EtOAc); <sup>1</sup>H NMR (500 MHz, CDCl<sub>3</sub>):  $\delta$ =8.09–8.07 (m, 2H, Ar-H), 7.61 (m, 2H, Ar-H), 7.46 (d,  $J$ =1.8 Hz, 1H, Ar-H), 7.40 (dd,  $J$ =2.3, 8.5 Hz, 1H, Ar-H), 7.18 (d,  $J$ =8.5 Hz, 1H, Ar-H), 5.61–5.58 (m, 2H, H-1, H-3), 5.50 (dd,  $J$ =2.0, 3.5 Hz, 1H, H-2), 5.41 (t,  $J$ =10.0 Hz, 1H, H-4), 4.31 (dd,  $J$ =5.9, 12.8 Hz, 1H, H-6a), 4.14–4.09 (m, 2H, H-5, H-6b), 3.94 (s, 3H, OCH<sub>3</sub>), 2.37 (s, 3H, CH<sub>3</sub>), 2.22, 2.08, 2.05, 2.04 ppm (4 s, 12H, 4 OAc); <sup>13</sup>C NMR (125 MHz, CDCl<sub>3</sub>):  $\delta$ =170.55, 170.06, 169.98, 169.75, 167.00 (5 CO), 154.05, 144.94, 134.54, 130.10, 130.02, 128.54, 128.05, 126.66, 125.76, 114.46 (12C, Ar-C), 95.84 (C-1), 69.48 (C-5), 69.37 (C-2), 68.98 (C-3), 65.81 (C-4), 62.13 (C-6), 52.12 (OCH<sub>3</sub>), 21.06, 20.91, 20.72, 20.70 (4 COCH<sub>3</sub>), 16.40 ppm (CH<sub>3</sub>); HRMS:  $m/z$ : calcd for C<sub>29</sub>H<sub>32</sub>NaO<sub>12</sub> [M+Na]<sup>+</sup>: 595.1786, found: 595.1786; elemental analysis calcd (%) for C<sub>29</sub>H<sub>32</sub>O<sub>12</sub>: C 60.84, H 5.63, found: C 60.76, H 5.80.

**Methyl 4'-(2,3,4,6-tetra-O-acetyl- $\alpha$ -D-mannopyranosyloxy)-3'-trifluoromethylbiphenyl-4-carboxylate (12c):** Prepared according to general procedure B from **10c** (100 mg, 0.175 mmol), **11** (34.6 mg, 0.193 mmol), Pd(dppf)Cl<sub>2</sub>·CH<sub>2</sub>Cl<sub>2</sub> (4.3 mg, 5.3  $\mu$ mol) and K<sub>3</sub>PO<sub>4</sub> (55.7 mg, 0.263 mmol). Yield: 100 mg (91%) as white solid.  $R_f$ =0.25 (PE/EtOAc, 2:1);  $[\alpha]_D^{20}$ +43.3 ( $c$ =1.00, EtOAc); <sup>1</sup>H NMR (500 MHz, CDCl<sub>3</sub>):  $\delta$ =8.13–8.11 (m, 2H, Ar-H), 7.87 (d,  $J$ =2.1 Hz, 1H, Ar-H), 7.75 (dd,  $J$ =2.2, 8.7 Hz, 1H, Ar-H), 7.63–7.61 (m, 2H, Ar-H), 7.35 (d,  $J$ =8.7 Hz, 1H, Ar-H), 5.70 (d,  $J$ =1.7 Hz, 1H, H-1), 5.57 (dd,  $J$ =3.5, 10.1 Hz, 1H, H-3), 5.50 (dd,  $J$ =2.0, 3.4 Hz, 1H, H-2), 5.43 (t,  $J$ =10.0 Hz, 1H, H-4), 4.30 (dd,  $J$ =5.6, 12.8 Hz, 1H, H-6a), 4.11–4.08 (m, 2H, H-5, H-6b), 3.95 (s, 3H, OCH<sub>3</sub>), 2.24, 2.07, 2.06, 2.05 ppm (4 s, 12H, 4 OAc); <sup>13</sup>C NMR (125 MHz, CDCl<sub>3</sub>):  $\delta$ =170.45, 169.96, 169.78, 169.65, 166.76 (5 CO), 152.94, 143.37, 134.59, 130.34, 129.40, 126.79, 126.14, 115.79 (12C, Ar-C), 95.67 (C-1), 69.91 (C-5), 69.15 (C-2), 68.56 (C-3), 65.50 (C-4), 61.97 (C-6), 52.25 (OCH<sub>3</sub>), 20.88, 20.71,

20.66 ppm (4C, 4 COCH<sub>3</sub>); HRMS: *m/z*: calcd for C<sub>29</sub>H<sub>29</sub>F<sub>3</sub>NaO<sub>12</sub> [*M*+Na]<sup>+</sup>: 649.1503, found: 649.1503.

**Methyl 4'-(2,3,4,6-tetra-O-acetyl- $\alpha$ -D-mannopyranosyloxy)-3'-methoxybiphenyl-4-carboxylate (12d):** Prepared according to general procedure B from **10d** (100 mg, 0.188 mmol), **11** (37.1 mg, 0.206 mmol), Pd(dppf)Cl<sub>2</sub>·CH<sub>2</sub>Cl<sub>2</sub> (4.6 mg, 5.6  $\mu$ mol) and K<sub>3</sub>PO<sub>4</sub> (59.9 mg, 0.282 mmol). Yield: 91 mg (83%) as white solid. *R*<sub>f</sub> = 0.25 (PE/EtOAc, 1:0.9); [ $\alpha$ ]<sub>D</sub><sup>20</sup> + 50.7 (*c* = 1.40, EtOAc); <sup>1</sup>H NMR (500 MHz, CDCl<sub>3</sub>):  $\delta$  = 8.10–8.08 (m, 2H, Ar-H), 7.62–7.60 (m, 2H, Ar-H), 7.19–7.13 (m, 3H, Ar-H), 5.64 (dd, *J* = 3.5, 10.0 Hz, 1H, H-3), 5.58 (dd, *J* = 1.8, 3.5 Hz, 1H, H-2), 5.53 (d, *J* = 1.7 Hz, 1H, H-1), 5.38 (t, *J* = 10.0 Hz, 1H, H-4), 4.34–4.28 (m, 2H, H-5, H-6a), 4.12 (m, 1H, H-6b), 3.94 (2 s, 6H, 2 OCH<sub>3</sub>), 2.21, 2.08, 2.05, 2.04 ppm (4 s, 12H, 4 OAc); <sup>13</sup>C NMR (125 MHz, CDCl<sub>3</sub>):  $\delta$  = 170.61, 170.02, 169.92, 169.83, 166.94 (5 CO), 151.01, 145.06, 144.92, 136.51, 130.13, 128.86, 126.87, 119.72, 119.32, 111.60 (12C, Ar-C), 97.50 (C-1), 69.48 (C-5), 69.43 (C-2), 68.91 (C-3), 66.12 (C-4), 62.29 (C-6), 56.01 (OCH<sub>3</sub>), 52.18 (CO<sub>2</sub>CH<sub>3</sub>), 20.95, 20.76, 20.74, 20.72 ppm (4 COCH<sub>3</sub>); HRMS: *m/z*: calcd for C<sub>29</sub>H<sub>32</sub>NaO<sub>13</sub> [*M*+Na]<sup>+</sup>: 611.1735, found: 611.1736.

**Methyl 4'-(2,3,4,6-tetra-O-acetyl- $\alpha$ -D-mannopyranosyloxy)-3'-cyclopropylbiphenyl-4-carboxylate (12e):** Prepared according to general procedure B from **10e** (100 mg, 0.184 mmol), **11** (36.4 mg, 0.202 mmol), Pd(dppf)Cl<sub>2</sub>·CH<sub>2</sub>Cl<sub>2</sub> (4.5 mg, 5.5  $\mu$ mol) and K<sub>3</sub>PO<sub>4</sub> (58.6 mg, 0.276 mmol). Yield: 60 mg (55%) as white solid. *R*<sub>f</sub> = 0.48 (PE/EtOAc, 2:1); [ $\alpha$ ]<sub>D</sub><sup>20</sup> + 53.0 (*c* = 0.70, EtOAc); <sup>1</sup>H NMR (500 MHz, CDCl<sub>3</sub>):  $\delta$  = 8.08–8.07 (m, 2H, Ar-H), 7.59–7.57 (m, 2H, Ar-H), 7.37 (dd, *J* = 2.4, 8.5 Hz, 1H, Ar-H), 7.19–7.17 (m, 2H, Ar-H), 5.64 (dd, *J* = 3.5, 10.1 Hz, 1H, H-3), 5.61 (d, *J* = 1.6 Hz, 1H, H-1), 5.54 (dd, *J* = 1.9, 3.4 Hz, 1H, H-2), 5.42 (t, *J* = 10.1 Hz, 1H, H-4), 4.31 (dd, *J* = 5.3, 12.2 Hz, 1H, H-6a), 4.19–4.10 (m, 2H, H-5, H-6b), 3.94 (s, 3H, OCH<sub>3</sub>), 2.22 (s, 3H, OAc), 2.17 (m, 1H, H-cPr), 2.08–2.05 (m, 9H, 3 OAc), 1.06–1.05 (m, 2H, CH<sub>2</sub>-cPr), 0.74–0.73 ppm (m, 2H, CH<sub>2</sub>-cPr); <sup>13</sup>C NMR (125 MHz, CDCl<sub>3</sub>):  $\delta$  = 170.55, 170.06, 170.02, 169.75, 166.98 (5 CO), 154.76, 145.12, 134.83, 133.56, 130.08, 128.58, 126.71, 125.33, 125.06, 114.84 (12C, Ar-C), 96.04 (C-1), 69.49 (C-5), 69.42 (C-2), 69.02 (C-3), 65.81 (C-4), 62.15 (C-6), 52.12 (OCH<sub>3</sub>), 20.91, 20.71 (4C, 4 COCH<sub>3</sub>), 9.78, 7.58 ppm (3C, cPr); elemental analysis calcd (%) for C<sub>29</sub>H<sub>32</sub>O<sub>12</sub>: C 62.20, H 5.72, found: C 62.00, H 5.86.

**Methyl 4'-(2,3,4,6-tetra-O-acetyl- $\alpha$ -D-mannopyranosyloxy)-3'-cyanobiphenyl-4-carboxylate (12f):** Prepared according to general procedure B from **10f** (100 mg, 0.189 mmol), **11** (37.5 mg, 0.208 mmol), Pd(dppf)Cl<sub>2</sub>·CH<sub>2</sub>Cl<sub>2</sub> (4.6 mg, 5.7  $\mu$ mol) and K<sub>3</sub>PO<sub>4</sub> (60.2 mg, 0.284 mmol). Yield: 92 mg (84%) as white solid. *R*<sub>f</sub> = 0.18 (PE/EtOAc, 2:1); [ $\alpha$ ]<sub>D</sub><sup>20</sup> + 61.4 (*c* = 0.80, EtOAc); <sup>1</sup>H NMR (500 MHz, CDCl<sub>3</sub>):  $\delta$  = 8.06–8.05 (m, 2H, Ar-H), 7.80 (d, *J* = 2.3 Hz, 1H, Ar-H), 7.72 (dd, *J* = 2.3, 8.8 Hz, 1H, Ar-H), 7.53–7.51 (m, 2H, Ar-H), 7.28 (d, *J* = 8.8 Hz, 1H, Ar-H), 5.64 (d, *J* = 1.7 Hz, 1H, H-1), 5.55 (dd, *J* = 3.5, 10.0 Hz, 1H, H-3), 5.49 (dd, *J* = 1.9, 3.4 Hz, 1H, H-2), 5.37 (t, *J* = 10.0 Hz, 1H, H-4), 4.24 (dd, *J* = 5.0, 12.4 Hz, 1H, H-6a), 4.12 (ddd, *J* = 2.2, 4.9, 10.0 Hz, 1H, H-5), 4.05 (dd, *J* = 2.2, 12.4 Hz, 1H, H-6b), 3.88 (s, 3H, OCH<sub>3</sub>), 2.16, 2.01, 1.99, 1.98 ppm (4 s, 12H, 4 OAc); <sup>13</sup>C NMR (125 MHz, CDCl<sub>3</sub>):  $\delta$  = 170.45, 170.01, 169.78, 169.54, 166.65 (5 CO), 156.84, 142.44, 135.67, 132.36, 129.77, 126.76, 115.99, 115.18, 104.47 (13C, Ar-C, CN), 96.63 (C-1), 70.24 (C-5), 69.17 (C-2), 68.49 (C-3), 65.48 (C-4), 60.85 (C-6), 20.88, 20.73, 20.71, 20.64 ppm (4 COCH<sub>3</sub>); HRMS: *m/z*: calcd for C<sub>29</sub>H<sub>29</sub>NNaO<sub>12</sub> [*M*+Na]<sup>+</sup>: 606.1582, found: 606.1583.

**Methyl 3'-fluoro-4'-( $\alpha$ -D-mannopyranosyloxy)biphenyl-4-carboxylate (13a):** Prepared according to general procedure C from **12a** (33 mg, 0.057 mmol). Yield: 15 mg (65%). [ $\alpha$ ]<sub>D</sub><sup>20</sup> + 114.3 (*c* = 0.30, MeOH); <sup>1</sup>H NMR (500 MHz, CD<sub>3</sub>OD):  $\delta$  = 7.98–7.97 (m, 2H, Ar-H),

7.63–7.61 (m, 2H, Ar-H), 7.42–7.36 (m, 3H, Ar-H), 5.45 (d, *J* = 1.7 Hz, 1H, H-1), 3.99 (dd, *J* = 1.9, 3.4 Hz, 1H, H-2), 3.82–3.84 (m, 4H, H-3, OCH<sub>3</sub>), 3.71–3.56 ppm (m, 4H, H-4, H-5, H-6); <sup>13</sup>C NMR (125 MHz, CD<sub>3</sub>OD):  $\delta$  = 168.34 (CO), 154.75 (d, *J* = 243.8 Hz, Ar-C), 145.6 (2C, Ar-C), 136.37 (d, *J* = 6.9 Hz, Ar-C), 130.20, 129.20, 127.80, 124.33, 120.33 (7C, Ar-C), 116.00 (d, *J* = 20.0 Hz, Ar-C), 101.40 (C-1), 75.97 (C-5), 72.31 (C-3), 71.82 (C-2), 68.18 (C-4), 62.65 (C-6), 52.65 ppm (OCH<sub>3</sub>); HRMS: *m/z*: calcd for C<sub>20</sub>H<sub>21</sub>FNaO<sub>8</sub> [*M*+Na]<sup>+</sup>: 431.1113, found: 431.1112.

**Methyl 4'-( $\alpha$ -D-mannopyranosyloxy)-3'-methylbiphenyl-4-carboxylate (13b):** Prepared according to general procedure C from **12b** (31 mg, 0.054 mmol). Yield: 16 mg (73%). [ $\alpha$ ]<sub>D</sub><sup>20</sup> + 110.5 (*c* = 0.35, MeOH); <sup>1</sup>H NMR (500 MHz, CD<sub>3</sub>OD):  $\delta$  = 7.96–7.94 (m, 2H, Ar-H), 7.60–7.58 (m, 2H, Ar-H), 7.40–7.37 (m, 2H, Ar-H), 7.22 (d, *J* = 8.5 Hz, 1H, Ar-H), 5.47 (d, *J* = 1.6 Hz, 1H, H-1), 3.97 (dd, *J* = 1.9, 3.4 Hz, 1H, H-2), 3.87 (dd, *J* = 3.4, 9.5 Hz, 1H, H-3), 3.82 (s, 3H, OMe), 3.67–3.52 (m, 3H, H-4, H-6), 3.46 (m, 1H, H-5), 2.21 ppm (s, 3H, Me); <sup>13</sup>C NMR (125 MHz, CD<sub>3</sub>OD):  $\delta$  = 168.56 (CO), 156.20, 146.86, 134.70, 131.07, 130.07, 130.54, 129.45, 128.92, 127.63, 126.85, 115.83 (12C, Ar-C), 99.76 (C-1), 75.55 (C-5), 72.64 (C-3), 72.11 (C-2), 68.31 (C-4), 62.68 (C-6), 52.59 ppm (OCH<sub>3</sub>), 16.54 (CH<sub>3</sub>); HRMS: *m/z*: calcd for C<sub>21</sub>H<sub>24</sub>NaO<sub>8</sub> [*M*+Na]<sup>+</sup>: 427.1363, found: 427.1370.

**Methyl 3'-trifluoromethyl-4'-( $\alpha$ -D-mannopyranosyloxy)biphenyl-4-carboxylate (13c):** Prepared according to general procedure C from **12c** (30 mg, 0.048 mmol). Yield: 14 mg (64%). [ $\alpha$ ]<sub>D</sub><sup>20</sup> + 113.1 (*c* = 0.40, MeOH); <sup>1</sup>H NMR (500 MHz, CD<sub>3</sub>OD):  $\delta$  = 8.11–8.10 (m, 2H, Ar-H), 7.92–7.90 (m, 2H, Ar-H), 7.75–7.73 (m, 2H, Ar-H), 7.63 (d, *J* = 8.4 Hz, 1H, Ar-H), 5.69 (d, *J* = 1.5 Hz, 1H, H-1), 4.09 (dd, *J* = 1.8, 3.3 Hz, 1H, H-2), 3.98–3.94 (m, 4H, H-3, OMe), 3.79–3.73 (m, 3H, H-4, H-6), 3.61 ppm (ddd, *J* = 2.3, 5.7, 9.6 Hz, 1H, H-5); <sup>13</sup>C NMR (125 MHz, CD<sub>3</sub>OD):  $\delta$  = 168.29 (CO), 155.54, 145.13, 134.74, 133.45, 131.36, 131.29, 130.32, 127.91, 127.85, 126.44, 117.80 (Ar-C), 100.27 (C-1), 76.13 (C-5), 72.24 (C-3), 71.74 (C-2), 68.09 (C-4), 62.67 ppm (C-6), 52.69 (OMe); HRMS: *m/z*: calcd for C<sub>21</sub>H<sub>21</sub>F<sub>3</sub>NaO<sub>8</sub> [*M*+Na]<sup>+</sup>: 481.1081, found: 481.1082.

**Methyl 4'-( $\alpha$ -D-mannopyranosyloxy)-3'-methoxybiphenyl-4-carboxylate (13d):** Prepared according to general procedure C from **12d** (32 mg, 0.055 mmol). Yield: 12 mg (52%). [ $\alpha$ ]<sub>D</sub><sup>20</sup> + 133.1 (*c* = 0.20, MeOH); <sup>1</sup>H NMR (500 MHz, CD<sub>3</sub>OD):  $\delta$  = 7.97–7.96 (m, 2H, Ar-H), 7.63–7.61 (m, 2H, Ar-H), 7.21–7.11 (m, 3H, Ar-H), 5.37 (d, *J* = 1.7 Hz, 1H, H-1), 4.00 (dd, *J* = 1.8, 3.4 Hz, 1H, H-2), 3.86 (dd, *J* = 3.5, 8.8 Hz, 1H, H-3), 3.82 (s, 6H, 2 CH<sub>3</sub>), 3.70–3.63 ppm (m, 4H, H-4, H-5, H-6); <sup>13</sup>C NMR (125 MHz, CD<sub>3</sub>OD):  $\delta$  = 168.50 (CO), 152.33, 147.40, 146.83, 136.56, 131.08, 129.76, 127.87, 120.86, 120.10, 112.54 (Ar-C), 101.51 (C-1), 75.66 (C-5), 72.40 (C-2), 72.00 (C-3), 68.34 (C-4), 62.70 (C-6), 56.61 (OMe), 52.63 ppm (OMe); HRMS: *m/z*: calcd for C<sub>21</sub>H<sub>24</sub>NaO<sub>9</sub> [*M*+Na]<sup>+</sup>: 443.1313, found: 443.1315.

**Methyl 3'-cyclopropyl-4'-( $\alpha$ -D-mannopyranosyloxy)biphenyl-4-carboxylate (13e):** Prepared according to general procedure C from **12e** (21 mg, 0.035 mmol). Yield: 10 mg (67%). [ $\alpha$ ]<sub>D</sub><sup>20</sup> + 101.6 (*c* = 0.24, MeOH); <sup>1</sup>H NMR (500 MHz, CD<sub>3</sub>OD):  $\delta$  = 8.07–8.05 (m, 2H, Ar-H), 7.68–7.67 (m, 2H, Ar-H), 7.46 (dd, *J* = 2.4, 8.5 Hz, 1H, Ar-H), 7.33 (d, *J* = 8.5 Hz, 1H, Ar-H), 7.21 (d, *J* = 2.4 Hz, 1H, Ar-H), 5.60 (d, *J* = 1.7 Hz, 1H, H-1), 4.13 (dd, *J* = 1.9, 3.3 Hz, 1H, H-2), 4.02 (dd, *J* = 3.4, 9.5 Hz, 1H, H-3), 3.93 (s, 3H, OMe), 3.81–3.74 (m, 3H, H-4, H-6), 3.69 (m, 1H, H-5), 2.19 (m, 1H, H-cPr), 1.01–0.99 (m, 2H, CH<sub>2</sub>-cPr), 0.76–0.74 ppm (m, 2H, CH<sub>2</sub>-cPr); <sup>13</sup>C NMR (125 MHz, CD<sub>3</sub>OD):  $\delta$  = 168.54 (CO), 156.92, 146.98, 135.00, 134.59, 131.07, 127.34, 127.67, 126.39, 125.34, 116.29 (12C, Ar-C), 100.14 (C-1), 75.61 (C-5), 72.64 (C-3), 72.14 (C-2), 68.33 (C-4), 62.71 (C-6), 52.60 (OCH<sub>3</sub>), 10.93,

8.06 ppm (3C, cPr); HRMS:  $m/z$ : calcd for  $C_{23}H_{26}NaO_8$   $[M+Na]^+$ : 453.1520, found: 453.1519.

**Methyl 3'-cyano-4'-( $\alpha$ -D-mannopyranosyloxy)biphenyl-4-carboxylate (13 f):** Prepared according to general procedure C from **12 f** (37 mg, 0.063 mmol). Yield: 19 mg (73%).  $[\alpha]_D^{20} + 101.1$  ( $c=0.30$ , MeOH);  $^1H$  NMR (500 MHz,  $CD_3OD$ ):  $\delta=8.00$ – $7.99$  (m, 2H, Ar-H), 7.90–7.85 (m, 2H, Ar-H), 7.65–7.63 (m, 2H, Ar-H), 7.50 (d,  $J=8.8$  Hz, 1H, Ar-H), 5.63 (s, 1H, H-1), 4.03 (m, 1H, H-2), 3.91 (dd,  $J=2.8$ , 9.4 Hz, 1H, H-3), 3.83 (s, 3H, OMe), 3.69–3.60 (m, 3H, H-4, H-6), 3.50 ppm (m, 1H, H-5);  $^{13}C$  NMR (125 MHz,  $CD_3OD$ ):  $\delta=168.22$  (CO), 159.29, 144.38, 135.61, 134.50, 133.08, 131.31, 130.56, 127.87, 117.36, 116.75, 104.35 (13C, Ar-C, CN), 100.62 (C-1), 76.39 (C-5), 72.27 (C-2), 71.62 (C-3), 68.07 (C-4), 62.64 (C-6), 52.71 ppm (OMe); HRMS:  $m/z$ : calcd for  $C_{21}H_{21}NNaO_8$   $[M+Na]^+$ : 438.1159, found: 438.1162.

**Sodium 3'-fluoro-4'-( $\alpha$ -D-mannopyranosyloxy)biphenyl-4-carboxylate (14 a):** Prepared according to general procedure D from **12 a** (50 mg, 0.087 mmol). Yield: 21 mg (58%).  $[\alpha]_D^{20} + 112.7$  ( $c=0.40$ , MeOH);  $^1H$  NMR (500 MHz,  $D_2O$ ):  $\delta=7.78$ – $7.77$  (m, 2H, Ar-H), 7.46–7.45 (m, 2H, Ar-H), 7.30–7.15 (m, 3H, Ar-H), 5.43 (s, 1H, H-1), 4.07 (s, 1H, H-2), 3.93 (d,  $J=3.3$  Hz, 1H, H-3), 3.68–3.62 ppm (m, 4H, H-4, H-5, H-6);  $^{13}C$  NMR (125 MHz,  $D_2O$ ):  $\delta=175.19$  (CO), 153.02 (d,  $J=242.6$  Hz, Ar-C), 142.52 (d,  $J=10.8$  Hz, Ar-C), 141.23 (Ar-C), 135.53 (d,  $J=6.4$  Hz, Ar-C), 135.07, 129.43, 126.25, 126.01, 122.96, 119.13 (Ar-C), 114.83 (d,  $J=19.4$  Hz, Ar-C), 99.32 (C-1), 73.65 (C-5), 70.23 (C-3), 69.67 (C-2), 66.35 (C-4), 60.52 ppm (C-6); HRMS:  $m/z$ : calcd for  $C_{19}H_{19}FNaO_8$   $[M+Na]^+$ : 417.0956, found: 417.0957.

**Sodium 4'-( $\alpha$ -D-mannopyranosyloxy)-3'-methylbiphenyl-4-carboxylate (14 b):** Prepared according to general procedure D from **12 b** (46 mg, 0.081 mmol). Yield: 5 mg (15%).  $[\alpha]_D^{20} + 85.7$  ( $c=0.20$ , MeOH);  $^1H$  NMR (500 MHz,  $D_2O$ ):  $\delta=7.78$ – $7.76$  (m, 2H, Ar-H), 7.53–7.52 (m, 2H, Ar-H), 7.43–7.37 (m, 2H, Ar-H), 7.10 (d,  $J=8.6$  Hz, 1H, Ar-H), 5.52 (d,  $J=1.6$  Hz, 1H, H-1), 4.07 (dd,  $J=1.9$ , 3.4 Hz, 1H, H-2), 3.95 (dd,  $J=3.5$ , 9.6 Hz, 1H, H-3), 3.63–3.50 (m, 4H, H-4, H-5, H-6), 2.14 ppm (s, 3H,  $CH_3$ );  $^{13}C$  NMR (125 MHz,  $D_2O$ ):  $\delta=153.33$ , 142.57, 134.59, 133.97, 129.47, 128.42, 126.25, 125.43, 114.99 (12C, Ar-C), 97.46 (C-1), 73.39 (C-5), 70.54 (C-3), 69.88 (C-2), 66.53 (C-4), 60.60 (C-6), 15.31 ppm ( $CH_3$ ); HRMS:  $m/z$ : calcd for  $C_{20}H_{22}NaO_8$   $[M+Na]^+$ : 413.1207, found: 413.1209.

**Sodium 3'-trifluoromethyl-4'-( $\alpha$ -D-mannopyranosyloxy)biphenyl-4-carboxylate (14 c):** Prepared according to general procedure D from **12 c** (45 mg, 0.072 mmol). Yield: 25 mg (74%).  $[\alpha]_D^{20} + 94.2$  ( $c=0.30$ , MeOH);  $^1H$  NMR (500 MHz,  $D_2O$ ):  $\delta=7.83$ – $7.81$  (m, 3H, Ar-H), 7.75 (d,  $J=8.7$  Hz, 1H, Ar-H), 7.57–7.55 (m, 2H, Ar-H), 7.31 (d,  $J=8.8$  Hz, 1H, Ar-H), 5.64 (s, 1H, H-1), 4.09 (d,  $J=1.5$  Hz, 1H, H-2), 3.94 (dd,  $J=3.4$ , 9.7 Hz, 1H, H-3), 3.67–3.60 (m, 3H, H-4, H-6), 3.54 ppm (m, 1H, H-5);  $^{13}C$  NMR (125 MHz,  $D_2O$ ):  $\delta=175.25$  (CO), 152.40, 141.31, 135.09, 133.53, 131.93, 129.46, 126.34, 125.59, 115.86 (12C, Ar-C), 97.20 (C-1), 73.68 (C-5), 70.19 (C-3), 69.58 (C-2), 66.36 (C-4), 60.55 ppm (C-6); HRMS:  $m/z$ : calcd for  $C_{20}H_{19}F_3NaO_8$   $[M+Na]^+$ : 467.0924, found: 467.0923.

**Sodium 4'-( $\alpha$ -D-mannopyranosyloxy)-3'-methoxybiphenyl-4-carboxylate (14 d):** Prepared according to general procedure D from **12 d** (47 mg, 0.080 mmol). Yield: 10 mg (29%).  $[\alpha]_D^{20} + 115.1$  ( $c=0.30$ , MeOH);  $^1H$  NMR (500 MHz,  $D_2O$ ):  $\delta=7.81$ – $7.79$  (m, 2H, Ar-H), 7.54–7.53 (m, 2H, Ar-H), 7.19–7.11 (m, 3H, Ar-H), 5.43 (d,  $J=1.6$  Hz, 1H, H-1), 4.10 (dd,  $J=1.8$ , 3.5 Hz, 1H, H-2), 3.96 (dd,  $J=3.5$ , 9.0 Hz, 1H, H-3), 3.78 (s, 3H, OCH<sub>3</sub>), 3.70–3.62 ppm (m, 4H, H-4, H-5, H-6);  $^{13}C$  NMR (125 MHz,  $D_2O$ ):  $\delta=175.24$  (CO), 149.53, 144.24, 142.42, 135.59, 134.75, 129.40, 126.41, 119.86, 118.03, 111.44 (12C, Ar-C), 99.23 (C-1), 73.53 (C-5), 70.32 (C-3), 69.78 (C-2), 66.40 (C-4), 60.54

(C-6), 55.81 ppm (OCH<sub>3</sub>); HRMS:  $m/z$ : calcd for  $C_{20}H_{22}NaO_9$   $[M+Na]^+$ : 429.1156, found: 429.1154.

**Sodium 3'-cyclopropyl-4'-( $\alpha$ -D-mannopyranosyloxy)biphenyl-4-carboxylate (14 e):** Prepared according to general procedure D from **12 e** (28 mg, 0.047 mmol). Yield: 6 mg (26%).  $[\alpha]_D^{20} + 149.8$  ( $c=0.20$ , MeOH);  $^1H$  NMR (500 MHz,  $D_2O$ ):  $\delta=7.79$ – $7.77$  (m, 2H, Ar-H), 7.48–7.46 (m, 2H, Ar-H), 7.30 (d,  $J=7.8$  Hz, 1H, Ar-H), 7.07–7.05 (m, 2H, Ar-H), 5.52 (s, 1H, H-1), 4.10 (m, 1H, H-2), 3.98 (dd,  $J=3.4$ , 9.5 Hz, 1H, H-3), 3.69–3.62 (m, 4H, H-4, H-5, H-6), 1.99 (m, 1H, H-cPr), 0.86–0.84 (m, 2H, CH<sub>2</sub>-cPr), 0.58–0.56 ppm (m, 2H, CH<sub>2</sub>-cPr);  $^{13}C$  NMR (125 MHz,  $D_2O$ ):  $\delta=175.34$  (CO), 153.82, 142.58, 134.57, 134.34, 133.74, 129.38, 126.26, 125.01, 124.01, 115.47 (12C, Ar-C), 97.88 (C-1), 73.47 (C-5), 70.55 (C-3), 69.93 (C-2), 66.46 (C-4), 60.57 (C-6), 9.16, 7.26, 7.06 ppm (cPr); HRMS:  $m/z$ : calcd for  $C_{22}H_{24}ONaO_8$   $[M+Na]^+$ : 439.1363, found: 439.1363.

**Sodium 3'-cyano-4'-( $\alpha$ -D-mannopyranosyloxy)biphenyl-4-carboxylate (14 f):** A two-neck flask was charged with **10 f** (150 mg, 0.28 mmol), 4-carboxybenzene boronic acid pinacol ester (**15**) (77 mg, 0.31 mmol), Pd(dppf)Cl<sub>2</sub>·CH<sub>2</sub>Cl<sub>2</sub> (7 mg, 0.008 mmol), K<sub>3</sub>PO<sub>4</sub> (89 mg, 0.42 mmol) and a stirring bar. The flask was evacuated and flushed with argon, then anhydrous DMF (2 mL) was added under a stream of argon. The mixture was degassed in an ultrasonic bath and flushed with argon for 5 min, and then stirred at 80 °C overnight. The reaction mixture was cooled to RT, diluted with EtOAc (50 mL), and washed with H<sub>2</sub>O (50 mL) and brine (50 mL). The organic layer was dried over Na<sub>2</sub>SO<sub>4</sub> and concentrated in vacuo. The residue was purified by MPLC on silica gel (CH<sub>2</sub>Cl<sub>2</sub>/MeOH, 10:1–8:1) to afford the biphenyl intermediate (162 mg). The intermediate was dissolved in dry MeOH (4 mL) and treated with freshly prepared 1 M NaOMe/MeOH (28  $\mu$ L) for 4 h at RT. The reaction mixture was neutralized with Amberlyst-15 (H<sup>+</sup>), filtered and concentrated. The crude product was transformed into the sodium salt by passing through a small column of Dowex 50X8 (Na<sup>+</sup> form) ion-exchange resin. After concentration the residue was purified by MPLC (RP-18, H<sub>2</sub>O) followed by size-exclusion chromatography (P-2 gel, H<sub>2</sub>O) to give **14 f** (19 mg, 17%) as a white solid after final lyophilization from H<sub>2</sub>O.  $[\alpha]_D^{20} + 75.3$  ( $c=0.20$ , MeOH);  $^1H$  NMR (500 MHz,  $D_2O$ ):  $\delta=7.86$ – $7.79$  (m, 4H, Ar-H), 7.53–7.52 (m, 2H, Ar-H), 7.31 (d,  $J=8.9$  Hz, 1H, Ar-H), 5.64 (d,  $J=1.9$  Hz, 1H, H-1), 4.11 (dd,  $J=1.9$ , 3.4 Hz, 1H, H-2), 4.00 (dd,  $J=3.5$ , 9.7 Hz, 1H, H-3), 3.73–3.65 (m, 3H, H-4, H-6), 3.58 ppm (ddd,  $J=2.4$ , 5.5, 9.9 Hz, 1H, H-5);  $^{13}C$  NMR (125 MHz,  $D_2O$ ):  $\delta=175.12$  (CO), 156.82, 140.37, 134.39, 133.56, 131.83, 129.58, 126.25, 116.82, 115.78, 102.08 (13C, Ar-C, CN), 98.09 (C-1), 73.97 (C-5), 70.29 (C-3), 69.54 (C-2), 66.36 (C-4), 60.56 ppm (C-6); HRMS:  $m/z$ : calcd for  $C_{21}H_{21}NNaO_8$   $[M+Na]^+$ : 424.1003, found: 424.1003.

### 3-Bromobenzyl 2,3,4,6-tetra-O-acetyl- $\alpha$ -D-mannopyranoside

**(17 a):** Prepared according to general procedure A from **8**<sup>[12]</sup> and 3-bromobenzyl alcohol (**16 a**). Yield: 100 mg (34%) as colorless oil.  $R_f=0.43$  (PE/EtOAc, 2:1);  $[\alpha]_D^{20} + 42.0$  ( $c=1.40$ , EtOAc);  $^1H$  NMR (500 MHz,  $CDCl_3$ ):  $\delta=7.48$ – $7.46$ , 7.30–7.24 (m, 4H, Ar-H), 5.37 (dd, 1H,  $J=3.4$ , 10.1 Hz, H-3), 5.33–5.29 (m, 2H, H-2, H-4), 4.88 (d, 1H,  $J=1.3$  Hz, H-1), 4.68, 4.54 (A, B of AB,  $J=12.1$  Hz, 2H, CH<sub>2</sub>Ar), 4.29 (dd, 1H,  $J=5.2$ , 12.3 Hz, H-6a), 4.07 (dd, 1H,  $J=2.3$ , 12.3 Hz, H-6b), 3.99 (ddd, 1H,  $J=2.4$ , 5.2, 9.9 Hz, H-5), 2.15, 2.13, 2.05, 2.00 ppm (4 s, 12H, 4 OAc);  $^{13}C$  NMR (125 MHz,  $CDCl_3$ ):  $\delta=170.59$ , 169.98, 169.87, 169.69 (4 CO), 138.49, 131.34, 131.09, 130.24, 126.66, 122.57 (Ar-C), 96.83 (C-1), 69.43, 69.02, 68.90, 68.78 (C-2, C-3, C-5, CH<sub>2</sub>Ar), 66.03 (C-4), 62.36 (C-6), 20.86, 20.76, 20.68 ppm (4C, COCH<sub>3</sub>); ESI-MS:  $m/z$ : calcd for  $C_{21}H_{25}BrNaO_{10}$   $[M+Na]^+$ : 539.05, found: 539.14.

**5-Bromo-2-chlorobenzyl 2,3,4,6-tetra-O-acetyl- $\alpha$ -D-mannopyranoside (17b):** Prepared according to general procedure A from **8**<sup>[12]</sup> and 5-bromo-2-chlorobenzyl alcohol (**16b**). Yield: 152 mg (48%) as a white solid.  $R_f$ =0.56 (PE/EtOAc, 2:1);  $[\alpha]_D^{20} + 48.0$  ( $c=1.50$ , EtOAc); <sup>1</sup>H NMR (500 MHz, CDCl<sub>3</sub>):  $\delta$ =7.48 (t,  $J=1.8$  Hz, 1H, Ar-H), 7.38 (s, 1H, Ar-H), 7.35 (d,  $J=1.8$  Hz, 1H, Ar), 5.33 (m, 3H, H-2, H-3, H-4), 4.88 (d,  $J=1.5$  Hz, 1H, H-1), 4.65, 4.51 (A, B of AB,  $J=12.3$  Hz, 2H, CH<sub>2</sub>Ar), 4.30 (dd,  $J=5.3$ , 12.3 Hz, 1H, H-6a), 4.09 (dd,  $J=2.4$ , 12.3 Hz, 1H, H-6b), 3.98 (ddd,  $J=2.4$ , 5.2, 9.7 Hz, 1H, H-5), 2.16, 2.13, 2.05, 2.01 ppm (4 s, 12H, 4 OAc); <sup>13</sup>C NMR (125 MHz, CDCl<sub>3</sub>):  $\delta$ =170.58, 169.98, 169.89, 169.69 (4 CO), 139.77, 135.35, 129.25, 126.85, 122.91 (6C, Ar-C), 96.96 (C-1), 69.33, 68.93, 68.24 (4C, C-2, C-3, C-5, CH<sub>2</sub>Ar), 65.98 (C-4), 62.38 (C-6), 20.86, 20.77, 20.68 ppm (4C, 4COCH<sub>3</sub>); ESI-MS:  $m/z$ : calcd for C<sub>21</sub>H<sub>24</sub>BrClNaO<sub>10</sub> [M+Na]<sup>+</sup>: 573.01, found: 573.06.

**2-Bromobenzyl 2,3,4,6-tetra-O-acetyl- $\alpha$ -D-mannopyranoside (17c):** Prepared according to general procedure A from **8**<sup>[12]</sup> and 2-bromobenzyl alcohol (**16c**). Yield: 140 mg (47%) as a white solid.  $R_f$ =0.55 (petrol ether/EtOAc, 2:1);  $[\alpha]_D^{20} + 44.6$  ( $c=2.10$ , EtOAc); <sup>1</sup>H NMR (500 MHz, CDCl<sub>3</sub>):  $\delta$ =7.57 (dd,  $J=1.0$ , 8.0 Hz, 1H, Ar-H), 7.47 (dd,  $J=1.4$ , 7.6 Hz, 1H, Ar-H), 7.35 (td,  $J=1.1$ , 7.5 Hz, 1H, Ar-H), 7.20 (td,  $J=1.7$ , 7.9 Hz, 1H, Ar-H), 5.41 (dd,  $J=3.5$ , 10.0 Hz, 1H, H-3), 5.35 (dd,  $J=1.8$ , 3.5 Hz, 1H, H-2), 5.31 (t,  $J=9.9$  Hz, 1H, H-4), 4.98 (d,  $J=1.6$  Hz, 1H, H-1), 4.83, 4.61 (A, B of AB,  $J=12.7$  Hz, 2H, CH<sub>2</sub>Ar), 4.29 (dd,  $J=5.8$ , 12.6 Hz, 1H, H-6a), 4.10–4.06 (m, 2H, H-6b, H-5), 2.17, 2.12, 2.04, 2.00 ppm (4 s, 12H, 4 OAc); <sup>13</sup>C NMR (125 MHz, CDCl<sub>3</sub>):  $\delta$ =170.64, 170.02, 169.88, 169.72 (4 CO), 135.77, 132.69, 129.58, 129.49, 127.64, 122.96 (Ar-C), 97.33 (C-1), 69.48, 69.30, 69.10, 68.84 (C-2, C-3, C-5, CH<sub>2</sub>Ar), 66.05 (C-4), 62.35 (C-6), 20.88, 20.76, 20.69 ppm (4C, 4COCH<sub>3</sub>); ESI-MS:  $m/z$ : calcd for C<sub>21</sub>H<sub>25</sub>BrNaO<sub>10</sub> [M+Na]<sup>+</sup>: 539.05, found: 539.14.

**Methyl 3'-[(2,3,4,6-tetra-O-acetyl- $\alpha$ -D-mannopyranosyloxy)methyl]biphenyl-4-carboxylate (18a):** Prepared according to general procedure B from **17a** (87.0 mg, 0.167 mmol), **11** (33.1 mg, 0.184 mmol), Pd(dppf)Cl<sub>2</sub>·CH<sub>2</sub>Cl<sub>2</sub> (4.1 mg, 5.0  $\mu$ mol) and K<sub>3</sub>PO<sub>4</sub> (53.2 mg, 0.251 mmol). Yield: 70 mg (73%) as colorless oil.  $R_f$ =0.30 (PE/EtOAc, 2:1);  $[\alpha]_D^{20} + 41.2$  ( $c=1.00$ , EtOAc); <sup>1</sup>H NMR (500 MHz, CDCl<sub>3</sub>):  $\delta$ =8.13–8.11 (m, 2H, Ar-H), 7.68–7.67 (m, 2H, Ar-H), 7.60–7.58 (m, 2H, Ar-H), 7.48 (t,  $J=4.7$  Hz, 1H, Ar-H), 7.39 (d,  $J=7.7$  Hz, 1H, Ar-H), 5.41 (dd,  $J=3.4$ , 10.0 Hz, 1H, H-3), 5.33–5.30 (m, 2H, H-2, H-4), 4.94 (d,  $J=1.5$  Hz, 1H, H-1), 4.79, 4.64 (A, B of AB,  $J=12.0$  Hz, 2H, CH<sub>2</sub>Ar), 4.30 (dd,  $J=5.0$ , 12.1 Hz, 1H, H-6a), 4.09–4.03 (m, 2H, H-6b, H-5), 3.94 (s, 3H, OMe), 2.15, 2.11, 2.04, 2.00 ppm (4 s, 12H, 4 OAc); <sup>13</sup>C NMR (125 MHz, CDCl<sub>3</sub>):  $\delta$ =170.64, 170.03, 169.91, 169.73, 166.94 (5 CO), 145.11, 140.41, 136.97, 130.15, 129.27, 129.09, 127.94, 127.22, 127.11 (12C, Ar-C), 96.76 (C-1), 69.57, 69.09, 68.94, 66.12 (C-2, C-3, C-5, CH<sub>2</sub>Ar), 62.40 (C-4), 60.38 (C-6), 52.15 (OMe), 20.89, 20.77, 20.69 ppm (4C, 4COCH<sub>3</sub>); ESI-MS:  $m/z$ : calcd for C<sub>29</sub>H<sub>32</sub>NaO<sub>12</sub> [M+Na]<sup>+</sup>: 595.18, found: 595.21.

**Methyl 3'-[(2,3,4,6-tetra-O-acetyl- $\alpha$ -D-mannopyranosyloxy)methyl]-4'-chlorobiphenyl-4-carboxylate (18b):** Prepared according to general procedure B from **17b** (143 mg, 0.260 mmol), **11** (51.5 mg, 0.286 mmol), Pd(dppf)Cl<sub>2</sub>·CH<sub>2</sub>Cl<sub>2</sub> (6.4 mg, 7.8  $\mu$ mol) and K<sub>3</sub>PO<sub>4</sub> (82.8 mg, 0.390 mmol). Yield: 133 mg (84%) as colorless oil.  $R_f$ =0.30 (PE/EtOAc, 2:1);  $[\alpha]_D^{20} + 45.9$  ( $c=1.20$ , EtOAc); <sup>1</sup>H NMR (500 MHz, CDCl<sub>3</sub>):  $\delta$ =8.13–8.11 (m, 2H, Ar-H), 7.65–7.64 (m, 2H, Ar-H), 7.57 (t,  $J=1.8$  Hz, 1H, Ar-H), 7.47 (s, 1H, Ar-H), 7.37 (s, 1H, Ar-H), 5.40 (dd,  $J=3.4$ , 10.1 Hz, 1H, H-3), 5.33–5.29 (m, 2H, H-2, H-4), 4.93 (d,  $J=1.4$  Hz, 1H, H-1), 4.76, 4.61 (A, B of AB,  $J=12.1$  Hz, 2H, CH<sub>2</sub>Ar), 4.31 (dd,  $J=5.2$ , 12.3 Hz, 1H, H-6a), 4.11 (dd,  $J=2.3$ , 12.3 Hz, 1H, H-6b), 4.03 (ddd,  $J=2.4$ , 5.2, 9.9 Hz, 1H, H-5), 3.95 (s, 3H, OMe), 2.16, 2.12, 2.05, 2.00 ppm (4 s, 12H, 4OAc); <sup>13</sup>C NMR

(125 MHz, CDCl<sub>3</sub>):  $\delta$ =170.61, 170.02, 169.90, 169.72, 166.75 (5 CO), 143.68, 142.16, 138.79, 135.11, 130.26, 129.68, 127.14, 125.14 (12C, Ar-C), 96.85 (C-1), 68.99, 68.89, 68.85, 66.07 (C-2, C-3, C-5, CH<sub>2</sub>Ar), 62.42 (C-4), 60.39 (C-6), 52.23 (OMe), 20.89, 20.78, 20.71, 20.69 ppm (4COCH<sub>3</sub>); ESI-MS:  $m/z$ : calcd for C<sub>29</sub>H<sub>31</sub>ClNaO<sub>12</sub> [M+Na]<sup>+</sup>: 629.14, found: 629.10.

**Methyl 2'-[(2,3,4,6-tetra-O-acetyl- $\alpha$ -D-mannopyranosyloxy)methyl]biphenyl-4-carboxylate (21):** Prepared according to general procedure B from **17c** (115 mg, 0.223 mmol), **11** (44.1 mg, 0.245 mmol), Pd(dppf)Cl<sub>2</sub>·CH<sub>2</sub>Cl<sub>2</sub> (5.5 mg, 6.7  $\mu$ mol) and K<sub>3</sub>PO<sub>4</sub> (71.0 mg, 0.335 mmol). Yield: 120 mg (94%) as colorless oil.  $R_f$ =0.41 (PE/EtOAc, 2:1);  $[\alpha]_D^{20} + 38.3$  ( $c=2.00$ , EtOAc); <sup>1</sup>H NMR (500 MHz, CDCl<sub>3</sub>):  $\delta$ =8.11–8.10 (m, 2H, Ar-H), 7.51–7.48 (m, 1H, Ar-H), 7.45–7.41 (m, 4H, Ar-H), 7.29 (m, 1H, Ar-H), 5.27–5.21 (m, 2H, H-3, H-4), 5.19 (dd,  $J=1.9$ , 3.3 Hz, 1H, H-2), 4.77 (d,  $J=1.4$  Hz, 1H, H-1), 4.67, 4.34 (A, B of AB,  $J=11.3$  Hz, 2H, CH<sub>2</sub>Ar), 4.13 (dd,  $J=5.2$ , 12.5 Hz, 1H, H-6a), 3.94 (s, 3H, OMe), 3.90 (dd,  $J=2.2$ , 12.3 Hz, 1H, H-6a), 3.52 (ddd,  $J=2.2$ , 5.1, 9.3 Hz, 1H, H-5), 2.13, 2.05, 2.04, 1.99 ppm (4 s, 12H, 4 OAc); <sup>13</sup>C NMR (125 MHz, CDCl<sub>3</sub>):  $\delta$ =170.52, 169.95, 169.82, 169.74, 166.77 (5 CO), 145.48, 141.44, 133.46, 129.99, 129.91, 129.58, 129.22, 128.52, 128.21 (12C, Ar-C), 97.20 (C-1), 69.47 (C-2), 68.98 (C-3), 68.48 (C-5), 68.13 (CH<sub>2</sub>Ar), 65.88 (C-4), 62.15 (C-6), 52.18 (OMe), 20.85, 20.66, 20.62 ppm (4C, 4COCH<sub>3</sub>); ESI-MS:  $m/z$ : calcd for C<sub>29</sub>H<sub>32</sub>NaO<sub>12</sub> [M+Na]<sup>+</sup>: 595.18, found: 595.21.

**Methyl 3'-[( $\alpha$ -D-mannopyranosyloxy)methyl]biphenyl-4-carboxylate (19a):** Prepared according to general procedure C from **18a** (24 mg, 0.042 mmol). Yield: 11 mg (65%).  $R_f$ =0.40 (CH<sub>2</sub>Cl<sub>2</sub>/MeOH, 8:1);  $[\alpha]_D^{20} + 68.0$  ( $c=0.34$ , MeOH); <sup>1</sup>H NMR (500 MHz, CD<sub>3</sub>OD):  $\delta$ =8.11–8.09 (m, 2H, Ar-H), 7.77–7.75 (m, 2H, Ar-H), 7.70 (s, 1H, Ar-H), 7.63 (d,  $J=7.6$  Hz, 1H, Ar-H), 7.49 (t,  $J=7.6$  Hz, 1H, Ar-H), 7.45 (d,  $J=7.6$  Hz, 1H, Ar-H), 4.90 (d,  $J=1.8$  Hz, 1H, H-1), 4.86, 4.63 (A, B of AB,  $J=12.0$  Hz, 2H, CH<sub>2</sub>Ar), 3.94 (s, 3H, OMe), 3.89–3.87 (m, 2H, H-2, H-3), 3.79–3.73 (m, 2H, H-4, H-6a), 3.68–3.64 ppm (m, 2H, H-5, H-6b); <sup>13</sup>C NMR (125 MHz, CD<sub>3</sub>OD):  $\delta$ =168.42 (CO), 146.91, 141.31, 139.97, 131.13, 130.20, 129.07, 128.17, 127.91, 127.67 (12C, Ar-C), 100.76 (C-1), 75.02 (C-5), 72.65 (C-3), 72.22 (C-2), 69.73 (CH<sub>2</sub>Ar), 68.65 (C-4), 62.98 (C-6), 52.66 ppm (OMe); HRMS:  $m/z$ : calcd for C<sub>21</sub>H<sub>24</sub>NaO<sub>8</sub> [M+Na]<sup>+</sup>: 427.1363, found: 427.1361.

**Methyl 4'-chloro-3'-[( $\alpha$ -D-mannopyranosyloxy)methyl]biphenyl-4-carboxylate (19b):** Prepared according to general procedure C from **18b** (40 mg, 0.066 mmol). Yield: 26 mg (90%).  $R_f$ =0.19 (CH<sub>2</sub>Cl<sub>2</sub>/MeOH, 8:1);  $[\alpha]_D^{20} + 101.8$  ( $c=0.50$ , MeOH); <sup>1</sup>H NMR (500 MHz, CD<sub>3</sub>OD):  $\delta$ =8.06 (d,  $J=8.4$  Hz, 2H, Ar-H), 7.69 (d,  $J=8.4$  Hz, 2H, Ar-H), 7.57–7.56 (m, 2H, Ar-H), 7.41 (s, 1H, Ar-H), 4.87 (s, 1H, H-1), 4.80, 4.58 (A, B of AB,  $J=12.3$  Hz, 2H, CH<sub>2</sub>Ar), 3.91 (s, 3H, OMe), 3.87–3.83 (m, 2H, H-2, H-3), 3.74–3.57 ppm (m, 4H, H-4, H-5, H-6); <sup>13</sup>C NMR (125 MHz, CD<sub>3</sub>OD):  $\delta$ =168.74 (CO), 145.78, 143.68, 142.71, 136.55, 131.75, 131.31, 129.02, 128.77, 127.95, 126.63 (12C, Ar-C), 101.47 (C-1), 75.65 (C-5), 73.16 (C-3), 72.65 (C-2), 69.49 (CH<sub>2</sub>Ar), 69.13 (C-4), 63.49 (C-6), 53.26 ppm (OMe); HRMS:  $m/z$ : calcd for C<sub>21</sub>H<sub>23</sub>ClNaO<sub>8</sub> [M+Na]<sup>+</sup>: 461.0974, found: 461.0975.

**Methyl 2'-[( $\alpha$ -D-mannopyranosyloxy)methyl]biphenyl-4-carboxylate (22):** Prepared according to general procedure C from **21** (48 mg, 0.084 mmol). Yield: 16 mg (47%).  $R_f$ =0.42 (CH<sub>2</sub>Cl<sub>2</sub>/MeOH, 8:1);  $[\alpha]_D^{20} + 61.9$  ( $c=0.90$ , MeOH); <sup>1</sup>H NMR (500 MHz, CD<sub>3</sub>OD):  $\delta$ =8.11–8.09 (m, 2H, Ar-H), 7.57 (m, 1H, Ar-H), 7.51–7.49 (m, 2H, Ar-H), 7.43–7.40 (m, 2H, Ar-H), 7.31 (m, 1H, Ar-H), 4.71 (A of AB,  $J=11.4$  Hz, 1H, CH<sub>2</sub>Ar), 4.70 (d,  $J=1.5$  Hz, 1H, H-1), 4.38 (B of AB,  $J=11.4$  Hz, 1H, CH<sub>2</sub>Ar), 3.75–3.60 (m, 5H, H-2, H-3, H-4, H-6), 3.95 (s, 3H, OMe), 3.40 ppm (ddd,  $J=3.0$ , 5.6, 6.8 Hz, 1H, H-5); <sup>13</sup>C NMR

(125 MHz, CD<sub>3</sub>OD):  $\delta$  = 168.42 (CO), 147.33, 142.66, 136.03, 130.83, 130.53, 130.47, 129.26, 129.15 (12C, Ar-C), 101.14 (C-1), 74.78 (C-5), 72.60 (C-3), 72.18 (C-2), 68.37 (2C, C-4, CH<sub>2</sub>Ar), 62.71 ppm (C-6), 52.69 (OMe); HRMS:  $m/z$ : calcd for C<sub>21</sub>H<sub>24</sub>NaO<sub>8</sub>Na [M + Na]<sup>+</sup>: 427.1363, found: 427.1367.

**Sodium 3'-[( $\alpha$ -D-mannopyranosyloxy)methyl]biphenyl-4-carboxylate (6):** Prepared according to general procedure D from **18a** (35 mg, 0.061 mmol). Yield: 24 mg (96%). [ $\alpha$ ]<sub>D</sub><sup>20</sup> + 64.5 ( $c$  = 0.30, MeOH/H<sub>2</sub>O 1:1); <sup>1</sup>H NMR (500 MHz, D<sub>2</sub>O):  $\delta$  = 7.80–7.78 (m, 2H, Ar-H), 7.50–7.43 (m, 4H, Ar-H), 7.31–7.24 (m, 2H, Ar-H), 4.82 (s, 1H, H-1), 4.58, 4.40 (A, B of AB,  $J$  = 11.5 Hz, 2H, CH<sub>2</sub>Ar), 3.82 (m, 1H, H-2), 3.75–3.50 ppm (m, 5H, H-3, H-4, H-5, H-6); <sup>13</sup>C NMR (125 MHz, D<sub>2</sub>O):  $\delta$  = 175.14 (CO), 142.69, 140.05, 137.34, 135.01, 129.46, 129.28, 127.92, 126.87, 126.64 (12C, Ar-C), 99.40 (C-1), 72.84 (C-5), 70.51 (C-3), 70.01 (C-2), 69.29 (CH<sub>2</sub>Ar), 66.61 (C-4), 60.71 ppm (C-6); HRMS:  $m/z$ : calcd for C<sub>20</sub>H<sub>22</sub>NaO<sub>8</sub> [M + Na]<sup>+</sup>: 413.1207, found: 413.1211.

**Sodium 4'-chloro-3'-[( $\alpha$ -D-mannopyranosyloxy)methyl]biphenyl-4-carboxylate (20):** Prepared according to general procedure D from **18b** (54 mg, 0.089 mmol). Yield: 4 mg (10%). [ $\alpha$ ]<sub>D</sub><sup>20</sup> + 44.7 ( $c$  = 0.30, MeOH); <sup>1</sup>H NMR (500 MHz, D<sub>2</sub>O):  $\delta$  = 7.86 (d,  $J$  = 7.8 Hz, 2H, Ar-H), 7.58–7.56 (m, 3H, Ar-H), 7.46, 7.34 (2 s, 2H, Ar-H), 4.90 (s, 1H, H-1), 4.58, 4.50 (A, B of AB,  $J$  = 12.3 Hz, 2H, CH<sub>2</sub>Ar), 3.91 (s, 1H, H-2), 3.78–3.75 (m, 2H, H-3, H-4), 3.71–3.59 ppm (m, 3H, H-5, H-6); <sup>13</sup>C NMR (125 MHz, D<sub>2</sub>O):  $\delta$  = 174.76 (CO), 141.82, 141.55, 139.40, 134.37, 129.56, 127.34, 126.74, 126.62, 125.15 (12C, Ar-C), 99.99 (C-1), 72.96 (C-5), 70.55 (C-3), 70.04 (C-2), 68.72 (CH<sub>2</sub>Ar), 66.66 (C-4), 60.77 ppm (C-6); HRMS:  $m/z$ : calcd for C<sub>20</sub>H<sub>21</sub>ClNaO<sub>8</sub> [M + Na]<sup>+</sup>: 447.0817, found: 447.0816.

**Sodium 2'-[( $\alpha$ -D-mannopyranosyloxy)methyl]biphenyl-4-carboxylate (23):** Prepared according to general procedure D from **21** (78 mg, 0.137 mmol). Yield: 26 mg (46%). [ $\alpha$ ]<sub>D</sub><sup>20</sup> + 53.2 ( $c$  = 0.40, MeOH); <sup>1</sup>H NMR (500 MHz, D<sub>2</sub>O):  $\delta$  = 7.91–7.89 (m, 2H, Ar-H), 7.43–7.34 (m, 5H, Ar-H), 7.26 (m, 1H, Ar-H), 4.68 (s, 1H, H-1), 4.57, 4.31 (A, B of AB,  $J$  = 10.8 Hz, 2H, CH<sub>2</sub>Ar), 3.57 (m, 1H, H-2), 3.46–3.39 (m, 4H, H-3, H-4, H-6), 2.83 ppm (m, 1H, H-5); <sup>13</sup>C NMR (125 MHz, D<sub>2</sub>O):  $\delta$  = 173.20 (CO), 144.48, 141.80, 133.47, 132.43, 130.69, 129.95, 129.27, 128.96, 128.32 (12C, Ar-C), 99.90 (C-1), 72.44 (C-5), 70.33 (C-3), 69.82 (C-2), 68.14 (CH<sub>2</sub>Ar), 65.99 (C-4), 60.25 ppm (C-6); HRMS:  $m/z$ : calcd for C<sub>20</sub>H<sub>22</sub>NaO<sub>8</sub> [M + Na]<sup>+</sup>: 413.1207, found: 413.1208.

**4-(4,4,5,5-Tetramethyl)-1,3,2-dioxaborolan-2-yl)phenyl 2,3,4,6-tetra-O-acetyl- $\alpha$ -D-mannopyranoside (27):** A microwave tube was charged with **26**<sup>[37]</sup> (240 mg, 0.55 mmol), KOAc (161 mg, 1.65 mmol), bis(pinacolato)diboron (152 mg, 0.60 mmol) and Pd(dppf)Cl<sub>2</sub>·CH<sub>2</sub>Cl<sub>2</sub> (13 mg, 0.017 mmol). The tube was closed, evacuated and flushed with argon. Then anhydrous DMF (1 mL) was added under a stream of argon. The mixture was degassed in an ultrasonic bath and flushed with argon for 5 min, and then heated by microwave irradiation at 120 °C for 2 h. The reaction mixture was cooled to RT and diluted with CH<sub>2</sub>Cl<sub>2</sub>/H<sub>2</sub>O (100 mL, 1:1). The organic layer was washed with H<sub>2</sub>O (50 mL) and brine (50 mL), dried over Na<sub>2</sub>SO<sub>4</sub> and concentrated. The residue was purified by MPLC (toluene/EtOAc, 4:1) to afford **27** (120 mg, 50%) as colorless oil. [ $\alpha$ ]<sub>D</sub><sup>20</sup> + 58.1 ( $c$  = 0.60, EtOAc); <sup>1</sup>H NMR (500 MHz, CDCl<sub>3</sub>):  $\delta$  = 7.76 (d,  $J$  = 8.6 Hz, 2H, Ar-H), 7.08 (d,  $J$  = 8.6 Hz, 2H, Ar-H), 5.58–5.55 (m, 2H, H-1, H-3), 5.45 (dd,  $J$  = 1.9, 3.4 Hz, 1H, H-2), 5.37 (t,  $J$  = 10.0 Hz, 1H, H-4), 4.28 (dd,  $J$  = 5.0, 12.0 Hz, 1H, H-6a), 4.05–4.02 (m, 2H, H-6b, H-5), 2.20, 2.05, 2.03 (3 s, 12H, 4 OAc), 1.33 ppm (s, 12H, 4 CH<sub>3</sub>); <sup>13</sup>C NMR (125 MHz, CDCl<sub>3</sub>):  $\delta$  = 170.55, 169.91, 169.74 (4C, 4 CO), 157.98, 136.62, 136.58, 115.67 (5C, Ar-C), 95.44 (C-1), 83.77 (Ar-C), 69.37 (C-2), 69.21 (C-5), 68.87 (C-3), 65.92 (C-4), 62.06 (C-6),

24.86, 24.58 (4C, 4 CH<sub>3</sub>), 20.87, 20.69 ppm (4C, 4 COCH<sub>3</sub>); ESI-MS:  $m/z$ : calcd for C<sub>26</sub>H<sub>35</sub>BNaO<sub>12</sub> [M + Na]<sup>+</sup>: 573.21, found: 573.32.

**Methyl 2-[4'-(2,3,4,6-tetra-O-acetyl- $\alpha$ -D-mannopyranosyloxy)biphenyl-4-yl]acetate (29):** Prepared according to general procedure B from methyl 2-(4-bromophenyl)acetate (**28**, 41.2 mg, 0.180 mmol), **27** (109 mg, 0.198 mmol), Pd(dppf)Cl<sub>2</sub>·CH<sub>2</sub>Cl<sub>2</sub> (4.4 mg, 5.4  $\mu$ mol) and K<sub>3</sub>PO<sub>4</sub> (57.3 mg, 0.270 mmol). Yield: 35 mg (34%) as yellow oil.  $R_f$  = 0.25 (petrol ether/EtOAc 2:1); [ $\alpha$ ]<sub>D</sub><sup>20</sup> + 75.09 ( $c$  = 0.8, EtOAc); <sup>1</sup>H NMR (500 MHz, CDCl<sub>3</sub>):  $\delta$  = 7.52–7.49 (m, 4H, Ar-H), 7.35–7.33 (m, 2H, Ar-H), 7.17–7.14 (m, 2H, Ar-H), 5.60–5.56 (m, 2H, H-1, H-3), 5.47 (dd,  $J$  = 1.8, 3.5 Hz, 1H, H-2), 5.38 (t,  $J$  = 10.0 Hz, 1H, H-4), 4.29 (dd,  $J$  = 5.0, 11.9 Hz, 1H, H-6a), 4.15–4.08 (m, 2H, H-6b, H-5), 3.71 (s, 3H, OMe), 3.66 (s, 2H, ArCH<sub>2</sub>), 2.21, 2.06, 2.05, 2.03 ppm (4 s, 12H, 4 OAc); <sup>13</sup>C NMR (125 MHz, CDCl<sub>3</sub>):  $\delta$  = 171.99, 170.53, 169.99, 169.95, 169.76 (5 CO), 155.09, 139.26, 135.72, 132.83, 129.73, 128.21, 127.03, 116.82 (12C, Ar-C), 95.87 (C-1), 69.43 (C-2), 69.23 (C-5), 68.91 (C-3), 65.99 (C-4), 62.15 (C-6), 52.11 (OMe), 40.78 (ArCH<sub>2</sub>), 20.88, 20.71, 20.70, 20.67 ppm (4 COCH<sub>3</sub>); ESI-MS:  $m/z$ : calcd for C<sub>29</sub>H<sub>32</sub>NaO<sub>12</sub> [M + Na]<sup>+</sup>: 595.18, found: 595.21.

**Methyl 2-[4'-(2,3,4,6-tetra-O-acetyl- $\alpha$ -D-mannopyranosyloxy)biphenyl-4-yl]cyclopropanecarboxylate (33):** Prepared according to general procedure B from methyl 1-(4-bromophenyl)cyclopropanecarboxylate (**32**, 42.6 mg, 0.167 mmol), **27** (101 mg, 0.184 mmol), Pd(dppf)Cl<sub>2</sub>·CH<sub>2</sub>Cl<sub>2</sub> (4.1 mg, 5.0  $\mu$ mol) and K<sub>3</sub>PO<sub>4</sub> (53.2 mg, 0.251 mmol). Yield: 60 mg (56%) as colorless oil.  $R_f$  = 0.31 (PE/EtOAc, 2:1); [ $\alpha$ ]<sub>D</sub><sup>20</sup> + 70.2 ( $c$  = 1.00, EtOAc); <sup>1</sup>H NMR (500 MHz, CDCl<sub>3</sub>):  $\delta$  = 7.54–7.48 (m, 4H, Ar-H), 7.40–7.39 (m, 2H, Ar-H), 7.17–7.14 (m, 2H, Ar-H), 5.59 (dd,  $J$  = 3.55, 10.1 Hz, 1H, H-3), 5.56 (d,  $J$  = 1.6 Hz, 1H, H-1), 5.46 (dd,  $J$  = 1.9, 3.5 Hz, 1H, H-2), 5.38 (t,  $J$  = 10.0 Hz, 1H, H-4), 4.29 (dd,  $J$  = 5.1, 12.0 Hz, 1H, H-6a), 4.15–4.09 (m, 2H, H-6b, H-5), 3.65 (s, 3H, OMe), 2.21, 2.06, 2.05, 2.03 (4 s, 12H, 4 OAc), 1.64–1.62 (m, 2H, cPr), 1.27–1.16 ppm (m, 2H, cPr); <sup>13</sup>C NMR (125 MHz, CDCl<sub>3</sub>):  $\delta$  = 175.04, 170.53, 169.98, 169.95, 169.75 (5 CO), 155.10, 139.25, 138.43, 135.76, 130.94, 128.24, 126.61, 116.80 (12C, Ar-C), 95.89 (C-1), 69.44 (C-5), 69.23 (C-2), 68.90 (C-3), 66.00 (C-4), 62.15 (C-6), 52.42 (OMe), 28.67 (cPr), 20.71, 20.68 (4C, 4 COCH<sub>3</sub>), 16.75 ppm (cPr); ESI-MS:  $m/z$ : calcd for C<sub>31</sub>H<sub>34</sub>NaO<sub>12</sub> [M + Na]<sup>+</sup>: 621.19, found: 621.26.

**Methyl 2-[4'-( $\alpha$ -D-mannopyranosyloxy)biphenyl-4-yl]acetate (30):** Prepared according to general procedure C from **29** (30 mg, 0.052 mmol). Yield: 20 mg (95%).  $R_f$  = 0.25 (CH<sub>2</sub>Cl<sub>2</sub>/MeOH, 8:1); [ $\alpha$ ]<sub>D</sub><sup>20</sup> + 116.0 ( $c$  = 0.50, MeOH); <sup>1</sup>H NMR (500 MHz, CD<sub>3</sub>OD):  $\delta$  = 7.57–7.53 (m, 4H, Ar-H), 7.34–7.33 (m, 2H, Ar-H), 7.22–7.20 (m, 2H, Ar-H), 5.54 (d,  $J$  = 1.5 Hz, 1H, H-1), 4.05 (dd,  $J$  = 1.8, 3.3 Hz, 1H, H-2), 3.95 (dd,  $J$  = 3.4, 9.5 Hz, 1H, H-3), 3.82–3.74 (m, 3H, H-4, H-6), 3.71 (s, 3H, OMe), 3.66 (s, 2H, ArCH<sub>2</sub>), 3.65 ppm (ddd,  $J$  = 2.5, 5.2, 9.7 Hz, 1H, H-5); <sup>13</sup>C NMR (125 MHz, CD<sub>3</sub>OD):  $\delta$  = 174.02 (CO), 157.50, 140.77, 136.22, 134.29, 130.81, 129.00, 127.77, 118.13 (12C, Ar-C), 100.23 (C-1), 75.42 (C-5), 72.45 (C-3), 72.03 (C-2), 68.38 (C-4), 62.70 (C-6), 52.49 (OMe), 41.34 ppm (ArCH<sub>2</sub>); HRMS:  $m/z$ : calcd for C<sub>21</sub>H<sub>24</sub>NaO<sub>8</sub> [M + Na]<sup>+</sup>: 427.1363, found: 427.1363.

**Methyl 2-[4'-( $\alpha$ -D-mannopyranosyloxy)biphenyl-4-yl]cyclopropanecarboxylate (34):** Prepared according to general procedure C from **33** (38 mg, 0.063 mmol). Yield: 9 mg (33%).  $R_f$  = 0.33 (CH<sub>2</sub>Cl<sub>2</sub>/MeOH, 8:1); [ $\alpha$ ]<sub>D</sub><sup>20</sup> + 108.0 ( $c$  = 0.30, MeOH); <sup>1</sup>H NMR (500 MHz, CD<sub>3</sub>OD):  $\delta$  = 7.46–7.39 (m, 4H, Ar-H), 7.28–7.26 (m, 2H, Ar-H), 7.10–7.07 (m, 2H, Ar-H), 5.42 (d,  $J$  = 1.7 Hz, 1H, H-1), 3.93 (dd,  $J$  = 1.9, 3.4 Hz, 1H, H-2), 3.82 (dd,  $J$  = 3.4, 9.4 Hz, 1H, H-3), 3.69–3.61 (m, 3H, H-4, H-6), 3.53 (m, 4H, OMe, H-5), 1.49–1.47 (m, 2H, cPr), 1.14–1.11 ppm (m, 2H, cPr); <sup>13</sup>C NMR (125 MHz, CD<sub>3</sub>OD):  $\delta$  = 157.50, 140.87, 139.51, 136.26, 132.03, 129.04, 127.43, 118.11 (12C, Ar-C),

100.20 (C-1), 75.43 (C-5), 72.42 (C-3), 72.02 (C-2), 68.34 (C-4), 62.68 (C-6), 52.81 (OME), 17.20 ppm (2C, cPr); HRMS:  $m/z$ : calcd for  $C_{23}H_{26}NaO_8$   $[M+Na]^+$ : 453.1520, found: 453.1523.

**Sodium 2-[4'-( $\alpha$ -D-mannopyranosyloxy)biphenyl-4-yl]acetate (31):** Prepared according to general procedure D from **29** (59 mg, 0.103 mmol). Yield: 17 mg (40%).  $[\alpha]_D^{20} + 94.0$  ( $c=0.20$ , MeOH/H<sub>2</sub>O 1:1); <sup>1</sup>H NMR (500 MHz, D<sub>2</sub>O):  $\delta=7.61$  (d,  $J=8.6$  Hz, 2H, Ar-H), 7.55 (d,  $J=8.0$  Hz, 2H, Ar-H), 7.31 (d,  $J=8.0$  Hz, 2H, Ar-H), 7.19 (d,  $J=8.6$  Hz, 2H, Ar-H), 5.60 (s, 1H, H-1), 4.13 (m, 1H, H-2), 4.00 (dd,  $J=3.2, 8.5$  Hz, 1H, H-3), 3.75–3.67 (m, 4H, H-4, H-5, H-6), 3.51 ppm (s, 2H, ArCH<sub>2</sub>); <sup>13</sup>C NMR (125 MHz, D<sub>2</sub>O):  $\delta=154.94, 137.93, 136.29, 135.08, 129.76, 128.07, 126.72, 117.49$  (12C, Ar-C), 98.20 (C-1), 73.37 (C-5), 70.40 (C-3), 69.89 (C-2), 66.58 (C-4), 60.65 (C-6), 43.89 ppm (ArCH<sub>2</sub>); HRMS:  $m/z$ : calcd for  $C_{20}H_{22}NaO_8$   $[M+Na]^+$ : 413.1207, found: 413.1208.

**Sodium 2-[4'-( $\alpha$ -D-mannopyranosyloxy)biphenyl-4-yl]cyclopropanecarboxylate (35):** Prepared according to general procedure D from **33** (59 mg, 0.099 mmol). Yield: 10 mg (23%).  $[\alpha]_D^{20} + 95.0$  ( $c=0.20$ , dioxane/H<sub>2</sub>O 1:1); <sup>1</sup>H NMR (500 MHz, D<sub>2</sub>O):  $\delta=7.62$ –7.60 (m, 2H, Ar-H), 7.54–7.53 (m, 2H, Ar-H), 7.38–7.19 (m, 4H, Ar-H), 5.60 (s, 1H, H-1), 4.13 (m, 1H, H-2), 4.00 (m, 1H, H-3), 3.75–3.67 (4H, H-4, H-5, H-6), 1.33 (s, 2H, cPr), 1.01 ppm (s, 2H, cPr); <sup>13</sup>C NMR (125 MHz, D<sub>2</sub>O):  $\delta=128.67, 126.10, 124.37, 115.47$  (12C, Ar-C), 96.18 (C-1), 71.35 (C-5), 68.38 (C-3), 67.87 (C-2), 64.56 (C-4), 58.62 (C-6), 12.66 ppm (2C, cPr); HRMS:  $m/z$ : calcd for  $C_{22}H_{24}NaO_8$   $[M+Na]^+$ : 439.1363, found: 439.1363.

### Competitive binding assay

A recombinant protein consisting of the CRD of FimH linked with a thrombin cleavage site (TH) to a His<sub>6</sub>-tag (FimH-CRD-Th-His<sub>6</sub>) was expressed in *E. coli* strain HM125 and purified by affinity chromatography.<sup>[16]</sup> To determine the affinity of the various FimH antagonists, a competitive binding assay described previously<sup>[16]</sup> was applied. Microtiter plates (F96 MaxiSorp, Nunc) were coated with a 10  $\mu$ g mL<sup>-1</sup> solution of FimH-CRD-Th-His<sub>6</sub> in 20 mM HEPES, 150 mM NaCl, and 1 mM CaCl<sub>2</sub>, pH 7.4 (assay buffer), 100  $\mu$ L per well, overnight at 4 °C. The coating solution was discarded, and the wells were blocked with 3% BSA in assay buffer (150  $\mu$ L per well) for 2 h at 4 °C. After three washing steps with assay buffer (150  $\mu$ L per well), a fourfold serial dilution of the test compound (50  $\mu$ L per well) in assay buffer containing 5% DMSO and streptavidin-peroxidase coupled Man- $\alpha$ (1–3)[Man- $\alpha$ (1–6)]-Man- $\beta$ (1–4)-GlcNAc- $\beta$ (1–4)-GlcNAc $\beta$  polyacrylamide (TM-PAA) polymer (50  $\mu$ L per well of a 0.5  $\mu$ g mL<sup>-1</sup> solution) were added. On each individual microtiter plate, *n*-heptyl  $\alpha$ -D-mannopyranoside (**1**) was tested in parallel. The plates were incubated for 3 h at 25 °C and 350 rpm and then carefully washed four times with 150  $\mu$ L per well assay buffer. After the addition of 100  $\mu$ L per well of 2,2'-azino-di-(3-ethylbenzthiazoline-6-sulfonic acid) (ABTS) substrate, the colorimetric reaction was allowed to develop for 4 min and then was stopped by the addition of 2% aqueous oxalic acid before the optical density (OD) was measured at 415 nm on a microplate reader (Spectramax 190, Molecular Devices, CA, USA). The IC<sub>50</sub> values of the compounds tested in duplicate were calculated with Prism software (GraphPad Software Inc., La Jolla, CA, USA). The IC<sub>50</sub> defines the molar concentration of the test compound that decreases the maximal specific binding of TM-PAA polymer to FimH-CRD by 50%. The relative IC<sub>50</sub> (rIC<sub>50</sub>) is the ratio of the IC<sub>50</sub> of the test compound to the IC<sub>50</sub> of *n*-heptyl  $\alpha$ -D-mannopyranoside (**1**).

### Cell-based flow cytometry assay

The assay was performed as described previously.<sup>[17]</sup> Briefly, 5637 cells (DSMZ, Braunschweig, Germany) were grown to confluence in 24-well plates. Before infection, a serial dilution of test compound in 5% DMSO, PBS (Sigma-Aldrich) was prepared. GFP-labeled UTI89 bacteria (200  $\mu$ L) in RPMI 1640 medium (Invitrogen, Basel, Switzerland) were pre-incubated with test compound (25  $\mu$ L) for 10 min at RT. The bacteria-antagonist mixtures were then added to the monolayers of 5637 cells. The multiplicity of infection (MOI) was 1:50 (cell/bacteria). To homogenize the infection, plates were centrifuged at RT for 3 min at 600 g. After an incubation time of 1.5 h at 37 °C, infected cells were washed four times with RPMI 1640 medium and suspended in ice-cold PBS for 5–20 min (treatment with ice-cold PBS results in the detachment of the infected cells). Cells were then kept in the dark until analysis. Samples were measured with a CyAn ADP flow cytometer (Beckman-Coulter, Brea, CA, USA) and analyzed by gating on the eukaryotic cells based on forward (FSC) and side scatter (SSC), which excludes unbound labeled bacteria and debris from analysis. A total of 10<sup>4</sup> cells were measured per sample. Data were acquired in a linear mode for the SSC and logarithmic mode for FSC and the green fluorescent channel FL1-H (GFP). The mean fluorescence intensity (MFI) of GFP was counted as a surrogate marker for the adherence of bacteria. Quantification of adhesion was evaluated with the FlowJo software 9.0.1 (Tree Star Inc., Ashland, OR, USA). IC<sub>50</sub> values were determined by plotting the concentration of the antagonist in a logarithmic mode versus the MFI and by fitting the curve with Prism software (GraphPad, inhibition curve, variable slope), ( $n=2-3$ , in duplicate/triplicate).

### Isothermal titration calorimetry (ITC)

For the ITC experiments, the His tag in FimH-CRD-Th-His<sub>6</sub> was cleaved.<sup>[16]</sup> Briefly, the protein (1 mg) was incubated with 10 U thrombin (T-6884, Sigma-Aldrich) in 20 mM Tris-HCl, pH 8.4, 150 mM NaCl and 2.5 mM CaCl<sub>2</sub> (cleavage buffer) at 20 °C for 16 h. The mixture was then applied to a gel filtration column (Bio-Prep SE100/17, Bio-Rad) attached to an FPLC system. The chromatography was run with assay buffer and analyzed by SDS-PAGE. The fractions containing FimH-CRD were pooled and concentrated by ultrafiltration (MWCO10, Sartorius AG, Tagelswangen, Switzerland). The ITC experiments were performed using a VP-ITC instrument from MicroCal Inc. (GE Healthcare, Northampton, MA, USA). The measurements were performed at 25 °C. Prior to measurements, the protein was dialyzed in assay buffer (10 mM HEPES, 150 mM NaCl, 1 mM CaCl<sub>2</sub>, pH 7.4 (HBS-Ca)). Injections of 3–5  $\mu$ L ligand solutions (150  $\mu$ M) were added at an interval of 10 min into the sample cell solution containing FimH-CRD (8–22  $\mu$ M, sample cell volume 1.4523 mL) with stirring at 307 rpm. Protein concentration was determined by HPLC-UV against a BSA standard.<sup>[38]</sup> The quantity  $c = Mt(0) K_D^{-1}$ , where  $Mt(0)$  is the initial macromolecule concentration, is of importance in titration microcalorimetry. The  $c$  values ranged between 300 and 3200. Because the smallest reliable volumes were injected, sigmoidal curves were obtained. Control experiments injecting ligand solution into buffer without protein showed that the heat of dilution was small and constant. Baseline correction and peak integration were accomplished using Origin 7 as described by the manufacturer (OriginLab, Northampton, MA, USA). The first injection was always excluded from data analysis because it usually suffers from sample loss during the mounting of the syringe and the equilibration preceding the actual titration. A three-parameter ( $N$  (stoichiometry),  $K_D$  (dissociation constant) and  $\Delta H^\circ$  (change in enthalpy) nonlinear least-square data fitting was per-

formed in a Microsoft Excel spreadsheet using the Solver add-in (Frontline System)<sup>[39,40]</sup> according to binding isotherms published by Ziegler and Seelig.<sup>[41]</sup>

Thermodynamics parameters were calculated from Equation (4).

$$\Delta G = \Delta H - T\Delta S = RT \ln K_D = -RT \ln K_A \quad (4)$$

where  $\Delta G$ ,  $\Delta H$ , and  $\Delta S$  are the changes in free energy, enthalpy, and entropy of binding, respectively,  $T$  is the absolute temperature, and  $R$  is the universal gas constant ( $8.314 \text{ J mol}^{-1} \text{ K}^{-1}$ ).

#### Determination of pharmacokinetic parameters

**Materials:** Dimethyl sulfoxide (DMSO), 1-octanol, Dulbecco's modified Eagle's medium (DMEM) high glucose, L-glutamine solution, penicillin–streptomycin solution, Dulbecco's phosphate-buffered saline (DPBS), and trypsin–EDTA solution were purchased from Sigma–Aldrich. MEM nonessential amino acid (MEM-NEAA) solution, fetal bovine serum (FBS), and DMEM without sodium pyruvate and phenol red were bought from Invitrogen. PAMPA System Solution, GIT-0 Lipid Solution, and Acceptor Sink Buffer were ordered from plon (Woburn, MA, USA). Acetonitrile (MeCN) was bought from Acros Organics. The Caco-2 cells were kindly provided by Prof. G. Imanidis, FHNW, Muttenz, Switzerland and originated from the American Type Culture Collection (Rockville, MD, USA).

#### Parallel artificial membrane permeation assay (PAMPA)

Values of  $\log P_e$  were determined in a 96-well format with the PAMPA<sup>[33]</sup> permeation assay. For each compound, measurements were performed at three pH values (5.0, 6.2, 7.4) in quadruplicate. For this purpose, 12 wells of a deep-well plate, i.e., four wells per pH value, were filled with 650  $\mu\text{L}$  System Solution. Samples (150  $\mu\text{L}$ ) were withdrawn from each well to determine the blank spectra by UV spectroscopy (SpectraMax 190). Then, analyte dissolved in DMSO was added to the remaining System Solution to yield 50  $\mu\text{M}$  solutions. To exclude precipitation, the optical density was measured at 650 nm, with 0.01 being the threshold value. Solutions exceeding this threshold were filtered. Afterward, samples (150  $\mu\text{L}$ ) were withdrawn to determine the reference spectra. Further 200  $\mu\text{L}$  were transferred to each well of the donor plate of the PAMPA sandwich P/N 110 163 (plon, Woburn MA, USA). The filter membranes at the bottom of the acceptor plate were impregnated with 5  $\mu\text{L}$  of GIT-0 Lipid Solution, and 200  $\mu\text{L}$  of Acceptor Sink Buffer were filled into each acceptor well. The sandwich was assembled, placed in the GutBox, and left undisturbed for 16 h. It was then disassembled, and samples (150  $\mu\text{L}$ ) were transferred from each donor and acceptor well to UV plates. Quantification was performed by both UV spectroscopy and LC–MS;  $\log P_e$  values were calculated with the aid of the PAMPA Explorer Software (plon, version 3.5).

#### Colorectal adenocarcinoma (Caco-2) cell permeation assay

Caco-2 cells were cultivated in tissue culture flasks (BD Biosciences, Franklin Lakes, NJ, USA) with DMEM high-glucose medium containing L-glutamine (2 mM), nonessential amino acids (0.1 mM), penicillin (100  $\text{U mL}^{-1}$ ), streptomycin (100  $\mu\text{g mL}^{-1}$ ), and FBS (10%). The cells were kept at 37 °C in humidified air containing 5%  $\text{CO}_2$ , and the medium was changed every second day. When ~90% confluence was reached, the cells were split in a 1:10 ratio and distributed to new tissue culture flasks. At passage numbers between 60

and 65, they were seeded at a density of  $5.3 \times 10^5$  cells per well to Transwell 6-well plates (Corning Inc., Corning, NY, USA) with 2.5 mL culture medium in the basolateral and 1.8 mL in the apical compartment. The medium was renewed on alternate days. Permeation experiments were performed between days 19 and 21 post-seeding. Prior to the experiment, the integrity of the Caco-2 monolayers was evaluated by measuring the transepithelial electrical resistance (TEER) with an Endohm tissue resistance instrument (World Precision Instruments Inc., Sarasota, FL, USA). Only wells with TEER values  $> 300 \Omega \text{ cm}^2$  were used. Experiments were performed in the apical-to-basolateral (absorptive) and basolateral-to-apical (secretory) directions in triplicate. Transport medium (DMEM without sodium pyruvate and phenol red) was withdrawn from the donor compartments of three wells and replaced by the same volume of compound stock solutions to reach an initial sample concentration of 62.5  $\mu\text{M}$ . The Transwell plate was then shaken (250 rpm) in the incubator. Samples (40  $\mu\text{L}$ ) were withdrawn after 15, 30, and 60 min from the donor and acceptor compartments, and their concentrations were determined by LC–MS. Apparent permeability coefficients ( $P_{app}$ ) were calculated according to the equation

$$P_{app} = \frac{dQ}{dt} \times \frac{1}{A \times c_0} \quad (5)$$

where  $dQ/dt$  is the permeability rate,  $A$  the surface area of the monolayer, and  $c_0$  the initial concentration in the donor compartment.<sup>[42]</sup> After the experiment, TEER values were assessed again for each well and results from wells with values  $< 300 \Omega \text{ cm}^2$  were discarded.

#### $\log D_{7.4}$ determination

The *in silico* prediction tool ALOGPS<sup>[43]</sup> was used to estimate the  $\log P$  values of the compounds. Depending on these values, the compounds were classified into three categories: hydrophilic compounds ( $\log P < 0$ ), moderately lipophilic compounds ( $0 \leq \log P \leq 1$ ) and lipophilic compounds ( $\log P > 1$ ). For each category, two different ratios (volume of 1-octanol to volume of buffer) were defined as experimental parameters (Table 4).

**Table 4.** Compound classification based on estimated  $\log P$  values.<sup>[43]</sup>

Compound type	$\log P$	Ratio (1-octanol)/(buffer)
hydrophilic	$< 0$	30:140, 40:130
moderately lipophilic	0–1	70:110, 110:70
lipophilic	$> 1$	3:180, 4:180

Equal amounts of phosphate buffer (0.1 M, pH 7.4) and 1-octanol were mixed and shaken vigorously for 5 min to saturate the phases. The mixture was left until separation of the two phases occurred, and the buffer was retrieved. Stock solutions of the test compounds were diluted with buffer to a concentration of 1  $\mu\text{M}$ . For each compound, six determinations, i.e., three determinations per 1-octanol/buffer ratio, were performed in different wells of a 96-well plate. The respective volumes of buffer containing analyte (1  $\mu\text{M}$ ) were pipetted to the wells and covered by saturated 1-octanol according to the chosen volume ratio. The plate was sealed with aluminum foil, shaken (1350 rpm, 25 °C, 2 h) on a Heidoph Titramax 1000 plate shaker (Heidolph Instruments GmbH & Co. KG, Schwabach, Germany) and centrifuged (2000 rpm, 25 °C,

5 min, 5804 R Eppendorf centrifuge, Hamburg, Germany). The aqueous phase was transferred to a 96-well plate for analysis by LC-MS.

$\log D_{7.4}$  was calculated from the 1-octanol/buffer ratio ( $o/b$ ), the initial concentration of the analyte in buffer ( $1 \mu\text{M}$ ), and the concentration of the analyte in the aqueous phase ( $c_B$ ) with equation:

$$\log D_{7.4} = \log \left( \frac{1 \mu\text{M} - c_B}{c_B} \times \frac{1}{o : b} \right) \quad (6)$$

### Solubility

Solubility was determined in a 96-well format using the  $\mu\text{SOL}$  Explorer solubility analyzer (plon, version 3.4.0.5). For each compound, measurements were performed at three pH values (3.0, 5.0, 7.4) in triplicates. For this purpose, nine wells of a deep-well plate, that is, three wells per pH value, were filled with 300  $\mu\text{L}$  of an aqueous universal buffer solution. Aliquots (3  $\mu\text{L}$ ) of a compound stock solution (10–50 mM in DMSO) were added and thoroughly mixed. The final sample concentration was 0.1–0.5 mM, the residual DMSO concentration was 1.0% ( $v/v$ ) in the buffer solutions. After 15 h, the solutions were filtered (0.2  $\mu\text{m}$  96-well filter plates) using a vacuum to collect manifold (Whatman Ltd., Maidstone, UK) to remove any precipitates. Equal amounts of filtrate and *n*-propanol were mixed and transferred to a 96-well plate for UV detection (190–500 nm). The amount of material dissolved was calculated by comparison with UV spectra obtained from reference samples, which were prepared by dissolving compound stock solution in a 1:1 mixture of buffer and *n*-propanol (final concentrations 0.017–0.083 mM).

### LC-MS measurements

Analyses were performed using an 1100/1200 Series HPLC System coupled to a 6410 Triple Quadrupole mass detector (Agilent Technologies, Inc., Santa Clara, CA, USA) equipped with electrospray ionization. The system was controlled with the Agilent MassHunter Workstation Data Acquisition software (version B.01.04). The column used was an Atlantis T3  $C_{18}$  column (2.1  $\times$  50 mm) with a 3  $\mu\text{m}$  particle size (Waters Corp., Milford, MA, USA). The mobile phase consisted of two eluents: solvent A ( $\text{H}_2\text{O}$ , containing 0.1% formic acid,  $v/v$ ) and solvent B (MeCN, containing 0.1% formic acid,  $v/v$ ), both delivered at 0.6  $\text{mL min}^{-1}$ . The gradient was ramped from 95% A/5% B to 5% A/95% B over 1 min, and then held at 5% A/95% B for 0.1 min. The system was then brought back to 95% A/5% B, resulting in a total duration of 4 min. MS parameters such as fragmentor voltage, collision energy, and polarity were optimized individually for each analyte, and the molecular ion was followed for each compound in the multiple reaction monitoring mode. The concentrations of the analytes were quantified by the Agilent Mass Hunter Quantitative Analysis software (version B.01.04).

### Abbreviations

Caco-2 cells, colorectal adenocarcinoma cells; CRD, carbohydrate recognition domain;  $D$ , distribution coefficient octanol/ $\text{H}_2\text{O}$ ; GFP, green fluorescent protein; HPLC, high-performance liquid chromatography;  $\text{IC}_{50}$ , half-maximal inhibitory concentration; ITC, isothermal titration calorimetry; MFI, mean fluorescence intensity; PAMPA, parallel artificial membrane permeability assay;  $P_{\text{app}}$ , apparent per-

meability coefficient;  $P_e$ , effective permeation value; SAR, structure–activity relationship; SPR, structure–property relationship; UPEC, uropathogenic *E. coli*; UTI, urinary tract infection.

### Acknowledgement

Financial support from the Swiss National Science Foundation (SNF interdisciplinary grant K-32K1-120904) is gratefully acknowledged.

**Keywords:** bacterial adhesin · FimH antagonists · flow cytometry · isothermal titration calorimetry · urinary tract infections

- [1] a) T. M. Hooton, W. E. Stamm, *Infect. Dis. Clin. North Am.* **1997**, *11*, 551–581; b) T. J. Wiles, R. R. Kulesus, M. A. Mulvey, *Exp. Mol. Pathol.* **2008**, *85*, 11–19; c) S. D. Fihn, *N. Engl. J. Med.* **2003**, *349*, 259–266.
- [2] C. Svanborg, G. Godaly, *Infect. Dis. Clin. North Am.* **1997**, *11*, 513–529.
- [3] a) J. D. Schilling, S. J. Hultgren, *Int. J. Antimicro. Ag.* **2002**, *19*, 457–460; b) M. G. Blango, M. A. Mulvey, *Antimicrob. Agents Chemother.* **2010**, *54*, 1855–1863.
- [4] G. Capitani, O. Eidam, R. Glockshuber, M. G. Grutter, *Microbes Infect.* **2006**, *8*, 2284–2290.
- [5] a) M. A. Mulvey, *Cell Microbiol.* **2002**, *4*, 257–271; b) S. G. Gouin, A. Wellens, J. Bouckaert, J. Kovensky, *ChemMedChem* **2009**, *4*, 749–755.
- [6] N. Sharon, *Biochim. Biophys. Acta.* **2006**, *1760*, 527–537.
- [7] a) N. Firon, I. Ofek, N. Sharon, *Biochem. Biophys. Res. Commun.* **1982**, *105*, 1426–1432; b) N. Firon, I. Ofek, N. Sharon, *Carbohydr. Res.* **1983**, *120*, 235–249; c) N. Sharon, *FEBS Lett.* **1987**, *217*, 145–157.
- [8] D. Choudhury, A. Thompson, V. Stojanoff, S. Langermann, J. Pinkner, S. J. Hultgren, S. D. Knight, *Science* **1999**, *285*, 1061–1066.
- [9] a) C. S. Hung, J. Bouckaert, D. Hung, J. Pinkner, C. Widberg, A. DeFusco, C. G. Auguste, R. Strouse, S. Langermann, G. Waksman, S. J. Hultgren, *Mol. Microbiol.* **2002**, *44*, 903–915; b) J. Bouckaert, J. Berglund, M. Schembri, E. D. Genst, L. Cools, M. Wuhler, C. S. Hung, J. Pinkner, R. Slättergard, A. Zavalov, D. Choudhury, S. Langermann, S. J. Hultgren, L. Wyns, P. Klemm, S. Oscarson, S. D. Knight, H. De Greve, *Mol. Microbiol.* **2005**, *55*, 441–455; c) A. Wellens, C. Garofalo, H. Nguyen, N. Van Gerven, R. Slättergard, J.-P. Hernalsteens, L. Wyns, S. Oscarson, H. De Greve, S. Hultgren, J. Bouckaert, *PLoS ONE* **2008**, *3*, e2040.
- [10] a) N. Firon, S. Ashkenazi, D. Mirelman, I. Ofek, N. Sharon, *Infect. Immun.* **1987**, *55*, 472–476; b) T. K. Lindhorst, S. Kötter, J. Kubisch, U. Krallmann-Wenzel, S. Ehlers, V. Kren, *Eur. J. Org. Chem.* **1998**, 1669–1674; c) O. Sperling, A. Fuchs, T. K. Lindhorst, *Org. Biomol. Chem.* **2006**, *4*, 3913–3922; d) Z. Han, J. S. Pinker, B. Ford, R. Obermann, W. Nolan, S. A. Wildman, D. Hobbs, T. Ellenberger, C. K. Cusumano, S. J. Hultgren, J. W. Janetka, *J. Med. Chem.* **2010**, *53*, 4779–4792; e) T. Klein, D. Abgottspon, M. Wittwer, S. Rabbani, J. Herold, X. Jiang, S. Kleeb, C. Lüthi, M. Scharenberg, J. Bezençon, E. Gubler, L. Pang, M. Smieško, B. Cutting, O. Schwarzd, B. Ernst, *J. Med. Chem.* **2010**, *53*, 8627–8641; f) O. Schwarzd, S. Rabbani, M. Hartmann, D. Abgottspon, M. Wittwer, S. Kleeb, A. Zalewski, M. Smieško, B. Cutting, B. Ernst, *Bioorg. Med. Chem.* **2011**, *19*, 6454–6473; g) C. K. Cusumano, J. S. Pinkner, Z. Han, S. E. Greene, B. A. Ford, J. R. Crowley, J. P. Henderson, J. W. Janetka, S. J. Hultgren, *Sci. Transl. Med.* **2011**, *3*, 109ra115; h) J. Berglund, J. Bouckaert, H. De Greve, S. Knight, *Anti-Adhesive Compounds to Prevent and Treat Bacterial Infections*, Intl. Pat. PCT/US 2005/089733, **2005**.
- [11] Glide, version 5.7, Schrödinger, LLC, New York, NY (USA), **2011**.
- [12] I. L. Scott, R. V. Market, R. J. DeOrazio, H. Meckler, T. P. Kogan, *Carbohydr. Res.* **1999**, *317*, 210–216.
- [13] C. A. Ocasio, T. S. Scanlan, *Bioorg. Med. Chem.* **2008**, *16*, 762–770.
- [14] M. Prieto, E. Zurita, E. Rosa, L. Muñoz, P. Lloyd-Williams, E. Giralt, *J. Org. Chem.* **2004**, *69*, 6812–6820.
- [15] M. Ishikawa, Y. Hashimoto, *J. Med. Chem.* **2011**, *54*, 1539–1554.
- [16] S. Rabbani, X. Jiang, O. Schwarzd, B. Ernst, *Anal. Biochem.* **2010**, *407*, 188–195.



- [17] M. Scharenberg, D. Abgottspon, E. Cicek, X. Jiang, O. Schwardt, S. Rabani, B. Ernst, *Assay Drug Dev. Technol.* **2011**, *9*, 455–464.
- [18] J. Bouckaert, J. Mackenzie, J. L. de Paz, B. Chipwaza, D. Choudhury, A. Zavialov, K. Mannerstedt, J. Anderson, D. Pierard, L. Wyns, P. H. Seeberger, S. Oscarson, H. De Greve, S. D. Knight, *Mol. Microbiol.* **2006**, *61*, 1556–1568.
- [19] G. Zhou, W. J. Mo, P. Sebbel, G. W. Min, T. A. Neubert, R. Glockshuber, *J. Cell Sci.* **2001**, *114*, 4095–4103.
- [20] P. Aprikian, V. Tchesnokova, B. Kidd, O. Yakovenko, V. Yarov-Yaroyov, E. Trinchina, V. Vogel, W. Thomas, E. Sokurenko, *J. Biol. Chem.* **2007**, *282*, 23437–23446.
- [21] I. Le Trong, P. Aprikian, B. A. Kidd, M. Forero-Shelton, V. Tchesnokova, P. Rajagopal, V. Rodriguez, G. Interlandi, R. Klevit, V. Vogel, R. E. Stenkamp, E. V. Sokurenko, W. E. Thomas, *Cell* **2010**, *141*, 645–655.
- [22] D. Abgottspon, G. Rölli, L. Hosch, A. Steinhuber, X. Jiang, O. Schwardt, B. Cutting, M. Smieško, U. Jenal, B. Ernst, A. Trampuz, *J. Microbiol. Methods* **2010**, *82*, 249–255.
- [23] a) J. E. Ladbury, *Biochem. Soc. Trans.* **2010**, *38*, 888–893; b) G. A. Holdgate, W. H. Ward, *Drug Discovery Today* **2005**, *10*, 1543–1550; c) R. Perozco, G. Folkers, L. Scapozza, *J. Recept. Signal Transduction Res.* **2004**, *24*, 1–52; d) J. E. Ladbury, G. Klebe, E. Freire, *Nat. Rev. Drug Discovery* **2010**, *9*, 23–27; e) K. P. Murphy, D. Xie, K. S. Thompson, L. M. Amzel, E. Freire, *Proteins* **1994**, *18*, 63–67.
- [24] a) B. Baum, L. Muley, M. Smolinski, A. Heine, D. Hangauer, G. Klebe, *J. Mol. Biol.* **2010**, *397*, 1042–1054; b) M. C. Chervenak, E. J. Toone, *J. Am. Chem. Soc.* **1994**, *116*, 10533–10539; c) J. E. DeLorbe, J. H. Clements, M. G. Teresk, A. P. Benfield, H. R. Plake, L. E. Millspaugh, S. F. Martin, *J. Am. Chem. Soc.* **2009**, *131*, 16758–16770.
- [25] S. Cabani, P. Gianni, V. Mollica, L. Lepori, *J. Solution Chem.* **1981**, *10*, 563–595.
- [26] A. V. Finkelstein, J. Janin, *Protein Eng.* **1989**, *3*, 1–3.
- [27] K. P. Murphy, *Biophys. Chem.* **1994**, *51*, 311–326.
- [28] E. Freire, *Drug Discovery Today* **2008**, *13*, 869–874.
- [29] a) T. S. G. Olsson, M. A. Williams, W. R. Pitt, J. E. Ladbury, *J. Mol. Biol.* **2008**, *384*, 1002–1017; b) C. Diehl, O. Engstrom, T. Delaine, M. Hakanson, S. Genheden, K. Modig, H. Leffler, U. Ryde, U. J. Nilsson, M. Akke, *J. Am. Chem. Soc.* **2010**, *132*, 14577–14589.
- [30] Phase, version 3.3, Schrödinger, LLC, New York, NY (USA), **2011**.
- [31] a) B. A. Williams, M. C. Chervenak, E. J. Toone, *J. Biol. Chem.* **1992**, *267*, 22907–22911; b) E. J. Toone, *Curr. Opin. Struc. Biol.* **1994**, *4*, 719–728; c) T. K. Dam, C. F. Brewer, *Chem. Rev.* **2002**, *102*, 387–429; d) M. Ambrosi, N. R. Cameron, B. G. Davis, *Org. Biomol. Chem.* **2005**, *3*, 1593–1608; e) E. Garcia-Hernandez, R. A. Zubillaga, E. A. Chavelas-Adame, E. Vazquez-Contreras, A. Rojo-Dominguez, M. Costas, *Protein Sci.* **2003**, *12*, 135–142.
- [32] H. Van de Waterbeemd, D. A. Smith, K. Beaumont, D. K. Walker, *J. Med. Chem.* **2001**, *44*, 1313–1333.
- [33] M. Kansy, F. Senner, K. Gubernator, *J. Med. Chem.* **1998**, *41*, 1007–1010.
- [34] A. Avdeef, S. Bendels, L. Di, B. Faller, M. Kansy, K. Sugano, Y. Yamauchi, *J. Pharm. Sci.* **2007**, *96*, 2893–2909.
- [35] C. A. Lipinski, *J. Pharmacol. Toxicol. Methods* **2000**, *44*, 235–249.
- [36] J. Kasuga, M. Ishikawa, M. Yonehara, M. Makishima, Y. Hashimoto, H. Miyachi, *Bioorg. Med. Chem.* **2010**, *18*, 7164–7173.
- [37] R. Roy, S. K. Das, F. Santoyo-González, F. Hernández-Mateo, T. K. Dam, C. F. Brewer, *Chem. Eur. J.* **2000**, *6*, 1757–1762.
- [38] a) F. Bitsch, R. Aichholz, J. Kallen, S. Geisse, B. Fournier, J. M. Schlaeppli, *Anal. Biochem.* **2003**, *323*, 139–149; b) S. Mesch, K. Lemme, H. Koliwer-Brandl, D. S. Strasser, O. Schwardt, S. Kelm, B. Ernst, *Carbohydr. Res.* **2010**, *345*, 1348–1359.
- [39] G. Kemmer, S. Keller, *Nat. Protoc.* **2010**, *5*, 267–281.
- [40] O. O. Krylova, N. Jahnke, S. Keller, *Biophys. Chem.* **2010**, *150*, 105–111.
- [41] A. Ziegler, J. Seelig, *Biophys. J.* **2004**, *86*, 254–263.
- [42] P. Artursson, J. Karlsson, *Biochem. Biophys. Res. Commun.* **1991**, *175*, 880–885.
- [43] a) VCCLAB, Virtual Computational Chemistry Laboratory, 2005, <http://www.vcclab.org> (accessed May 3, 2012); b) I. V. Tetko, J. Gasteiger, R. Todeschini, A. Mauri, D. Livingstone, P. Ertl, V. A. Palyulin, E. V. Radchenko, N. S. Zefirov, A. S. Makarenko, V. Y. Tanchuk, V. V. Prokopenko, *J. Comput. Aid. Mol. Des.* **2005**, *19*, 453–463.

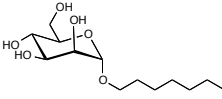
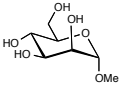
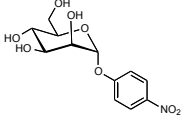
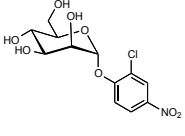
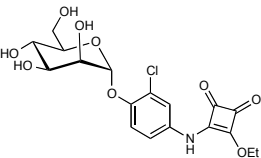
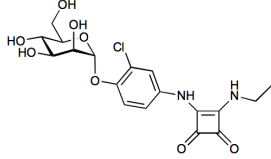
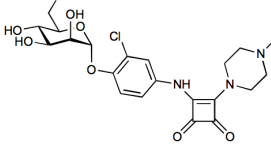
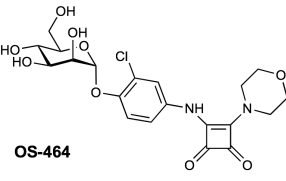
Received: March 6, 2012

Revised: April 27, 2012

Published online on May 29, 2012

## Flow cytometry assay results

Table 1. IC<sub>50</sub> values obtained for OS compounds.

Compound	Structure	FACS Inhibition Assay	
		IC <sub>50</sub> [μM]	rIC <sub>50</sub>
<i>n</i> -heptyl α-D-mannopyranoside (reference)		3.9 ± 1.6	1
α-D-methyl mannoside		249.2 ± 62.3	63.8
pNpα mannoside		3.2 ± 0.69	0.82
OS386		1.06 ± 0.47	0.27
OS394		0.035 ± 0.008	0.009
OS420		0.13 ± 0.02	0.033
OS421		0.11 ± 0.2	0.028
OS464	 OS-464	0.12 ± 0.06	0.03

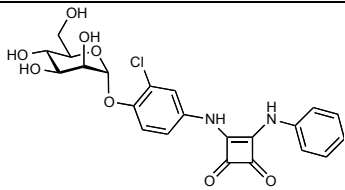
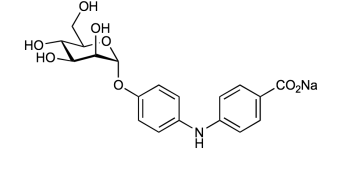
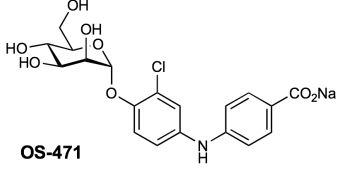
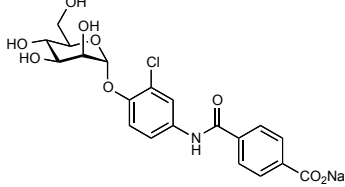
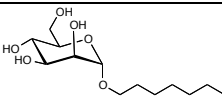
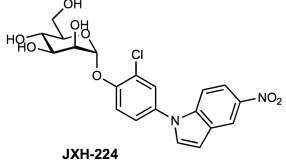
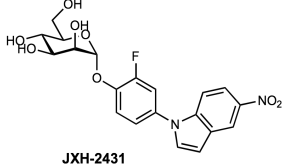
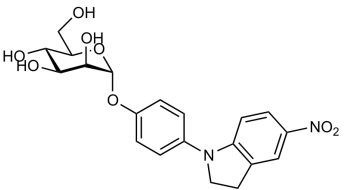
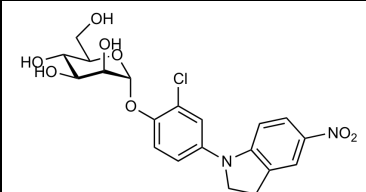
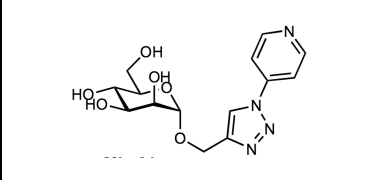
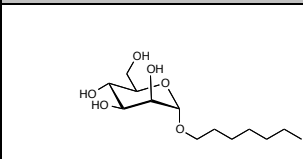
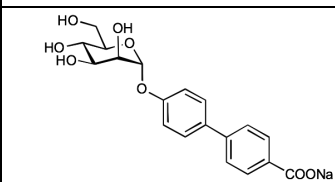
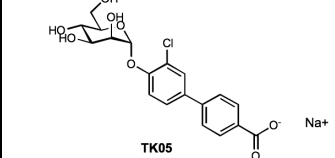
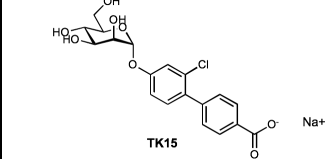
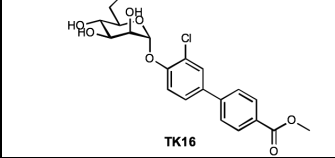
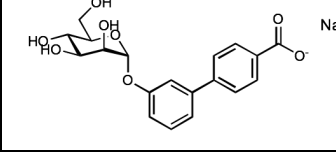
OS397		$0.09 \pm 0.01$	0.02
OS452		$0.72 \pm 0.003$	0.19
OS471	 OS-471	$0.61 \pm 0.13$	0.15
OS487		0.2	0.05

Table 2. IC<sub>50</sub> values obtained for JXH and Mha compounds.

Compound	Structure	FACS Inhibition Assay	
		IC <sub>50</sub> [μM]	rIC <sub>50</sub>
<i>n</i> -heptyl α-D-manno-pyranoside (reference)		$3.9 \pm 1.6$	1
JXH-224	 JXH-224	$0.59 \pm 0.045$	0.15
JXH-2431	 JXH-2431	1.02	0.26
MH17		$0.14 \pm 0.05$	0.04

<b>Mh31?</b>		$0.04 \pm 0.02$	0.01
<b>Mha31</b>		$21.5 \pm 1.49$	5.5

**Table 3.** IC<sub>50</sub> values obtained for biphenyl compounds from JXH and TK.

Compound	Structure	FACS Inhibition Assay	
		IC <sub>50</sub> [ $\mu$ M]	rIC <sub>50</sub>
<b><i>n</i>-heptyl <math>\alpha</math>-D-manno-pyranoside (reference)</b>		$3.9 \pm 1.6$	1
<b>JXH2372</b>		$0.86 \pm 0.56$	0.22
<b>TK05</b>		$0.33 \pm 0.05$	0.085
<b>TK15</b>		$0.53 \pm 0.06$	0.135
<b>TK16</b>		$0.24 \pm 0.043$	0.06
<b>TK18</b>		$4.45 \pm 1.9$	1.14

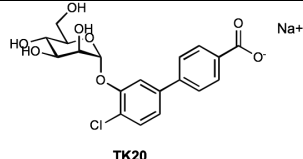
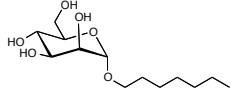
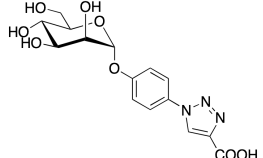
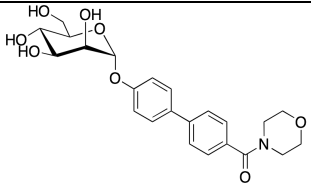
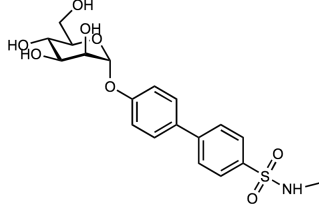
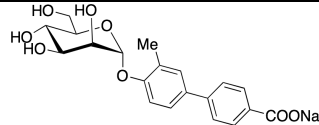
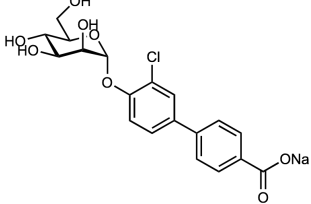
TK20	 <p style="text-align: center;">TK20</p>	0.78 ± 0.16	0.2
------	---	-------------	-----

Table 4. IC<sub>50</sub> values obtained for PLJ compounds.

Compound	Structure	FACS Inhibition Assay	
		IC <sub>50</sub> [μM]	rIC <sub>50</sub>
<i>n</i> -heptyl α-D-mannopyranoside (reference)		3.9 ± 1.6	1
PLJ01066A		2.7 ± 0.26	0.69
PLJ01076A		0.83 ± 0.15	0.21
PLJ01089A		4.9	1.27
PLJ01179B		1.83 ± 0.14	0.47
PLJ01178B		1.95 ± 0.36	0.5

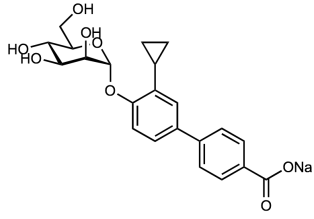
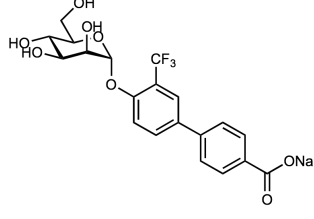
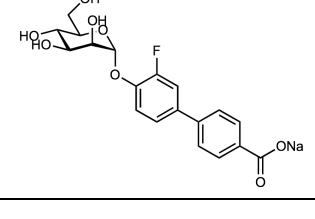
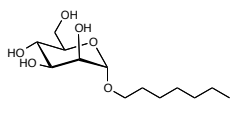
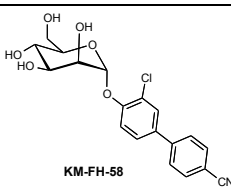
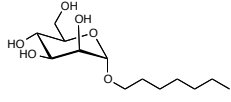
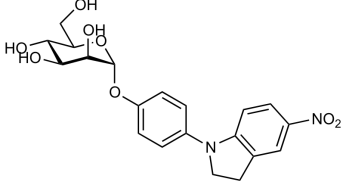
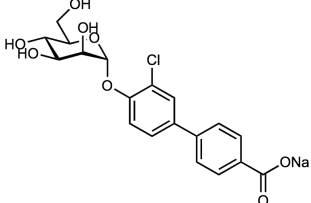
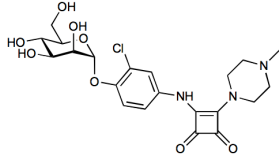
<b>PLJ01181B</b>		$4.85 \pm 0.79$	1.2
<b>PLJ01194B</b>		$0.89 \pm 0.1$	0.23
<b>PLJ01175B</b>		$1.54 \pm 0.31$	0.39

Table 5. IC<sub>50</sub> values obtained for KM compounds

Compound	Structure	FACS Inhibition Assay	
		IC <sub>50</sub> [μM]	rIC <sub>50</sub>
<b><i>n</i>-heptyl α-D-manno-pyranoside (reference)</b>		$3.9 \pm 1.6$	1
<b>KM FH58</b>	 KM-FH-58		

**Table 6.** IC<sub>50</sub> values obtained with *Klebsiella pneumoniae* (C3091 strain)

Compound	Structure	FACS Inhibition Assay	
		IC <sub>50</sub> [μM]	rIC <sub>50</sub>
<b><i>n</i>-heptyl α-D-manno-pyranoside (reference)</b>		7.82 ± 1.65	1
<b>MH17</b>		0.21 ± 0.11	0.027
<b>PLJ01178B</b>		0.33 ± 0.22	0.042
<b>OS421</b>		0.21 ± 0.08	0.027

## **Part II: The lectin DC-SIGN**

---

**DC-SIGN Abstract**

---



## Abstract DC-SIGN

Dendritic cell-specific ICAM-3-grabbing non-integrin (DC-SIGN) is a pathogen recognition receptor (PRR) and abundantly expressed on immature dendritic cells (DCs). The binding of pathogens via PRRs mediates phagocytosis, DC maturation and migration from peripheral tissues to draining lymph nodes. After lysosomal degradation, the processed antigen particles are presented to naïve T-cells, resulting in the stimulation of adaptive immune responses. However, a variety of pathogens including HIV-1 use the interaction with DC-SIGN on DCs as initial entry port to their host. These pathogens are able to circumvent the intracellular degradation process and impair DC maturation. DC-SIGN recognizes mannose-containing glycoconjugates and fucose-containing blood-group antigens, such as Lewis<sup>x</sup> (Le<sup>x</sup>), Lewis<sup>a</sup> (Le<sup>a</sup>), and Lewis<sup>y</sup> (Le<sup>y</sup>), in the envelope of viruses and the membranes of parasites. DC-SIGN is therefore considered as a potential drug target for the treatment and prevention of a number of infectious diseases. Consequently, considerable efforts are made to develop DC-SIGN antagonists. These new anti-infectives would inhibit DC-SIGN-pathogen interaction and block the initial step of an infection, as well as the pathogen dissemination.

This thesis addresses the issue of improving the recombinant expression of the carbohydrate recognition domain of DC-SIGN by investigating the effect of different signal peptides on the expression of recombinant protein in CHO-K1 cells. The usage of the luciferase signal peptide of the copepod *Gaussia princeps* led to a drastic improvement of the protein yield compared to the standard interleukin-2 signal peptide. The recombinant protein was used for the evaluation of binding potentials of novel FimH antagonists. A target-based binding assay was developed and a series of antagonists were measured, with the focus on Lewis type structures. Combination of binding assays, mutational analysis, STD NMR studies, and computational modeling revealed a new binding mode with improved affinity for phenyl group-substituted Le<sup>a</sup> compounds. Therefore these compounds display a novel class of potential anti-infectives.

## **Part II: The lectin DC-SIGN**

---

### **DC-SIGN Chapter 1: Introduction**

---

## **DC-SIGN Introduction**

### **Pathogen recognition receptors on dendritic cells**

Dendritic cells (DCs) are specialized antigen presenting cells that play a major role in the initiation and differentiation of immune responses, operating at the interface between innate and adaptive immunity [1]. Immature DCs are abundantly found in peripheral tissues throughout the body, where they recognize invading microorganisms with pattern recognition receptors (PRRs) on their cell surfaces [2]. Antigen binding triggers pathogen uptake by receptor-mediated phagocytosis and antigen processing in lysosomal compartments. Binding also results in DC maturation and migration from the periphery to the lymphoid organs. Here the DCs present pathogenic peptides on major histocompatibility complex (MHC)-class I/II molecules on its surface to resting T cells. Transient interaction between the antigen-MHC complex and the T cell receptor leads to T cell activation and initiation of an adaptive immune response [3].

Depending on their tissue localization and differentiation state, DCs express distinct patterns of PRRs and costimulatory molecules. PRRs recognize pathogen-associated molecular patterns (PAMPs) of microorganisms such as bacterial cell wall components or liposaccharides, as well as double stranded RNA of viruses. DCs are equipped with several different classes of PRRs, including Toll-like receptors (TLRs) [4], scavenger receptors [5], and C-type lectin receptors (CTLs) [6]. These receptors differ in their ligand specificity, and an activation of the DC triggers receptor-specific immune responses [7]. TLRs preferably bind to bacterial and viral lipopolysaccharides (LPS) [8], leading to the release of pro-inflammatory cytokines (IFNs, IL12) and an up-regulation of costimulatory molecules important for T cell activation. Scavenger receptors recognize lipoproteins, while CTLs recognize carbohydrate structures, both leading to pathogen endocytosis and processing in lysosomal compartments [5, 9]. Furthermore, binding of CTLs to self-glycoproteins induces tolerance and maintenance of immune homeostasis, and also mediates cell-cell adhesion and migration processes. Since pathogens generally express several PAMPs, they can simultaneously stimulate multiple PRRs on a single cell. This may result in an interplay of the PRRs and a cross talk between intracellular signaling pathways, tailoring the elicited immune response [10-12].

### The C-type lectin DC-SIGN

C-type lectin receptors share primary structural homology in their carbohydrate recognition domain (CRD) and most CTLs bind sugars in a calcium-dependent manner. The very large family of CTLs includes many endocytotic receptors, proteoglycans [13], as well as all selectins and collectins. The family can be divided in two subgroups, based on an amino-acid motif that is involved in the sugar binding. The CRD of mannose-type C-type lectins contains a Glu-Pro-Asn (EPN) motif, whereas the galactose-type lectins contain a Gln-Pro-Asp (QPD) sequence. EPN motif-containing lectins preferably bind to mannose- or fucose-terminated glycans, whereas QPD motif-containing lectins prefer galactose- or *N*-acetylgalactosamine-terminated glycans [14]. Both types are involved in many immune system functions. They play crucial roles in inflammatory responses, are involved in innate immunity by pathogen recognition and their elimination, and in activation processes of cells of the adaptive immunity. One abundantly expressed EPN-type C-type lectin on dendritic cells and macrophage subpopulations [15] is DC-SIGN, which shapes the immune responses against various pathogens. DC-SIGN is mainly expressed on myeloid DCs, but also found on dermal DCs, interstitial DCs, and a subset of DCs in the blood [16, 17]. This receptor was first described in 1992 by Curtis *et al.* as a membrane associated PRR with a high affinity for the glycoprotein (gp120) on HIV-1 [18]. In 2000, Geijtenbeek and colleagues found the same molecule mediating intercellular interactions with ICAM-3 (intercellular adhesion molecule-3) on resting T cells in the lymphatic tissue [19]. Since up to that time the interaction between DCs and T cells had only been attributed to integrins, they named the protein “DC-specific ICAM-3 grabbing non-integrin” or DC-SIGN.

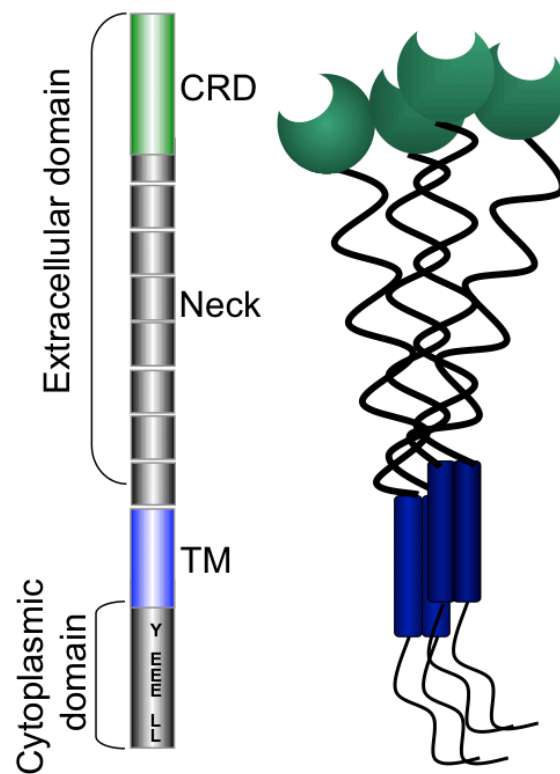


**Figure 1.** Schematic representation of the type II transmembrane protein DC-SIGN. DC-SIGN consists of a cytoplasmic domain bearing the di-leucin motif, tri-acidic internalization motifs and the tyrosin residue, associated with signal transduction. The cytoplasmic domain connects to the transmembrane domain (TM) and the extracellular domain. The extracellular domain is composed of the neck region, characterized by seven and a half repeats of 23 amino acids, and the carbohydrate recognition domain (CRD). DC-SIGN forms tetramers, facilitated by hydrophobic interactions between the neck regions of the monomers.

DC-SIGN is a tetrameric type II transmembrane protein [20], consisting of an N-terminal cytoplasmic domain, connected via a short hydrophobic transmembrane domain to the extracellular domain (Figure 1). Certain amino acid motifs within the intracellular domain, as *e.g.* a di-leucin based motif and a tri-acidic cluster (Glu-Glu-Glu), regulate the internalization and the recycling of the receptor [17]. It also contains a YxxL motif that has been associated with intracellular signaling [21, 22]. The extracellular domain consists of a neck region and the carbohydrate recognition domain (CRD). The hydrophobic neck region bears seven complete and one incomplete tandem repeats of 23 amino acids and is crucial for the tetramerization of the lectin. The globular CRD is composed of 12  $\beta$ -strands, two  $\alpha$ -helices and three disulfide bridges, and is the ligand-binding part of the molecule [23]. It binds two  $\text{Ca}^{2+}$  ions, one being essential for the assembly of the tertiary structure, the other for the

binding of the ligand [24]. DC-SIGN recognizes mannose-containing glycoconjugates [25] and fucose-containing blood-group antigens, such as Lewis<sup>x</sup> (Le<sup>x</sup>), Lewis<sup>a</sup> (Le<sup>a</sup>), and Lewis<sup>y</sup> (Le<sup>y</sup>) [26], in the envelope of viruses and the membranes of parasites. It was shown that DC-SIGN binds to branched high-mannose glycans [24] with a minimum of three internal ( $\alpha 1 \rightarrow 3$ ,  $\alpha 1 \rightarrow 6$ ) or two terminal mannose residues [24]. The receptor multimerization increases the binding avidity for ligands containing repetitive sugar moieties, by forming multivalent interactions. Due to the multimerization, DC-SIGN prefers mannose residues with distinct spatial arrangements [24, 25, 27]. Ultimately, it defines the set of pathogens that are recognized by DC-SIGN, by promoting ligand specificity [28]. An effective binding of various mannose- and fucose-containing oligosaccharides is also provided by DC-SIGN conformational flexibility upon ligand binding [29]. Furthermore, it was shown that DC-SIGN tetramers are organized in clusters in lipid microdomains within the membrane (lipid rafts), which further promote ligand binding, internalization, and signal transduction [30, 31]. As a common feature for endocytotic receptors, DC-SIGN releases ligands at low pH. This allows the separation of DC-SIGN from ligands in the endosomes and the subsequent recycling of the free receptor to the cell surface [32]. Important ligands for DC-SIGN are for example Le<sup>x</sup> containing liposaccharides (LPS) of *Helicobacter pylori* [33], the cell wall component ManLAM of *Mycobacterium tuberculosis* [34, 35], and the envelope glycoprotein gp120 of HIV-1 [20, 36].

Apart from its function as PRR and endocytotic receptor by recognizing PAMPs on microbial surfaces, DC-SIGN also acts as a cell-cell adhesion molecule that binds to endogenous ligands such as ICAM-2 or ICAM-3. ICAM-2 binding on vascular endothelial cells contributes to transendothelial migration [37, 38] of the DC. Interaction with ICAM-3, expressed on resting T cells in the lymph nodes, stabilizes the formation of the synapse between the antigen-MHC class II complex and the T cell receptor, resulting in T cell activation [20]. DCs also interact with neutrophils via DC-SIGN-Mac1 or CEACAM-1 interaction. Neutrophils are part of the innate immunity and mediate immediate removal of pathogens. The interaction with neutrophils directly at the site of an infection activates DCs and instructs them to guide the T cells towards a Th1 response [39]. However, the major function of DC-SIGN is its participation in the initiation of an immune response by pathogen capture [26, 40]. Pathogen binding by DC-SIGN leads to an uptake of the pathogen, DC maturation and initiation of the adaptive immune response.

### DC-SIGN signaling and HIV-1 infection

Pathogens recognized by DC-SIGN are generally internalized and immediately degraded by the DC. However, a variety of pathogens exploit DC-SIGN to infect their host, including viruses (HIV-1 [20, 36], Ebola virus [41], Hepatitis C virus (HCV) [42, 43], Dengue virus [44], Herpes simplex virus [45], SARS corona virus [46]), bacteria (*M.tuberculosis* [34, 35]), fungi (*Candida albicans* [47]) and parasites (Leishmania [26]). These pathogens are able to circumvent the intracellular degradation process and use the interaction with DC-SIGN on DCs as initial entry port to their host. In case of HIV-1, the virus survives inside of the DCs in multivesicular bodies. It retains its infectiveness until the infected DC has migrated from the site of infection to the lymph node, where HIV-1 is efficiently transmitted to CD4<sup>+</sup> T cells (Figure 2).

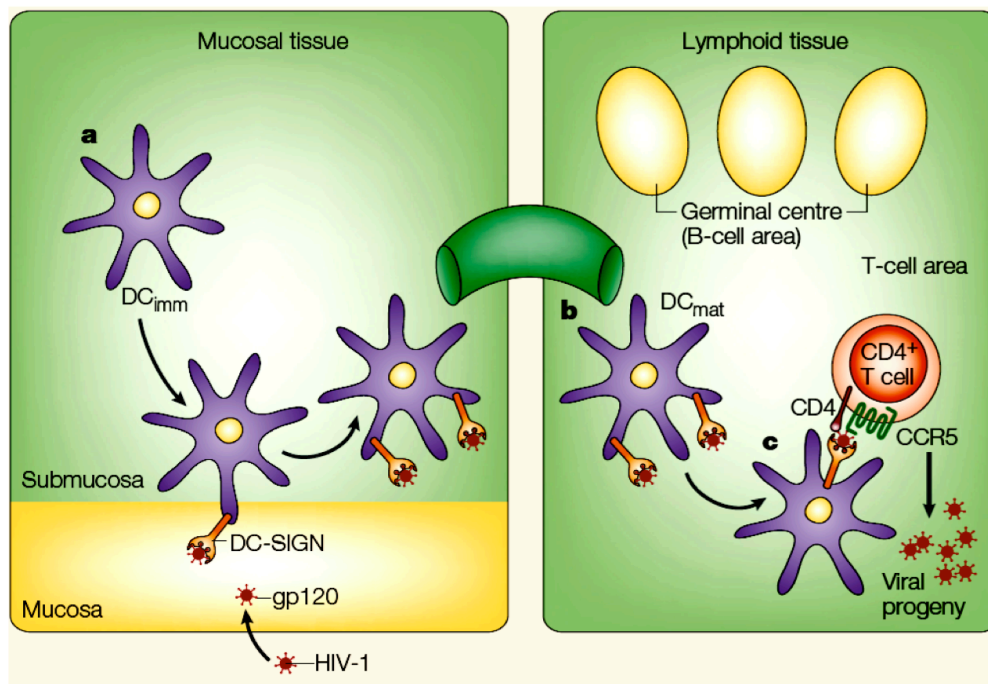


**Figure 2.** Role of dendritic cells and DC-SIGN in HIV-1 infection, taken from [9]. The immature DC binds via DC-SIGN to the envelope protein gp120 on HIV-1, which has entered peripheral tissues of the host (mucosa, skin). The activated DC migrates via the lymph vessels to secondary lymphoid organs, where it encounters resting T cells. HIV-1 can evade the normal degradation processes and is thus able to infect CD4<sup>+</sup>/CCR5 T cells. This process is termed “infection *in trans*”.

The pathogens exploit DC-SIGN signaling to benefit their survival and dissemination. Up to now, it is still speculative how ligand binding leads to the induction of signal transduction by DC-SIGN. However, it is known that DC-SIGN signaling can either function independently,

or it can modulate the responses of other PRRs such as TLRs [48]. The triggered signaling and the specific modulation of immune responses are tailored to the type of pathogen involved and can therefore differ between pathogens. Signaling by *M.tuberculosis*, HIV-1, and *C.albicans* activates Raf-1 by interacting with Ras-1, which induces Raf-1 phosphorylation of the residues Y340/341 or S338 by Src kinases or Pak [49, 50] (Figure 3). The activation of Raf-1 mediates phosphorylation of the transcription factor NFκB subunit 65 at residue S276. In addition, NFκB needs to be previously activated by TLR signaling. The active heterodimers of subunits p65 and p50 then translocate into the nucleus, where they bind to the promoters of target genes and initiate their transcription. The NFκB activation upon TLR stimulation is essential for the induction of DC-SIGN triggered immune responses. The activity of p65, which is the transcriptionally active component, is regulated by several posttranslational modifications, such as phosphorylation and acetylation. DC-SIGN-dependent phosphorylation by Raf-1 induces the acetylation of p65, resulting in enhanced and sustained transcription of the IL-10 gene [51]. Thus, DC-SIGN signaling controls NFκB activity and modulates TLR responses. IL-10 is an immunosuppressive cytokine, but it is presumed that p65 acetylation also modulates pro-inflammatory genes. The net immune response is dependent on the entity of cytokines that are stimulated by DC-SIGN signaling, and this needs to be further investigated. However, almost all pathogens binding to DC-SIGN cause chronic infections and successfully manipulate the Th1/Th2 balance. Promoting Th2 cell proliferation is often crucial for virulence and persistence of intracellular pathogens [52]. Furthermore, Gringhuis *et al.* have demonstrated that mannose- and fucose-presenting pathogens induce different TLR-induced DC-SIGN signaling pathways. Mannose containing pathogens, such as HIV-1 and *M.tuberculosis* enhance IL-10, IL-12, and IL-6 secretion, while fucose-containing ligands induce IL-10, but suppress IL-12 and IL-6 secretion [53].



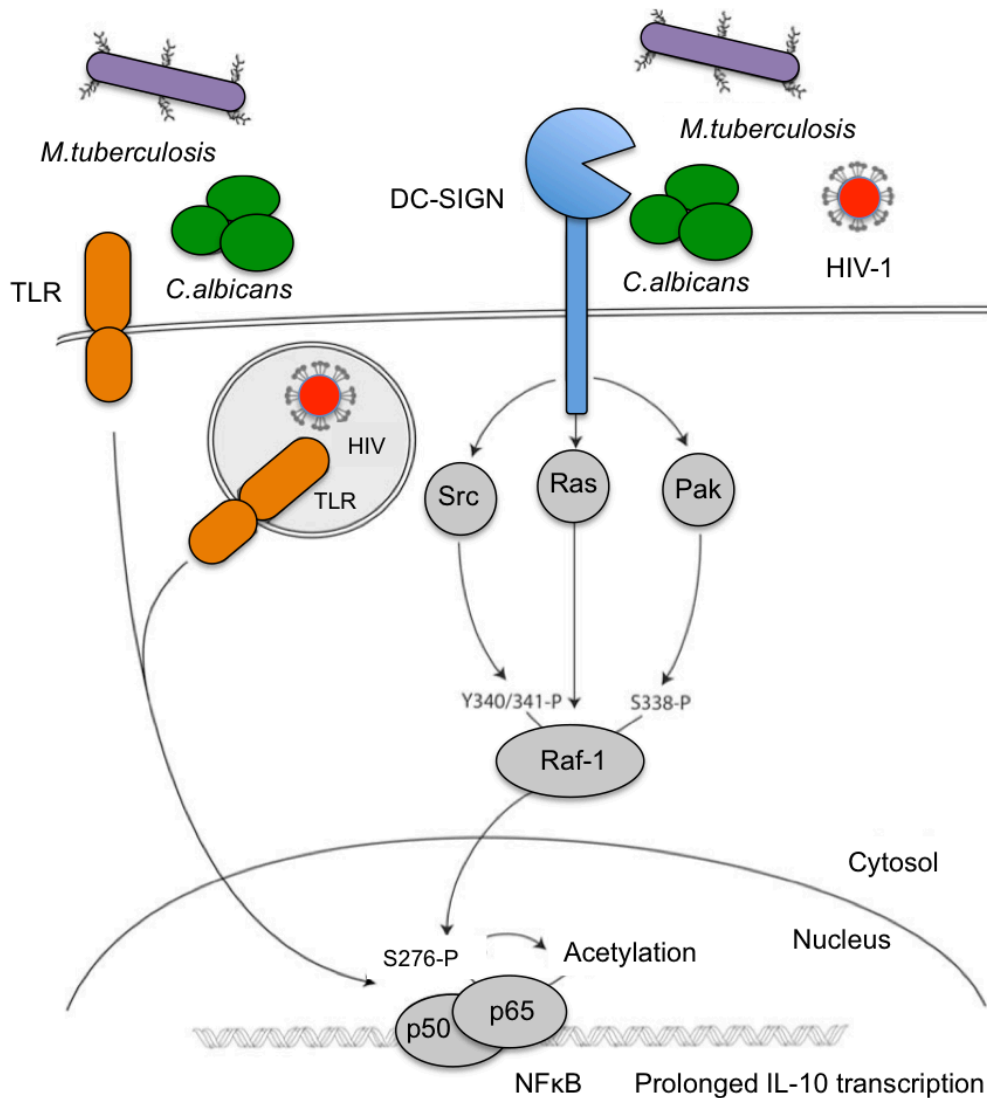


**Figure 3.** Signaling pathway in DCs, triggered by binding to HIV-1, *C.albicans*, and *M.tuberculosis* (adapted from [54]). The pathogens bind with different PAMPs to TLRs and DC-SIGN. TLR signaling activates NFκB, a heterodimer composed of the subunits p65 and p50. Upon activation NFκB translocates into the nucleus, where it binds to target DNA sequences, such as the IL-10 promoter. DC-SIGN binding to Ras induces the activation of Raf-1 and its subsequent phosphorylation via src kinases or Pak. Activated Raf-1 triggers the phosphorylation of the p65 subunit of NFκB, eliciting its acetylation. This posttranslational modification enhances NFκB activity and results in a prolonged IL-10 transcription.

In the case of HIV-1, it was shown that its virulence requires signaling elicited by the binding of viral ssRNA to endosomal TLR8, as well as by the binding of gp120 to DC-SIGN. Binding to TLR8 activates NFκB, which then binds to proviral DNA integrated in the host genome. NFκB initiates transcription by RNA polymerase II (RNAPII), but an additional

phosphorylation of the RNAPII induced by DC-SIGN signaling is necessary to prolong the transcriptional activity. This modification is crucial for the transcription of full-length viral transcripts, and thus pivotal for HIV-1 virulence [55, 56]. In addition to this effect and the enhanced transcription of IL-10 via NF $\kappa$ B, DC-SIGN signaling also impairs dendritic cell maturation and T cell proliferation [57], thereby promoting systemic infection of the host. Furthermore, it was shown that upon HIV-1 infection DC-SIGN expression gets up-regulated, which further enhances the infectivity [58]. However, it is presumed that the suppression of the immune response by the pathogen via DC-SIGN also benefits the host, since it prevents an excessive immune activation, which might harm the host as well.

### **The carbohydrate recognition domain (CRD) of DC-SIGN**

The DC-SIGN CRD was co-crystalized with different mannosides [32, 59] and lacto-*N*-fucopentaose III (LNFP III), which contains the Le<sup>x</sup> trisaccharide [32]. These studies revealed a shallow binding site of DC-SIGN. In this binding site, mannose complexes the Ca<sup>2+</sup>-ion with its 3- and 4-OH in an equatorial-equatorial manner, whereas the 3- and 4-OH of the LNFP III fucose complex the Ca<sup>2+</sup>-ion in an equatorial-axial manner (Figure 4). Therefore, the fucose is tipped in comparison to the mannose and is able to form additional tight van der Waals contacts with the 2-OH to Val351. The galactose moiety in the Le<sup>x</sup> motif contributes to the binding by forming water-bridged hydrogen bonds via the 4-OH with Asp367 and Glu358, and via the 6-OH with Leu371. The GlcNAc of Le<sup>x</sup> is positioned in a vertical manner and points towards the solvent (Figure 5). Mannose-containing oligosaccharides involve an extended secondary binding site lined by Phe313. This amino acid seems to contribute to the selectivity as well as to the affinity [32] (Figure 6). Mannose- and fucose-based ligands show overlapping, but distinct binding modes. These differences might be the reason for the different biological effects of mannose- and fucose-based ligands, as discussed earlier [33].

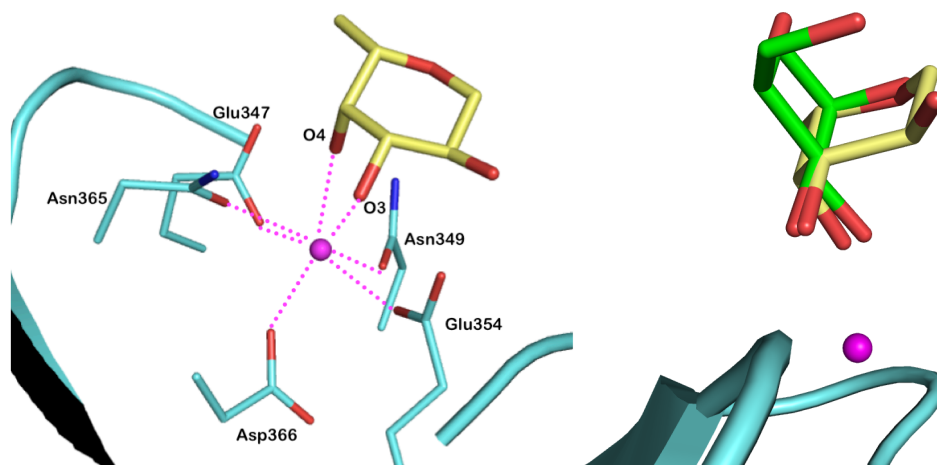


**Figure 4.** Coordination of  $\text{Ca}^{2+}$  by terminal 3- and 4-OHs of fucose in LNFP III (left). Since  $\text{Ca}^{2+}$  (magenta sphere) is coordinated by one equatorial and one axial OH group, fucose is “tipped” (yellow carbons, right) compared to mannose, coordinating the  $\text{Ca}^{2+}$  by two equatorial OH groups (green carbons) (PDB entry 1SL5 [32], modeled by Sameh Eid).

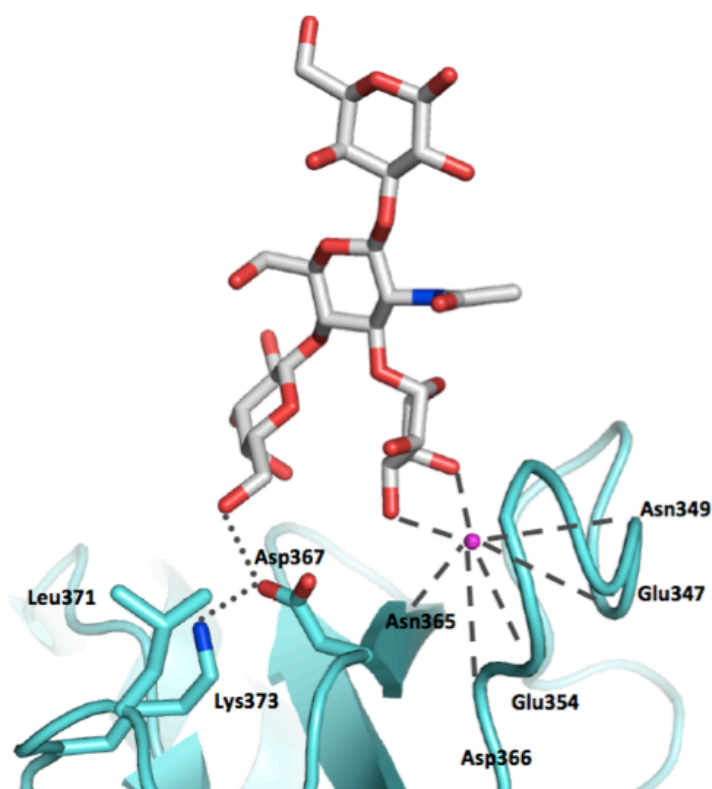


**Figure 5.** Binding mode of the resolved part of LNFP. Dashed lines show  $\text{Ca}^{2+}$  (magenta sphere) coordination by 3- and 4-OH of fucose. The galactose moiety points towards the solvent (PDB entry 1SL5 [32], modeled by Sameh Eid).

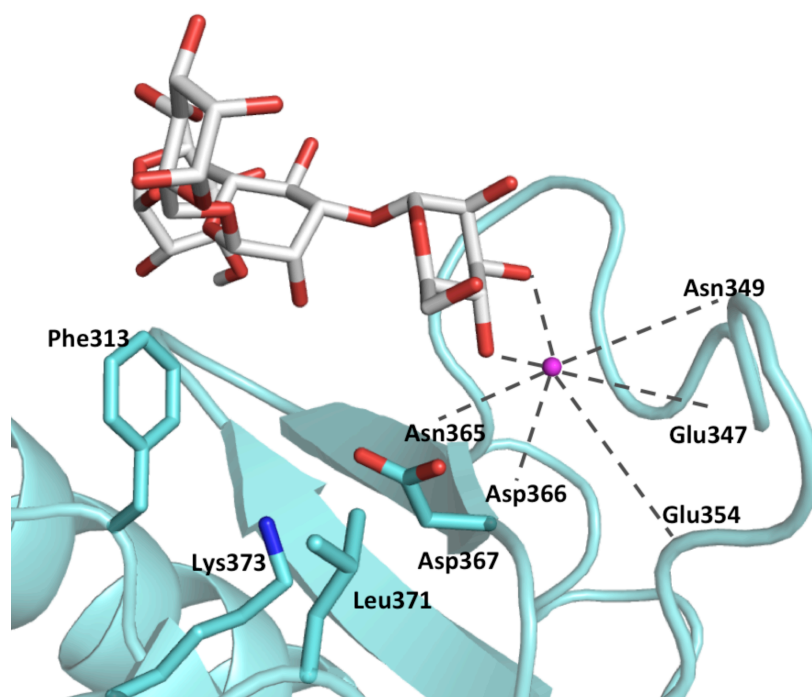


**Figure 6.** Binding mode of the resolved part of Man<sub>4</sub> (green carbons). Dashed lines show Ca<sup>2+</sup> (magenta sphere) coordination by 3- and 4-OH of mannose. Man-2 and Man-3 are interacting with a secondary binding site lined by Phe313. (PDB entry 1SL4 [32], modeled by Sameh Eid).

### DC-SIGN antagonists

Since a variety of pathogens use the interaction with DC-SIGN on DCs as initial entry port to their host, DC-SIGN is considered as a potential therapeutic target for the treatment and prevention of a number of infectious diseases [60]. Consequently, *considerable efforts* are made to develop DC-SIGN antagonists [23, 25, 61, 62]. These new anti-infectives would inhibit DC-SIGN-pathogen interaction and block the initial step in an infection and the pathogen dissemination.

To date, studies have only shown *in vitro* data on the investigation of antagonists. Poor pharmacokinetic properties of carbohydrate-based antagonists make the design of therapeutically applicable and active compounds a challenging task. The main carbohydrate ligand for DC-SIGN on glycoproteins of pathogens is the high-mannose glycan Man<sub>9</sub>GlcNAc<sub>2</sub>, with a moderate affinity in the micromolar range (gp120, GP1, etc.) [59, 63]. Affinities of monosaccharides such as D-mannose, L-fucose, and methyl- $\alpha$ -D-mannopyranoside are generally weak with K<sub>D</sub>-values in the millimolar range [25]. Up to now, several approaches to enhance the affinity of ligands by generating multivalent antagonists were explored. Oligomannose glycodendrons successfully block DC-SIGN in a glycan array

assay and an ELISA based assay, with affinities in the nanomolar range [64]. Furthermore, oligomannoside-functionalized gold glyco-nanoparticles were able to inhibit DC-SIGN-mediated trans-infection of T cells by HIV-1 at nanomolar concentrations [65]. Sattin *et al.* showed that a tetravalent dendron containing four copies of a linear trimannose mimic inhibited trans-HIV infection at low micromolar concentrations [66]. Although these polyvalent molecules are not suitable for a systemic administration due to their poor pharmacokinetic properties and toxicity, they might be administrated topically at the sites of infection, e.g. at mucosal surfaces.

Binding affinities of Lewis-type structures to DC-SIGN have not been extensively determined so far, although they show much higher selectivity [67]. Monovalent Le<sup>x</sup> exhibits an affinity in the low millimolar range [61], whereas Le<sup>a</sup> shows a slightly higher relative binding affinity to DC-SIGN [63]. Recently, fucose-based Le<sup>x</sup> mimics, with a fucosylamide linker replacing the metabolically unstable  $\alpha$ -glycosidic bond were synthesized. These exhibit similar affinities to Le<sup>x</sup>, but with low binding affinities to the C-type lectin Langerin [61, 67]. Monovalent non-carbohydrate inhibitors with IC<sub>50</sub> values in the micromolar range were identified in a high-throughput fluorescence-based competition assay and were also effective in DC-SIGN-dependent cell adhesion assays [68]. The binding mode of these non-carbohydrate ligands remains unknown. Furthermore, DNA aptamers against DC-SIGN were selected, exhibiting affinities in the nanomolar range [69]. Recently, the hydrophobic region lined with Phe313 was employed to improve affinity of glycomimetic DC-SIGN antagonists [70]. Mannopyranosides substituted with a phenyl ring exhibited an increased binding affinity, implying that the phenyl ring makes contributing hydrophobic interactions with the Phe313. Le<sup>x</sup> structures with a sialylated or sulfated 3-OH group of galactose abrogated binding to DC-SIGN. Based on the crystal structure these ligand exclusions could be caused by steric hindrances of Phe313 and by electrostatic repulsion [32].

Since DC-SIGN is a pathogen recognition receptor with signaling functions, DC-SIGN antagonists are also potential agonists that might activate the receptor upon binding. In fact, it might even be that antagonists activate different signaling cascades, depending on their structure. With no integral assay existing up to now, analysis of the exact biological effects of novel antagonists remains a future challenge. And although one can deduce great potential for the developed DC-SIGN antagonists from *in vitro* assays, there is still a great need for improving affinity, selectivity and drug-like properties of DC-SIGN antagonists, before a potent anti-infective can be developed.

---

**Literature**

1. Banchereau J, Briere F, Caux C, Davoust J, Lebecque S, Liu YT, Pulendran B, Palucka K, *Annu. Rev. Immunol.* **2000**, *18*:767.
2. Banchereau J, Steinman RM, *Nature* **1998**, *392*(6673):245-252.
3. Clark GJ, Angel N, Kato M, Lopez JA, MacDonald K, Vuckovic S, Hart DNJ, *Microbes Infect* **2000**, *2*(3):257-272.
4. Underhill DM, Ozinsky A, *Curr. Opin. Immunol.* **2002**, *14*(1):103-110.
5. Peiser L, Mukhopadhyay S, Gordon S, *Curr. Opin. Immunol.* **2002**, *14*(1):123-128.
6. Weis W, *Abstr Pap Am Chem Soc.* **1998**, *215*(1-2):22.
7. Janeway CA, Jr., Medzhitov R, *Annu. Rev. Immunol.* **2002**, *20*:197-216.
8. Akira S, *J. Invest. Dermatol.* **2003**, *121*(5):1234-1234.
9. Figdor CG, van Kooyk Y, Adema GJ, *Nat. Rev. Immunol.* **2002**, *2*(2):77-84.
10. Creagh EM, O'Neill LAJ, *Trends Immunol.* **2006**, *27*(8):352-357.
11. Gantner BN, Simmons RM, Canavera SJ, Akira S, Underhill DM, *J. Exp. Med.* **2003**, *197*(9):1107-1117.
12. Hunger RE, Surovy AM, Hassan AS, Braathen LR, Yawalkar N, *Br. J. Dermatol.* **2008**, *158*(4):691-697.
13. Aspegren A, Miura R, Bourdoulous S, Shimonaka M, Heinegard D, Schachner M, Ruoslahti E, Yamaguchi Y, *Proc. Natl. Acad. Sci. U.S.A.* **1997**, *94*(19):10116-10121.
14. Taylor, M.E. and Drickamer, K, Introduction to glycobiology, *Oxford University Press*, Oxford. **2003**, 207 pp.
15. Granelli-Piperno A, Pritsker A, Pack M, Shimeliovich I, Arrighi JF, Park CG, Trumpfheller C, Piguet V, Moran TM, Steinman RM, *J. Immunol.* **2005**, *175*(7):4265-4273.
16. Geijtenbeek TBH, van Vliet SJ, Engering A, t Hart BA, van Kooyk Y, *Annu. Rev. Immunol.* **2004**, *22*:33-54.
17. Engering A, Geijtenbeek TBH, van Vliet SJ, Wijers M, van Liempt E, Demaurex N, Lanzavecchia A, Franssen J, Figdor CG, Piguet V *et al*, *J. Immunol.* **2002**, *168*(5):2118-2126.
18. Curtis BM, Scharnowske S, Watson AJ, *Proc. Natl. Acad. Sci. U.S.A.* **1992**, *89*(17):8356-8360.
19. Geijtenbeek TBH, Torensma R, van Vliet SJ, van Duijnhoven GCF, Adema GJ, van Kooyk Y, Figdor CG, *Cell* **2000**, *100*(5):575-585.

20. Geijtenbeek TBH, Torensma R, Kwon D, van Vliet SJ, van Duijnhoven GCF, Adema GJ, KewalRamani V, Littman D, Figdor CG, van Kooyk Y, *Tissue Antigens*. **2000**, 55(Supplement 1):56.
21. Fuller GLJ, Williams JAE, Tomlinson MG, Eble JA, Hanna SL, Pohlmann S, Suzuki-Inoue K, Ozaki Y, Watson SP, Pearce AC, *J. Biol. Chem.* **2007**, 282(17):12397-12409.
22. Gantner BN, Simmons RM, Underhill DM, *EMBO J.* **2005**, 24(6):1277-1286.
23. Feinberg H, Guo Y, Conroy E, Mitchell D, Alvarez R, Blixt O, Taylor M, Drickamer K, Weis W, *Glycobiology* **2005**, 15(11):35.
24. Feinberg H, Mitchell DA, Drickamer K, Weis WI, *Science* **2001**, 294(5549):2163-2166.
25. Mitchell DA, Fadden AJ, Drickamer K, *J. Biol. Chem.* **2001**, 276(31):28939-28945.
26. Appelmelk BJ, van Die I, van Vliet SJ, Vandenbroucke-Grauls C, Geijtenbeek TBH, van Kooyk Y, *J. Immunol.* **2003**, 170(4):1635-1639.
27. Geijtenbeek TBH, van Duijnhoven GCF, van Vliet SJ, Krieger E, Vriend G, Figdor CG, van Kooyk Y, *J. Biol. Chem.* **2002**, 277(13):11314-11320.
28. Frison N, Taylor ME, Soilleux E, Bousser MT, Mayer R, Monsigny M, Drickamer K, Roche AC, *J. Biol. Chem.* **2003**, 278(26):23922-23929.
29. Menon S, Rosenberg K, Graham SA, Ward EM, Taylor ME, Drickamer K, Leckband DE, *Proc. Natl. Acad. Sci. U.S.A.* **2009**, 106(28):11524-11529.
30. Cambi A, de Lange F, van Maarseveen NM, Nijhuis M, Joosten B, van Dijk E, de Bakker BI, Fransen JAM, Bovee-Geurts PHM, van Leeuwen FN *et al*, *J. Cell Biol.* **2004**, 164(1):145-155.
31. Koopman M, Cambi A, Joosten B, Garcia-Parajo MF, Figdor CG, van Hulst NF, *Biophys. J.* **2004**, 86(1):363A-364A.
32. Guo P, Feinberg H, Conroy E, Mitchell DA, Alvarez R, Blixt O, Taylor ME, Weis WI, Drickamer K, *Nat. Struct. Mol. Biol.* **2004**, 11(7):591-598.
33. Gringhuis SI, den Dunnen J, Litjens M, van der Vlist M, Geijtenbeek TB, *Nat. Immunol.* **2009**, 10(10):1081-1088.
34. Geijtenbeek TBH, van Vliet SJ, Koppel EA, Sanchez-Hernandez M, Vandenbroucke-Grauls C, Appelmelk B, van Kooyk Y, *J. Exp. Med.* **2003**, 197(1):7-17.
35. Tailleux L, Schwartz O, Herrmann JL, Pivert E, Jackson M, Amara A, Legres L, Dreher D, Nicod LP, Gluckman JC *et al*, *J. Exp. Med.* **2003**, 197(1):121-127.

36. Gurney KB, Elliott J, Nassanian H, Song C, Soilleux E, McGowan I, Anton PA, Lee B, *J. Virol.* **2005**, *79*(9):5762-5773.
37. Geijtenbeek TBH, Krooshoop D, Bleijs DA, van Vliet SJ, van Duijnhoven GCF, Grabovsky V, Alon R, Figdor CG, van Kooyk Y, *Nat. Immunol.* **2000**, *1*(4):353-357.
38. Garcia-Vallejo JJ, van Liempt E, Martins PdC, Beckers C, van het Hof B, Gringhuis SI, Zwaginga J-J, van Dijk W, Geijtenbeek TBH, van Kooyk Y *et al*, *Mol. Immunol.* **2008**, *45*(8):2359-2369.
39. Ludwig IS, Geijtenbeek TBH, van Kooyk Y, *Curr Opin Pharmacol.* **2006**, *6*(4):408-413.
40. Cambi A, Figdor CG, *Curr. Opin. Cell Biol.* **2003**, *15*(5):539-546.
41. Alvarez CP, Lasala F, Carrillo J, Muniz O, Corbi AL, Delgado R, *J. Virol.* **2002**, *76*(13):6841-6844.
42. Lozach PY, Lortat-Jacob H, de Lavalette AD, Staropoli I, Foung S, Amara A, Houles C, Fieschi F, Schwartz O, Virelizier JL *et al*, *J. Biol. Chem.* **2003**, *278*(22):20358-20366.
43. Ludwig IS, Lekkerkerker A, Depla E, Depraetere S, van Kooyk Y, Geijtenbeek T, *Immunobiology* **2004**, *209*(4-6):390.
44. Tassaneetrithep B, Burgess TH, Granelli-Piperno A, Trumpfherer C, Finke J, Sun W, Eller MA, Pattanapanyasat K, Sarasombath S, Birx DL *et al*, *J. Exp. Med.* **2003**, *197*(7):823-829.
45. de Jong MAWP, de Witte L, Bolmstedt A, van Kooyk Y, Geijtenbeek TBH, *J. Gen. Virol.* **2008**, *89*:2398-2409.
46. Han DP, Lohani M, Cho MW, *J. Virol.* **2007**, *81*(21):12029-12039.
47. Cambi A, Gijzen K, de Vries JM, Torensma R, Joosten B, Adema GJ, Netea MG, Kullberg BJ, Romani L, Figdor CG, *Eur. J. Immunol.* **2003**, *33*(2):532-538.
48. van Vliet SJ, den Dunnen J, Gringhuis SI, Geijtenbeek TBH, van Kooyk Y, *Curr. Opin. Immunol.* **2007**, *19*(4):435-440.
49. Gringhuis SI, den Dunnen J, Litjens M, Hof Bvh, van Kooyk Y, Geijtenbeek TBH, *Immunity* **2007**, *26*(5):605-616.
50. Wellbrock C, Karasarides M, Marais R, *Nat. Rev. Mol. Cell Biol.* **2004**, *5*(11):875-885.
51. Hayden MS, Ghosh S, *Genes Dev* **2004**, *18*(18):2195-2224.
52. van Kooyk Y, Geijtenbeek TBH, *Nat. Rev. Immunol.* **2003**, *3*(9):697-709.



53. Gringhuis SI, den Dunnen J, Litjens M, van der Vlist M, Geijtenbeek TBH, *Nat. Immunol.* **2009**, *10*(10):1081-U1058.
54. den Dunnen J, Gringhuis SI, Geijtenbeek TB, *Cancer Immunol. Immunother.* **2009**, *58*(7):1149-1157.
55. Gringhuis SI, van der Vlist M, van den Berg LM, den Dunnen J, Litjens M, Geijtenbeek TBH, *Nat. Immunol.* **2010**, *11*(5):419-U481.
56. Gringhuis SI, Geijtenbeek TBH, *Methods Enzymol.* **2010**, *480*:151-64.
57. Hodges A, Sharrocks K, Edelmann M, Baban D, Moris A, Schwartz O, Drakesmith H, Davies K, Kessler B, McMichael A *et al*, *Nat. Immunol.* **2007**, *8*(6):569-577.
58. Sol-Foulon N, Moris A, Nobile C, Boccaccio C, Engering A, Abastado JP, Heard JM, van Kooyk Y, Schwartz O, *Immunity* **2002**, *16*(1):145-155.
59. Feinberg H, Castelli R, Drickamer K, Seeberger PH, Weis WI, *J. Biol. Chem.* **2007**, *282*(6):4202-4209.
60. Ernst B, Magnani JL, *Nat Rev Drug Discov* **2009**, *8*(8):661-677.
61. Timpano G, Tabarani G, Anderluh M, Invernizzi D, Vasile F, Potenza D, Nieto PM, Rojo J, Fieschi F, Bernardi A, *Chembiochem* **2008**, *9*(12):1921-1930.
62. Borrok MJ, Kiessling LL, *J. Am. Chem. Soc.* **2007**, *129*:12780-12785.
63. van Liempt E, Bank CMC, Mehta P, Garcia-Vallejo JJ, Kawar ZS, Geyer R, Alvarez RA, Cummings RD, van Kooyk Y, van Die I, *FEBS Lett.* **2006**, *580*(26):6123-6131.
64. Wang SK, Liang PH, Astronomo RD, Hsu TL, Hsieh SL, Burton DR, Wong CH, *Proc. Natl. Acad. Sci. U.S.A.* **2008**, *105*(10):3690-3695.
65. Martinez-Avila O, Bedoya LM, Marradi M, Clavel C, Alcamí J, Penades S, *Chembiochem* **2009**, *10*(11):1806-1809.
66. Sattin S, Daggetti A, Thepaut M, Berzi A, Sanchez-Navarro M, Tabarani G, Rojo J, Fieschi F, Clerici M, Bernardi A, *ACS Chem. Biol.* **2010**, *5*(3):301-312.
67. Andreini M, Doknic D, Sutkeviciute I, Reina JJ, Duan J, Chabrol E, Thepaut M, Moroni E, Doro F, Belvisi L *et al*, *Org. Biomol. Chem.* **2011**, *9*(16):5778-5786.
68. Garber KC, Wangkanont K, Carlson EE, Kiessling LL, *Chem. Commun. (Camb.)* **2010**, *46*(36):6747-6749.
69. Hui Y, Shan L, Lin-Fu Z, Jian-Hua Z, *Mol. Cell. Biochem.* **2007**, *306*(1-2):71-77.
70. Obermajer N, Sattin S, Colombo C, Bruno M, Svajger U, Anderluh M, Bernardi A, *Mol. Divers.* **2011**, *15*(2):347-360.

## **Part II: The lectin DC-SIGN**

---

**DC-SIGN Chapter 2: Results and discussion**

**Manuscript 1**

---

## Optimization of Recombinant Protein Expression in the Mammalian Cell System by the Choice of the Signal Peptide

Meike Scharenberg, Mirco Cassina, Said Rabbani, and Beat Ernst\*

Institute of Molecular Pharmacy, Pharmacenter, University of Basel, Switzerland  
Klingelbergstrasse 50, 4056 Basel, Switzerland

Meike Scharenberg, [meike.scharenberg@unibas.ch](mailto:meike.scharenberg@unibas.ch), +41 61 267 1559

Mirco Cassina, [mirco.cassina@stud.unibas.ch](mailto:mirco.cassina@stud.unibas.ch), +41 61 267 1559

Said Rabbani, [Said.rabbani@unibas.ch](mailto:Said.rabbani@unibas.ch), +41 61 267 1559

\*Correspondence to Prof. Dr. Beat Ernst, Institute of Molecular Pharmacy, Pharmacenter, University of Basel, Klingelbergstrasse 50, CH-4056 Basel, Switzerland

Tel: +41 61 267 1551

Fax: +41 61 267 1552

Email: [beat.ernst@unibas.ch](mailto:beat.ernst@unibas.ch)

For submission to Protein Expression and Purification.

**Keywords:** Mammalian expression system, CHO cells, Kozak sequence, signal peptide, *Gaussia princeps* luciferase, interleukin-2, DC-SIGN.

**Abbreviations:** AA, amino acid; ABTS, 2,2'-azino-di-(3-ethylbenzthiazoline-6-sulfonic acid); BSA, bovine serum albumin; CHO cells, chinese hamster ovary cells; CRD; carbohydrate recognition domain; DC, dendritic cell; DC-SIGN, DC-specific ICAM-3-grabbing non-integrin; EDTA, ethylenediaminetetraacetic acid; FCS, fetal calf serum; IgG, immunoglobulin G; IL, interleukin; Le<sup>a</sup>, Lewis<sup>a</sup>; ss, signal peptide; OD, optical density; PAA, polyacrylamide; HEPES, 4-(2-hydroxyethyl)-piperazine-1-ethanesulfonic acid; PRR, pathogen recognition receptor; SDS, sodium dodecylsulfate; SRP, signal recognition particles.

## Abstract

Proteins such as enzymes and receptors are indispensable tools in the drug discovery and development process. The growing number of tests necessary to proof the *in vitro* effect of a drug candidate requires high amounts of high quality proteins. In this study we investigated the effect of different signal peptides on the expression of recombinant human DC-SIGN in CHO-K1 cells. DC-SIGN is considered a potential therapeutic target for the treatment and prevention of various infectious diseases, such as HIV-1. However, testing the potency of DC-SIGN antagonists requires preparative amounts of this protein. We engineered CHO-K1 cell lines that stably overexpress the carbohydrate recognition domain (CRD) of DC-SIGN. The cDNA of the DC-SIGN gene was fused to an extended Kozak sequence in combination with different signal peptides. The usage of the luciferase signal peptide of the copepod *Gaussia princeps* led to a drastic improvement of the protein yield, compared to the standard interleukin-2 signal peptide. This communication emphasizes the role of genetic refinement for high-level production of recombinant genes.

## Introduction

Quantitative amounts of highly pure and active proteins are required for the supply of proteins for therapeutic purposes and during the early phase of drug development, *e.g.* for the characterization of ligand-protein interactions and screening applications. Protein expression is commonly performed in mammalian, bacterial, yeast, or insect cells [1]. Although the expression of recombinant proteins in mammalian cells is less efficient and more expensive compared to other systems [2-4], the quality of the protein compensates for these drawbacks, especially when expressing human proteins with complex posttranslational modifications. Posttranslational modifications are limited in bacteria and yeast, and missing modifications can negatively influence the functionality of the protein of interest [5]. In addition, the expression of mammalian proteins in bacteria often leads to their accumulation as inclusion bodies. *In vitro* refolding of inclusion bodies into proteins with native conformations is a cumbersome and time-consuming process. Therefore, mammalian cells have become the system of preference for the production of human proteins for research and clinical applications [5].

Increasing the expression of recombinant proteins in the mammalian cell system has been either achieved by refining growth conditions or by genetic engineering of the expression vector, increasing both transcription and translation levels [6-9]. According to Marilyn Kozak, translation efficiency in eukaryotic cells can be enhanced to a great extent by using a distinct translation initiation code in mRNAs, called the Kozak sequence [6]. That sequence was found to be a consensus sequence for initiation in higher eukaryotes and can be used to enhance the expression of recombinant proteins. It was shown, that an adenine (A) or a guanine (G) in position -3 (*i.e.* three nucleotides upstream from the AUG codon) and a G in position +4 boosted the recognition efficiency of the AUG codon by the scanning ribosomes more than 60%. Up to three repeats of the three-nucleotide motif G(A)CC preceding the AUG triplet further enhances this effect.

Recently, it was demonstrated that individual signal peptides (secretion signal, ss) show high variations in their secretion efficiency of proteins [10-12]. Although there is little homology in the overall amino acid sequence, signal peptides consist of three domains, a positively charged N-terminus, a hydrophobic central core and a C-terminal cleavage region [13]. Studies revealed that the basic N-terminal and the hydrophobic core regions are essential for protein translocation by mediating the interaction with signal recognition particles (SRPs). The physical properties of both regions influence the affinity of the signal peptide for SRPs

and hence the efficiency of the protein export. Zhang *et al.* [10] investigated the influence of single amino acid mutations in the commonly used human interleukin-2 signal peptide (IL-2 ss) on the protein secretion level. They were able to augment the secretion up to 3.5 fold by increasing the basicity and the hydrophobicity of the IL-2 signal peptide. Knappskog *et al.* [14] demonstrated that the use of a luciferase signal peptide derived from the marine copepod *Gaussia princeps* led to a substantial increase of the expression of human endostatin. However, the efficiency of the signal peptide seems to be dependent on the target protein. Up to date, human endostatin is the only mammalian protein equipped with a *Gaussia princeps* luciferase signal peptide that has been investigated. A quantitative evaluation on absolute protein expression yields induced by different signal peptides has not yet been reported.

In this study, we investigated the recombinant expression of the human DC-specific ICAM-3-grabbing non-integrin (DC-SIGN). DC-SIGN is a pathogen recognition receptor (PRR) and abundantly expressed on immature dendritic cells (DCs) [15]. The binding of pathogens via PRRs mediates phagocytosis, DC maturation and migration from peripheral tissues to draining lymph nodes. After lysosomal degradation, the processed antigen particles are presented to naïve T-cells, resulting in the stimulation of adaptive immune responses [16]. However, a variety of pathogens including HIV-1 use the interaction with DC-SIGN on DCs as initial entry port to their host. These pathogens are able to circumvent the intracellular degradation process and impair DC maturation [17, 18]. DC-SIGN is therefore considered as a potential drug target for the treatment and prevention of a number of infectious diseases [19]. Consequently, considerable efforts are made to develop DC-SIGN antagonists [20-23]. The evaluation of such antagonists requires preparative amount of protein.

In this study three constructs were investigated, in which the human DC-SIGN cDNA was combined with an extended Kozak sequence and different signal peptides. The constructs were transfected into CHO cells and after selection of stable clones the protein expression was quantitatively evaluated. Here, we demonstrate that the choice of the signal peptide is a crucial factor for enhancing protein expression in mammalian cells. The *Gaussia princeps* luciferase signal peptide was superior to the commonly used interleukin-2 signal peptide, which is known for its efficient secretion *in vivo*. Protein quality control was performed using a target-based binding assay, which also allows the determination of IC<sub>50</sub> values for DC-SIGN antagonists.

## Material and Methods

**Cloning of DC-SIGN-CRD-IgG-Fc.** The plasmid containing the full-length cDNA of DC-SIGN was kindly provided by Daniel A. Mitchell (Glycobiology Institute, Department of Biochemistry, University of Oxford). Standard molecular techniques [24] were used for the cloning of the DC-SIGN-carbohydrate recognition domain. Three different DC-SIGN-CRD-IgG-Fc inserts (DC-SIGN: GenBank accession no. M98457, aa residues 250-404) were generated, each of them containing the extended Kozak sequence and either the IL-2 ss (GenBank accession no. NM\_000586), a modified IL-2 ss (Table 1), or a codon-usage optimized *Gaussia princeps* luciferase ss (GenBank accession no. AY015993). Overhang primers containing the signal peptides were used on the original plasmid (pFUSE-hIgG2-Fc2 vector, Lucerne, Switzerland) encoding DC-SIGN-CRD-IgG-Fc. The inserts were ligated into the corresponding cloning site of the pcDNA3.1(+) expression vector (Invitrogen, Lucerne, Switzerland) using the *Bam*HI and *Eco*RV restriction sites. The N-terminal sequences of each construct are summarized in Table 1.

The plasmids were transformed into chemo-competent DH5 $\alpha$  *E. coli* (Novagen Lucerne, Switzerland). After mini-preparation and restriction control, the correctness of the inserts was confirmed by DNA sequencing (Microsynth, Switzerland).

**Cell culture.** CHO-K1 cells (American Type Culture Collection No. CCL-61<sup>TM</sup>) were cultivated in Ham's Nutrient Mixture F-12 supplemented with 2 mM L-glutamate (Invitrogen, Paisley, UK), 10% fetal calf serum (FCS, Invitrogen, Paisley, UK), 100 U/mL penicillin, and 100  $\mu$ g/mL streptomycin (both Sigma-Aldrich, Basel, Switzerland). The cells were subcultivated twice a week. Cells used for protein production were not subcultured, but the supernatant was collected and replaced by fresh medium every six days.

**Production of stable cell lines.** FuGENE<sup>®</sup> HD transfection reagent (Roche Applied Science, Rotkreuz, Switzerland) was used to transfect CHO-K1 cells according to the manufacturer's instructions. To obtain stable populations, positively transfected cells were selected by cultivation in growth medium supplemented with 0.5 mg/ml G418 (Gibco, Invitrogen Lucerne, Switzerland). Clonal populations were generated using the limiting dilution technique. For each construct 20 clones were cultured and screened for recombinant protein expression. The selected cell clones were cultured in 12-well plates and after six days cultivation the medium was tested for the presence of DC-SIGN by immunoblot analysis.



DC-SIGN producing clones were seeded into 150 cm<sup>2</sup> cell culture flasks and cultivated for six days without medium exchange.

**Protein purification.** Purification of the recombinant protein was achieved by applying conditioned medium in loading buffer I (20 mM Tris/HCl, pH 7.6, 150 mM NaCl, 0.05% (v/v) Tween-20<sup>TM</sup>) onto a protein A-sepharose column (BioVision, Mountain View, CA, USA), attached to a fast protein liquid chromatography apparatus (BioLogic (FPLC) system, BioRad, Reinach BL, Switzerland). The protein was eluted in elution buffer I (0.5 M acetic acid/ammonium acetate, pH 3.4). The collected protein was further purified on a L-fucose-sepharose column using loading buffer II (20 mM Tris/HCl, pH 7.8, 0.5 M NaCl, 25 mM CaCl<sub>2</sub>) and elution buffer II (20 mM Tris/HCl, pH 7.8, 0.5 M NaCl, 2 mM EDTA). For long-term storage, the purified protein was frozen at -80 °C

**SDS-PAGE analysis.** Protein purity was verified by SDS-PAGE analysis on a 15% non-reducing polyacrylamide gel according to the method of Laemmli [25]. Following gel electrophoresis, the gel was stained with a coomassie solution as described in [26].

**Immunoblot analysis.** Conditioned medium of each clone was resolved on a 12% SDS-PAGE under reducing conditions and transferred onto a nitrocellulose membrane (Bio-Rad, Reinach, Switzerland). The membrane was blocked with 3% bovine serum albumin (BSA, Sigma, Steinheim, Germany) in PBS-buffer and incubated with a monoclonal rabbit anti-DC-SIGN-CRD primary antibody (1:5000, Sigma, Buchs, Switzerland). As secondary antibody an alkaline phosphatase coupled anti-rabbit IgG (Sigma, Buchs, Switzerland) was used. After three washing steps the membrane was developed with the NBT-BCIP solution (Fluka, Buchs, Switzerland).

**Preparation of horseradish peroxidase coupled polyacrylamide glycopolymer.** Biotinylated Lewis<sup>a</sup> (Le<sup>a</sup>)-PAA polymer (20 μL, 1 mg/mL) was mixed with 80 μL assay buffer, 20 μL FCS and 80 μL streptavidin-horseradish peroxidase-conjugate (500 U/mL) and incubated for 2 h at 37 °C [27]. The complex was stable for several weeks when stored at 4 °C.

**Le<sup>a</sup>-PAA binding assay.** A polymer-based binding assay for DC-SIGN was developed based on the assay reported in [27]. The compounds **1**, **2**, and **3** were purchased from ChemDiv (San

Diego, CA, USA, (**1**, K784-1581; **2**, K784-1848; **3**, K593-1866). D-mannose, methylmannoside, L-fucose, and D-glucose were purchased from Sigma-Aldrich (Basel, Switzerland). Flat-bottom 96-well microtiter plates (F96 MaxiSorp, Nunc) were coated with 100  $\mu\text{L}$ /well of a 2.5  $\mu\text{g}/\text{mL}$  solution of DC-SIGN-CRD-IgG-Fc in assay buffer (20 mM HEPES, 150 mM NaCl, 1 mM  $\text{CaCl}_2$ , pH 7.4) overnight at 4 °C. The coating solution was discarded and the wells were blocked with 200  $\mu\text{L}$ /well of 3% BSA in assay buffer for 2 h at 4 °C. After three washing steps with assay buffer, either a dilution series of the polymer 100  $\mu\text{L}$ /well (0-3  $\mu\text{g}/\text{mL}$  for  $\text{EC}_{50}$  determination) or a mixture of test compound for  $\text{IC}_{50}$  determinations (50  $\mu\text{L}$ /well, dilution series) and  $\text{Le}^{\text{a}}$ -PAA (50  $\mu\text{L}$ /well, 0.5  $\mu\text{g}/\text{mL}$ ) in assay buffer were added. The plates were incubated for 3 h at room temperature and 350 rpm and then washed with assay buffer. After the addition of the ABTS-substrate (100  $\mu\text{L}$ /well), the colorimetric reaction was allowed to develop for 2 min, then stopped by the addition of 2% aqueous oxalic acid before the optical density (OD) was measured at 415 nm on a microplate-reader (Spectramax 190, Molecular Devices, California, USA). The  $\text{EC}_{50}$  or  $\text{IC}_{50}$ -values were calculated with the prism software (GraphPad Software, Inc, La Jolla, USA). The  $\text{IC}_{50}$  defines the molar concentration of the test compound that reduces the maximal specific binding of  $\text{Le}^{\text{a}}$ -PAA to DC-SIGN-CRD by 50%.

## Results and discussion

**Generation of DC-SIGN-CRD-IgG-Fc constructs.** Three different expression vectors (Table 1) encoding the DC-SIGN-CRD were generated by standard molecular biology methods [24]. The constructs were ligated into the pcDNA3.1(+) plasmid and transfected into CHO K1 cells. After the selection of stable clones, the effect on protein expression efficiency was evaluated. In the starting construct pFuse-hIgG2-Fc2 the gene of interest was incorporated between an IL-2 signal peptide and a human IgG2-Fc2 part. It contained a non-extended Kozak-sequence (sequence: gcc acc atg). In the newly designed vectors, DC-SIGN-CRD-Fc2 was provided with an extended Kozak sequence (sequence: gcc gcc acc atg g\*). The guanine (marked \*) at position +4 was inserted using a codon coding for glycine (gga), leading to an elongation of the proceeding signal peptides by this amino acid. Glycine was assumed to have no influence on the secretion process, since it is a small and uncharged amino acid. In this study, the commonly used IL-2 signal peptide (IL-2 ss), a modified IL-2 signal peptide (IL-2mod ss) with increased basicity and hydrophobicity, as well as a codon-

usage optimized *Gaussia princeps* luciferase signal peptide (luciferase ss) were tested for their secretion efficiency.

Construct name	Sequence
Original IL-2 ss	5` atg tac agg atg caa ctc ctg tct tgc att gca cta agt ctt gca ctt gtc acg aat tcg 3` MYRMQLLSCIALSLALVTNS
Kozak-IL-2 ss	5` gcc gcc acc atg gga tac agg atg caa ctc ctg tct tgc att gca cta agt ctt gca ctt gtc acg aat tcg 3` MGYRMQLLSCIALSLALVTNS
Kozak-IL-2mod ss	5` gcc gcc acc atg gga cgg* agg atg caa ctc ctc* ctg tct tgc att gca cta ttg* ctt gca ctt gtc acg aat tcg 3` MGR*RMQLLL*SCIALL*LALVTNS
Kozak-luciferase ss	5` gcc gcc acc atg gga gtg aag gtg ctg ttc gcc ctg atc tgc atc gcc gtc gcc gag gcc 3` MGVKVLFALICIAVAEA

**Table 1.** Plasmid constructs with their N-terminal DNA- and amino acid- sequence including Kozak sequence and signal peptide (ss). DNA sequences corresponding to the Kozak sequence are shaded in grey. \*Modified amino acids in the IL-2mod ss.

The IL-2mod ss was designed based on the study by Zhang *et al.* [10]. There, they modified the basic and the hydrophobic region of the IL-2 ss and separately investigated their effect on human endostatin expression. Increasing basicity and hydrophobicity of each region enhanced protein expression by factor 2, compared to the parental IL-2 ss. We decided to combine the modified parts that exhibited the most beneficial effect on endostatin expression in one single signal peptide, and test its impact on DC-SIGN secretion (Table 2).

**Table 2.** Design of the IL-2mod ss, based on studies by Zhang *et al.* [10]. Listed are the expression yields (f) of the IL-2 ss 1 and IL-2 ss 2 relative to the native IL-2 ss found in [10]. IL-2 ss 1 was modified in the basic region, IL-2 ss 2 was modified in the hydrophobic region. IL-2mod ss is a combination of the two modified signal peptides 1 and 2. Polar, neutral amino acids (AA) are highlighted in grey, basic AA in black, hydrophobic AA are not highlighted.

Signal peptide	f	basic			hydrophobic								polar									
IL-2 ss	1	M	Y	R	M	Q	L	L	S	C	I	A	L	S	L	A	L	V	T	N	S	
IL-2 ss 1	2.2	M	R	R	M	Q	L	L	S	C	I	A	L	S	L	A	L	V	T	N	S	
IL-2 ss 2	2.9	M	Y	K	M	Q	L	L	L	S	C	I	A	L	L	L	A	I	V	T	N	S
IL-2mod ss		M	R	R	M	Q	L	L	L	S	C	I	A	L	L	L	A	L	V	T	N	S

**Quantification of protein expression by stably transfected CHO-K1 cells.** DC-SIGN expression by stably transfected CHO-K1 cells was analyzed in conditioned culture medium via affinity purification, using protein A- and L-fucose-sepharose columns. Absolute protein yields were then determined by HPLC. Table 3 summarizes the absolute yields of DC-SIGN-CRD-IgG obtained from the medium samples. The construct with an extended Kozak sequence and the standard IL-2 signal peptide (Kozak-IL-2 ss) showed a 3.6-fold increase in protein expression, compared to the original construct with a non-extended Kozak sequence only. This effect may either result from the beneficial effect of the extended Kozak sequence, or it may attribute to the non-isogenic backgrounds (pcDNA3.1(+) and pFUSE-hIgG-Fc2 vector) and the diverging promoters (hCMV, hEF1-HTLV prom) of both constructs. However, for a valid comparison of the effect of the different signal peptides, we only compared the newly designed constructs that have the same isogenic background. The luciferase signal peptide proved to be most efficient, with a 2-fold increase (6.5 mg/mL) in protein yield compared to the IL-2 signal peptide (3.6 mg/mL). Surprisingly, we obtained a protein yield of only 1.2 mg/mL for the IL-2mod signal peptide, meaning a 3-fold reduction compared to the standard IL-2 signal peptide.

**Table 3.** DC-SIGN-CRD-IgG-Fc expression yields for stably transfected cells. Absolute protein yields in mg per liter culture medium, after six days of culture.

Construct	Protein yield in mg/L
IL-2 ss original	1.0
Kozak-IL-2 ss	3.6
Kozak-IL-2mod ss	1.2
Kozak-luciferase ss	6.5

Additionally, stably expressing cell populations derived from individual cell clones were generated and evaluated for recombinant protein expression. We used immunoblot analysis and Le<sup>a</sup>-PAA binding assays to identify DC-SIGN-expressing clones (Figure 1).

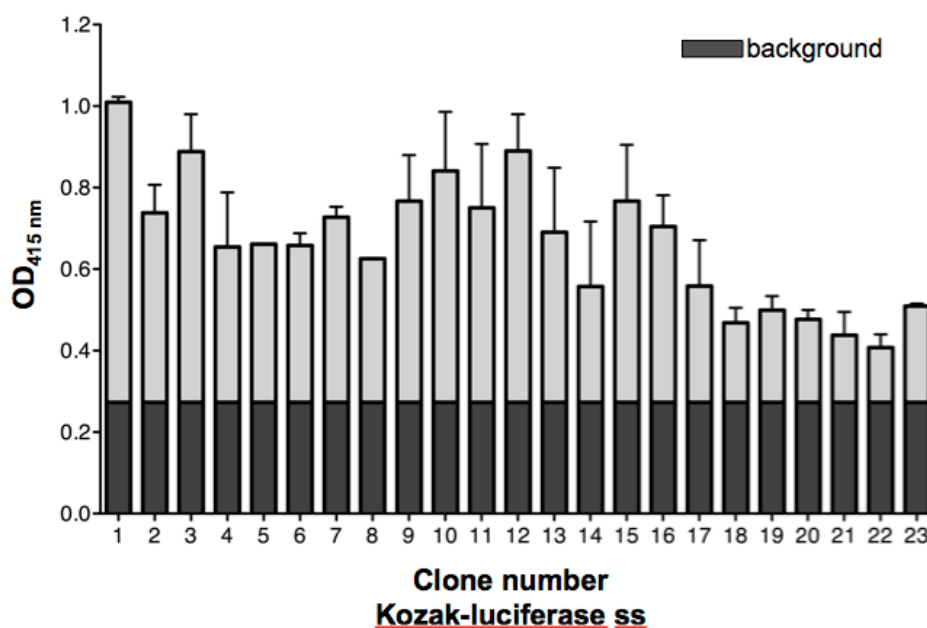


**Figure 1.** Le<sup>a</sup>-PAA binding assay for screening CHO-K1 single cell clones that are stably transfected with the Kozak-luciferase ss construct. 100  $\mu$ L cell medium per cell clone was coated over night on 96-well microtiter plates and the binding to the Le<sup>a</sup>-PAA (1  $\mu$ g/mL) was measured. The strength of the signal correlates with the amount of DC-SIGN-CRD-Fc2 in the coated medium. Background signals (dark grey) are Le<sup>a</sup>-PAA binding to medium of untransfected CHO-K1 cells. The assay was performed in triplicates.

The results confirmed the expression of active protein in all generated cell lines. However, great differences in the extent of synthesized proteins were detectable between the individual clones. We used the clonal populations with the highest signals in the PAA-binding assay for further cultivation and analysis. Conditioned medium from each population was collected and purified over a protein A-sepharose column. Based on the areas under the curve of the respective FPLC peaks, we selected the two best-producing clones of each construct. For these candidates, the absolute protein yields were determined by HPLC. The obtained yields of the best-producing clonal populations confirmed the results for the different signal peptides that we had observed with the pooled clones (Table 4).

**Table 4.** DC-SIGN-CRD-IgG-Fc expression yield for the best producing stable cell lines of each construct. Absolute protein yields in mg/L.

Construct	Protein yield in mg/L
IL-2 ss original	1.2
Kozak-IL-2 ss	9.5
Kozak-IL-2mod ss	1.0
Kozak-luciferase ss (clone nr. 1)	19.6

Influencing the translation process by inserting an extended Kozak sequence (Kozak-IL-2 ss cell line) resulted in a 8-fold higher protein yield compared to the original IL-2 ss cell line. Furthermore, by fusing the *Gaussia princeps* luciferase signal peptide and the extended Kozak sequence an even higher protein yield was obtained. Clone 1 produced 19.5 mg DC-SIGN per liter culture medium, which represents a two-fold augmented expression compared to the best Kozak-IL-2 ss clone and a 16-fold increase to the original IL-2 clone. The hydrophobic IL-2mod signal peptide exhibited an adverse rather than a beneficial effect on protein secretion. The protein quantity of the best Kozak-IL-2mod ss clone was ten times less than for the Kozak-IL-2 ss cell line. The reason for this might be, that the enhanced basicity and hydrophobicity of this signal peptide results either in a very low, or in a very high affinity for the SRPs. Both effects would interfere with the translocation process of the protein. Additionally, it might be that the signal peptide interacts with the connected protein, resulting in reduced secretion efficiencies. This effect is likely to vary between proteins, since the

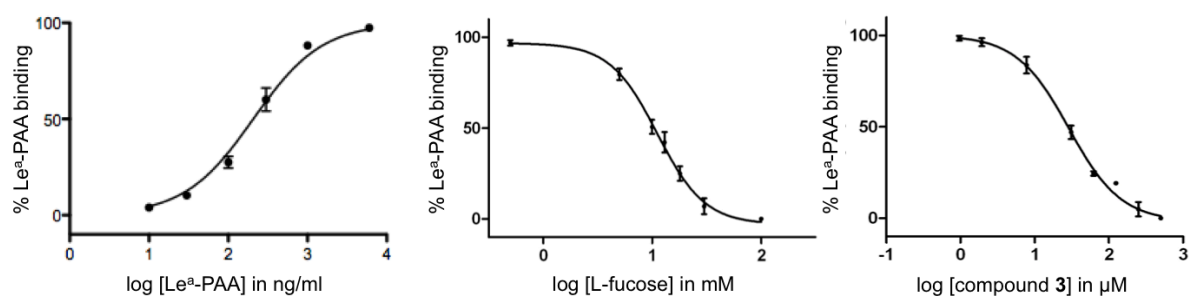
strength of the intramolecular interactions depends on the structure and biophysical properties of the recombinant protein.

The superior efficacy of the *Gaussia princeps* luciferase signal peptide is in agreement with the published data, where its beneficial effect on human endostatin secretion was reported [14]. The analysis of the amino acid sequence of the luciferase signal peptide revealed a higher hydrophobicity of the core region in comparison to the native IL-2 signal peptide (Table 5). This analysis confirmed the findings of Zhang *et al.* that enhanced hydrophobicity of the signal peptide significantly improves protein secretion.

**Table 5.** Comparison of the amino acid (AA) sequences from the native IL-2 ss, the IL-2mod ss and the *G. princeps* luciferase ss. Polar, neutral AA are highlighted in light grey, acidic AA in darker grey, basic AA in black, hydrophobic AA are not highlighted.

	basic			hydrophobic										polar						
IL-2 ss	M	Y	R	M	Q	L	L	S	C	I	A	L	S	L	A	L	V	T	N	S
IL-2 mod. ss	M	R	R	M	Q	L	L	S	C	I	A	L	L	L	A	L	V	T	N	S
G. luciferase ss	M	V	K	V	L	F	A	L	I	C	I	A	V					A	E	A

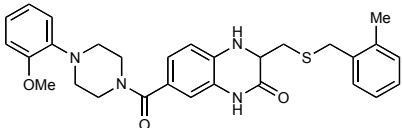
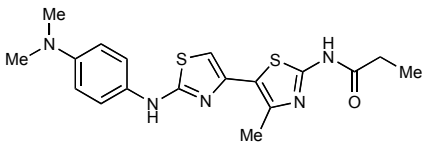
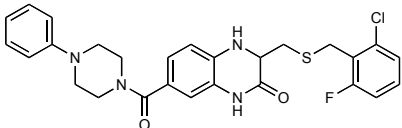
**Le<sup>a</sup>-PAA binding assay.** To verify the activity of the purified DC-SIGN proteins, Le<sup>a</sup>-PAA binding assays were performed (Figure 2, Table 6). DC-SIGN bound the Le<sup>a</sup>-PAA with an EC<sub>50</sub> value of 89 ng/ml, which confirmed the activity of the protein. L-Fucose, D-mannose, methylmannoside, and D-glucose inhibited the Le<sup>a</sup>-PAA binding to DC-SIGN with an IC<sub>50</sub> value of 5.3 mM, 9.6 mM, 8.7 mM, and 22.5 mM, respectively. These values are consistent with data from the literature [22]. Furthermore, non-carbohydrate inhibitors **1**, **2**, **3** exhibited strong inhibitory potencies with IC<sub>50</sub> values in the μM range (24-127 μM). However, our values were higher than the reported values in the literature [21], which can be explained by the different assay formats and by the low solubility of these compounds. The developed target-based competition assay can be employed as a fast screening assay for new DC-SIGN antagonists.



**Figure 2.** EC<sub>50</sub> determination of DC-SIGN to the Le<sup>a</sup>-PAA and IC<sub>50</sub> determination of D-mannose, L-fucose and compound **3** using the Prism software. The assay was performed in triplicates.



**Table 6:** EC<sub>50</sub> value for Le<sup>a</sup>-PAA to DC-SIGN and inhibitory potencies (IC<sub>50</sub>) of DC-SIGN ligands. The IC<sub>50</sub> values were determined with the Le<sup>a</sup>-PAA binding assay as described in the material and methods section and compared to those reported in the literature [21, 22].

	Competitive binding assay	In literature
<b>EC<sub>50</sub> Le<sup>a</sup>-PAA [ng/ml]</b>	89.6 ± 19.7	
<b>DC-SIGN antagonists</b>	<b>IC<sub>50</sub></b>	<b>IC<sub>50</sub></b>
<b>L-fucose</b>	5.3 ± 0.8 mM	6.7 ± 0.5 mM [22]
<b>D-mannose</b>	9.6 ± 1.1 mM	13.1 ± 0.4 mM [22]
<b>methyl mannoside</b>	8.7 ± 2.2 mM	12.5 ± 0.5 mM [22]
<b>D-glucose</b>	22.5 ± 1.2 mM	23 ± 1 mM [22]
<b>1</b>		
	42.7 ± 5.7 μM	2.0 ± 1 μM [21]
<b>2</b>		
	127.3 ± 40.5 μM	1.6 ± 0.5 μM [21]
<b>3</b>		
	24.2 ± 5.5 μM	7.3 ± 3.5 μM [21]

## Conclusion

In summary, the results of this study confirmed the possibility to substantially improve the efficacy of mammalian expression systems by inserting an extended Kozak sequence at the translation start, and by choosing an appropriate signal peptide. The luciferase signal peptide derived from the copepod *Gaussia princeps* showed a superior functionality compared to the interleukin-2 signal peptide, with more than two-fold higher protein yield. Therefore, we can strongly recommend the usage of this luciferase signal peptide as an alternative to the commonly used interleukin-2 signal peptide.

## References

1. Andersen DC, Krummen L, *Curr. Opin. Biotechnol.* **2002**, 13(2):117-123.
2. Gerngross TU, *Nat. Biotechnol.* **2004**, 22(12):1589-1589.
3. Baez J, Olsen D, Polarek JW, *Appl. Microbiol. Biotechnol.* **2005**, 69(3):245-252.
4. Swartz JR, *Curr. Opin. Biotechnol.* **2001**, 12(2):195-201.
5. Wurm FM, *Nat. Biotechnol.* **2004**, 22(11):1393-1398.
6. Kozak M, *J Mol Biol.* **1987**, 196(4):947-950.
7. Le Hir H, Nott A, Moore MJ, *Trends Biochem Sci.* **2003**, 28(4):215-220.
8. Gopalkrishnan RV, Christiansen KA, Goldstein NI, DePinho RA, Fisher PB.: *Nucleic Acids Research* **1999**, 27(24):4775-4782.
9. Kalwy S, Rance J, Young R, *Mol. Biotechnol.* **2006**, 34(2):151-156.
10. Zhang L, Leng QX, Mixson AJ, *J Gene Med* **2005**, 7(3):354-365.
11. Trosse C, Ravneberg H, Stern B, Pryme IF, *Gene Regul Syst Bio* **2007**, 1:303-312.
12. S Stern, B., Olsen, L.C., Tröbe, C., Ravneberg, H. and Pryme, I.F, *Trends Cell Mol. Biol.* **2007**, 2:1-17.
13. Martoglio B, Dobberstein B, *Trends Cell Biol.* **1998**, 8(10):410-415.
14. Knappskog S, Ravneberg H, Gjerdrum C, Trosse C, Stern B, Pryme IF, *J Biotechnol.* **2007**, 128(4):705-715.
15. Geijtenbeek TBH, Torensma R, van Vliet SJ, van Duijnhoven GCF, Adema GJ, van Kooyk Y, Figdor CG, *Cell* **2000**, 100(5):575-585.
16. Figdor CG, van Kooyk Y, Adema GJ, *Nat. Rev. Immunol.* **2002**, 2(2):77-84.
17. Geijtenbeek TBH, Torensma R, Kwon D, van Vliet SJ, van Duijnhoven GCF, Adema GJ, KewalRamani V, Littman D, Figdor CG, van Kooyk Y, *Cell.* **2000**, 100(5):587-97.
18. Gurney KB, Elliott J, Nassanian H, Song C, Soilleux E, McGowan I, Anton PA, Lee B, *J Virol* **2005**, 79(9):5762-5773.
19. Ernst B, Magnani JL, *Nat Rev Drug Discov* **2009**, 8(8):661-677.
20. Timpano G, Tabarani G, Anderluh M, Invernizzi D, Vasile F, Potenza D, Nieto PM, Rojo J, Fieschi F, Bernardi A, *Chembiochem.* **2008**, 9(12):1921-1930.
21. Borrok MJ, Kiessling LL, *J Am Chem Soc.* **2007**, 129:12780-12785.
22. Mitchell DA, Fadden AJ, Drickamer K, *J Biol Chem.* **2001**, 276(31):28939-28945.
23. Feinberg H, Guo Y, Conroy E, Mitchell D, Alvarez R, Blixt O, Taylor M, Drickamer K, Weis W, *Glycobiology* **2005**, 15(11):35.
24. Sambrook J, Fritsch EF, Maniatis T, *Cold Spring Harbor Laboratory Press, NY*, **1989**.

25. Laemmli UK, *Nature* **1970**, 227(5259):680-&.
26. Dyballa N, Metzger S, *J Vis Exp.* **2009**, 3: pii: 1431.
27. WeitzSchmidt G, Stokmaier D, Scheel G, Nifantev NE, Tuzikov AB, Bovin NV, *Anal. Biochem.* **1996**, 238(2):184-190.



## **Part II: The lectin DC-SIGN**

---

### **DC-SIGN Chapter 2: Results and discussion**

#### **Manuscript 2**

---

**Binding of Lewis<sup>a/x</sup> to DC-SIGN: Nature of aglycone  
determines binding mode**

Katharina Mayer,<sup>‡</sup> Meike Scharenberg,<sup>‡</sup> Sameh Eid,<sup>‡</sup> Katrin Lemme, Arjan Odedra, Brian Cutting, Said Rabbani, Angelo Vedani, Beat Ernst\*

Institute of Molecular Pharmacy, Pharmacenter, University of Basel, Klingelbergstr.50, 4056 Basel, Switzerland

\* Corresponding author: Prof. Beat Ernst, Institute of Molecular Pharmacy, Pharmacenter of the University of Basel, Klingelbergstrasse 50, CH-4056 Basel, Tel: +41 61 2671551, Fax: +41 61 2671552; e-mail: [beat.ernst@unibas.ch](mailto:beat.ernst@unibas.ch)

<sup>‡</sup> These authors contributed equally to this work

**Abstract**

Dendritic cells (DCs) have the function of presenting antigens to other processing cells of the immune system, particularly T-cells. DC-SIGN (DC-specific intramolecular adhesion molecule-3-grabbing non-integrin) is one of the major receptors on DCs involved in the uptake of pathogens and has gained increasing interest over the last decade as it is crucially involved in infections caused by HIV-1, Ebola virus, *Mycobacterium tuberculosis*, and various other pathogens. High-mannosylated *N*-glycans or L-Fuc-containing trisaccharide motifs such as the Lewis blood group antigens Lewis<sup>a</sup> and Lewis<sup>x</sup>, which are surface components of these microorganisms, mediate binding to DC-SIGN.

Crystallographic data for DC-SIGN in complex with a Lewis<sup>x</sup>-containing pentasaccharide suggest that the terminal sugar residues, L-Fuc and D-galactose, are predominantly involved in binding. We elucidated the interaction of Lewis<sup>a</sup> as well as Lewis<sup>x</sup> bearing two different aglycones with DC-SIGN. Binding assays together with STD NMR analysis revealed distinct, substitution-dependent binding modes. Eventually, molecular modelling and mutagenesis studies support the assumption of a switch of the binding mode when introducing hydrophobic residues at the reducing end of the Lewis trisaccharides. Based on this information a new series of potential high- affinity DC-SIGN antagonists can be designed.



## 1. Introduction

Immature dendritic cells (DCs), found in peripheral tissues throughout the body, play an essential role in triggering the immune response as they are antigen-presenting cells.<sup>1,2</sup> DCs recognize and capture a broad variety of pathogens including viruses,<sup>3</sup> bacteria,<sup>4</sup> and yeasts<sup>5</sup> by pathogen recognition receptors (PRRs). Pathogen uptake by PRRs as well as inflammatory cytokines and chemokines (*e.g.* IL-4) trigger DC differentiation and migration to the lymphoid organs where the mature DCs present pathogenic peptides on the major histocompatibility complex (MHC) to resting T cells.

Dendritic cell-specific intercellular adhesion molecule-3 grabbing nonintegrin (DC-SIGN) is one of the main receptors on DCs for recognition and uptake of pathogens. Since its first discovery by Geijtenbeek *et al.* in 2000<sup>3</sup>, DC-SIGN gained popularity, particularly because a variety of pathogens exploit DC-SIGN to infect their host, including HIV, Ebola virus, and SARS.<sup>6,7,8</sup> The fact that different pathogens have capitalized on this infection strategy makes DC-SIGN an interesting target for a new class of anti-infectives.<sup>9</sup> In a study on the binding and transfer of HIV in human rectal mucosa cells, DC-SIGN<sup>+</sup> cells accounted for more than 90% of bound viruses although they represented only 1–5% of the total mucosal mononuclear cells. Furthermore, anti-DC-SIGN antibodies blocked more than 90% of HIV binding.<sup>10</sup>

DC-SIGN is a type II transmembrane protein with a C-terminal carbohydrate recognition domain (CRD). It is part of the C-type lectin family, which implies that ligand binding is Ca<sup>2+</sup>-dependent. The majority of pathogens bind with *N*-linked high-mannose oligosaccharides to DC-SIGN<sup>11,12</sup>, *e.g.* mannan structures on the gp120 envelope protein of HIV-1.<sup>13</sup> Besides oligomannosides, blood group antigens, such as Lewis<sup>x</sup> (Le<sup>x</sup>, Galβ(1-4)[Fucα(1-3)]GlcNAc) and Lewis<sup>a</sup> (Le<sup>a</sup>, Galβ(1-3)[Fucα(1-4)]GlcNAc) that are also commonly found on pathogens, are recognized by DC-SIGN.<sup>14-17</sup> Le<sup>x</sup> and Le<sup>a</sup> bind to DC-SIGN in the low millimolar range, with Le<sup>a</sup> exhibiting a slightly higher binding affinity than Le<sup>x</sup>.<sup>18,19</sup> Since pathogens present these rather low-affinity sugar motives in a multimeric form to the DC-SIGN tetramers, high binding avidities are observed.<sup>20,21</sup>

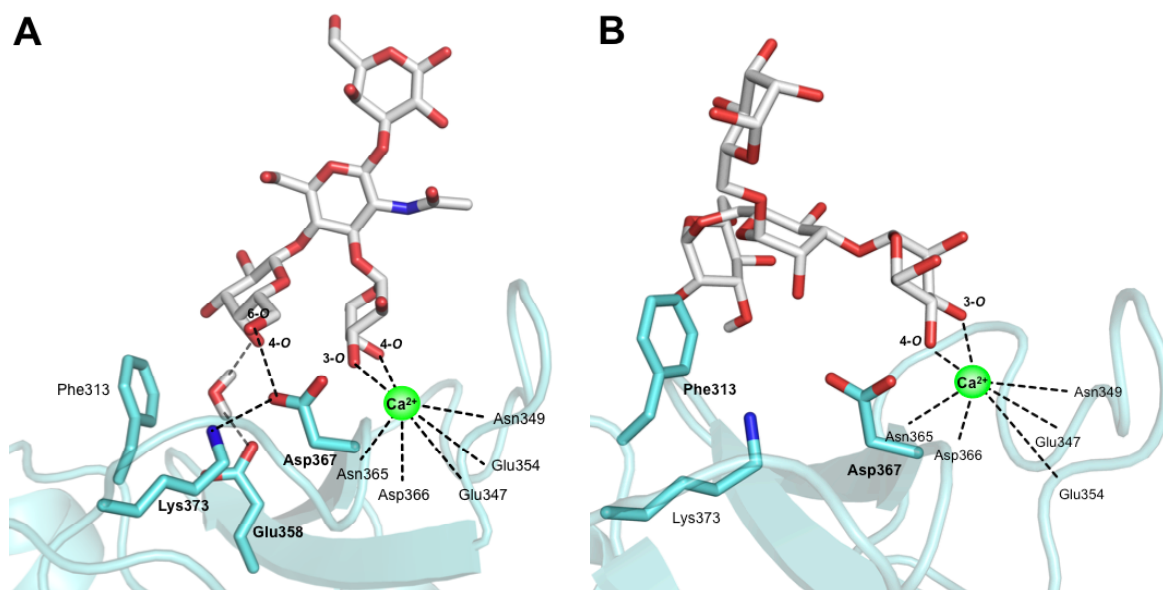


**Figure 1.** A) X-ray of LNFP III/CRD of DC-SIGN (PDB 1SL5).<sup>22</sup> The equatorial 3-OH and the axial 4-OH of L-Fuc coordinate the calcium ion. The interaction of 4-OH with Glu358 is mediated by a water molecule. 6-OH of D-galactose forms a H-bond with Asp367, which on its part is stabilized by an interaction with Lys373. B) X-ray of Man<sub>4</sub> {Man $\alpha$ (1-6)[Man $\alpha$ (1-3)]Man $\alpha$ (1-6)Man}/CRD of DC-SIGN (PDB 1SL4).<sup>14,22</sup> The calcium ion is coordinated by the equatorial 3- and the equatorial 4-OH of the terminal  $\alpha$ (1-3)-linked D-mannose. In addition, a hydrophobic contact of the terminal  $\alpha$ (1-6)-linked D-mannose further stabilizes the interaction.

Crystallographic data (PDB: 1SL5)<sup>22</sup> obtained from the CRD of DC-SIGN co-crystallized with lacto-*N*-fucopentaose III (LNFP III, Gal $\beta$ (1-4)[Fuc $\alpha$ (1-3)]GlcNAc $\beta$ (1-3)Gal $\beta$ (1-4)Glc) suggest that the equatorial 3- and axial 4-OH of the D-Fuc moiety coordinate the calcium ion (Figure 1A). For the 4-OH of the D-Gal moiety a water-bridged H-bond with Glu358 is proposed. In addition, a H-bond of 6-OH of D-Gal to Lys373, bridged by Asp367 is assumed.<sup>22</sup> For the CRD of DC-SIGN co-crystallized with oligomannosides (Man<sub>4</sub> and GlcNAc<sub>2</sub>Man<sub>3</sub>) a comparable docking mode was obtained. There the equatorial 3- and 4-OH of the  $\alpha$ (1-3)-linked mannose moiety complex the calcium ion (Figure 1B). In addition, Man<sub>4</sub> (PDB 1SL4) addresses a second binding site lined by Phe313, contributing to selectivity as well as affinity.<sup>14,22</sup> Only recently, Bernardi *et al.* took advantage of this additional hydrophobic contact for their design of glycomimetic DC-SIGN antagonists.<sup>23,24</sup>

In our program directed to the identification of high-affinity DC-SIGN antagonists, a large library of carbohydrates and mimetics thereof was screened. One interesting finding was the unexpectedly improved affinity discovered for Le<sup>x</sup> and Le<sup>a</sup> antigens with aromatic aglycones

( $\rightarrow$ 3,4) compared to the corresponding methyl glycosides ( $\rightarrow$ 1,2). When these derivatives adopt a binding mode similar to LNFP III,<sup>22</sup> the aglycones should point to the solvent and therefore not contribute to binding. To clarify whether a modified binding mode is responsible for the increased affinity, the binding epitopes of the Le<sup>a</sup> and Le<sup>x</sup> derivatives **1-4** were analyzed by STD NMR and docking studies.

## 2. Results and Discussion

**2.1. Binding Affinities for Lewis Structures.** For the determination of the affinities of methyl Le<sup>x</sup> (**1**), methyl Le<sup>a</sup> (**2**), phenyl Le<sup>x</sup> (**3**) and phenyl Le<sup>a</sup> (**4**) (Table 1) a cell-free competitive binding was developed. It is based on the competition of a biotinylated polyacrylamide glycopolymer (Le<sup>a</sup>-polyacrylamide, Le<sup>a</sup>-PAA) and the ligand of interest for the CRD of DC-SIGN. A soluble recombinant protein consisting of the DC-SIGN CRD-Fc (amino acid residues 250-404) was expressed in CHO-K1 cells and purified by affinity chromatography (protein A- and L-fucose-sepharose column). For the determination of IC<sub>50</sub> values, a microtiter plate coated with DC-SIGN CRD-Fc was incubated with biotinylated Gal $\beta$ (1-3)[Fuc $\alpha$ (1-4)]GlcNAc $\beta$ -polyacrylamide (Le<sup>a</sup>-PAA) polymer conjugated to streptavidin-horseradish peroxidase and the DC-SIGN antagonist in a serial dilution. The assay was performed in duplicates and repeated three times for each compound. To ensure comparability of different ligands, the reference compound L-fucose was tested in parallel on each individual microtiter plate.

L-Fuc and D-mannose were used as reference compounds showing IC<sub>50</sub> values of 7.6 mM and 9.1 mM, respectively. These affinities correlate well with published data.<sup>20</sup> Phenyl Le<sup>x</sup> (**3**) (IC<sub>50</sub> 1.2 mM) and phenyl Le<sup>a</sup> (**4**) (IC<sub>50</sub> 0.9 mM) showed a two- to threefold increase in affinity compared to corresponding methyl derivatives [IC<sub>50</sub> 2.3 mM for methyl Le<sup>x</sup> (**1**) and 2.9 mM for methyl Le<sup>a</sup> (**2**)]. For phenyl Le<sup>a</sup> (**4**), the best antagonist in this series, we also performed isothermal titration calorimetry (ITC) experiments. The K<sub>D</sub> of 582  $\mu$ M for phenyl Le<sup>a</sup> (**4**) confirms the results of the polymer binding assay with affinity in the micromolar range. As observed for the majority of carbohydrate-lectin interactions,<sup>25-27</sup> the binding is enthalpy driven ( $\Delta H = -28.0 \pm 2.0$  kJ/mol,  $T\Delta S = -9.5 \pm 2.1$  kJ/mol).

When the Le<sup>x</sup>- and Le<sup>a</sup>-motifs bind comparable to LNFP III,<sup>22</sup> only the L-Fuc and D-Gal moiety participate in binding, whereas the D-GlcNAc moiety as well as the aglycone point to the solvent. Therefore, the observed beneficial effect of the aromatic aglycone was unexpected.

**Table 1.** The cell-free competitive binding assay is based on the competition of a biotinylated Le<sup>a</sup>-PAA with the antagonist of interest for the CRD of DC-SIGN. The assay was performed in duplicates and repeated three times for each compound. To ensure comparability of different ligands, the reference compound L-Fuc was tested in parallel on each individual microtiter plate. ITC experiments were performed at 25 °C. Thermodynamic parameters were calculated according to the equation  $\Delta G = RT \ln K_D = \Delta H - T\Delta S$ ; n.d. not determined.

Ligand	Competitive binding assay, IC <sub>50</sub>	Isothermal titration calorimetry, K <sub>D</sub>
D-mannose	9.1 ± 1.3 mM	n.d.
L-fucose	7.6 ± 2.6 mM	n.d.
Me Le <sup>x</sup> (methyl Galβ(1-4)[Fucα(1-3)]βGlcNAc) ( <b>1</b> )	2.3 ± 0.1 mM	n.d.
Me Le <sup>a</sup> (methyl Galβ(1-3)[Fucα(1-4)]βGlcNAc) ( <b>2</b> )	2.9 ± 0.5 mM	n.d.
Ph Le <sup>x</sup> (phenyl Galβ(1-4)[Fucα(1-3)]βGlcNAc) ( <b>3</b> )	1.2 ± 0.5 mM	n.d.
Ph Le <sup>a</sup> (phenyl Galβ(1-3)[Fucα(1-4)]βGlcNAc) ( <b>4</b> )	0.9 ± 0.3 mM	582 ± 40 μM

**2.2. Saturation Transfer Difference (STD) NMR Analysis.** For the interpretation of the unexpected higher affinities correlated with the phenyl aglycone of antagonists **3** and **4**, the binding epitopes of the Le<sup>a</sup> and Le<sup>x</sup> derivatives were characterized by STD NMR (Figure 2A-D), which is particularly suited for epitope mapping of ligand receptor couples with weak interactions.<sup>28-31</sup> STD NMR experiments are based on spin magnetization transfer from a macromolecule, the protein, to a smaller binding molecule, the ligand. The saturation transfer proceeds through space via dipolar coupling and is therewith dependent on the distance ( $r^{-6}$ ) of ligand hydrogens to the protein surface.

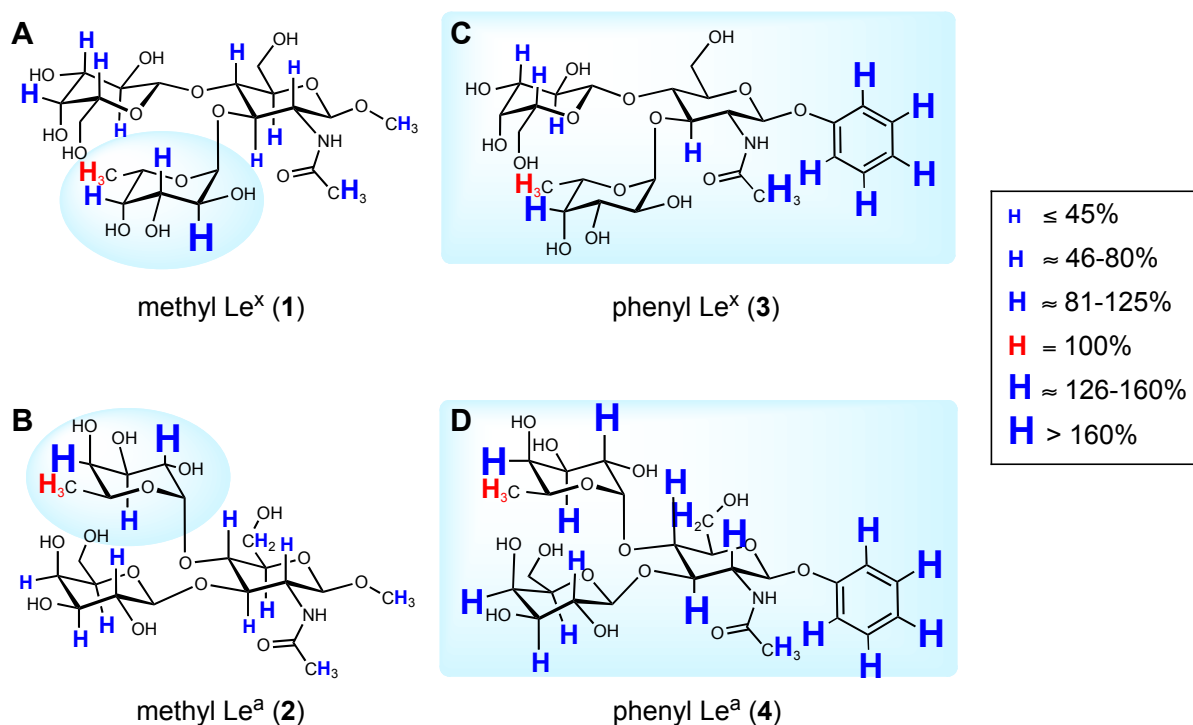


**Figure 2.** Binding epitopes of the Lewis antigens **1** - **4** interacting with DC-SIGN CRD-Fc determined by STD NMR. The contribution of each hydrogen to the STD epitope is quantified by forming the ratio of the signal intensities in the STD to those in the reference spectrum. These values are normalized to H-6 of D-Fuc (in red, 100%) to give the percentage epitope. STD values greater than 100% represent proximity to DC-SIGN CRD-Fc closer than that of the H-6 of D-Fuc. The letter size used for the hydrogens expresses the proximity to the protein, *i.e.* the relative amount of saturation transfer. The STD epitope for methyl Le<sup>x</sup> (**1**) is consistent with recently published data with respect to experimental accuracy.<sup>32</sup> Further details regarding the percentage epitope, sample preparation and parameters for the STD NMR measurement are available in the experimental section.

In the STD NMR analysis significantly higher STD values for the aromatic hydrogens (**3** and **4**, Figure 2C&D) compared to the methyl groups (in **1** and **2**, Figure 2A&B) were found. This clearly indicates spatial proximity of the aromatic aglycones to DC-SIGN. However, a comparison of the binding epitopes reveals further differences going beyond aglycones. For the D-GlcNAc moieties of methyl Le<sup>x</sup> (**1**) and Le<sup>a</sup> (**2**) the maximal STD values for ring hydrogens are smaller than for H-6 of D-Fuc (up to 75%), whereas for the phenyl derivatives **3** and **4** the values reach up to 165%. Especially for phenyl Le<sup>a</sup> (**4**), and to a lesser extent for phenyl Le<sup>x</sup> (**3**), high STD values (80-220%) are equally distributed over the entire structure. In contrast, for methyl Le<sup>x</sup> (**1**), methyl Le<sup>a</sup> (**2**) high STD values are predominantly located on the L-Fuc moiety. The latter finding corresponds with X-ray data when the Le<sup>x</sup>-containing

LNFP III is co-crystallized with DC-SIGN,<sup>22</sup> indicating the dominant role of the L-Fuc moiety in these binding epitopes.

**2.3. Molecular Modeling Studies.** Overall, the correlation of increased affinity with the presence of aromatic aglycones as well as the STD NMR data suggest a spatial proximity of the phenyl substituents to DC-SIGN. This is in contrast to the structural information deduced from the co-crystallization of LNFP III with the CRD of DC-SIGN.<sup>22</sup> For a possible solution of this riddle, docking studies were initiated. The crystal structure 1SL5<sup>22</sup> was used as starting point for the docking studies. The replacement of the internal D-Gal moiety in LNFP III by a methyl aglycone LNFP III → methyl Le<sup>x</sup> (**1**) is not expected to have a significant influence on its binding mode as indicated by the small STD value of the aglycone in **1** (Figure 2A). In addition, the proximity of the *N*-acetyl of the D-GlcNAc moiety to Val351 as proposed by the crystal structure (inter-proton distance of 2.5 Å)<sup>22</sup> is reflected by the increased STD value.

Automated docking of methyl Le<sup>x</sup> (**1**) positions the Le<sup>x</sup> subunit in close agreement (RMSD 0.7Å) with its orientation in the crystal structure<sup>22</sup> as shown in Figure 3A. In the docking pose of methyl Le<sup>a</sup> (**2**), on the other hand, the D-GlcNAc residue is flipped along its C1-O5 axis, thereby positioning L-Fuc moiety similar to the LNFP III crystal structure. Calcium coordination and H-bond network to L-Fuc are thus maintained (Figure 3B). In this new orientation D-Gal can establish the same characteristic H-bond to Asp367 as well. However, *N*-acetyl group of D-GlcNAc no longer forms a hydrophobic contact with Val351 but with Phe313 instead, with a much longer inter-proton distance of ~ 4.5 Å. This is in good agreement with the lower intensity of the STD NMR signal of the *N*-acetyl group of GlcNAc in methyl Le<sup>a</sup> (**2**, Figure 2B).

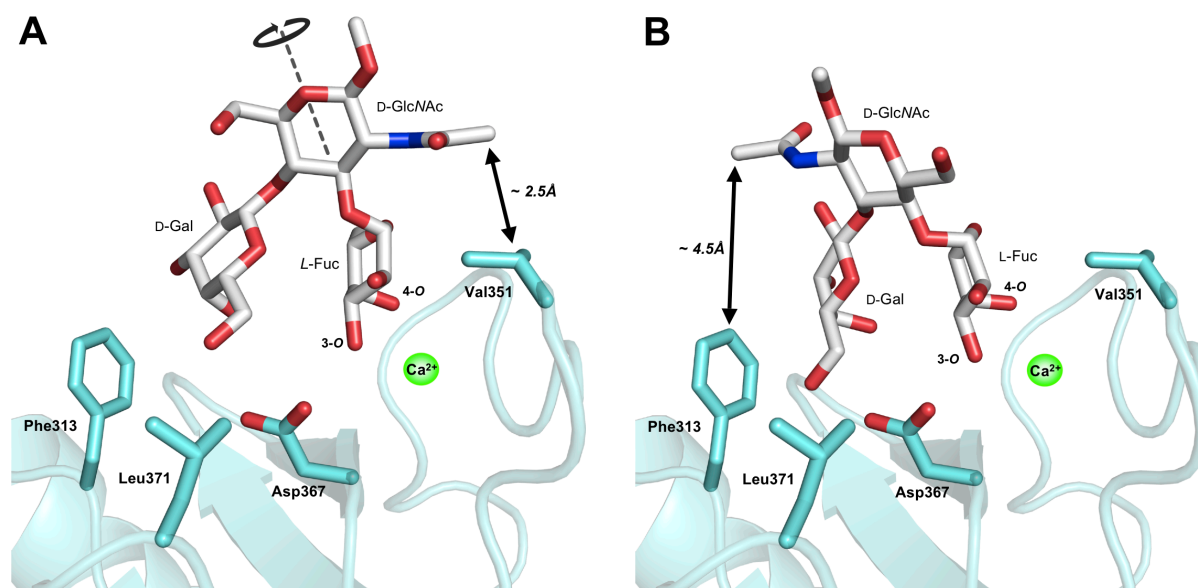


**Figure 3.** A) Docking modes of methyl  $\text{Le}^x$  (1) and B) methyl  $\text{Le}^a$  (2). Contacts between the *N*-acetyl groups and closest protein residues are highlighted with double-headed arrows.

A binding mode for phenyl  $\text{Le}^x$  (3) where the  $\text{Le}^x$  subunit adopts an analogous orientation to LNFP III (Figure 1A) is inconsistent with the significant saturation transfer observed for the aromatic protons, since the aglycone would point to the solvent with no close contacts to the protein (Figure 4A). The top-ranked pose from Glide XP<sup>33</sup> induced-fit docking presents an alternative pose where the ligand lies “flat” on the receptor and the phenyl aglycone makes a close contact with a hydrophobic cavity formed by the side chains of Phe313 and Leu371 (Figure 4B). This docking pose perfectly explains the large STD values of the aromatic protons of phenyl  $\text{Le}^x$  (3, Figure 2C), indicating a close proximity to DC-SIGN.

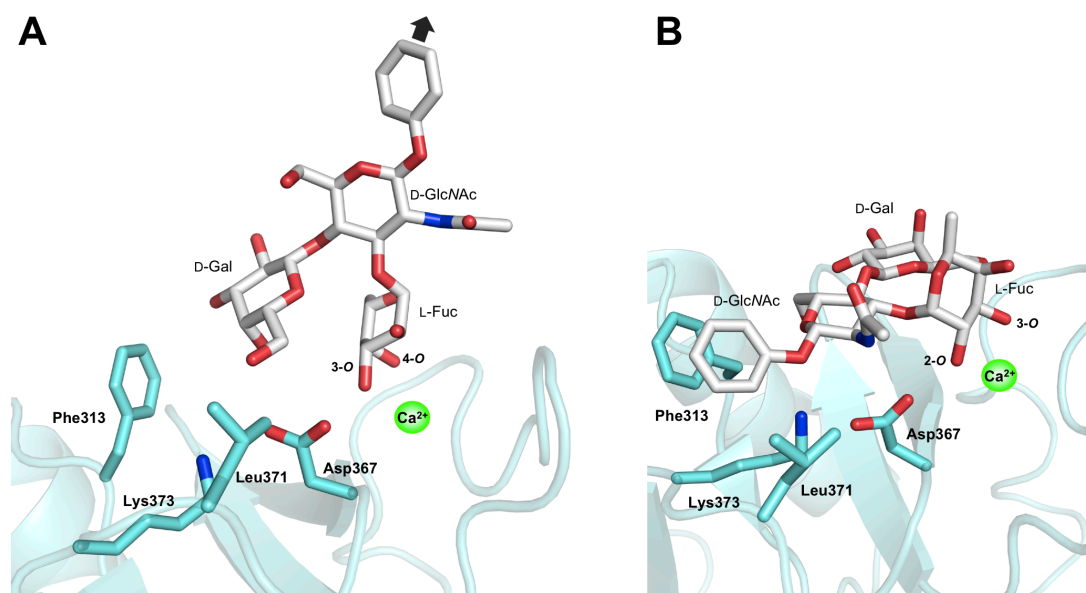


**Figure 4.** A) When phenyl Le<sup>x</sup> (**3**) binds to DC-SIGN in a manner comparable to methyl Le<sup>x</sup> (**2**) (Figure 3A) and LNFP III (Figure 1A), the phenyl aglycone points to the solvent (black arrow), not exhibiting an apparent protein contact. B) The induced-fit docking pose for phenyl Le<sup>x</sup> (**3**) shows an interaction of the phenyl aglycone with the hydrophobic cleft formed by Phe313 and Leu371, rationalizing the strong aromatic proton signals in STD NMR.

Because of smaller overlaps of the resonances in the H-NMR spectrum of phenyl Le<sup>a</sup> (**4**), its STD NMR analysis is more detailed. The automated docking pose of phenyl Le<sup>a</sup> (Figure 5) is similar to phenyl Le<sup>x</sup> (**3**) where L-Fuc coordinates to Ca<sup>2+</sup> via the two equatorial hydroxyl groups at the 2- and 3-position. In addition, H-bonds from 2-OH to both Glu354 and Asn365 and between 3-OH and Glu347 are formed. The D-Gal moiety lies close to the primary binding site forming two H-bonds from 6-OH to Glu347 and from 2-OH to Ser360 (not shown). The phenyl aglycone occupies the same hydrophobic pocket (Phe313 and Leu371) as phenyl Le<sup>x</sup> (**3**) (Figure 4B), rationalizing the large STD values for the aromatic protons (Figure 2D). Moreover, D-GlcNAc also interacts via a H-bond between its 6-OH and Asp367, which in turn bridges this H-bond to Lys373. In the proposed orientation, the D-GlcNAc moiety of phenyl Le<sup>a</sup> (**4**) is in closer contact with the receptor compared to methyl Le<sup>a</sup> (**2**) (Figure 3B), which explains the observed larger STD values for the D-GlcNAc protons. Dynamic stability of this novel binding mode was confirmed by molecular dynamics simulation.



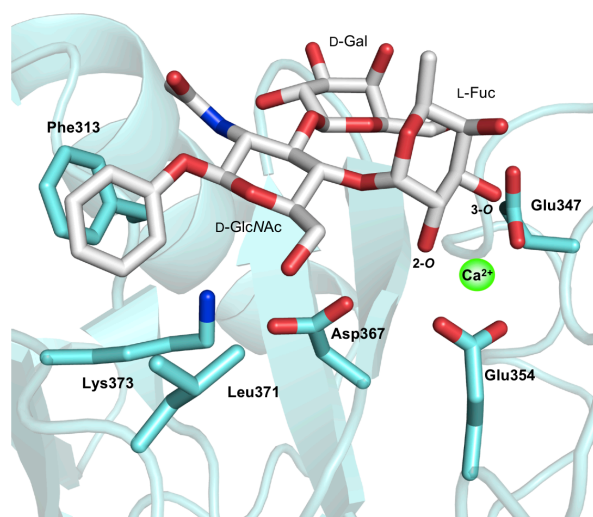


**Figure 5.** Binding mode of phenyl Le<sup>a</sup> (4) to DC-SIGN. Binding of the phenyl aglycone in the hydrophobic cleft formed by Phe313 and Leu371 and proximity of the D-GlcNAc moiety to protein surface coincides with the measured STD NMR values (Figure 2D).

**2.4. Mutagenesis Studies.** To further confirm the proposed hydrophobic interaction between Phe313 and the aromatic aglycone, the known DC-SIGN CRD F313A<sup>22</sup> was expressed and the binding affinities for methyl Le<sup>a</sup> (2) and phenyl Le<sup>a</sup> (4) were determined. Table 2 summarizes the results of the competitive binding assay with wild type and mutant DC-SIGN CRD. L-Fuc was included as reference compound. The F313A mutation should not have an impact on binding affinity of L-Fuc since the monosaccharide is assumed to bind exclusively in the primary binding site.<sup>22</sup> However, L-Fuc showed a lower IC<sub>50</sub> value for the mutant protein (IC<sub>50</sub> 3.9 mM) than for the wild type (IC<sub>50</sub> 7.6 mM). This can be explained by the lower affinity of Le<sup>a</sup>-PAA for the F313A mutant, reflected by the EC<sub>50</sub> value (Table 2). For a better comparison we state relative IC<sub>50</sub> values (rIC<sub>50</sub>) with L-Fuc as reference (Table 2).

**Table 2.** Results of the competitive binding assay for L-Fuc, methyl Le<sup>a</sup> (**2**), and phenyl Le<sup>a</sup> (**4**) with wild type and mutant DC-SIGN. The observed differences in the absolute inhibitory potencies between wild type and mutant are due to different binding affinities to Le<sup>a</sup>-PAA reflected by a higher EC<sub>50</sub> value (half maximal effective concentration) in case of the mutant protein. The rIC<sub>50</sub> values of methyl Le<sup>a</sup> (**2**) and phenyl Le<sup>a</sup> (**4**) with L-Fuc as reference were determined by dividing the respective IC<sub>50</sub> values by the IC<sub>50</sub> of L-Fuc; a value below 1 resembles higher affinity than L-Fuc. Detailed information on protein expression and competitive binding assay is given in the experimental section.

Ligand	DC-SIGN wild type	DC-SIGN F313A mutant
EC <sub>50</sub> Le <sup>a</sup> -PAA	66.9 ± 0.3 ng/ml	111.2 ± 0.2 ng/ml
rIC <sub>50</sub> L-Fuc	1	1
rIC <sub>50</sub> methyl Le <sup>a</sup> ( <b>2</b> )	0.38	0.46
rIC <sub>50</sub> phenyl Le <sup>a</sup> ( <b>4</b> )	0.12	0.43
Factor of <b>2</b> to <b>4</b>	3.2	1.1

In Figure 6, inhibition curves for methyl Le<sup>a</sup> (**2**) and phenyl Le<sup>a</sup> (**4**) with wild type and mutant DC-SIGN CRD-Fc are shown. Graph A visualizes the aforementioned difference in binding affinity of methyl Le<sup>a</sup> (**2**) and phenyl Le<sup>a</sup> (**4**) to wild type DC-SIGN (factor 3.2). In contrast, both compounds exhibited near identical binding affinities (factor 1.1, Figure 6B) for the F313A mutant, which indicates the omission of the beneficial hydrophobic contact of Phe313 with the phenyl aglycone.

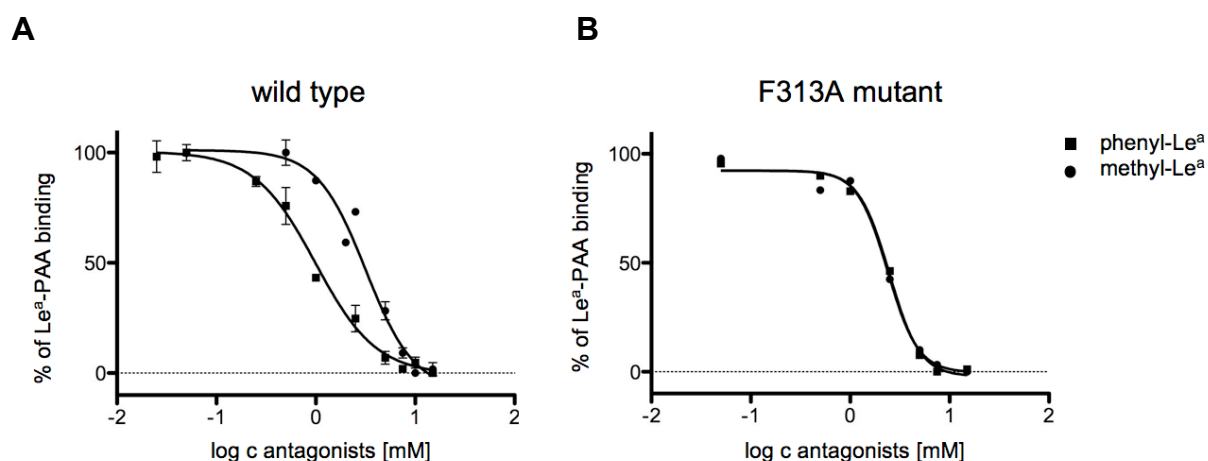


**Figure 6.** Inhibition curves for methyl Le<sup>a</sup> (**2**) and phenyl Le<sup>a</sup> (**4**) obtained from the competitive binding assay, with (A) wild type DC-SIGN and (B) F313A mutant.

### 3. Conclusion

STD NMR spectroscopy and molecular modeling supplemented with a protein mutation study were used to rationalize diverging binding modes of Le<sup>a</sup> and Le<sup>x</sup> antigens to DC-SIGN induced by the nature of the aglycone. The originally found improved binding affinity of phenyl Le<sup>x</sup> (**3**) and phenyl Le<sup>a</sup> (**4**) indicated a contribution of the phenyl aglycone to binding, presumably by a hydrophobic contact with the protein. Strong STD NMR values further confirmed this assumption. Docking and MD studies finally revealed a novel favorably interaction of the phenyl aglycone with a hydrophobic pocket formed by Phe313 and Leu371. With a single-point mutation of the DC-SIGN CRD the proposed interactions of the phenyl aglycone of **4** with Phe313 could be verified.

Here, we report an interesting example, illustrating how flexible binding modes on shallow protein surfaces can be, especially when the starting affinity is low, a situation often present in carbohydrate-lectin interactions. Therefore, improved affinities induced by structural modifications should be carefully analyzed regarding possible reorientations of binding modes. STD NMR experiments<sup>28,29</sup> represent an excellent tool for this endeavor. Based on the new binding mode of phenyl Le<sup>x</sup> (**3**) and phenyl Le<sup>a</sup> (**4**), the interaction within the hydrophobic pocket formed by Phe313 and Leu371 provides a promising rational for the design of more potent DC-SIGN antagonists.

Our study demonstrates the value of this additional interaction with the hydrophobic cleft formed by Phe313 and Leu371, which in fact leads to a switch in the binding mode for Le<sup>a</sup> and Le<sup>x</sup> upon introduction of an aromatic aglycone. Making use of this interaction is therewith a promising rational for the design of more potent DC-SIGN antagonists and was already approached with a series of glycomimetics by Bernardi et al., recently.<sup>24</sup>

### 4. Experimental section

**4.1. Ligands.** Methyl Le<sup>x</sup> (**1**) and methyl Le<sup>a</sup> (**2**) were purchased from Toronto Research Chemicals Inc. Phenyl Le<sup>x</sup> (**3**) and phenyl Le<sup>a</sup> (**4**) were prepared according to ref<sup>34</sup>.

**4.2. Cloning of DC-SIGN CRD-IgG(Fc).** Plasmids containing the full-length cDNA of DC-SIGN were kindly provided by Daniel A. Mitchell (Glycobiology Institute, Department of

Biochemistry, University of Oxford). Standard molecular techniques<sup>35</sup> were used for the cloning of the carbohydrate recognition domain of DC-SIGN (DC-SIGN CRD; aa residues 250-404, GenBank accession no. M98457). The DC-SIGN CRD encoding insert was amplified by PCR using specific forward and reverse primers containing the restriction sites *EcoRI* and *NcoI* (New England BioLabs, Allschwil, Switzerland), respectively. The insert was ligated into the corresponding cloning site of the pFUSE-hIgG2-Fc2 expression vector (Invivogen, Toulouse, France). The construct was amplified in chemocompetent DH5 $\alpha$  *E. coli* (Novagen, Lucerne, Switzerland). After plasmid minipreparation and restriction control, the construct correctness was confirmed by DNA sequencing.

**4.3. Expression and purification of DC-SIGN CRD-Fc.** CHO-K1 cells (American Type Culture Collection No. CCL-61<sup>TM</sup>) were cultivated in Ham's Nutrient Mixture F-12 (Invitrogen, Paisley, UK) supplemented with 2 mM L-glutamate, 10% fetal calf serum (FCS, Invitrogen, Paisley, UK), 100 U/mL penicillin, and 100  $\mu$ g/mL streptomycin (Sigma-Aldrich, Basel, Switzerland). The cells were cultivated as monolayers in tissue culture flasks (Nunc, Roskilde, Denmark). The CHO-K1 cells were transfected with the DC-SIGN CRD expression vector using the FuGENE<sup>®</sup> HD transfection reagent (Roche Applied Science, Rotkreuz, Switzerland) following to the instructions of the supplier. Stably transfected CHO-K1 cells were selected by treatment with Zeocin<sup>TM</sup> (0.5  $\mu$ g/ml, Invitrogen, Paisley, UK) and single clones were obtained by limiting dilution. For DC-SIGN CRD-Fc production the cells were cultivated as described above and the culture medium, containing the secreted DC-SIGN CRD-Fc chimera was harvested weekly, adjusted to pH 7.6 and sterile filtrated (conditioned medium).

The purification of the recombinant protein was achieved by applying conditioned medium on a protein A-sepharose column (BioVision, Mountain View, CA, USA) attached to a fast protein liquid chromatography apparatus (BioLogic (FPLC) system, BioRad, Reinach BL, Switzerland), which was previously equilibrated with loading buffer I (20 mM Tris/HCl, pH 7.6, 150 mM NaCl, 0.05% (v/v) Tween-20<sup>TM</sup>). The protein was eluted with elution buffer I (0.5 M acetic acid/ammonium acetate, pH 3.4). The collected protein was further purified on a L-Fuc-sepharose column (prepared in house) using loading buffer II (20 mM Tris/HCl, pH 7.8, 0.5 M NaCl, 25 mM CaCl<sub>2</sub>) and elution buffer II (20 mM Tris/HCl, pH 7.8, 0.5 M NaCl, 2 mM EDTA). For long-term storage, the protein was frozen at -80 °C.

**4.4. Cloning of the F313A DC-SIGN CRD mutant.** The PCR overlap extension method<sup>36</sup> was used for the substitution of the codon TTC against CGC at cDNA bp 968-970, resulting in the mutation of phenyl alanine 313 to an alanine. In a first step, two overlapping DNA fragments were generated separately, both using wild type DC-SIGN cDNA as template (PCR 1: primer fw: 5` g gaa ttc cat atg gaa cgc ctg tgc cac ccc 3` and primer F313A rv: 5` tcc aga agt aac cgc **gcg** acc tgg atg gga 3`; PCR 2: primer F313A fw: 5` aag tcc cat cca ggt **cgc** gcg gtt act tct 3` and primer rv: 5` cgc gga tcc tta cta cgc agg agg ggg gtt tgg g 3`). The two internal primers contained a mismatch for the site-directed base substitution (bold). In a second step, both overlapping DNA fragments were elongated to the full-length gene, containing the single point mutation. The *NdeI* and *BamHI* (New England BioLabs, Allschwil, Switzerland) treated insert was ligated into the corresponding cloning site of the expression vector pET-3a. After *E.coli* DH5 $\alpha$  transformation, plasmid minipreparation, the mutation was confirmed by DNA sequencing. Finally, for protein expression the construct was transformed into BL21 *E.coli* (Novagen, Lucerne, Switzerland).

**4.5. Expression and purification of F313A DC-SIGN CRD mutant.** Protein expression was carried out in TB medium (terrific broth) containing 100  $\mu$ g/mL ampicillin (Applichem, Darmstadt, Germany). The bacteria were cultured at 37 °C until an OD<sub>600</sub> of 1.0 was reached. The expression was induced by the addition of isopropyl- $\beta$ -D-thiogalactoside (IPTG, Applichem, Darmstadt, Germany) at the final concentration of 0.4 mM. The cells were further cultivated for 12 h, prior to harvesting by centrifugation at 4000 rpm for 20 min at 4 °C. For bacterial lysis, the pellet was dissolved in 20 mM Tris-HCl buffer, pH 7.8, 0.5 M NaCl, containing 1 mg/mL lysozym (Sigma, Buchs, Switzerland) and incubated for 30 min at 4 °C under shaking. The inclusion bodies were solubilized by addition of  $\beta$ -mercaptoethanol (0.01 % v/v), urea (8 M), and brief sonication followed by gentle rotation for 30 min at 4 °C. The mixture was centrifuged at 22000 rpm for 1 h at 4°C and the supernatant was diluted by slow addition of the fivefold volume loading buffer II. The mixture was dialyzed against 6 volumes of loading buffer II with 6 buffer exchanges. After dialysis, insoluble precipitate was removed by centrifugation at 22000 rpm for 1 h at 4°C. The protein was purified using a L-Fuc-sepharose column as described above.

Protein purity was confirmed by standard SDS-PAGE analysis<sup>37</sup> followed by Coomassie Brilliant Blue G-250 staining (Bio-Rad laboratories, Hercules, CA, USA). Protein

concentration was determined either by the Bradford method (Bio-Rad laboratories, Hercules, CA, USA) or with HPLC<sup>38</sup>.

**4.6. Competitive binding assay.** Biotinylated Le<sup>a</sup>-PAA polymer (20  $\mu$ L, 1 mg/mL, GlycoTech, Gaithersburg, MD, USA) was mixed with 80  $\mu$ L assay buffer (20 mM HEPES, 150 mM NaCl, 10 mM CaCl<sub>2</sub>, pH 7.4), 20  $\mu$ L FCS and 80  $\mu$ L streptavidin-horseradish peroxidase-conjugate (500 U/mL, Roche, Mannheim, Germany) and incubated for 2 h at 37 °C. The complex was stable for several weeks when stored at 4 °C.

Flat-bottom 96-well microtiter plates (F96 MaxiSorp, Nunc) were coated with 100  $\mu$ L/well of a 2.5  $\mu$ g/mL solution of DC-SIGN CRD-Fc protein in assay buffer overnight at 4 °C in a humidified chamber. The coating solution was discarded and the wells were blocked with 200  $\mu$ L/well of 3% bovine serum albumin (BSA, Sigma-Aldrich, Buchs, Germany) in assay buffer for 2 h at 4 °C. After three washing steps with assay buffer (150  $\mu$ L/well), a serial dilution of the test compound (25  $\mu$ L/well) in assay buffer and streptavidin-peroxidase coupled Le<sup>a</sup>-PAA (25  $\mu$ L/well, 0.25  $\mu$ g/mL final concentration) were added. Subsequent to an incubation of 3 h at room temperature and 350 rpm the plate was carefully washed four times with 200  $\mu$ L/well assay buffer. Le<sup>a</sup>-PAA binding was detected by addition of 100  $\mu$ L/well of ABTS-substrate (2,2'-azino-bis-(3-ethylbenzthiazoline-6-sulfonic acid, Invitrogen, Paisley, UK). The colorimetric reaction was allowed to develop for 2 min, then stopped by the addition of 2% aqueous oxalic acid before the optical density (OD) was measured at 415 nm on a microplate-reader (Spectramax 190, Molecular Devices, Ca, USA). The IC<sub>50</sub>-values were calculated using the Prism software (GraphPad Software, Inc, La Jolla, USA). The IC<sub>50</sub> (half maximal inhibitory concentration) defines the molar concentration of the test compound that reduces the maximal specific binding of carbohydrate-polymer to DC-SIGN-CRD-Fc by 50%.

For EC<sub>50</sub> determination (half maximal effective concentration) of the Le<sup>a</sup>-PAA, the assay was performed as described above with a serial dilution of Le<sup>a</sup>-PAA (0-3  $\mu$ g/mL) in absence of antagonist.

**4.7. Isothermal titration calorimetry.** ITC experiments were performed at 298 K and a reference power of 10  $\mu$ cal/sec under constant stirring speed of 307 rpm using a MicroCal VP-ITC instrument (MicroCal, Northampton, MA). The concentration of DC-SIGN CRD-Fc was determined by HPLC-UV against a standard curve of BSA at 210 nm<sup>38</sup> after extensive dialysis against 10 mM HEPES, 150 mM NaCl, 10 mM CaCl<sub>2</sub>, pH 7.4. The ligand was diluted in the dialysat. Injections of 3-5  $\mu$ l ligand solutions were added from a syringe at an

interval of 5 min into the sample cell solution containing DC-SIGN CRD-Fc (cell volume 1.45 ml). Control experiments were performed, where identical ligand solutions were injected into buffer without protein, and showed insignificant heat of dilution. The experimental data were fitted to a theoretical titration curve (one site binding model) using Origin software (version 7, MicroCal). The quantity  $c = Mt(0)/K_D$  with  $Mt(0)$  as initial macromolecule concentration, is of importance in titration microcalorimetry.<sup>39</sup> The experiments were performed with  $c$  values below 1. The stoichiometry was fixed to 1 (concentration expressed in terms of binding site) to allow reliable determination of  $K_D$  and  $\Delta H$ .<sup>40, 41</sup> Thermodynamic parameters were calculated from the equation 1,

$$\Delta G^\circ = \Delta H^\circ - T\Delta S^\circ = -RT\ln K_A = RT\ln K_D \quad (\text{eq. 1})$$

where  $\Delta G^\circ$ ,  $\Delta H^\circ$ , and  $\Delta S^\circ$  are the changes in free energy, enthalpy, and entropy of binding, respectively.  $T$  is the absolute temperature, and  $R = 8.314 \text{ J/mol/K}$ .

**4.8. STD NMR.** Experiments were performed on a Bruker 11.7 T spectrometer with an Avance III console at a temperature of 298 K. Shigemi NMR tubes with a sample volume of 250  $\mu\text{L}$  were used for the measurements. Each sample contained 20-30  $\mu\text{M}$  DC-SIGN CRD-Fc (dimer) and 1-2 mM ligand. A d-Tris buffer was used as solvent containing 20 mM d-TRIS (98% Cambridge Isotope Libraries), 4 mM  $\text{CaCl}_2$  and 150 mM NaCl in  $\text{D}_2\text{O}$  (99.8% Sigma-Aldrich) adjusted to a pH of 8.1 with HCl.

Using a pulse sequence modified from Meyer *et al.*<sup>28</sup> allows simultaneous saturation of the protein at two frequencies which leads to a more intense STD epitope. The cosine modulated E-Burp-1 pulse<sup>42</sup> for the on resonance spectrum was centered at 1555 Hz and resulted in two sidebands at 0 and 3110 Hz with a power of 53 dB.<sup>43</sup> The duration of each of the 40 E-Burp-1 pulses used to saturate the protein was 50 ms with a 1ms recovery between the pulses.

Off-resonance excitation was set to 26000 Hz. STD NMR experiments were performed applying a Watergate solvent suppression. Specific parameters were determined via preliminary experiments including negative control experiments with only ligand-containing sample to avoid artifacts from direct excitation. Scaling each STD signal on an off-resonance reference spectrum resulted in a relative binding epitope (approximate values).<sup>30</sup> Ligand resonances were assigned by using 2D NMR and 1D selective TOCSY experiments. Not all protons could be assigned doubtlessly, due to solvent suppression and partial signal overlap.

Detailed conditions: STD NMR of methyl-bearing compounds: 2 mM ligand with 20  $\mu$ M DC-SIGN CRD-Fc, STD NMR of phenyl Le<sup>a</sup>: 1 mM ligand with 20  $\mu$ M DC-SIGN CRD-Fc, STD NMR of phenyl Le<sup>x</sup>: 1 mM with 30  $\mu$ M DC-SIGN CRD-Fc; number of scans was typically 14k for on-resonance spectra and 512 for off-resonance spectra.

Experiments with different saturation times were performed for phenyl Le<sup>a</sup>. These data indicate an overall consistent epitope at either saturation times of 0.7, 1, 2, and 3 s and exclude misinterpretation due to T1 bias for different proton species.

**4.9. Docking studies.** All ligands were manually built using Maestro, and optimized using standard procedures. Model for DC-SIGN in complex with LNFP III was downloaded from the Protein Data Bank (code: 1SL5). Hydrogens were added and water molecules were removed using Maestro Protein Preparation Wizard. Partial charges were calculated from OPLS2005 force field while protonation states and oxidation states for metals were assigned by Epik<sup>44</sup>. Orientation of added hydrogens was sampled for optimal H-bond formation and the model was then refined by minimization within RMSD of 0.3Å.

GlideXP<sup>33</sup> was used for docking of novel ligands to DC-SIGN. To account for the possibility of side chain re-organization upon ligand binding the Induced-Fit Docking (IFD) methodology was employed<sup>45</sup>. The binding site was defined to include residues within 5 Å radius around the co-crystallized ligand LNFP III in the prepared complex. In the initial stages of IFD protocol amino acids within 5 Å radius around any found pose were considered as flexible, and their side chain conformations were optimized. Up to 50 poses were retained for each calculation within an energy window of 40 kcal/mol to allow for larger diversity in output poses. Prioritization was done by Standard Precision (SP)<sup>46</sup> scoring function in the initial soft-docking stage followed by more rigorous Extra Precision (XP)<sup>47</sup> scoring in the redocking stage. Output poses were then visually inspected for agreement with STD NMR experiment, and those showing considerable discrepancy were disregarded. Stability of the proposed modes was assessed using molecular dynamics.



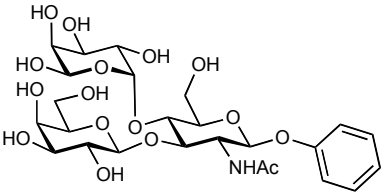
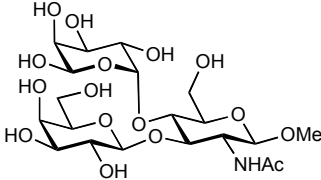
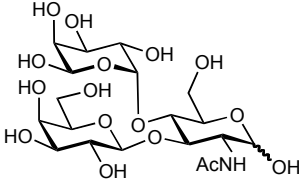
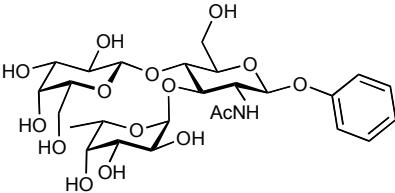
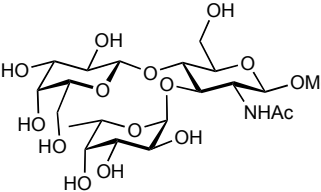
## References

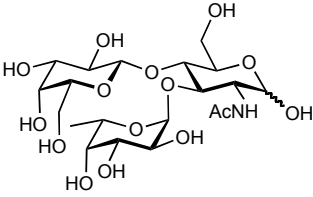
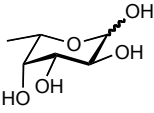
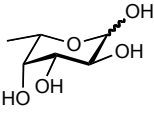
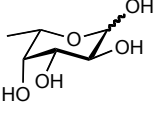
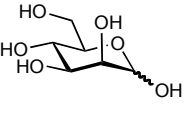
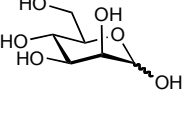
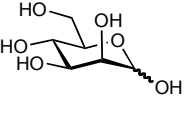
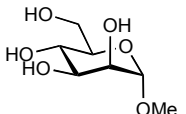
- (1) Hart, D. N. J.; Clark, G. J.; Dekker, J. W.; Fearnley, D. B.; Kato, M.; Hock, B. D., McLellan, A. D.; Neil, T.; Sorg, R. V., Sorg, U.; Summers, K. L.; Vuckovic, S. *Dendritic Cells in Fundamental and Clinical Immunology, Vol 3* **1997**, 417, 439-442.
- (2) Banchereau, J.; Steinman, R. M.; *Nature* **1998**, 392, 245-252.
- (3) Geijtenbeek, T. B. H.; Torensma, R.; van Vliet, S. J.; van Duijnhoven, G. C. F.; Adema, G. J.; van Kooyk, Y.; Figdor, C. G.; *Cell* **2000**, 100, 575-585.
- (4) Geijtenbeek, T. B. H.; van Vliet, S. J.; Koppel, E. A.; Sanchez-Hernandez, M.; Vandenbroucke-Grauls, C.; Appelmelk, B.; van Kooyk, Y. *J. Exp. Med.* **2003**, 197, 7-17.
- (5) Cambi, A.; Gijzen, K.; de Vries, J. M.; Torensma, R.; Joosten, B.; Adema, G. J.; Netea, M. G.; Kullberg, B. J.; Romani, L.; Figdor, C. G. *Eur. J. Immunol.* **2003**, 33, 532-538.
- (6) Geijtenbeek, T. B. H.; Kwon, D. S.; Torensma, R.; van Vliet, S. J.; van Duijnhoven, G. C. F.; Middel, J.; Cornelissen, I.; Nottet, H.; KewalRamani, V. N.; Littman, D. R.; Figdor, C. G.; van Kooyk, Y. *Cell* **2000**, 100, 587-597.
- (7) Marzi, A.; Gramberg, T.; Simmons, G.; Moller, P.; Rennekamp, A. J.; Krumbiegel, M.; Geier, M.; Eisemann, J.; Turza, N.; Saunier, B.; Steinkasserer, A.; Becker, S.; Bates, P.; Hofmann, H.; Pohlmann, S. *J. Virol.* **2004**, 78, 12090-12095.
- (8) Alvarez, C. P. *J. Virol.* **2002**, 76, 6841-6844.
- (9) Anderluh, M.; Jug, G.; Svajger, U.; Obermajer, N. *Curr. Med. Chem.* **2012**, 19, 992-1007.
- (10) Gurney, K. B.; Elliott, J.; Nassanian, H.; Song, C.; Soilleux, E.; McGowan, I.; Anton, P. A.; Lee, B. *J. Virol.* **2005**, 79, 5762-5773.
- (11) Bashirova, A. A.; Wu, L.; Cheng, J.; Martin, T. D.; Martin, M. P.; Benveniste, R. E.; Lifson, J. D.; KewalRamani, V. N.; Hughes, A.; Carrington, M. *J. Virol.* **2003**, 77, 217-227.
- (12) van Kooyk, Y.; Geijtenbeek, T. B. H. *Nat. Rev. Immunol.* **2003**, 3, 697-709.
- (13) Hong, P. W.; Flummerfelt, K. B.; de Parseval, A.; Gurney, K.; Elder, J. H.; Lee, B. *J. Virol.* **2002**, 76, 12855-12865.
- (14) Feinberg, H.; Mitchell, D. A.; Drickamer, K.; Weis, W. I. *Science* **2001**, 294, 2163-2166.
- (15) Van Die, I. *Glycobiology* **2003**, 13, 471-478.
- (16) Appelmelk, B. J. *J. Immunol.* **2003**, 170, 1635-1639.

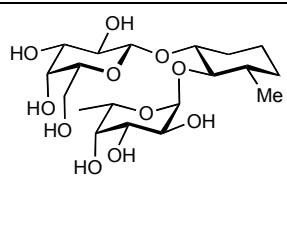
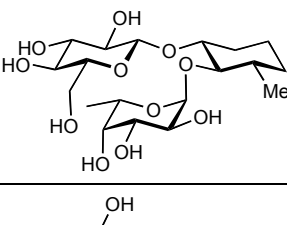
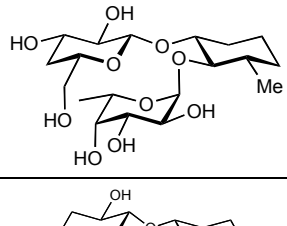
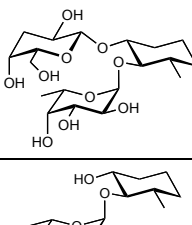
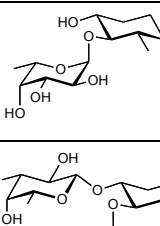
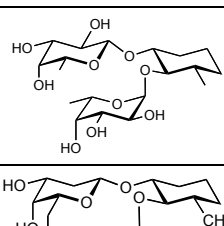
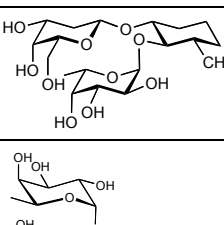
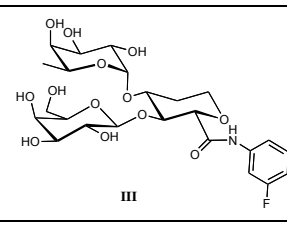
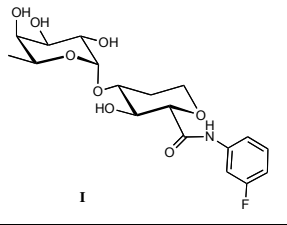
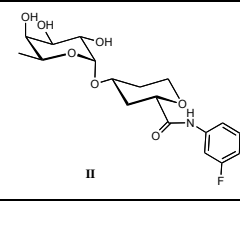
- 
- (17) Naarding, M. A.; Ludwig, I. S.; Groot, F.; Berkhout, B.; Geijtenbeek, T. B. H.; Pollakis, G.; Paxton, W. A. *J. Clin. Invest.* **2005**, *115*, 3256-3264.
- (18) Timpano, G.; Tabarani, G.; Anderluh, M.; Invernizzi, D.; Vasile, F.; Potenza, D.; Nieto, P. M.; Rojo, J.; Fieschi, F.; Bernardi, A. *ChemBioChem* **2008**, *9*, 1921-1930.
- (19) van Liempt, E.; Bank, C. M. C.; Mehta, P.; Garcia-Vallejo, J. J.; Kwar, Z. S.; Geyer, R.; Alvarez, R. A.; Cummings, R. D.; van Kooyk, Y.; van Die, I. *FEBS Lett.* **2006**, *580*, 6123-6131.
- (20) Mitchell, D. A.; Fadden, A. J.; Drickamer, K. *J. Biol. Chem.* **2001**, *276*, 28939-28945.
- (21) Feinberg, H.; Guo, Y.; Mitchell, D. A.; Drickamer, K.; Weis, W. I.; *J. Biol. Chem.* **2005**, *280*, 1327-1335.
- (22) Guo, Y.; Feinberg, H.; Conroy, E.; Mitchell, D.; Alvarez, R.; Blixt, O.; Taylor, M.; Weis, W. I.; Drickamer, K. *Nat. Struct. Mol. Biol.* **2004**, *11*, 591-598.
- (23) Obermajer, N.; Sattin, S.; Colombo, C.; Bruno, M.; Švajger, U.; Anderluh, M.; Bernardi, A. *Mol. Diversity* **2010**, 1-14.
- (24) Andreini, M.; Doknic, D.; Sutkeviciute, I.; Reina, J. J.; Duan, J.; Chabrol, E.; Thepaut, M.; Moroni, E.; Doro, F.; Belvisi, L.; Weiser, J.; Rojo, J.; Fieschi, F.; Bernardi, A. *Org. Biomol. Chem.* **2011**, *9*, 5778-5786.
- (25) Toone, E. J. *Curr. Opin. Struct. Biol.* **1994**, *4*, 719-728.
- (26) Ambrosi, M.; Cameron, N. R.; Davis, B. G. *Org. Biomol. Chem.* **2005**, *3*, 1593-1608.
- (27) Dam, T. K.; Brewer, C. F. *Chem. Rev.* **2002**, *102*, 387-429.
- (28) Mayer, M.; Meyer, B. *Angew. Chem., Int. Ed.* **1999**, *38*, 1784-1788.
- (29) Meyer, B.; Peters, T. *Angew. Chem., Int. Ed.* **2003**, *42*, 864-890.
- (30) Mayer, M.; Meyer, B. *J. Am. Chem. Soc.* **2001**, *123*(25), 6108-6117.
- (31) Haselhorst, T.; Lamerz, A.-C.; von Itzstein, M. **2009**, 1-12.
- (32) Guzzi, C.; Angulo, J.; Doro, F.; Reina, J. J.; Thepaut, M.; Fieschi, F.; Bernardi, A.; Rojo, J.; Nieto, P. M. *Org. Biomol. Chem.* **2011**, *9*, 7705-7712.
- (33) Glide, version 5.7, Schrödinger, LLC, New York, NY, 2011.
- (34) Su, Z.; Wagner, B.; Cocinero, E. J.; Ernst, B.; Simons, J. P. *Chem. Phys. Lett.* **2009**, *477*, 365-368.
- (35) Sambrook, J.; Fritsch, E. F.; Maniatis, T. Cold Spring Harbor Laboratory Press, NY, **1989**.
- (36) Ho, S. N.; Hunt, H. D.; Horton, R. M.; Pullen, J. K.; Bell, M. P.; McKean, D. J.; Pease, L. R. *FASEB J.* **1989**, *3*, A519.
- (37) Laemmli, U. K. *Nature* **1970**, *227*, 680-685.

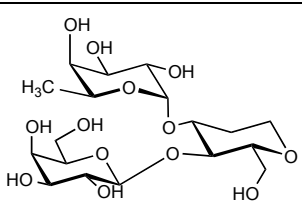
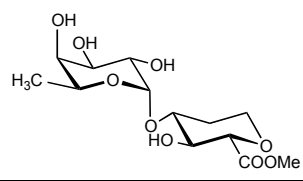
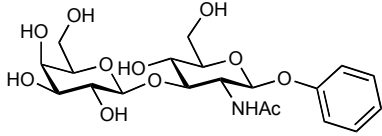
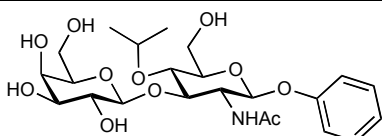
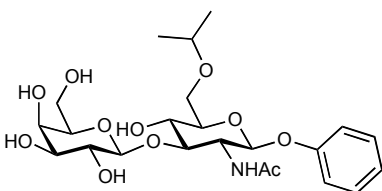
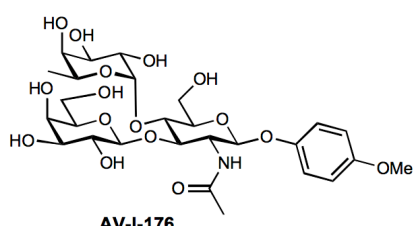
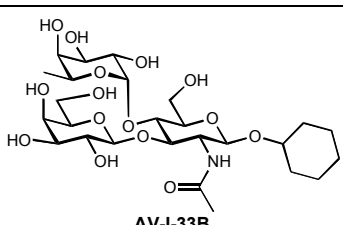
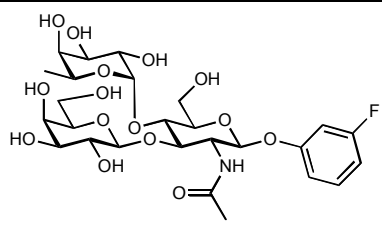
- (38) Bitsch, F.; Aichholz, R.; Kallen, J.; Geisse, S.; Fournier, B.; Schlaeppli, J.-M. *Anal. Biochem.* **2003**, *323*, 139-149.
- (39) Wiseman, T.; Williston, S.; Brandts, J. F.; Lin, L. N. *Anal. Biochem.* **1989**, *179*, 131-137.
- (40) Turnbull, W. B.; Daranas, A. H. *J. Am. Chem. Soc.* **2003**, *125*, 14859-14866.
- (41) Tellinghuisen, J. *Anal. Biochem.* **2008**, *373*, 395-397.
- (42) Geen, H.; Wimperis, S.; Freeman, R. *J. of Magn. Reson.* **1989**, *85*, 620-627.
- (43) Cutting, B.; Shelke, S. V.; Dragic, Z.; Wagner, B.; Gathje, H.; Kelm, S.; Ernst, B. *Magn. Reson. Chem.* **2007**, *45*, 720-724.
- (44) Shelley, J. C.; Cholleti, A.; Frye, L. L.; Greenwood, J. R.; Timlin, M. R.; Uchimaya, M. *J. Comput.-Aided Mol. Des.* **2007**, *21*, 681-691.
- (45) Sherman, W.; Day, T.; Jacobson, M. P.; Friesner, R. A.; Farid, R. *J. Med. Chem.* **2006**, *49*, 534-553.
- (46) Friesner, R. A.; Banks, J. L.; Murphy, R. B.; Halgren, T. A.; Klicic, J. J.; Mainz, D. T.; Repasky, M. P.; Knoll, E. H.; Shelley, M.; Perry, J. K.; Shaw, D. E.; Francis, P.; Shenkin, P. S. *J. Med. Chem.* **2004**, *47*, 1739-1749.
- (47) Friesner, R. A.; Murphy, R. B.; Repasky, M. P.; Frye, L. L.; Greenwood, J. R.; Halgren, T. A.; Sanschagrin, P. C.; Mainz, D. T. *J. Med. Chem.* **2006**, *49*, 6177-6196.

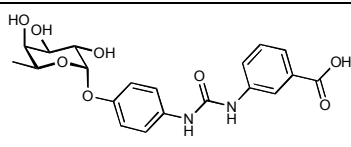
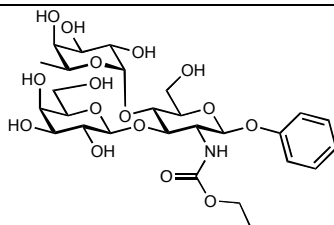
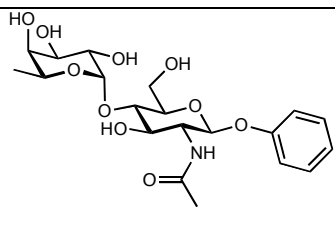
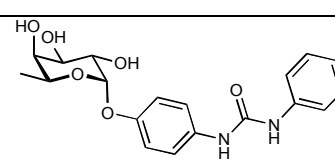
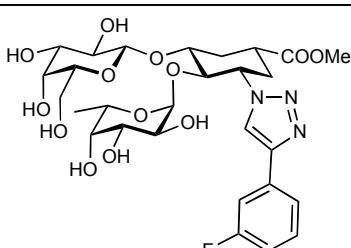
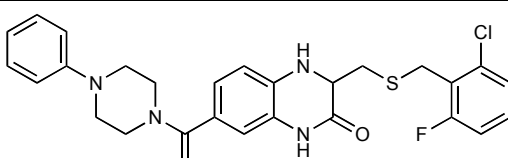
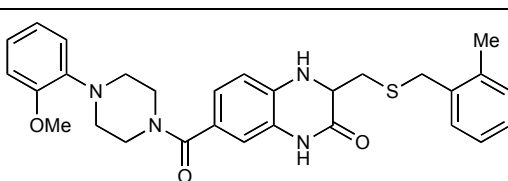
## Competitive binding assay results

Nr.	Structure	IC <sub>50</sub> (binding assay, Le <sup>a</sup> -PAA)	rIC <sub>50</sub>	Reference
<b>AV33</b> <b>(Ph Le<sup>a</sup>)</b>		0.28 mM/16.12.09 0.14 mM/11.02.10 0.46 mM/16.04.10 0.7 mM/20.04.10 0.75 mM/22.04.10 0.77 mM/23.04.10 1.39 mM/22.06.10 1.13 mM/24.06.10 0.71 mM/25.06.10 0.95 mM/21.07.10 1.3 mM/23.07.10 1.2 mM/24.11.10 1.1 mM/29.03.11 0.82 mM/30.03.11 0.67 mM/31.03.11 1.2 mM/01.04.11 0.64 mM/16.06.11 0.73 mM/17.06.11 0.99 mM/07.07.11	1 1	
<b>Me Le<sup>a</sup></b> (Toronto Research Chemicals, Canada)		2.45 mM/16.12.10 2.69 mM/24.06.10 1.96 mM/25.06.10 3.48 mM/19.10.10	8.75 3.7 2.7 3.6	Ph Le <sup>a</sup> Ph Le <sup>a</sup> Ph Le <sup>a</sup> Ph Le <sup>a</sup>
<b>Le<sup>a</sup></b>		2.8 mM/17.07.09	6.08, relative to mean value of AV33 results: 0.46 mM	Ph Le <sup>a</sup>
<b>BW558</b> <b>(Ph Le<sup>x</sup>)</b>		0.87 mM/16.12.09 0.29 mM/11.02.10 1.62 mM/14.10.10	3.1 2.1	Ph Le <sup>a</sup> Ph Le <sup>a</sup>
<b>Me Le<sup>x</sup></b> (Toronto Research Chemicals, Canada)		2.4 mM/24.06.10 2.2 mM/25.06.10	3.4 3.1	Ph Le <sup>a</sup> Ph Le <sup>a</sup>

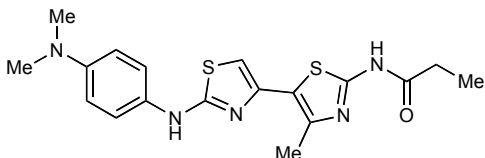
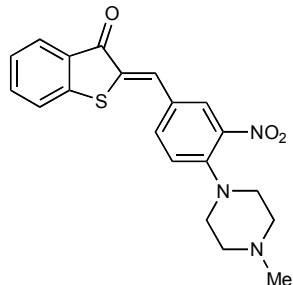
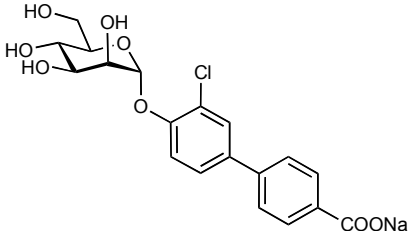
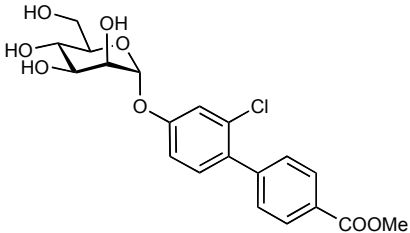
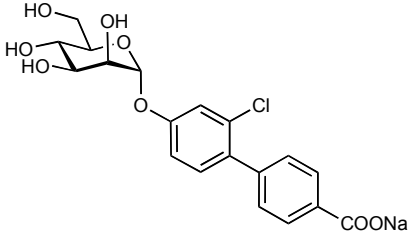
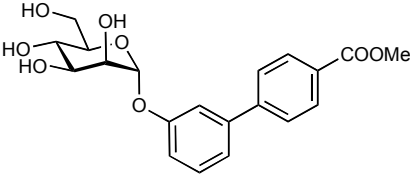
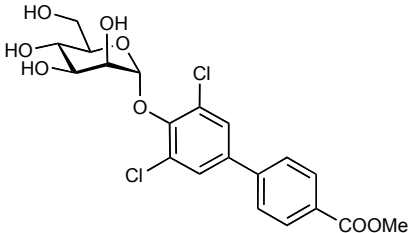
<b>Le<sup>x</sup></b>		3.8 mM/17.07.09	8.1, relative to mean value of AV33 results: 0.46 mM	Ph Le <sup>a</sup>
<b>L-fucose</b>		15.5 mM/10.10.08 10.8 mM/12.01.09 9.7 mM/20.02.09 6.2 mM/07.05.09 3.5 mM/08.05.09 13.9 mM/25.05.09 11.0 mM/09.02.10 11.4 mM/14.04.10 4.10 mM/15.04.10 4.86 mM/16.04.10 8.75 mM/20.04.10 5.4 mM/23.04.10 6.1 mM/23.04.10 9.58 mM/21.07.10	10.5 12.5 7.2	Ph Le <sup>a</sup> Ph Le <sup>a</sup> Ph Le <sup>a</sup>
<b>L-fucose</b>		4.06 mM/10.10.08 3.98 mM/10.03.09 3.0 mM/13.03.09 2.0 mM/30.06.10 2.5 mM/30.06.10 vs. trimannose- biotin-PAA	m. v.: 3.68 ± 0.59	Ph Le <sup>a</sup>
<b>L-fucose</b>		0.94 mM/09.06.10 1.10 mM/30.06.10 1.01 mM/30.06.10 vs. mannose-biotin- PAA		
<b>D-mannose</b>		7.7 mM/15.04.10 8.23 mM/21.04.10 10.31 mM/23.04.10 10.28 mM/18.08.10		
<b>D-mannose</b>		1.7 mM/09.06.10 1.27 mM/30.06.10 2.1 mM/18.08.10 vs. mannose-biotin- PAA		
<b>D-mannose</b>		2.72 mM/30.06.10 2.58 mM/30.06.10 2.5 mM/18.08.10 vs. trimannose- biotin-PAA		
<b>Me α-D-mannoside</b>		10.3 mM/12.01.09 6.8 mM/24.06.10 7.1 mM/25.06.10	9.6 10	Ph Le <sup>a</sup> Ph Le <sup>a</sup>
<b>D-glucose</b>		21.6 mM/24.06.10 23.3 mM/25.06.10	30.4 32.8	Ph Le <sup>a</sup> Ph Le <sup>a</sup>

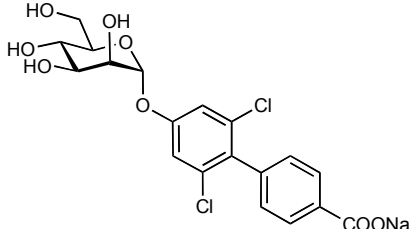
<b>KM 65</b> <b>KM 80</b>		0.79 mM/11.02.10	5.7	Ph Le <sup>a</sup>
		1.67 mM/22.04.10	2.2	Ph Le <sup>a</sup>
		1.69 mM/23.04.10	2.2	Ph Le <sup>a</sup>
		1.69 mM/22.06.10	1.2	Ph Le <sup>a</sup>
		1.35 mM/24.06.10	1.2	Ph Le <sup>a</sup>
		2.45 mM/21.07.10	2.5	Ph Le <sup>a</sup>
		2.5 mM/ 23.07.10	1.9	Ph Le <sup>a</sup>
<b>KM 73</b>		0.84 mM/11.02.10	6	Ph Le <sup>a</sup>
		1.39 mM/22.04.10	1.84	Ph Le <sup>a</sup>
		1.79 mM/23.04.10	2.3	Ph Le <sup>a</sup>
		1.4 mM/24.06.10	1.2	
		2.56 mM/21.07.10	2.7	
<b>KM 106</b>		1.9 mM/22.04.10	2.5	Ph Le <sup>a</sup>
		2.36 mM/23.04.10	3.0	Ph Le <sup>a</sup>
		3.14 mM/22.06.10	2.3	Ph Le <sup>a</sup>
		2.15 mM/24.06.10	1.9	Ph Le <sup>a</sup>
		3.75 mM/21.07.10	3.9	Ph Le <sup>a</sup>
<b>KM 149</b>		1.8 mM/22.06.10	1.3	Ph Le <sup>a</sup>
		1.6 mM/22.06.10	1.6	Ph Le <sup>a</sup>
		2.37 mM/21.07.10	2.5	Ph Le <sup>a</sup>
		2.65 mM/ 23.07.10	2.0	Ph Le <sup>a</sup>
<b>KM 151</b>		4.25 mM/22.06.10	3.1	Ph Le <sup>a</sup>
		2.25 mM/24.06.10	2	Ph Le <sup>a</sup>
		3.35 mM/21.07.10	3.5	Ph Le <sup>a</sup>
		2.95 mM/ 23.07.10	2.3	Ph Le <sup>a</sup>
<b>KM 153</b>		5.6 mM/22.06.10	5.6	Ph Le <sup>a</sup>
		3.7 mM/24.06.10	3.6	Ph Le <sup>a</sup>
		4.79 mM/21.07.10	5.0	Ph Le <sup>a</sup>
<b>KM 166</b>		2.73 mM/21.07.10	2.9	Ph Le <sup>a</sup>
		2.34 mM/ 23.07.10	1.8	Ph Le <sup>a</sup>
		1.35 mM/07.07.11	1.35	
<b>KM 244</b>		0.98 mM/30.03.11	1.2	Ph Le <sup>a</sup>
		1.22 mM/17.06.11	1.6	Ph Le <sup>a</sup>
<b>KM 232</b>		1.84 mM/30.03.11	2.24	Ph Le <sup>a</sup>
		0.29 mM/16.06.11	0.45	Ph Le <sup>a</sup>
		1.33 mM/07.07.11	1.33	Ph Le <sup>a</sup>
<b>KM 256</b>		1.2 mM/30.03.11	1.45	Ph Le <sup>a</sup>
		0.36 mM/16.06.11	0.56	Ph Le <sup>a</sup>
		1.34 mM/07.07.11	1.34	

<b>KM 280</b>		0.36 mM/16.06.11 0.63 mM/17.06.11	0.56 0.86	Ph Le <sup>a</sup> Ph Le <sup>a</sup>
<b>KM 277</b>		1.05 mM/16.06.11 1.2 mM/17.06.11	1.64 1.64	Ph Le <sup>a</sup> Ph Le <sup>a</sup>
<b>AV124</b>		No inhibition		
<b>AV137</b>		no inhibition!		
<b>AV144</b>		low solubility! low inhibition starting at approx. 5 mM!		
<b>AV176</b>	 <b>AV-I-176</b>	1.02 mM/ 25.08.10 1.76 mM/ 25.10.10		
<b>AV33b</b>	 <b>AV-I-33B</b>	3.14 mM/ 25.08.10 2.79 mM/ 25.10.10		
<b>AV257</b>	 <b>AV-257</b>	1.01 mM/ 01.04.11	0.84	Ph Le <sup>a</sup>

<b>AV278</b>	 <p style="text-align: center;"><b>AV-278</b></p>	3.89 mM/ 01.04.11	3.24	Ph Le <sup>a</sup>
<b>AV267</b>	 <p style="text-align: center;"><b>AV-267</b></p>	0.97 mM/ 31.03.11	1.44	Ph Le <sup>a</sup>
<b>AV270</b>	 <p style="text-align: center;"><b>AV-270</b></p>	1.99 mM/ 31.03.11	2.97	Ph Le <sup>a</sup>
<b>AV256</b>	 <p style="text-align: center;"><b>AV-256</b></p>	2.54 mM/ 31.03.11	3.79	Ph Le <sup>a</sup>
<b>GMI-1084 (Glyco- Mimetics)</b>		<b>0.76 mM</b> /07.05.09 <b>0.45 mM</b> /08.05.09 <b>0.93 mM</b> /29.05.09		
<b>K784- 1848 (Kiessling)</b>		<b>17.09 μM</b> /27.08.09 <b>26.37 μM</b> /15.09.09 <b>28.33 μM</b> /17.09.09		
<b>K784- 1581 (Kiessling)</b>		<b>49.34 μM</b> /27.08.09 <b>39.45 μM</b> /15.09.09 <b>39.25 μM</b> /17.09.09		



<b>K593-1866</b> (Kiesling)		<b>80.51 <math>\mu</math>M</b> /27.08.09 <b>149.3 <math>\mu</math>M</b> /15.09.09 <b>152.1 <math>\mu</math>M</b> /17.09.09		
<b>K584-1572</b> (Kiesling)		<b>n.d.</b> /27.8.09 <b>178.1 <math>\mu</math>M</b> /15.09.09 <b>261.7 <math>\mu</math>M</b> /17.09.09		
<b>TK05</b>		17.02.09 <b>no inhibition up to 1 mM</b> vs. trimannose PPA		
<b>TK14</b>		17.02.09 <b>no inhibition up to 1 mM</b> vs. trimannose PPA		
<b>TK15</b>		17.02.09 12.03.09 <b>no inhibition up to 1 mM</b> vs. trimannose PPA		
<b>TK17</b>		17.02.09 <b>no inhibition up to 1 mM</b> vs. trimannose PPA		
<b>TK22</b>		12.03.09 <b>no inhibition up to 1 mM</b> vs. trimannose PPA		

<b>TK28</b>		17.02.09 <b>no inhibition up to 1 mM</b> vs. trimannose PPA		
-------------	---	---	--	--

## CURRICULUM VITAE

NAME	<b>MEIKE SCHARENBERG</b>
PLACE OF BIRTH	<b>HANNOVER, GERMANY</b>
DATE OF BIRTH	<b>12.04.1982</b>
<b>EDUCATION AND WORK EXPERIENCE</b>	
MARCH 2008 – DEC. 2011	<b>PHD THESIS</b> <b>UNIVERSITY OF BASEL, INSTITUTE OF MOLECULAR PHARMACY, PHARMACENTER, BASEL, SWITZERLAND</b> SUPERVISOR: <b>PROF. DR. BEAT ERNST</b> “BIOLOGICAL CHARACTERIZATION OF THE LECTINS DC-SIGN AND FIMH: PUTATIVE TARGETS FOR NOVEL ANTI-INFECTIVES“
MAY – NOV. 2007	<b>DIPLOMA THESIS</b> <b>HANNOVER MEDICAL SCHOOL, GERMANY</b> INSTITUTE FOR CELLULAR CHEMISTRY SUPERVISOR: <b>PROF. DR. RITA GERARDY-SCHAHN</b> TITLE: “CHARACTERISATION OF THE GALNACTA IN COMPARISON WITH THE DHHC PROTEIN-DEPENDENT GALNACTB FROM <i>DROSOPHILA MELANOGASTER</i> ”
JULY – SEPT. 2006	<b>INTERNSHIP (AS PART OF DIPLOMA STUDIES)</b> <b>UNIVERSITY OF CANTERBURY, CHRISTCHURCH, NEW ZEALAND</b> SUPERVISOR: ASSOC. PROF. DR. JACK HEINEMANN “THE INTEGRON/GENE CASSETTE SYSTEM IN <i>CAMPYLOBACTER SSP.</i> “
2002 - 2007	<b>DIPLOMA STUDY IN BIOCHEMISTRY</b> LEIBNIZ UNIVERSITY OF HANNOVER / HANNOVER MEDICAL SCHOOL MAJOR SUBJECTS: BIOCHEMISTRY, IMMUNOLOGY, BIOPHYSICAL CHEMISTRY
2001 - 2002	<b>TEACHER TRAINING COURSE, MAJOR SUBJECTS: CHEMISTRY, BIOLOGY</b> UNIVERSITY OF HANNOVER, GERMANY
JUNE 2001	<b>ABITUR/ A LEVELS</b> GYMNASIUM LUTHERSCHULE, HANNOVER, GERMANY
1994 - 2001	<b>SECONDARY SCHOOL</b> GYMNASIUM LUTHERSCHULE, HANNOVER, GERMANY
<b>TEACHING</b>	
2008 - 2011	<b>TEACHING ASSIGNMENT</b> FIMH PROJECT MEETINGS, UNIVERSITY OF BASEL
2008 - 2011	<b>SUPERVISION OF PRACTICAL COURSES IN BIOLOGY</b> FOR UNDERGRADUATE PHARMACY STUDENTS, UNIVERSITY OF BASEL
2010 - 2011	<b>PLANNING AND SUPERVISION OF MASTER THESES</b> FOR FOUR MASTER STUDENTS IN TOTAL, UNIVERSITY OF BASEL

## ADDITIONAL DIPLOMA

- 2009 **BACHELOR EXAM IN “MOLECULAR DRUG MECHANISMS” FOR PHARMACISTS**  
UNIVERSITY OF BASEL
- 2009 **GRADUATE COURSE “KEY ISSUES IN DRUG DISCOVERY & DEVELOPMENT”**  
DEPARTMENT OF PHARMACEUTICAL SCIENCES, UNIVERSITY OF BASEL
- 2009 **GE HEALTHCARE WORKSHOP BIACORE BASIC**  
MUNICH, GERMANY

## PRESENTATIONS AND POSTERS

- GORDON CONFERENCE  
GLYCOBIOLOGY, LUCCA,  
ITALY, MAY 2011
- “DISTINCT BINDING-MODES FOR SUBSTITUTED LEWIS STRUCTURES TO DC-SIGN“  
**ORAL PRESENTATION AND POSTER**

## PUBLICATIONS

- ASSAY AND DRUG  
DEVELOPMENT  
TECHNOLOGIES, 2011
- A FLOW CYTOMETRY-BASED ASSAY FOR SCREENING FIMH ANTAGONISTS  
**MEIKE SCHARENBERG**, DANIELA ABGOTTSPON, EVELIN CICEK,  
XIAOHUA JIANG, OLIVER SCHWARDT, SAID RABBANI, AND BEAT ERNST
- CELLULAR AND  
MOLECULAR LIFE SCIENCES,  
2011
- ““ADD-ON” DOMAINS OF DROSOPHILA  $\beta$ 1,4-N-ACETYLGALACTOSAMINYL-  
TRANSFERASE B IN THE STEM REGION AND ITS PILOT PROTEIN.”  
BENJAMIN KRAFT, ANITA JOHSWICH, GWENDA KAUCZOR, **MEIKE SCHARENBERG**,  
RITA GERARDY-SCHAHN UND HANS BAKKER
- JOURNAL OF MEDICINAL  
CHEMISTRY, 2010
- “FIMH ANTAGONISTS FOR THE ORAL TREATMENT OF URINARY TRACT INFECTIONS:  
FROM DESIGN AND SYNTHESIS TO *IN VITRO* AND *IN VIVO* EVALUATION“  
TOBIAS KLEIN, DANIELA ABGOTTSPON, MATTHIAS WITTEW, SAID RABBANI,  
JANNO HEROLD, XIAOHUA JIANG, SIMON KLEEB, CHRISTINE LUTHI,  
**MEIKE SCHARENBERG**, JACQUELINE BEZENCON, ERICH GUBLER, LIJUAN PANG,  
MARTIN SMIESKO, BRIAN CUTTING, OLIVER SCHWARDT, AND BEAT ERNST